OAK RIDGE NATIONAL LABORATORY LIBRARIES

3 4456 0578506 8

ORNL/NUREG-17

Cy. 66

Zirconium Metal-Water Oxidation Kinetics IV. Reaction Rate Studies

J. V. Cathcart
R. E. Pawel
R. A. McKee
R. E. Druschel
G. J. Yurek
J. J. Campbell
S. H. Jury

Prepared for the U.S. Nuclear Regulatory Commission
Office of Nuclear Regulatory Research
Under Interagency Agreements 40-551-75 and 40-552-75

OAK RIDGE NATIONAL LABORATORY
CENTRAL RESEARCH LIBRARY
DOCUMENT COLLECTION
LIBRARY LOAN COPY
DO NOT TRANSFER TO ANOTHER PERSON
If you wish someone else to see this
document, send in name with document
and the library will arrange a loan.

OAK RIDGE NATIONAL LABORATORY
OPERATED BY UNION CARBIDE CORPORATION FOR THE ENERGY RESEARCH AND DEVELOPMENT ADMINISTRATION

Printed in the United States of America. Available from
National Technical Information Service
U.S. Department of Commerce
5285 Port Royal Road, Springfield, Virginia 22161
Price: Printed Copy $7.75; Microfiche $3.00

This report was prepared as an account of work sponsored by the United States Government. Neither the United States nor the Energy Research and Development Administration, the United States Nuclear Regulatory Commission, nor any of their employees, nor any of their contractors, subcontractors, or their employees, makes any warranty, express or implied, or assumes any legal liability or responsibility for the accuracy, completeness or usefulness of any information, apparatus, product or process disclosed, or represents that its use would not infringe privately owned rights.

ORNL/NUREG-17
Dist. Category NRC-3

Contract No. W-7405-eng-26

METALS AND CERAMICS DIVISION

ZIRCONIUM METAL-WATER OXIDATION KINETICS IV. REACTION RATE STUDIES

J. V. Cathcart, R. E. Pawel, R. A. McKee, R. E. Druschel,
G. J. Yurek, J. J. Campbell, and S. H. Jury

Manuscript Completed — July 19, 1977

Date Published — August 1977

Prepared for the
U.S. Nuclear Regulatory Commission
Office of Nuclear Regulatory Research
Under Interagency Agreements 40-551-75 and 40-552-75

OAK RIDGE NATIONAL LABORATORY
Oak Ridge, Tennessee 37830
operated by
UNION CARBIDE CORPORATION
for the
ENERGY RESEARCH AND DEVELOPMENT ADMINISTRATION

CONTENTS

SUMMARY vii
ABSTRACT 1
INTRODUCTION 2
EXPERIMENTAL PROCEDURES 3
Thermocouple Selection and Calibration 4
Thermocouple-Specimen Compatibility 6
Apparatus Description-MaxiZWOK 10
MaxiZWOK Temperature Control and Recording Systems . . . 14
Apparatus Description-MiniZWOK 14
MiniZWOK Temperature Control and Recording System 17
Potential Errors in Temperature Measurements 18
Thermal Shunting 19
Thermal Shunting in the MiniZWOK Apparatus 20
Thermal Shunting in the MaxiZWOK Apparatus 21
Electrical Shunting 22
Parasitic EMF's 22
Data Acquisition System Errors 23
Thermocouple Calibration Errors 23
Temperature Gradients in the Sample 23
Decalibration of Thermocouples 25
Tab Attachment Effects 25
Evaluation of Temperature Errors 27
Determinant Errors 27
Indeterminant Errors 27
Indeterminant Errors in MiniZWOK 29
Indeterminant Errors in MaxiZWOK 34
Total Error Estimates 34
Weight Gain Tests 35
Characterization of Zircaloy-4 PWR Tube Specimens 38
EXPERIMENTAL RESULTS FOR ISOTHERMAL OXIDATION 39
Primary Isothermal Data Set — MiniZWOK Apparatus 40
Time-Temperature Cycles 40
Normalization of Time-Temperature Excursions 43

Metallographic Procedures 45
Phase Thickness Measurements 46
Results 50
Correlation of the Data 58
Oxide-Alpha Thickness Ratios 72
Comparison of Isothermal Kinetic Data 73
Scoping Tests 76
Isothermal Oxidation Tests in MaxiZWOK 76
Data and Results 79
Correlation of Data and Comparisons 81
Mixed Gas Experiments 85
Alloy Composition Variation 93
Summary of Isothermal Scoping Test Results 98
COMPUTER CODES AND TRANSIENT-TEMPERATURE OXIDATION 98
Isothermal Model Verification 100
Mixed-Temperature Experiments 102
Transient Temperature Oxidation Experiments 105
Anomalous Transient Temperature Oxidation 109
CONCLUSIONS AND RECOMMENDATIONS 117
ACKNOWLEDGMENTS 120
REFERENCES 121
APPENDIX A -- ERROR ANALYSIS 125
INTRODUCTION 125
STATISTICAL TREATMENT OF ISOTHERMAL OXIDATION RATE DATA 125
Data 126
Prediction Equations for Rate Constants. 126
Confidence Intervals at the 95% Level 140
Individual Confidence Limits 140
(Upper 95%/Upper 90%) for Estimator $\hat{A}$. 141
(Upper 95%/Upper 90%) for $\hat{Q}$ 143
Joint Confidence Intervals 144
MAXIMUM ABSOLUTE ERROR LIMITS FOR EXPERIMENTAL PROCEDURES 144
Temperature Measurement Errors 144
Time Measurement Errors 150

Thickness Measurement Errors 151
Uncertainty in Parabolic Rate Constants 156
Uncertainties in A and Q 158
Indeterminant Errors 158
SIGNIFICANCE OF ABSOLUTE ERROR ESTIMATES 160
REFERENCES 162
APPENDIX B — HYDROGEN ANALYSES FOR OXIDIZED SPECIMENS 163
INTRODUCTION 163
ANALYTICAL RESULTS 163
EVALUATION OF ANALYTICAL DATA 168
DISCUSSION OF THE ANALYTICAL RESULTS 169
As-Received Tubing 169
Two-Sided Oxidation 169
One-Sided Oxidation 169
Mechanism of Hydrogen Absorption 170
Transient Temperature Oxidation 173
POSSIBLE EFFECTS OF DISSOLVED HYDROGEN ON OXIDATION RATES 173
Indirect Evidence 174
Self-Consistency of Rate Data 174
Comparison with Other Data 174
Experiments in Pure Oxygen 175
Analysis of Possible Effects 175
Effects in the Alpha and Beta Phases 176
Effects in the Oxide 178
Experimental Results for Oxidation in Oxygen 179
Discussion of Results 181
Hydrogen Effects in the Beta Phase Only 181
Effects in the Oxide Only 185
CONCLUSIONS 196
REFERENCES 197

SUMMARY

The isothermal reaction rates of steam and Zircaloy-4 were determined at 50°C (90°F) intervals from 900 to 1500°C (1652–2732°F). The following correlations were obtained for oxide, alpha, and Xi layer growth and for total oxygen consumption:

$$\delta_\phi^2/2 = 0.01126 \exp(-35890/RT) \text{ cm}^2/\text{s for } 1000°C < T \leq 1500°C,$$
$$\delta_\alpha^2/2 = 0.7615 \exp(-48140/RT) \text{ cm}^2/\text{s for } 900°C \leq T \leq 1500°C,$$
$$\delta_\xi^2/2 = 0.3412 \exp(-41700/RT) \text{ cm}^2/\text{s for } 1000°C < T \leq 1500°C,$$
$$\delta_\tau^2/2 = 0.1811 \exp(-39940/RT) \text{ (g/cm}^2)^2/\text{s for } 1000°C < T \leq 1500°C,$$

where the $\delta_K^2/2$ are the parabolic rate constants ($\delta_K^2/2 = K\ dK/dt$), ϕ, α, ξ refer to oxide, alpha and Xi layer growth, respectively, and τ represents total oxygen consumed. The correlations for ϕ, ξ, and τ are not valid below $\sim$ 1000°C (1832°F) because below this temperature the oxide layer growth does not follow parabolic kinetics.

The conditions under which these data were obtained were carefully characterized and the experimental procedures fully documented, especially with regard to the accuracy of temperature, time, and phase thickness measurements. The data were subjected to a rigorous statistical analysis, and at the midpoint of the reciprocal temperature determinations [$\sim$ 1200°C (2192°F)] the uncertainty on $\delta_K^2/2$ at the 90% confidence level was 2.5, 5.8, 1.5, and 1.7% for the oxide, alpha, Xi, and total oxygen rate constants, respectively. At the extremes of the temperature range these uncertainties were somewhat greater; e.g., at 1500°C (2732°F) values of 4.3, 10.1, 2.6, and 2.9%, respectively, were obtained. An absolute error analysis is also supplied. Within the limits thus established and for the comparatively ideal oxidation conditions used, we consider this isothermal data set to be highly reliable.

A series of scoping tests demonstrated that neither steam flow rate (above steam starvation levels); steam temperature; the presence of reasonable concentrations of oxygen, nitrogen, or hydrogen in the steam; nor small variations in alloy composition significantly influence the isothermal oxidation rate of Zircaloy-4.

Two computer codes, SIMTRAN and BILD5, were written that together successfully predict the thickness of the compact oxide and oxygen-stabilized alpha layers formed and total oxygen consumed during most transient temperature oxidation experiments. Exceptions involve certain postulated two-peak LOCAs where the phenomenon of "anomalous transient temperature oxidation" is observed. The probable mechanism of this effect is discussed in detail in the body of the report. The computer codes also do not model the formation of alpha incursions or precipitates in the beta regions of the fuel tubes during the cooling phase of a temperature transient.

Areas in which it is suggested that further correlations be developed or additional research performed include: (1) the effect of fuel tube deformation on oxidation rate; (2) the phenomenon of the formation of alpha incursions as related to the mechanical properties of Zircaloy-4; and (3) anomalous transient temperature oxidation effects.

ZIRCONIUM METAL-WATER OXIDATION KINETICS IV. REACTION RATE STUDIES

J. V. Cathcart, R. E. Pawel, R. A. McKee, R. E. Druschel, G. J. Yurek,* J. J. Campbell, and S. H. Jury†

ABSTRACT

The isothermal rates of oxide, oxygen-stabilized alpha, and Xi layer growth and of total oxygen consumption of Zircaloy-4 in steam were determined from 900 to 1500°C (1652—2732°C) and described in terms of analytical expression for the appropriate parabolic rate constants. Comparison of the results with existing rate data demonstrates the relative conservatism of the Baker-Just correlation. Scoping tests of the effects on isothermal oxidation rates of such system parameters as steam flow rate, injection temperature, and purity and of small changes in alloy composition showed these variables to have small or negligible effects. Experimental transient temperature oxidation behavior was found to be predictable by computer codes designed for that purpose; the only exception found was the case of certain hypothetical two-peak LOCA's. The probable cause for this exception is discussed in terms of the monoclinic-tetragonal phase transformation of the oxide. An error analysis of the oxidation data is presented in both statistical and analytical terms, and possible kinetic effects of hydrogen dissolved in oxidized samples are considered and concluded to be negligible.

---

*Dept. of Materials Science and Engineering, Massachusetts Institute of Technology, Cambridge, MA 02139.

†Consultant, University of Tennessee, Knoxville, TN.

INTRODUCTION

Models of hypothetical loss-of-coolant accidents for light water nuclear power reactors generally involve an excursion in temperature for parts of the reactor core in which the reaction of the Zircaloy fuel rods with the steam environment may become appreciable. The effects of the Zircaloy-steam reaction must be considered in the emergency core cooling system design because of their potential influence on both the thermal and mechanical behavior of the system. Thus, it has been considered important to establish a capability to evaluate and predict quantitatively the extent of the oxidation reaction during transient temperature exposures.

The primary purpose of the present program is to provide reliable kinetic measurements describing the reaction of Zircaloy with steam at high temperatures. This information will provide a basic data set to be used as input to computer codes to predict the oxidation behavior of LWR fuel cladding during the various temperature excursions anticipated for hypothetical LOCA's. This report constitutes the final report of the oxidation kinetics phase of this research. Previous reports of this work, which contain many of the details not emphasized here, are the Quarterly Report series,[1] several topical reports,[2-5] and other publications.[6-7]

The oxidation of Zircaloy at temperatures above the alpha-beta transformation will generally result in two distinct product layers growing into the host beta: the outermost oxide phase, and an intermediate layer of oxygen-stabilized alpha. During cooling of the specimen to room temperature, the beta core transforms back to alpha. However, the metallographic appearance of this material is significantly different from that of the oxygen-stabilized alpha, and the "prior beta" is easily recognized. The growth rates of these product layers are conveniently measured parameters that may be used to describe the oxidation kinetics. In addition, it is possible to utilize the phase thickness measurements, in conjunction with other information, to calculate the total oxygen consumption. The bulk of the experimental effort in this program was directed at obtaining kinetic data for these parameters over the

temperature range 900–1500°C. In addition, computer codes were developed that utilized these data to predict oxidation behavior during transient temperature reactions.

EXPERIMENTAL PROCEDURES

The accurate measurement of reaction kinetics at elevated temperatures requires a considerable effort in order to keep experimental errors within acceptable limits. The apparatuses and procedures utilized in this program were developed with these problems in mind, and particular attention was directed throughout the research to assure that accurate temperature measurements would be characteristic of all experiments.

In order to accomplish all of the necessary tests, two experimental steam oxidation apparatuses were constructed. Both apparatuses utilized the multispecimen technique to examine the reaction kinetics. The first, called MaxiZWOK, was based on a high thermal inertia furnace system, with steam at or near the desired reaction temperature being passed over the specimen. In this apparatus, the temperature of the specimen was not controlled directly but was governed by its response to the heat transfer from its steam and furnace environment. With this apparatus tests could be conducted at comparatively high steam flow rates and insertion temperatures. The second apparatus, called MiniZWOK, was based on a low thermal inertia furnace system in which the specimen was heated in flowing steam by a powerful radiant heating furnace. In this case, the specimen temperature was controlled directly by regulating the power to the furnace. A temperature programming capability for this system made it convenient for performing both isothermal and transient-temperature oxidation experiments.

Both apparatuses were developed and improved during the course of this investigation and the chronology of these changes can be followed in the Quarterly Reports.[1] The most important changes came about in an effort to improve the accuracy of temperature measurements of the specimen during oxidation. For example, the original MiniZWOK apparatus was designed to oxidize both inner and outer surfaces of the Zircaloy

tube specimens. Preliminary experiments with this apparatus uncovered a number of problems involving temperature measurements that were alleviated when the system was modified to allow oxidation on the outer tube surfaces only.

Thermocouple Selection and Calibration

A prime goal in the Thermometry Task of this program was to provide temperature measurements traceable to the International Practical Temperature Scale of 1968 (IPTS-68). In the temperature range 900 to 1500°C (1652–2732°F), the IPTS-68 is based on two instruments: (1) the Pt vs Pt–10% Rh thermocouple, which spans the range 630.74 to 1064.43°C (∿ 1167–1948°F), and (2) above 1064.43°C (∿ 1948°F), a radiation pyrometer using the Planck Law of radiation with 1064.43°C (∿ 1948°F), as the reference temperature and a value of 0.014388 meter-kelvin for C_2 in the radiance equation.[8]

Because of its convenience and superior characteristics for both the oxidation and diffusion experiments, nominal Pt vs Pt–10% Rh thermocouples (type S) were used as our primary means for determining temperature. The supplies of platinum and Pt–10% Rh reference grade thermocouple wire were obtained from the Sigmund Cohn Corporation.* Individual lots were fabricated from the same heat in order to minimize calibration differences. Several wire diameters were specified, but subsequent testing revealed no differences in the performance of thermocouples made from 0.008, 0.025, and 0.051 cm (0.003, 0.010, 0.020 in.) diam wires. Therefore, for the sake of ease of handling, the 0.025 cm (0.010 in.) diam wire was used exclusively in all later experiments.

Prior to calibration all thermocouple wires were subjected to an air anneal. The initial annealing schedule, 6 hr at 1300°C (2372°F), produced no difficulties with the pure platinum wire, but the tensile strength of the Pt–10% Rh was reduced by 30% and its total elongation by 45%. This deterioration of mechanical properties was shown metallographically to be related to excessive grain growth in the wire during

---

*Sigmund Cohn Corp., 121 S. Columbus Ave., Mt. Vernon, NY, 10553.

the anneal; the average grain size after anneal was about half the wire diameter. Therefore, a less demanding annealing schedule was adopted: 2 min at 1400°C (2552°F), 20 min at 1200°C (2192°F), 1 hr at 1000°C (1832°F), and 2 hr at 500°C (932°F). This treatment produced wires composed of relatively small, equiaxed grains, and the mechanical properties of the wires were not degraded.

The actual calibration of the various thermocouple combinations was carried out in the Metrology Research and Development Laboratory, Instruments and Controls Division, Oak Ridge National Laboratory. The procedure used involved several comparison calibrations of the thermocouple wires to 1500°C (2732°F). Several thermocouples, including two NBS-calibrated Pt vs Pt—10% Rh thermocouples, were connected to a common hot junction and the emf values of various pairs compared with the standards. A detailed description of the calibration procedure was given in a previous report.[3]

The data obtained indicated that the thermoelectric properties of our wires were excellent. The Pt vs Pt—10% Rh wire behaved very much like the NBS-calibrated thermocouples.

This calibration procedure represented an attempt to achieve, under ideal conditions, measurements of temperature with maximum uncertainty of ±2°C (3.6°F) on IPTS-68 at 1500°C (2732°F). Below 1064°C (1947°F), estimated uncertainties of thermocouple calibrations were less than ±0.2°C (0.36°F) at fixed points and less than ±0.3°C (0.54°F) for table values between fixed points.[9] These uncertainties increased above 1064°C (1947°F). At 1450°C (2646°F) an uncertainty of ±1°C (1.8°F) is given for an NBS calibrated Pt vs Pt—10% Rh thermocouple, and we estimated an uncertainty of ±1.5°C (2.7°F) for our thermocouples at 1500°C (2732°F). Thus our goal of an uncertainty of ±2°C (3.6°F) at 1500°C (2732°F) appears to be realized except for possible problems associated with thermocouple decalibration during installation and use.

We addressed this latter concern by submitting for recalibration a Pt vs Pt—10% Rh thermocouple that had been used in several experiments between 900 and 1475°C (1652—2687°F) for approximately 3 hr. This thermocouple was tested to 1000°C (1832°F), and the results of the

recalibration gave no evidence of decalibration problems. Portions of a similar thermocouple were also submitted for chemical analysis. There was no indication of significant contamination which might lead to decalibration of the thermocouples.

A feature of our experimental procedure that mitigates decalibration difficulties is the fact that in a normal experiment the thermocouple hot junction is made by welding the thermocouple leads to a small tab of tantalum that is in turn welded directly to the specimen. At the end of an experiment the leads are clipped off just below the hot junction, and an entirely new hot junction is formed on the next specimen. Thus any contaminants near the hot junction are eliminated before they have time to diffuse far enough along the thermocouple wires to produce problems.

Thermocouple-Specimen Compatibility

The Zircaloy-steam reaction is highly exothermic ($\Delta H \approx 140$ kcal/mole in the temperature range of interest), and significant self-heating of a Zircaloy specimen can occur under conditions where the rate of oxidation is high. Therefore, in order to monitor accurately the temperature of an oxidizing sample, we considered it essential that metal-to-metal contact be maintained at all times between the specimen and the thermocouples.

Unfortunately, platinum-base thermocouples cannot be attached directly to Zircaloy specimens used in experiments above $\sim$ 1150°C (2102°F) because of the formation of a low melting [1185°C (2165°F)] Pt-Zr eutectic (see Fig. 1). We circumvented this problem by inserting tantalum or iridium tabs [2 × 2 × 0.075 mm (0.08 × 0.08 × 0.003 in.)] between the thermocouple and the specimen. The thermocouple leads were first spot welded together on the tabs, and the tabs were then spot welded to the specimen.

Tantalum proved to be an excellent tab material when used in vacuum, as in our diffusion experiments, or in an inert gas, as in our low thermal inertia oxidation apparatus (see below). A Zr-Ta eutectic melting at $\sim$ 1850°C (3362°F) has been reported[11] but produced no problems.

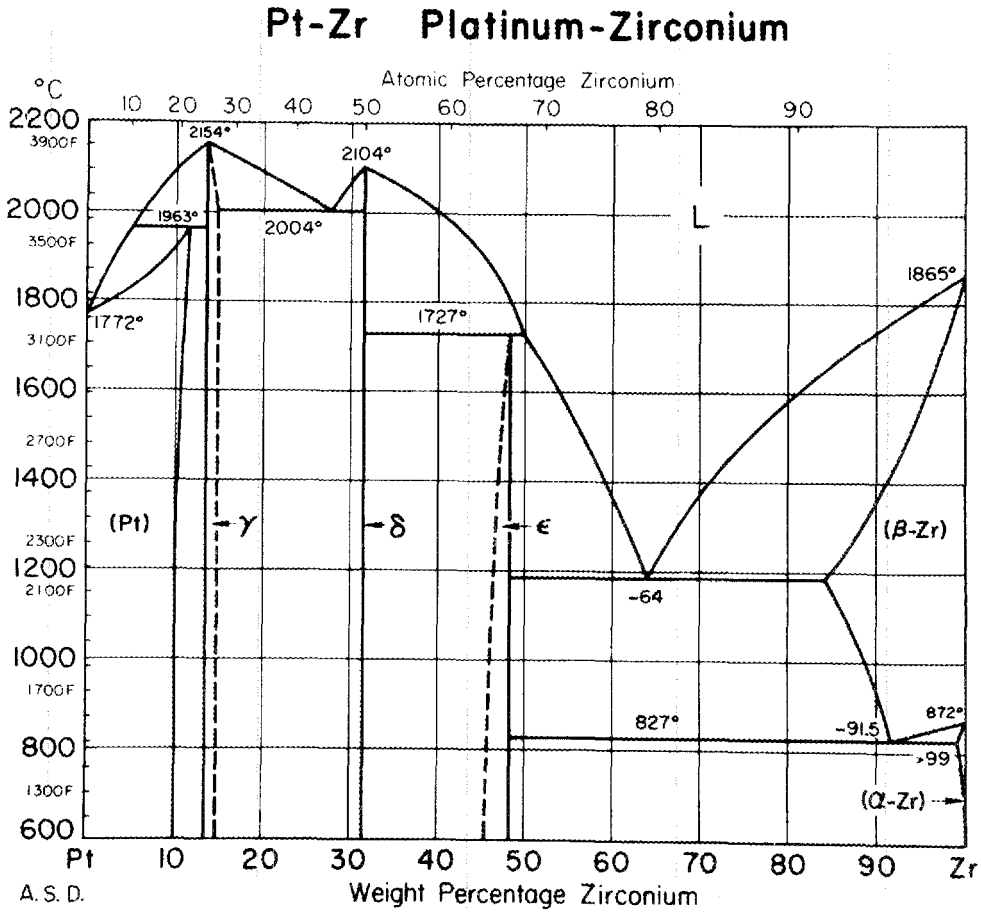

Fig. 1. Platinum-Zirconium Phase Diagram After Hawkins and Hultgren.[10]

A narrow diffusion zone between a tab and a Zircaloy diffusion specimen could be detected after a 30 min anneal at 1450°C (2642°C), but because the junction between tab and specimen always consisted of metal with good thermal conductivity, we see no reason to question the validity of this form of thermocouple attachment. No Pt-Ta phase diagram appears to be available, but metallographic examinations of the Pt-Ta interface showed little evidence of interaction. The only disadvantage of the tantalum tabs was the necessity to protect them from steam during our oxidation experiments. A cross-section through a thermocouple-tab-specimen weld area is shown in Fig. 2. The specimen was from an experiment in the MiniZWOK apparatus, (S-74), in which oxidation for 339 s at 1153°C (2107°F) took place. A good connection between the thermocouple bead, the tab, and the specimen is seen to exist.

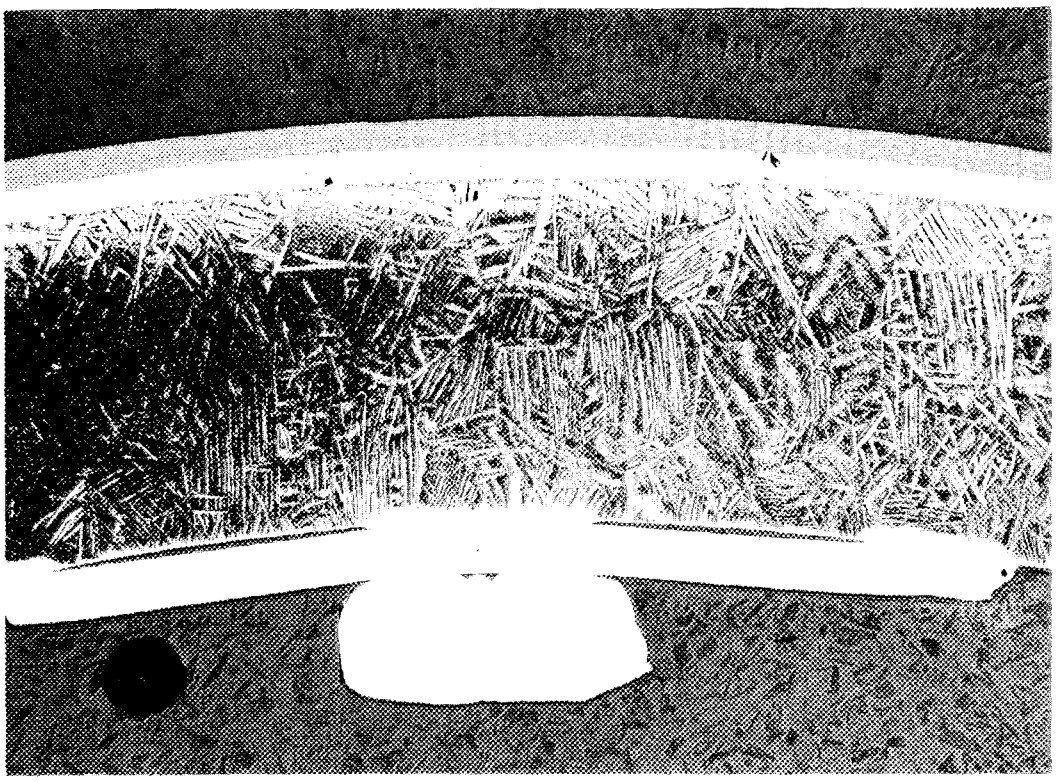

Fig. 2. Cross Section Through Thermocouple and Tantalum Tab Spot Welded to Zircaloy-4 Specimen. Outer surface of specimen tube was oxidized 339 s at 1153°C (2107°F). 75×.

Because it was much more difficult to protect the thermocouple tabs in the preliminary version (two-sided oxidation) of the MiniZWOK apparatus, we originally employed iridium tabs for use in steam where, in the temperature range of interest, iridium is inert. We were unable to find a Zr-Ir phase diagram in the literature, and preliminary annealing tests[1a] in vacuum did indicate the formation of a Zr-Ir eutectic between 1200 and 1300°C (2192–2372°F). However, in these tests the specimen was heated at a rate of 400°C/hr (720°F/hr), thus providing ample time for interdiffusion between the sample and tab. In a much shorter test, at a temperature of ∿ 1400°C (2552°F) and carried out under the time-temperature regime shown in Fig. 3, the thermocouple did remain attached to the specimen throughout the experiment. Subsequent metallographic examination of the specimen (Fig. 4) showed evidence of liquation in both the tab and the specimen. However, melting was confined to the immediate vicinity of the tab, the tab itself was not penetrated (thus

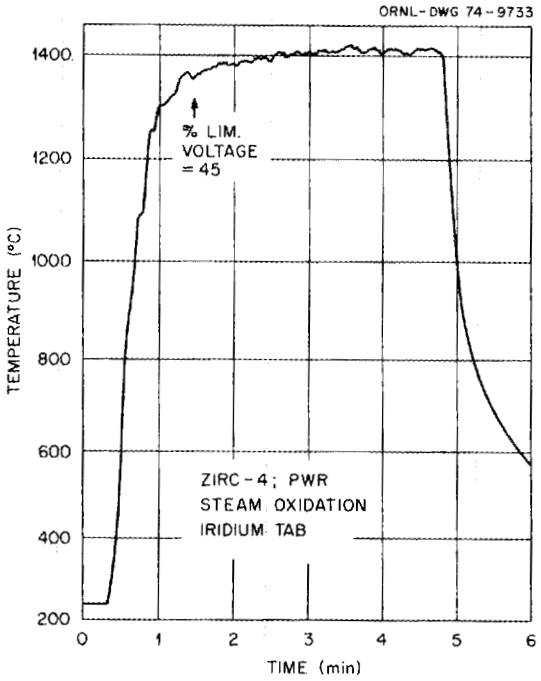

Fig. 3. Recorder Trace of Time-Temperature Regime Used in Test of Iridium Thermocouple Tab on Zircaloy-4.

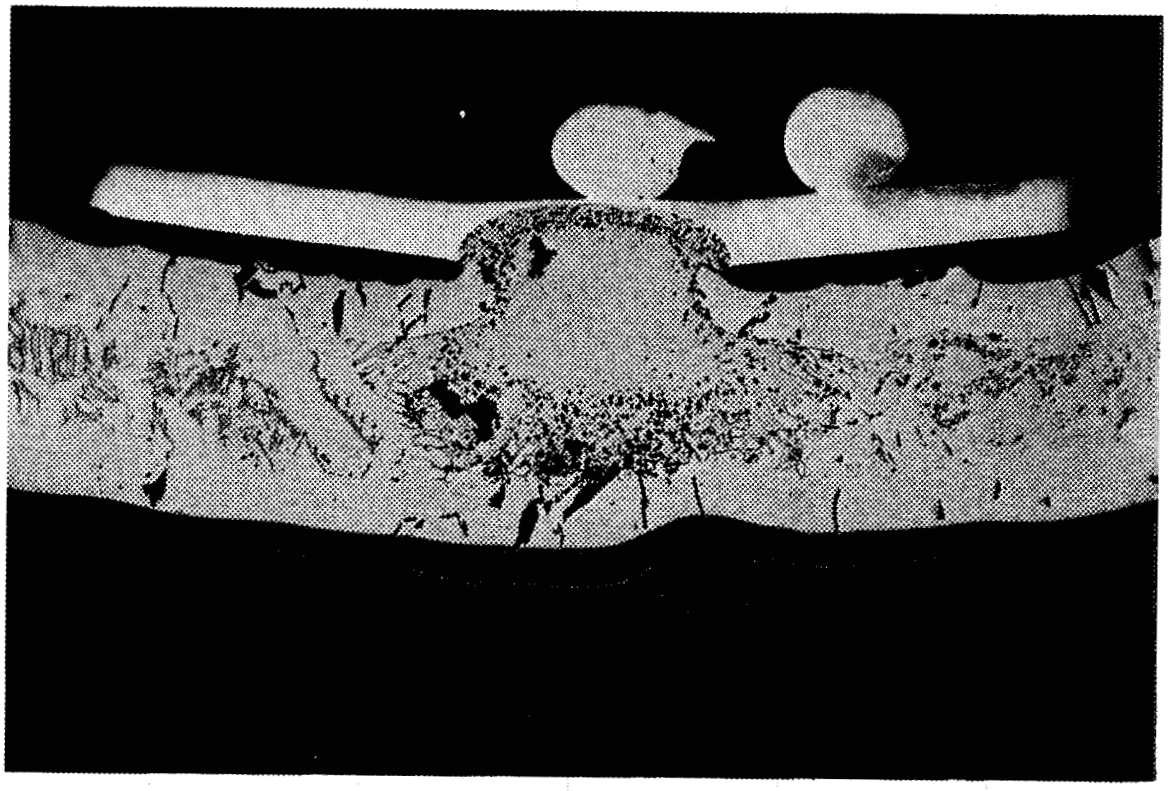

Fig. 4. Cross Section of Zircaloy-4 PWR Tube Specimen after Exposure in Steam According to the Temperature Cycle of Fig. 3. This illustrates the interaction zone associated with the weld between the iridium tab (on inside of tube) and the specimen. As polished, bright field, 62×.

protecting the thermocouple leads from attack), and good physical and thermal contact was maintained between the tab and specimen throughout the experiment. For these reasons and because we anticipated oxidation experiments of durations considerably less than 4 min at these very high temperatures, we were confident that iridium tabs could have been used successfully as needed in our oxidation rate studies. The modification of the MiniZWOK apparatus to produce oxidation only on the outer surface made it more practical to use the tantalum tabs.

Apparatus Description-MaxiZWOK

The MaxiZWOK steam oxidation apparatus is shown schematically in Fig. 5. The main components of this system are the superheated steam and distilled water supplies, the furnace and reaction tube, the specimen insertion device, and the instrumentation arrangements. The apparatus provides for superheating steam at high flow rates and brings it in contact with Zircaloy tubing specimens under well-documented conditions.

The incoming steam (65 psig) from the ORNL plant steam system passes through a separator, is metered, and enters the superheater at a pressure of 55–60 psig. Tests on the plant steam have revealed that the oxygen is maintained at less than 0.5 ppm, total soluble gases are less than 15 ppm, and total solids are approximately 0.4 ppm. The superheater consists of two coils of 0.95 cm (3/8 in.) OD Inconel 600 tubes that are resistance-heated. Power to the coils is furnished by four 5 KVA step-down transformers each fed by a Variac. The temperature of the Inconel at several points near the top (and hottest portion) of the superheater is monitored at all times as part of the "surveillance" thermocouple system. The superheater system is well-insulated with high temperature material (Kaowool). This arrangement proved capable of delivering approximately 1 lb/min of steam at temperatures up to 1000°C (1832°F) to the reaction chamber. Inconel tube temperatures approaching 1200°C (2192°F) were common. At these mass flow rates, the linear velocity of the steam was estimated to be about 20 m/s (66 ft/s) in the reaction chamber, and a few hundred m/s in the superheater tube.

ORNL-DWG 74-6057R

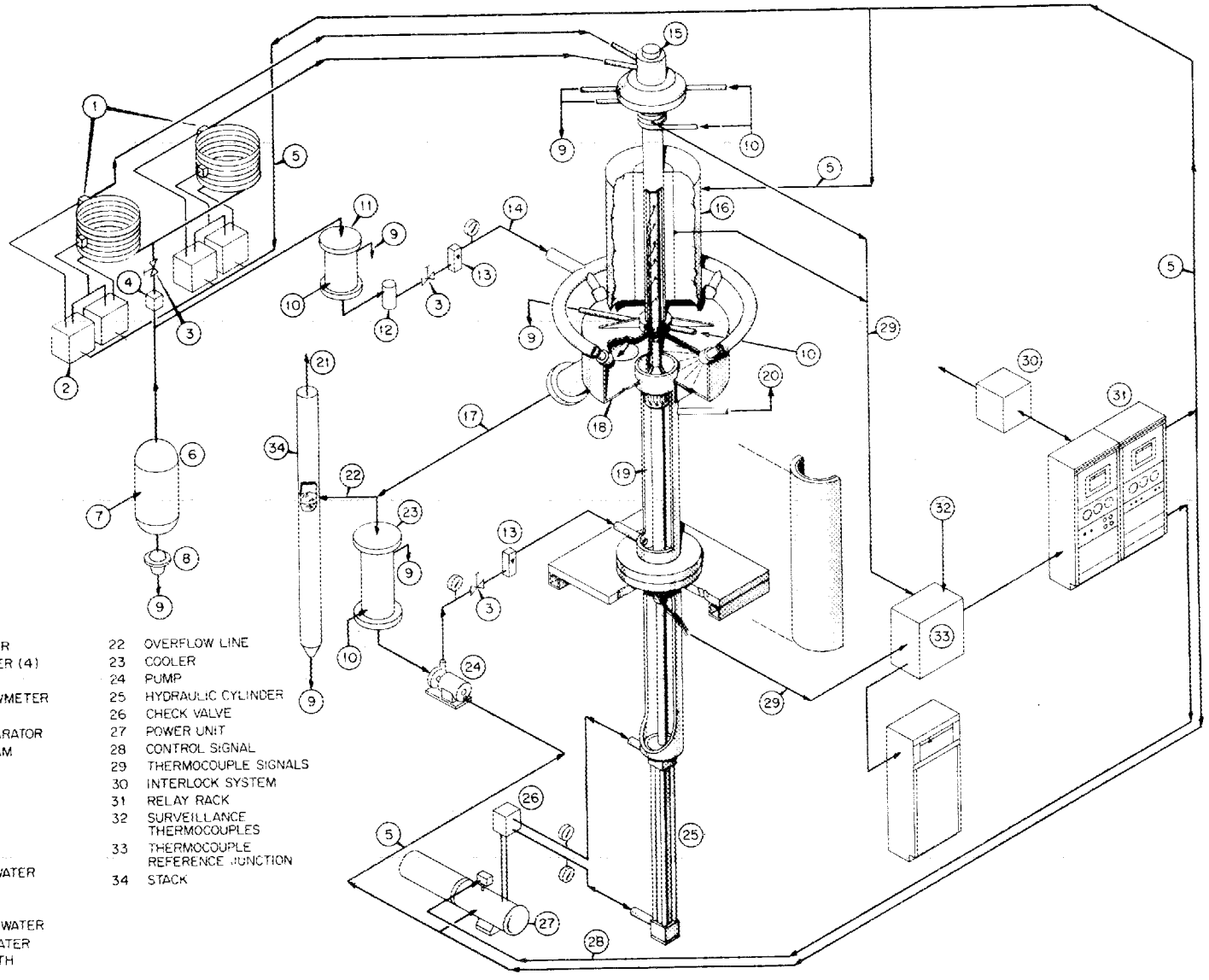

1 SUPERHEATER
2 TRANSFORMER (4)
3 VALVE
4 STEAM FLOWMETER
5 POWER
6 STEAM SEPARATOR
7 PLANT STEAM
8 TRAP
9 DRAIN
10 WATER
11 CONDENSER
12 FILTER
13 ROTAMETER
14 DISTILLED WATER
15 HEADER
16 REACTOR
17 STEAM AND WATER
18 DESUPERHEATER
19 QUENCH BATH
20 VENT
21 STEAM
22 OVERFLOW LINE
23 COOLER
24 PUMP
25 HYDRAULIC CYLINDER
26 CHECK VALVE
27 POWER UNIT
28 CONTROL SIGNAL
29 THERMOCOUPLE SIGNALS
30 INTERLOCK SYSTEM
31 RELAY RACK
32 SURVEILLANCE THERMOCOUPLES
33 THERMOCOUPLE REFERENCE JUNCTION
34 STACK

Fig. 5. Schematic Diagram of the MaxiZWOK Oxidation Apparatus.

The steam enters the top of the reaction chamber through an Inconel "header", where the steam temperature is measured by a Pt/Pt-10% Rh thermocouple attached to a platinum support located in the middle of the steam stream. The output of this thermocouple actuates a Speedomax H recorder-controller system that maintains the inlet steam temperature at the desired value by pulsing power to the superheater.

The reaction chamber consists of a 2" ID alumina tube surrounded by a muffle furnace. The primary purpose of the furnace is to prevent excessive heat losses from the steam before it contacts the specimen and to prevent excessive radiation losses from the specimen to the chamber wall. A thermocouple located in the annular region between the furnace and the specimen tube is used in conjunction with another Speedomax H system to control the power to the furnace. Generally, the furnace temperature is set equal to (or slightly above) the inlet steam temperature.

As shown in Fig. 5, a fraction of the steam leaving the separator is condensed and cooled for use in the steam desuperheater and specimen quench bath. Thus, all water coming in contact with the specimen in the apparatus is distilled water.

The surveillance thermocouple system consists of twelve Chromel-Alumel thermocouples located at important points on the apparatus. A twelve-point recorder operates continuously during the course of an experiment, serving as an early warning system for incipient troubles in critical parts of the apparatus. Particular attention needs to be paid to temperatures in the superheater system in order to prevent them from becoming excessive. The possibility of a rupture of a superheater tube operating at a high-temperature, high-flow condition creates some interesting scenarios.

The specimen consists of a 46 cm (18 in.) length of Zircaloy tubing. A small segment of the tube in close proximity to the thermocouple stations actually serves as the basic specimen; the remainder functions simply as support for the specimen and the thermocouple leads.

The specimen is cut from a standard PWR tube section. At a point approximately 20 cm (8 in.) from the forward end, a series of staggered

"ventilation" slots is cut in the tube in order to provide a path for the steam flow through the interior of the tube and to interfere with heat conduction from the upper end of the tube to its cooler lower portions. The tube is then cleaned thoroughly with a detergent solution, washed in alcohol, rinsed with distilled water, and dried.

Three thermocouple installations are made on the specimen. Generally, all three are located on the outside of the tube, 120° apart, at a point 5 cm (2 in.) from the upper end. After oxidation, the tube is sectioned at this elevation for appropriate metallographic measurements. If desired, a different arrangement of the thermocouples can be made. As mentioned previously, the thermocouples are 0.025 cm (0.010 in.) Pt/Pt—10% Rh calibrated, reference-grade materials encased in high-purity alumina to a distance of about 1.2 cm (0.5 in.) from the welded junctions. The ceramic tubes are positioned along the axis of the tube and are held in place with several Nichrome wires. The outputs of the three thermocouples attached to the specimen are fed directly to one single-channel and one two-channel Esterline-Angus recorders. The specimen temperature from insertion to quench can thus be monitored at various chart speeds and sensitivities. In addition, a switch is available to read the specimen thermocouple output directly on a Leeds and Northrup K-3 potentiometer.

The instrumented specimen is installed in the apparatus in a collet chuck located atop the plunger of a small hydraulic ram that serves as the insertion system. The thermocouple connections are completed via terminals located on a bakelite cylinder beneath the chuck. With the specimen in place, the panel door to the specimen chamber is fixed tightly in place with clamps. Distilled water is circulated in the specimen chamber to keep the specimen cool prior to its insertion into the reaction tube; this arrangement, in conjunction with the spray desuperheater, also serves as an efficient quench bath at the conclusion of the experiment.

Very concisely, an experiment in MaxiZWOK is conducted as follows:
(1) The instrumented specimen is mounted in the specimen chamber.
(2) With steam flowing through the system, power to the steam superheater coils is increased until the desired steam temperature is reached.

Concurrently, the furnace temperature, measured by a thermocouple located in the annulus between the furnace wall and the reaction tube, is brought into control at the desired value. (3) The hydraulic insertion system is activated, driving the specimen into the reaction chamber. The time-temperature response of the specimen is monitored. (4) At the conclusion of the experiment, the specimen is withdrawn from the reaction chamber into the quench bath. The oxidized specimen is now ready for metallographic analysis.

MaxiZWOK Temperature Control and Recording Systems

Power to the steam superheater is controlled by the signal from the Pt vs Pt—10% Rh thermocouple located at the upper end of the reaction tube. An ice bath cold junction is utilized, and control is provided by an L&N Speedomax H recorder-controller. The furnace temperature is controlled by the Chromel-Alumel thermocouple in the furnace annulus, again using a Speedomax H controller with a built-in temperature compensator. The outputs from measuring Pt vs Pt—10% Rh thermocouples are fed into two Esterline Angus, Model 1102S recorders; one of the couples is wired through an L&N DPDT, low-thermal-emf, copper switch so that its signal can also be read on the K-3 potentiometer. The calibration of the Esterline Angus recorders is checked before and after each experiment using a portable potentiometer; however, as in the case of MiniZWOK, the accepted temperatures are based on the K-3 potentiometer readings.

At the control temperature, a MaxiZWOK specimen is subjected to temperature oscillations of about ±2°C (3.6°F). Two frequencies and amplitudes of oscillations were observed related to the independent control of the steam superheater and furnace temperatures.

Apparatus Description-MiniZWOK

The bulk of the reaction rate experiments were performed in the MiniZWOK apparatus, a low thermal inertia system in which the temperature of the specimen (rather than that of its surroundings) is controlled in a programmed time-temperature excursion. A schematic diagram of the MiniZWOK steam oxidation apparatus is shown in Fig. 6. As mentioned

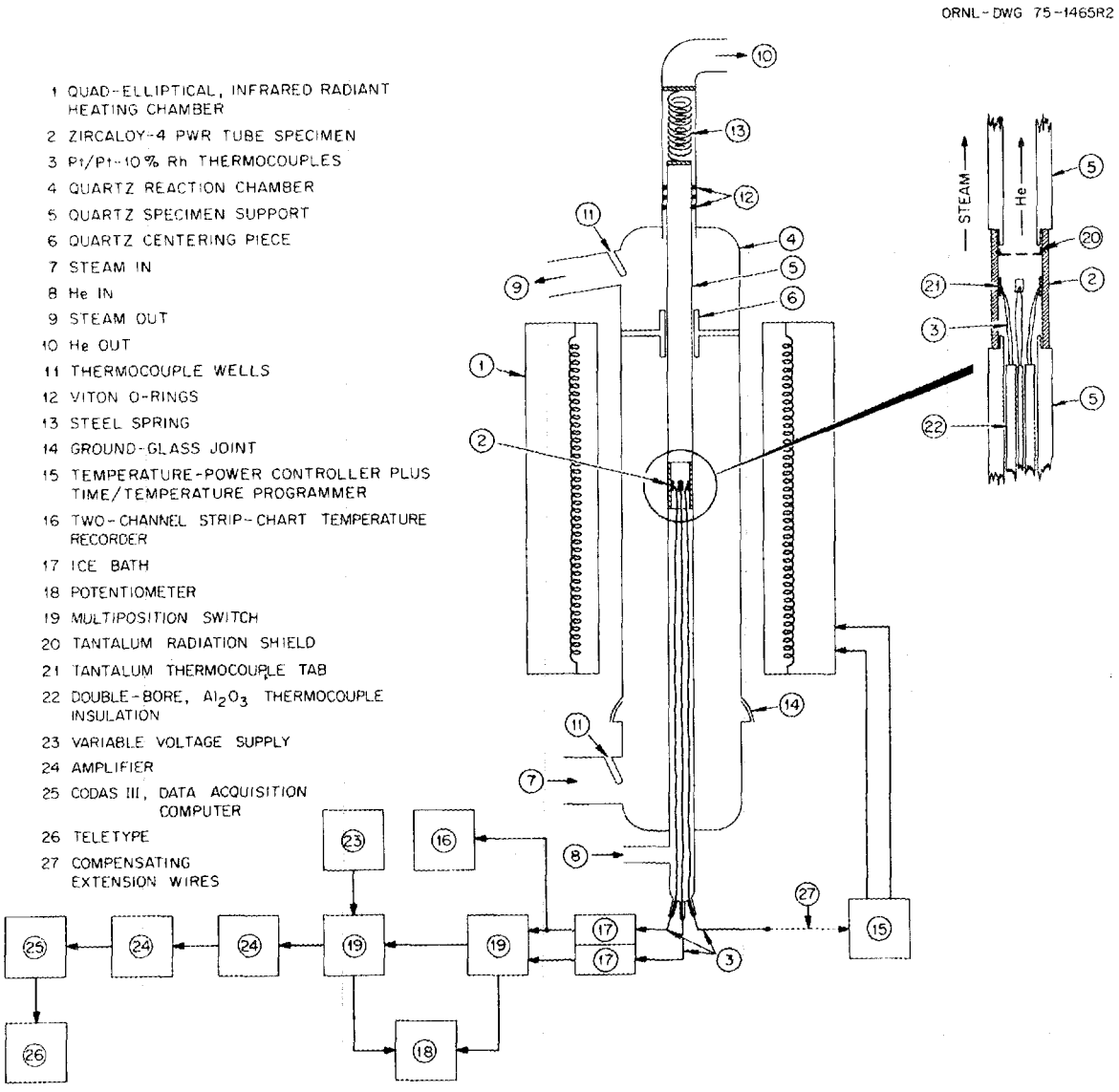

Fig. 6. Schematic Diagram of the MiniZWOK Oxidation Apparatus.

previously, this apparatus has been improved in a number of ways since its inception and has performed efficiently in producing well-characterized experiments under rather extreme experimental conditions.

The reaction chamber consists of a 60 mm (2.36 in.) OD quartz tube 60 cm (23.6 in.) long with a Zircaloy-4 PWR tube specimen [30 mm long by 10.92 mm OD by 9.65 mm ID (1.18 × 0.430 × 0.380 in.)] supported at its center between two smaller quartz tubes. During an experiment, steam flows past the outside surface of the specimen, and a slight positive pressure of helium is maintained inside the support tubes in

order to prevent ingress of steam to the interior of the specimen. A helium flow rate of ∿ 0.2 cc/s is used for this purpose. Steam is generated in an all-glass boiler (not shown in the figure). For most experiments the steam flow rate was adjusted to 30 g/min (0.066 lb/min) which corresponds to a linear velocity of about 1 m/s (3 ft/s) past the specimen in the reaction tube.

The furnace surrounding the reaction chamber is a Research, Inc. quadelliptical radiant heating chamber, Model E-4, with a hot zone of 25.4 cm (10 in.). Specimen heating rates in excess of 150°C/s (270°F/s) can be attained with this unit, and the response of both the furnace and its controller is very fast. These characteristics, plus the fact that the furnace is controlled directly by the specimen temperature, prevent specimen over-heating and allow essentially isothermal conditions to be maintained during oxidation.

The specimen is instrumented with three Pt vs Pt-10% Rh thermocouples. As described earlier, the hot junctions are formed by spot welding the thermocouple leads to small tantalum tabs [2 × 2 × 0.075 mm (0.08 × 0.08 × 0.003 in.)] that are in turn welded to the interior of the sample near its midpoint. One thermocouple is connected to the temperature controller, and the other two are used as measuring couples. The two measuring couples are positioned 180 degrees apart at the same elevation. Depending upon the duration of the experiment and the desired sensitivity, the temperature-time excursion of the specimen as sampled by each of the monitor thermocouples is determined by either a recorder chart output, multiple readings on the standard L & N K-3 potentiometer, or the CODAS (Computer Operated Data Acquisition System). These measuring systems will be discussed later.

This general design was adopted so that the tantalum thermocouple tabs could be protected from the steam and also to minimize thermal shunting effects. The latter purpose is also served by the tantalum heat shield inserted into the upper portion of the specimen. A lower heat shield is formed by the ends of the double-bore, DeGussit AL-23, high-purity alumina insulators used to separate the lower portions of the thermocouple leads. The upper parts of insulators are within the

furnace and also serve to preheat the helium before it reaches the interior of the specimen.

An experiment in MiniZWOK may be described briefly as follows: (1) The instrumented specimen is mounted in the apparatus as shown in the illustration. (2) The steam and helium flow is started and sufficient time is allowed to purge the air from the apparatus. During this period the furnace is on at very low power to eliminate condensation in the vicinity of the specimen, which is maintained at a temperature less than 200°C (392°F). (3) the CODAS is activated for the two monitor thermocouples. (4) The specimen is now driven through the desired time-temperature cycle by means of the programmable controller which actuates the quadelliptical radiant heating furnace surrounding the specimen. Sufficient cooling is available to perform an effective quench at the end of an "isothermal" experiment. (5) After the experiment, the specimen is removed from the apparatus for analysis. The thermocouple tabs are left in place so that the metallographic measurements can be referenced to the monitor thermocouple positions.

MiniZWOK Temperature Control and Recording System

The instrumentation for this apparatus is more complex than that for MaxiZWOK and is indicated schematically in Fig. 6. All Pt vs Pt—10% Rh thermocouple wires are led out of the system uninterrupted through ports sealed with silicone rubber or Teflon and from thence to an ice bath where they join low thermal emf copper telephone wires.

Temperature control of the specimen is maintained with a Research, Inc. Model D-30 MicroThermac Controller associated with a Data-Trak Programmer for virtually any time-temperature regime. The signals from the two measuring thermocouples, after passing through a thermal free, multiposition switch (contact resistance < 0.001 ohm, thermal emf < 1 μV), may be (1) read on an L & N K-3 potentiometer, (2) recorded by a two-channel strip chart recorder (Esterline Angus, Model 1102S, a multi-span unit with calibrated zero), or (3) fed to the computer operated data acquisition system (CODAS). The CODAS system has been described in detail elsewhere.[12] In our system the CODAS computer periodically

reads the thermocouple emf (25 readings in 2 msec), calculates an average emf for a specified number of readings, converts the emf to temperature according to the emf-temperature calibration for our particular Pt vs Pt—10% Rh thermocouple wires, and either prints the time and the averaged temperature at specified intervals with the aid of a teletype or records this information on magnetic tape for later retrieval. The CODAS system is calibrated directly before and after each experiment with a Dial-A-Source voltage unit (General Resistance, Inc., Model DAS-47A1) that itself is compared against our K-3 potentiometer.

Care was exercised in properly wiring, grounding, and shielding the various components of the MiniZWOK control and recording system in order to eliminate ground loops and other parasitic emf's. In addition it was found that considerable high frequency noise was introduced into the system by the operation of the silicon-controlled rectifiers of the furnace power supply. For this reason a low band pass filter with a cutoff above 50 Hz was installed between the multiposition switch and the CODAS amplifier (items 19 and 24 in Fig. 6). The filter, installed in each copper lead, consisted of a series-connected, 50 Ω, manganin-wire wound resistor grounded through a 60 μF mylar capacitor.

The temperature control capability exhibited by this system, for both isothermal and transient-temperature experiments, was excellent. In the isothermal control regions only small temperature fluctuations, ∿±1°C (±1.8°F), about the control temperature were observed.

Potential Errors in Temperature Measurements

Considerable care must be exercised in the use of thermocouples at high temperatures if serious temperature errors are to be avoided. This caution is particularly relevant in systems where experimental requirements create less than ideal conditions. We have considered the following list of potential error sources in relation to the ZMWOK program:

1. Thermal shunting
2. Electrical shunting
3. Parasitic emf's
4. Data acquisition system errors

5. Thermocouple calibration errors
6. Temperature gradients in the sample
7. Decalibration of thermocouples
8. Tab attachment effects.

In this section we discuss the error sources listed above as they apply to each of the apparatuses used in the program.

Thermal Shunting

The term "thermal shunting" is used here to mean the shunting of heat to or from the thermocouple hot junction by convection, conduction, or radiation. The process is illustrated in Fig. 7 for the case of thermal shunting by convection. Cool steam flowing past the thermocouple leads reduces their temperature and causes a flow of heat from the hot junction to the leads. As a result the hot-junction temperature is lowered with a consequent reduction in the emf generated by the thermocouple, and the indicated specimen temperature is erroneously low.

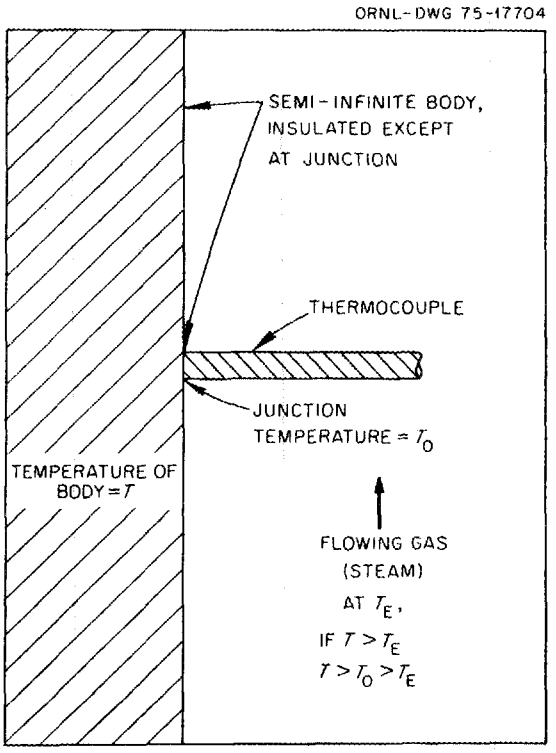

Fig. 7. Schematic Model Illustrating Nature of Thermal Shunting Errors.

Thermal shunting errors, or "perturbation" errors as they are sometimes called, have been discussed by a number of investigators[13] who have made suggestions both for minimizing the errors and for calculating their magnitude.

The analytical problem is essentially one of establishing an acceptable model for the heat transfer system, and then solving the heat flow equations so that the temperature at a given point in the absence of the sensor can be calculated. While such solutions have been obtained[14-16] for several cases relevant to the operation of thermocouples on specimens suspended in flowing gas streams, these solutions are generally based on oversimplified system geometries. Obviously, under these circumstances an experimental calibration of the system is desirable; but frequently it is impractical or even impossible to carry out such a direct calibration for a real system. For this reason we have taken the position that we should design our apparatuses in such a way as to minimize perturbation errors, while at the same time making use of existing computational procedures to estimate the magnitude of the errors involved and to guide the design work. Equations derived by Nusselt (reported by Jakob[14] and others) or Boelter[15] proved useful in the latter effort; and they have the added virtue that, because of the nature of the assumptions made in each derivation, the calculated perturbation error is believed to be greater than the actual error.

The results of these calculations, which predict thermal shunting errors of $\sim$ 3% of the difference between specimen and coolant temperatures, are recognized as being approximate. Their contribution, therefore, lies not so much in a precise prediction of error values but in the fact that they indicate the relationship between some of the important system parameters that affect temperature measurements errors, thereby suggesting means for reducing these errórs to a minimum. Our thermocouple installations are constructed with these ideas in mind. The details of these calculations are reported fully in a previous publication.[3]

Thermal Shunting in the MiniZWOK Apparatus — Our decision to construct the MiniZWOK apparatus as a one-sided oxidation system with steam on the outside and the thermocouples mounted internally was a

direct consequence of the need to minimize thermal shunting effects. Errors on the order of 100°C (180°F) have been observed in systems where the thermocouples were exposed to rapidly flowing cool steam.[17] A discussion of the magnitude of such errors may also be found in Jakob.[14] In MiniZWOK the thermocouples are subjected only to very slowly flowing helium, and the helium itself is preheated as it passes over the hot Al_2O_3 thermocouple insulation in the lower portion of the apparatus. In normal experiments the helium flow rate through the center tube of the apparatus is 0.24 cc/s, and no changes in the measured emf's of the thermocouples were noted when helium flow rates were varied from 0 to 4.9 cc/s (higher flow rates were not attempted) in the range of 900 to 1300°C (1652–2372°F), indicating the absence of any significant convective or conductive thermal shunting errors owing to the flow of helium past the thermocouples.

In order to minimize the possibility of radiative thermal shunting, a tantalum heat shield is located in the upper portion of the Zircaloy specimen (see Fig. 6). The Al_2O_3 thermocouple insulation located in the bottom specimen support tube also acts as a heat shield.

As already noted the thermocouples used in this apparatus are spot welded to tantalum tabs, and the tabs, in turn, are carefully spot welded to the interior of the specimen tubes. The thermocouple wires are led away from the tab along the tube wall in a path parallel to the axis of the tube to minimize conduction errors (see inset, Fig. 6). The vertical sections of thermocouple wire between the tabs and the double-bore Al_2O_3 insulation are covered with single-bore Al_2O_3 insulation.

These various design features and tests have led us to the conclusion that thermal shunting errors in the MiniZWOK apparatus are negligible.

Thermal Shunting in the MaxiZWOK Apparatus — Thermal shunting problems in this apparatus are relatively minor because in isothermal experiments both the steam and the furnace are at the same temperature. Thus, even though the thermocouples are exposed to rapidly flowing steam, there can be no cooling effect. The possibility of thermal shunting does arise in experiments in which substantial specimen self-heating occurs and in which the furnace temperature is higher than the steam

temperatures. We expect such errors to be minimal, however, because (1) the difference between steam and specimen temperatures is relatively small — at most in the neighborhood of 200°C (360°F), and (2) since the furnace temperature in many cases is higher than the specimen temperature, the errors due to convective losses (steam effects) will be of opposite sign to those related to radiative effects (furnace wall temperature). In the worst case, using the perturbation error analysis above, we estimate errors due to thermal shunting to be no more than $\sim$ 5°C (9°F).

Electrical Shunting

Thermocouple errors may arise due to electrical leakage of the thermocouple insulators or to thermionic emission between thermoelements or other metals in the system. These errors can be as large as several hundred degrees Celsius in certain environments and at very high temperatures [e.g., in argon at a pressure of 43 torr and at temperatures near 1800°C (3272°F)].[18] However, in the current work this phenomenon was not a problem. For example, the resistance of an open circuit thermocouple at 1300°C (2372°F) in the MiniZWOK apparatus was 5×10^5 ohms and 1.7×10^5 ohms at 1455°C (2651°F), which are much too high values to allow significant electrical shunting. A similar experiment in the MaxiZWOK apparatus produced a value of $\sim 10^4$ ohms. The decrease in resistivity relative to that measured in MiniZWOK was attributed to the fact that the lower ends of the MaxiZWOK thermocouples are exposed to the distilled water of the quench bath for the apparatus; however, a resistance of 10^4 ohms was still considered sufficiently high to preclude the existence of significant electrical shunting.

Parasitic EMF's

Temperature measurement errors can be caused by the presence of parasitic emf's in the electrical circuitry of thermocouples. Reference here is made to such effects as ground loops, noise pickup, and problems associated with the use of improper lead wires, reference junctions, feedthroughs, etc. The elimination of such error sources requires considerable care and the use of proper thermometry techniques. In

setting up the circuitry for all our systems we worked closely with representatives of the Instruments and Controls Division of ORNL, and the steps taken to overcome these problems have already been outlined.

Data Acquisition System Errors

Our primary standard used in measuring thermocouple emf's is a carefully calibrated Leeds and Northrup K-3 potentiometer. The accuracy of an individual measurements is given as 0.015% of the measured emf plus 0.5 μV. Thus at 1500°C (2732°F) for a Pt vs Pt—10% Rh thermocouple, the potentiometer has an accuracy of ∿ 0.2°C (0.36°F).

For our MiniZWOK experiments, time and temperature are also recorded with a Computer Operated Data Acquisition System (CODAS). This device is calibrated against the K-3 potentiometer at the beginning of each experiment, and recalibrations immediately after an experiment revealed no change. Thus, for short periods of time the accuracy of CODAS appears to be comparable to that of the K-3 itself.

Thermocouple Calibration Errors

Thermocouple calibration procedures and uncertainty limits were described in detail in an earlier section. This uncertainty is greatest at temperatures above the gold point [1064°C (1947°F)], and we estimate it to be ±1.5°C (2.7°F) at 1500°C (2732°F). Below the gold point the uncertainty is ±0.8°C (1.4°F). In situ calibration at the gold point was conducted in the MiniZWOK oxidation apparatus. This measurement indicated that the system uncertainty was less than 2°C (3.6°F) at these temperatures.

Temperature Gradients in the Sample

We have no evidence for the existence of temperature gradients within samples in the critical part of the tubing used as the specimen in the MaxiZWOK apparatus. The MiniZWOK samples, however, are not completely isothermal. For example, at 1200°C (2192°F) we observed a longitudinal gradient of ∿ 4°C/cm (7°F/cm) from the center to the ends of the specimens. There is also a circumferential variation (two-fold symmetry) in temperature. The quadelliptical furnace is built in two

hinged sections that can be opened to allow the insertion of the reaction tube. The hinge and corresponding opening on the other side of the furnace are located along the vertical center line of two opposed elliptic hemi-cylindrical reflecting surfaces. The positions of the cooler regions on a specimen correspond to the positions of the hinge and opening, leading to the conclusion that these imperfections in the reflecting surfaces reduce the efficiency of the furnace in these areas.

These temperature gradients cause no particular problem for our measurements of oxide and alpha layer thicknesses since we simply section the specimen at the thermocouple tabs and make our metallographic measurements in the immediate vicinity of the tabs where the temperature is known. We did, however, investigate the possibility that, because of the Seebeck effect, the existence of such thermal gradients could lead to the generation in the thermocouple of an additional emf that is proportional to the temperature difference between the two wires of the thermocouple at the hot junction.

A calculation was performed for a thermocouple whose hot junction consists of successive segments of Pt, Ta, and Pt—10% Rh. A temperature gradient is assumed to exist across the junction with $T_1 > T_2 > T_3$, T_1, T_2 and T_3 being the temperatures at the Pt/Ta junction, the midpoint of the Ta segment, and the Ta/Pt—10% Rh junction, respectively. Let E_M and E_T be, respectively, the emf's generated by the thermocouple and a similar thermocouple in which the Ta segment is removed. It can be shown that

$$E_M - E_T \approx (S_{Ta} - S_{Pt})(T_2 - T_1) + (S_{Ta} - S_{Pt/Rh})(T_3 - T_2) \quad , \qquad (1)$$

where the S_x's are the appropriate absolute Seebeck coefficients. The results of this calculation are tabulated in Table 1 for the case $T_1 - T_3 = 1°C$ (1.8°F).

The "Worst Case Error" listed in the table was calculated on the assumption that the thermocouple leads are welded at the edges of the tabs, thus producing a hot junction length of ∿ 2 mm. The worst temperature gradient in our sample is ∿ 0.8°C/mm (1.4°F/mm), thus creating a temperature gradient of 1.6°C (2.9°F) across the hot junction.

Table 1. Seebeck Effect Temperature Errors

Temperature (°C)	$E_M - E_T$/°C (μV/°C)	$(E_M - E_T/dE/dT)$/°C (°C/°C)	(°F/°C)	Worst Case Error[a] (°C)	(°F)
900	−13.70	−1.2	−2.2	−1.9	−3.4
1100	−18.60	−1.4	−2.5	−2.2	−4.0
1300	−22.70	−1.9	−3.4	−3.0	−5.5
1500	−26.2	−2.2	−4.0	−3.5	−6.3

[a]See text.

In light of these findings we adopted the procedure of welding the two thermocouple wires together and welding the junction thus formed to a tantalum tab in the orientation shown in Fig. 2. Thus, for a well-made thermocouple junction, the error due to the Seebeck effect is expected to be negligible.

The calculations given above were made for a Pt/Ta/Pt—10% Rh junction, whereas in actual practice the tantalum tab is attached to the Zircaloy tube. Thus the Zircaloy might also be expected to contribute to the Seebeck error. We have made a few rough determinations of the absolute Seebeck coefficient for Zircaloy-4, however, and find it to be approximately 1 μV greater than that for tantalum. Therefore, Eq. (1) may also be expected to give a reasonable estimate of the Seebeck effect temperature error for a Pt/Ta—Zr/Pt—10% Rh junction.

Decalibration of Thermocouples

This problem was discussed in the section on Thermocouple Calibration Procedures. As stated, we have found no indication of decalibration during times much longer than the duration of our experiments.

Tab Attachment Effects

As already pointed out, at temperatures above about 1100°C (2012°F) we find it necessary to insert small tantalum tabs between the Zircaloy and the thermocouples in order to circumvent the problem of the

low-melting Pt-Zr eutectic. The success of this arrangement obviously depends on establishing good thermal contact between the tabs and the specimen, and our normal procedure is to spot weld the tab to the specimen at several points. However, we have no way of determining prior to an experiment just how good the tab attachment might be, although in general it appears quite satisfactory. Note that "tab attachment effects" represent a special case of thermal shunting.

We have attempted to establish an upper bound for tab attachment errors in the MiniZWOK apparatus by performing an experiment in which one measuring thermocouple was attached to the specimen in the normal fashion while the second thermocouple was spot welded to a tab and the tab positioned in the approximate center of the specimen tube. Temperature differences of 9, 11, 10, and 15°C (16, 20, 18, and 27°F) were observed at 900, 1100, 1300, and 1500°C (1652, 2012, 2372, and 2732°F), respectively. In this experiment the flow rate of helium through the interior of the specimen was varied from 0 to ∿ 5 cc/s at each temperature; no change in the thermocouple readings was noted except at 900°C (1652°F) where a temperature drop of 1°C (1.8°F) was noted for the unattached thermocouple. These results set the maximum limits for temperature errors due to poor tab attachment.

Our regular experimental procedure requires an examination of both thermocouples and tabs after each experiment. Any indication of loose attachment, e.g., if the tab can be pulled loose with a pair of tweezers, causes us to regard that experiment as suspect. Any accidental leakage of steam into the interior of the specimen in quantities sufficient to produce significant oxidation of the thermocouple tabs also leads to a suspect experiment. Thus, in a normal experiment, errors due to poor tab attachment are expected to be much smaller than the maxima given above and should approach zero for good attachments.

One indication of the existence of tab attachment errors may be obtained by comparing the temperatures indicated by the two measuring thermocouples. Widely differing values suggest tab troubles. For example, if the tab to which the control and the first measuring thermocouple are attached makes poor thermal contact with the specimen,

the control thermocouple will sense a temperature lower than that of the specimen. The temperature of the specimen will thus increase until the emf required by the controller is generated by the control thermocouple. The first measuring thermocouple (attached to the same tab as the control thermocouple) will indicate approximately the expected temperature; however, the second measuring thermocouple (assumed to be well attached) will indicate a relatively high temperature — in this case the true temperature of the specimen.

The requirement that reasonable agreement exist between the two measuring thermocouple temperatures is not an absolute measure of tab attachment quality. Real temperature differences may exist in the specimen or both tabs may be poorly attached. With regard to the latter problem, the probability that the thermal attachment of both tabs will be equally poor seems small, but, clearly, the only real cure for tab attachment effects is to make sure that good bonding is achieved between tab and specimen, and we make every effort to see that that is done.

Evaluation of Temperature Errors

In this section we consider the magnitudes of the total temperature measurement errors in our experimental systems.

Determinant Errors

Certain parts of the temperature measuring system used with a given apparatus may be calibrated against external standards, and a quantitative estimate of the error associated with each component can be obtained; such errors are usually referred to as the determinant errors of the system. The determinant temperature errors for our steam oxidation apparatuses are summarized in Table 2.

Indeterminant Errors

It is considerably more difficult to specify quantitatively the indeterminant temperature measurement errors associated with our experimental systems. Indeterminant errors are those related to procedures or apparatus features not susceptible to direct, independent

Table 2. Determinant Temperature Errors in the MiniZWOK and MaxiZWOK Apparatuses

Error Source	Temperature Error, deg, at					
	900°C (°C)	1652°F (°F)	1200°C (°C)	2192°F (°F)	1500°C (°C)	2732°F (°F)
Uncertainty relative to IPTS-68	±0.3	±0.5	±0.7	±1.3	±1.0	±1.8
Thermocouple material variability	0.5	0.9	0.5	0.9	0.5	0.9
Potentiometer	0.15	0.28	0.19	0.34	0.24	0.43
Potentiometer readout	0.33	0.59	0.33	0.59	0.33	0.59
Thermal emf in copper leads	<0.01	<0.02	<0.01	<0.02	<0.01	<0.02
Reference (ice bath) temperature	0.01	0.02	0.01	0.02	0.01	0.02
TOTAL	±1.3	±2.3	±1.7	±3.2	±2.1	±3.7

calibration as are, for example, thermocouples. Examples of such errors include the problems of thermal and electrical shunting, decalibration of thermocouples, tab attachment effects, and spurious emf's associated with temperature gradients across the thermocouple hot junctions (the Seebeck effect).

Indeterminant Errors in MiniZWOK — On the basis of evidence cited in the section on Potential Errors we felt that indeterminant errors in temperature measurements in the MiniZWOK apparatus were acceptably small. The quantification of such errors is, however, extremely difficult, and the procedure finally adopted for that purpose in the Thermometry Report[3] is admittedly rather arbitrary (see also the section on Total Error Estimates below). For this reason and in consideration of the special need for accurate temperature measurements in the ZWOK project we continued throughout the entire program to perform experiments designed to check our original estimates of ±4°C (±7°F) and ±6°C (±11°F) as the maximum total uncertainty in temperature measurements at 900 and 1500°C (1652—2732°F), respectively.

Particularly in the MiniZWOK apparatus, which was used to obtain the base isothermal oxidation data set, these experimental checks have been exhaustive. In addition to the external calibrations and tests already described of the component parts of the thermometry assembly, *in situ* tests were performed to evaluate the accuracy of thermometry measurements under operating conditions. In one such experiment the calibration of the thermocouples was checked at the gold point [1064.43°C (1947.9°F)]. Using a standard MiniZWOK Zircaloy tube specimen, one recording thermocouple (designated T/C #1) was installed in the usual fashion, i.e., attached to a Ta tab that was welded to the inside wall of the specimen. A second recording thermocouple (T/C #2) was formed by attaching a Ta tab to a length of Pt wire, which was then located in the center of the specimen along the tube axis out of contact with the tube walls. One end of a thin gold wire was welded to the back of this tab, and the other end of the wire was attached to the Ta tab of T/C #1. The electrical circuit for T/C #2 was completed through the Pt-Rh leg of T/C #1. The output of both thermocouples was recorded by the CODAS, the

purpose of T/C #2 being to indicate by a loss of electrical continuity the time at which the gold wire melted. The output of the normal thermocouple, T/C #1, served to measure the temperature of the Ta tab at the moment of melting of the gold. The temperature of the sample was slowly increased to the expected melting point of gold, and melting occurred at a temperature of 1064 ± 2°C (1947 ± 4°F).

This test shows that the temperature of the thermocouple junction accurately reflected the temperature of the Ta tab to which it was attached. It demonstrates the accuracy of the external calibration of the thermocouples and indicates that all potential sources of error, save only thermal shunting, are small.

To evaluate thermal shunting errors, a specimen must be held at a known temperature and that temperature compared to the apparent specimen temperature as recorded by the thermocouple. This constraint was satisfied in experiments in which we used the temperatures for the α-β and α-γ transformations in zirconium and iron, respectively, and the melting point of gold as independent means of establishing the specimen temperature.

For the α-β transformation in zirconium, a cylinder of crystal-bar zirconium was machined into a tube having dimensions suitable for use in MiniZWOK. This specimen was instrumented in the standard manner and subjected to a steam oxidation experiment using techniques typical of previous experiments. The initial portion of this experiment (which was a transient-temperature test) involved a fast heat-up to 1400°C (2552°F) followed by a fast cool to 650°C (1202°F). The CODAS output describing the temperature-time response of the two monitor thermocouples during this part of the cycle is shown in Fig. 8a. The initial heating rate of the specimen was 200°C/s (360°F/s), and the inflection in the heating curve shown at about 860°C (1580°F) was a result of the endothermic alpha-to-beta transformation of the Zircaloy, which, for the pure material, takes place at 862 ± 5°C (1584 ± 9°F).

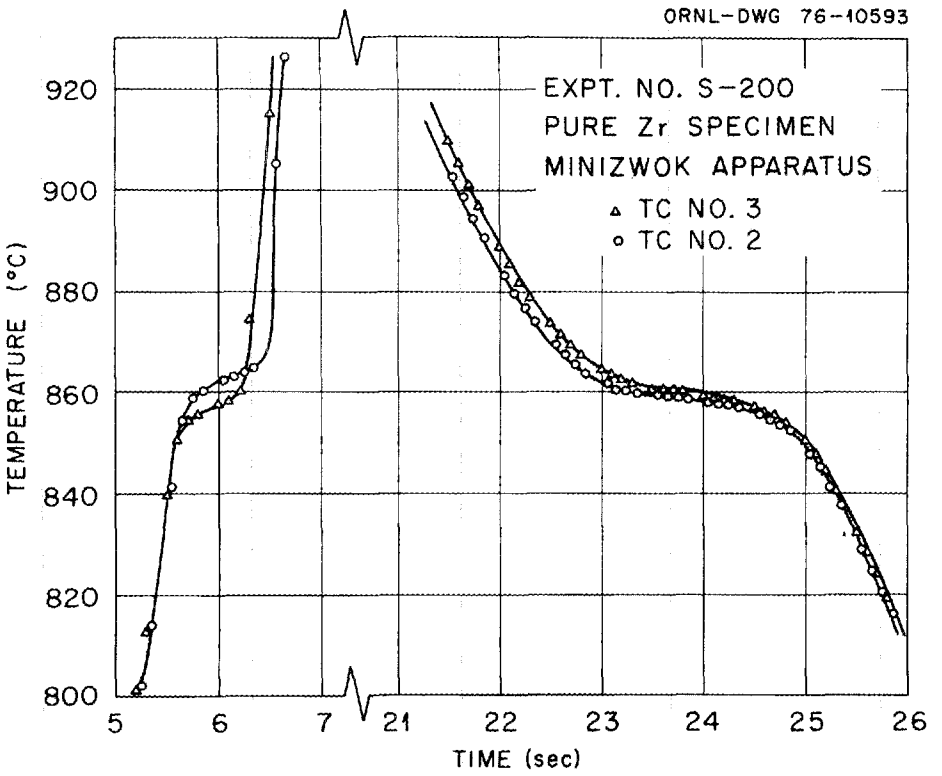

Fig. 8a. Time-Temperature Excursion for Pure Zr Specimen in MiniZWOK Apparatus. Note heating and cooling rates and α/β transition temperatures indicated by tab-mounted thermocouples.

The iron α-γ phase transition experiment was performed in a somewhat similar manner. A sheet of high purity iron* was formed into a tube of the same dimensions as a standard MiniZWOK specimen, and the thermocouples were welded directly to the specimen. The thermal arrest obtained on heating through the α-γ transition at a heating rate of ∿13°C/s occurred at 912.7 ± 0.1°C (1674.9 ± 0.2°F). While iron is by no means a standard reference material for temperature calibration, the accepted value for the α-γ transition temperature is 912°C (1674°F).

---

*Marz Iron obtained from Materials Research Corp. Vendor certified analysis (ppm by wt): 12 C, 60 O, 1.0 H, 10 N, <0.1 Al, 1.6 Na, 0.87 Mg, 0.70 P, 2.60 S, 0.80 Cl, 1.80 K, 0.80 Ca, 1.40 Ti, 0.60 Cu, <0.10 Si, 1.60 Cr, <0.10 Ni, 1.90 Zn, <0.10 Ga, <0.10 Zr, <0.10 Nb, <0.10 Mo, <0.10 Pd, <0.10 Ag, <0.10 In, <0.10 Sn, <0.10 Sb, <0.10 Ta, <0.10 Pt, <0.10 Au, <0.10 Pb, others <0.10.

Perhaps the most convincing evidence that thermal shunting errors were negligible in the MiniZWOK apparatus was provided by a test in which the specimen was held at the gold melting temperature. In order to avoid any lowering of the gold melting point as a result of the formation of a Au-Zr solid solution, this measurement was carried out in a special "Zircaloy oxide crucible" made by arranging a standard PWR Zircaloy-4 specimen concentrically inside a BWR tube of the same length, both tubes being held in a Zircaloy jig as shown in Fig. 8b. Because of the greater diameter of the BWR tube, an annular space approximately 0.075 cm (0.030 in.) was formed between the two tubes. The resulting "specimen" was then instrumented in the standard fashion and mounted in the MiniZWOK apparatus where the outer and inner BWR- and outer PWR-tube surfaces were oxidized in pure oxygen at ∿1000°C (1832°F) to form surface oxide layers ∿30 μm thick. The net result of this treatment was the conversion of the annular region of the sample into a "Zircaloy-oxide"

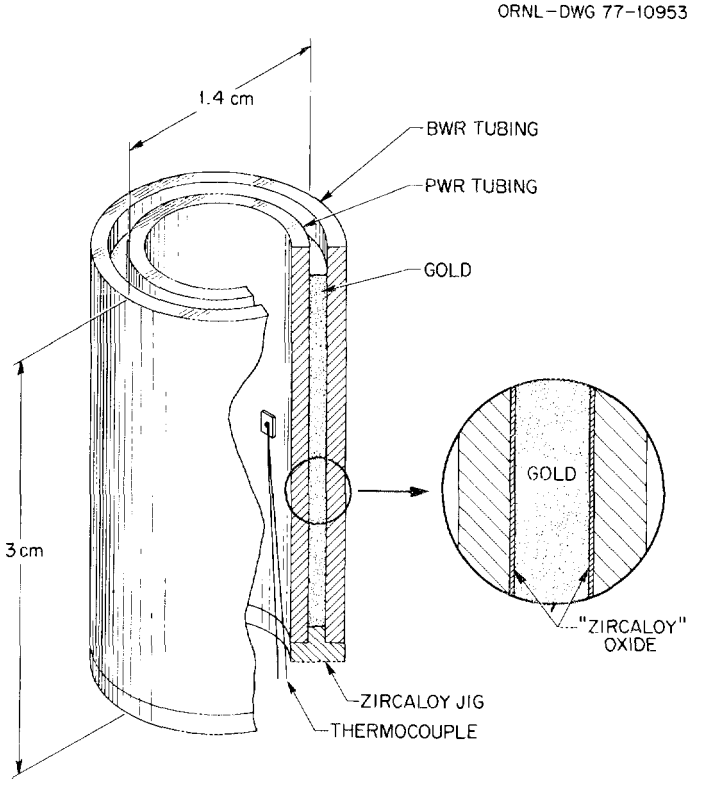

Fig. 8b. Schematic Drawing of the "Zircaloy Oxide Crucible" Used in the Gold-Point Determination.

crucible. Next the specimen-crucible was removed from the apparatus, a gold foil of melting-point-standard purity* was inserted into the annular crucible, and the entire assemblage was placed back in the MiniZWOK apparatus. The subsequent melting of the gold was done with flowing helium as an environment. The specimen was first driven through the melting point of gold to bring the gold into intimate contact with the oxide surface and then again driven through the transient pictured in Fig. 8c. This mode of heating was identical to that in an oxidation experiment except that when the temperature reached the melting point of gold, a thermal arrest occurred, causing the oxide-gold interface to be at a fixed and known temperature of 1064.4.[3] It is at this time

*Marz Gold obtained from Materials Research Corp. Vendor certified analysis (ppm by wt): 15C, <5.0 O, <1.00 H, <5.0 N, 0.20 Al, 0.10 Na, 0.02 Mg, <0.01 P, 0.13 S, 0.16 Cl, 0.40 K, 0.30 Ca, 0.01 Ti, 0.73 Fe, 1.30 Cu, 0.51 Si, <0.01 Cr, 0.05 Ni, 0.05 Zn, 0.06 Mo, 0.25 Pd, 4.20 Ag, <0.01 Sn, 0.02 Sb, <0.01 Pb.

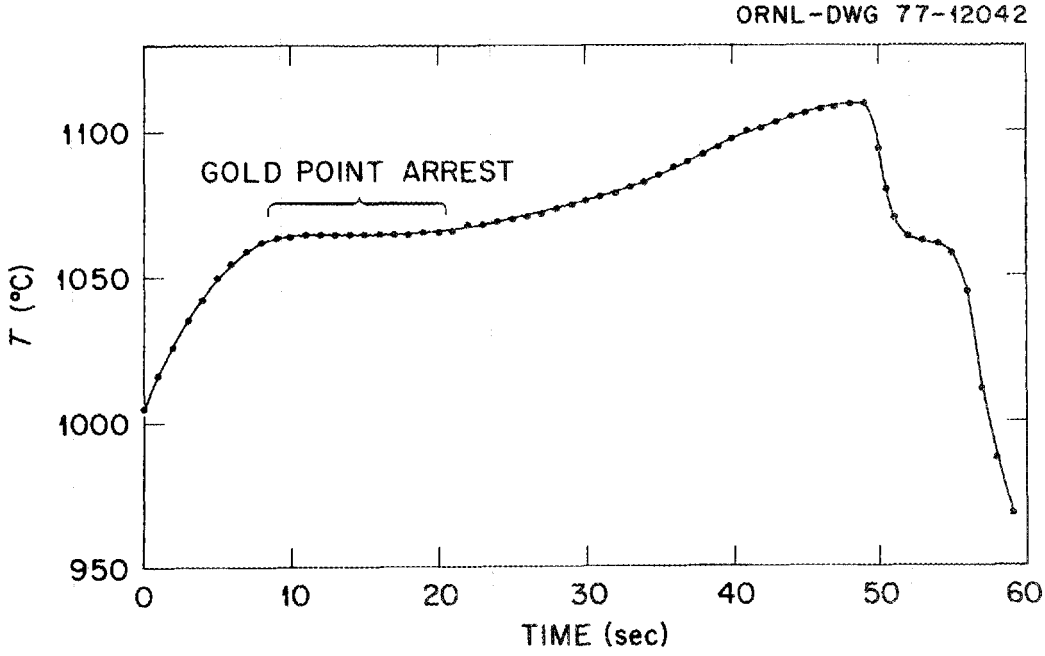

Fig. 8c. Time-Temperature Excursion for Gold-Point Determination in the MiniZWOK Apparatus.

that the difference in the recorded thermocouple temperature and the gold point is precisely the thermal shunting error. As is illustrated in Fig. 8c, the thermal arrest at the gold point lasted for approximately nine seconds, and with the temperature monitoring capability of CODAS, seventy-five temperature measurements were made over this time interval, the average temperature indicated by the thermocouple being 1064.4 ± 0.3°C.

Attempts were also made to perform an *in situ* nickel-point determination using the "Zircaloy-oxide" crucible and by other approaches. In all cases, however, severe experimental difficulties were encountered, for example, the melting down of the crucible as a result of the alloying of the nickel and Zircaloy when the oxide coating on the crucible either cracked due to thermal strains or because the oxide dissolved into the underlying Zircaloy as the sample was heated to the Ni melting temperature. For this reason we were unable to obtain a completely unambiguous comparison between indicated thermocouple temperatures and actual specimen temperatures at the upper end of the temperature range investigated. Nonetheless, the rather remarkable results obtained for the transformation temperatures of Zr and Fe and the melting point of gold strongly suggest that thermal shunting effects in the MiniZWOK apparatus were essentially negligible and that our estimates of maximum total temperature measurement uncertainties are valid and, if anything, somewhat conservative.

Indeterminant Errors in MaxiZWOK — Again for reasons already given, we believe that electrical shunting and thermocouple decalibrations errors are negligible in this apparatus. Errors due to thermal shunting are also very small for isothermal experiments, although we estimate that such errors may reach 5°C (9°F) in our "mixed temperature" experiments where the furnace temperature exceeds the steam temperature. The relative ease with which thermocouples may be installed and the absence of significant thermal gradients in this apparatus tend to minimize both the tab and Seebeck effects.

Total Error Estimates

The total temperature error for a given apparatus is the sum of the determinant and indeterminant errors for the system. The determinant errors for the MiniZWOK and MaxiZWOK apparatuses are listed above and we

have already cited evidence for our belief that the indeterminant errors are small. It is impossible to quantify them; however, in other studies[19] it has been observed that the probable absolute accuracy error of temperature measurements in a well designed system is two-to-three times the reproducibility. Thus, taking the determinant error as an estimate of reproducibility, we give as the probable temperature measurement error in MiniZWOK and for isothermal experiments in MaxiZWOK values ranging from ±4°C (7.2°F) at 900°C (1652°F) to ±6°C (10.8°F) at 1500°C (2732°F). During transient temperature tests in the MaxiZWOK apparatus where the temperatures of the steam, the furnace, and the specimen are all different, the temperature error may be slightly larger than that given above, the additional uncertainty reaching an estimated ±5°C (9°F) for those situations where, because of specimen self-heating, the specimen temperature is significantly above that of either the steam or the furnace.

Weight Gain Tests

In order to provide a measurement of the kinetics of total oxygen consumption during isothermal steam oxidation, it is necessary when using the multispecimen technique to obtain for each specimen a value of the oxygen uptake. Normally, this task would be accomplished by precision weight-gain measurements or by quantitative chemical analysis. However, both of these methods yield average values of the oxygen gain for the whole specimen or sample and, thus, care must be taken to insure that the entire specimen is uniformly reacted. In addition, for the weight gain method, the possible problems associated with the thermocouple installations, end effects, and the like, must be considered. These problems and others make the weight gain and chemical analysis methods unattractive for assessing the extent of the high temperature steam oxidation of Zircaloy fuel tubes.

An alternative procedure, based on the experimental observation that *compact* and relatively *uniform* layers of oxide and alpha-Zircaloy form during the reaction, is to calculate the total oxygen consumed from phase thickness measurements and diffusion calculations. This value is

obtained by computing the total oxygen associated with the oxide, alpha, and (prior) beta layers, and subtracting from this the amount of oxygen originally in the specimen. A basic assumption is that equilibrium values of the oxygen concentrations apply at the various interfaces. (It is common in calculations of this type to consider the oxide to be completely stoichiometric rather than having an oxygen gradient across it. Since the defect structure of Zircaloy oxide is not well established, a "conservative" estimate of total oxygen is obtained if the oxide is assumed to be stoichiometric. Unless otherwise noted, as in the case for calculating diffusion coefficients, we will report values of total oxygen based on stoichiometric oxide. Furthermore, linear oxygen concentration gradients are assumed for the alpha phase, and a simplified diffusion calculation is used to determine the amount of oxygen in the beta phase. The accuracy of the latter calculation was checked for several cases by a more sophisticated method and was found to be satisfactory.)

We selected the following expressions to represent the equilibrium solubility and diffusivity values for the Zircaloy-4-oxygen system over the temperature range of our experiments:

a. The concentration of oxygen in the oxide at the gas interface (stoichiometric oxide):

$$C_{ox/gas} = 1.511 \text{ g/cm}^3 \quad . \qquad \text{(Ref. 20)}$$

b. The concentration of oxygen in the oxide at the alpha phase interface (used in calculations where an oxygen concentration gradient across the oxide is considered):

$$C_{ox/\alpha} = 1.517 - 7.5 \times 10^{-5} \text{ T [°K] g/cm}^3 \quad . \qquad \text{(Ref. 21)}$$

c. The concentration of oxygen in the alpha phase at the oxide interface:

$$C_{\alpha/ox} = 0.4537 \text{ g/cm}^3 \quad . \qquad \text{(Refs. 22 and 23)}$$

d. The concentration of oxygen in the alpha phase at the beta phase interface:

$$C_{\alpha/\beta} = [-0.2263 + (\frac{T[°K]}{63.385} - 16.877)^{1/2}] \ .0649 \ g/cm^3 \qquad \text{(Ref. 24)}$$

$$(T > 1073°K)$$

e. The concentration of oxygen in the beta phase at the alpha phase interface:

$$C_{\beta/\alpha} = [\frac{T[°K] - 1081.7}{491.159}] \ .0649 \ g/cm^3 \qquad \text{(Ref. 24)}$$

$$(T > 1373°K)$$

$$C_{\beta/\alpha} = [-.00428 + (\frac{T[°K]}{392.46} - 3.1417)^{1/2}] \ .0649 \ g/cm^3 \qquad \text{(Ref. 24)}$$

$$(1233°K < T < 1373°F) \quad .$$

f. The diffusivity of oxygen in the beta phase:

$$D_\beta = .0263 \exp(-28{,}200/RT[°K]) \ cm^2/s \quad . \qquad \text{(Ref. 4)}$$

A direct comparison of the total oxygen values obtained by weight-gain measurements and by calculations based on the metallographic phase layer measurements is given in Table 3. These four experiments were

Table 3. A Comparison of Values for Total Oxygen Consumption by Weight-Gain and Metallographic Measurements. Oxidation of Batch B PWR tubes in steam at 1200°C (2192°F).

Time (s)	Layer Oxide (μm)	Thickness Alpha (μm)	Total Oxygen Consumed	
			Weight Gain (mg/cm^2)	Metallography (mg/cm^2)
62	25.3	33.0	5.31	5.29
142	36.5	50.8	7.61	7.76
171	38.9	51.7	8.17	8.22
188	41.4	57.0	8.73	8.80

conducted in an early version of the MiniZWOK apparatus, and particular attention was paid to the weighing procedures for the specimen before and after oxidation. The measured and calculated oxygen consumption values are seen to exhibit very good agreement for each case, and we regard this as further evidence that the metallographic method and associated computational procedures are acceptably accurate, at least for oxidation under isothermal conditions.

Characterization of Zircaloy-4 PWR Tube Specimens

The bulk of the oxidation experiments carried out in this program were conducted with Reactor Grade Zircaloy-4 PWR tubing from Sandvik Special Metals Corporation. This material was part of a larger quantity purchased specifically for use in a number of fuel cladding research programs sponsored by the Division of Reactor Safety Research of the Nuclear Regulatory Commission. The specifications and characterization of this tubing have been published previously[25] and will not be considered here. The partial chemical analyses of this material, along with comparative values from a second lot, designated Batch B, is presented in Table 4. The ORNL analyses for Fe and Cr were determined

Table 4. Nominal Analysis of Zircaloy-4 PWR Tubes Used in ZWOK Steam Oxidation Experiments

Element	ORNL Analysis Batch B Tubes	ORNL Analysis Sandvik Tubes	Vendor Analysis Sandvik Tubes	Vendor Analysis Sandvik Ingot
Sn	1.3 wt %	1.6 wt %		1.47 wt %
Fe	0.22	0.25		.21
Cr	0.10	0.12		.12
Ni	<.02			<.0035
Si	<.0015			.0080
O	1250 ppm	1200 ppm	1220 ppm	1240 ppm
C	100	90		110
N	15	30	33	32
H	15	25	20	5

by isotope dilution spark-source mass spectrometry methods with a probable error within 5 to 10% of the reported value. The Sn concentration was determined photoelectrically with an uncertainty of about 5% of the reported value. The agreement between the vendor and ORNL analyses for the Sandvik tubing is seen to be quite good. The concentrations of the metallic alloying elements in the Batch B material show some small differences compared to the Sandvik tubing. The Batch B tubing was used only in the preliminary oxidation studies and for one of the scoping test sequences. The tube dimensions (Sandvik: 1.092 cm OD, .0635 cm wall thickness; Batch B: 1.067 cm OD, .0686 cm wall thickness) were such that either could be used in our apparatuses without modification.

EXPERIMENTAL RESULTS FOR ISOTHERMAL OXIDATION

The main objective of the Reaction Rate Task of the Zirconium Metal-Water Oxidation Kinetic Program was to provide a basic set of isothermal oxidation rate parameters for Zircaloy-4 in steam at temperatures from 900 to 1500°C (1652 to 2732°F) obtained under carefully controlled experimental conditions. A number of scoping tests were also conducted. These were designed to establish the effect on the isothermal rate of oxidation of Zircaloy-4 of (a) the steam injection temperature, (b) steam flow rates, (c) the presence in the steam of gaseous impurities such as oxygen, hydrogen, and nitrogen, and (d) small variations in alloy composition. (Scoping tests of the effect of steam pressure are presently in progress and their results will be described in a subsequent report.) In addition, a number of transient-temperature oxidation tests were performed in order to provide a basis for testing our code predictions based on the isothermal data.

The primary data set for isothermal oxidation was obtained using the MiniZWOK oxidation apparatus. This apparatus proved to be extremely versatile and was also used for many of the scoping tests. The MaxiZWOK apparatus provided scoping test information (steam flow rate and insertion temperature) for oxidation at the lower temperatures of interest. A few "mixed-temperature" experiments, where the steam and furnace were

maintained at different temperatures, were also conducted in this apparatus.

Primary Isothermal Data Set — MiniZWOK Apparatus

The kinetics of the reaction between the standard batch of Sandvik Zircaloy-4 PWR fuel tubes and steam were studied under essentially isothermal conditions over the temperature range 900–1500°C (1652–2732°F) at 50°C (90°F) intervals. The MiniZWOK oxidation apparatus was utilized to produce series of oxidized specimens that were then examined by metallographic methods in order to obtain the basic kinetic parameters. For each temperature investigated, at least ten specimens were oxidized. The maximum oxidation time at each temperature was chosen to enable an accurate description of the kinetics to be obtained yet to avoid problems that arise at longer oxidation times where excessive oxygen solution in the beta phase occurs.

Most of the data-gathering procedures have been discussed in detail in previous Quarterly Reports.[1] We will include here a general description of the techniques used emphasizing only those points that have not previously received attention. The procedures outlined in the preceeding chapter of this report describing the apparatus were followed. For all of the experiments involved in the primary data set, the steam flow rate was set at approximately 30 g/min (0.066 lb/min) corresponding to a linear velocity of about 1 m/s (3 ft/s) past the specimen in the apparatus.

Time-Temperature Cycles

The time-temperature cycles used to approximate the isothermal exposures were set into the programmer for the temperature controller prior to each experiment. Generally these experiments involved heating the specimens to the desired temperature at rates in excess of 100°C/s (180°F/s), holding the specimen at constant temperature, within about ±1°C, for the required time, and finally cooling the specimen at initial rates greater than 100°C/s (180°F/s). Two time-temperature curves illustrating typical isothermal experiments are shown in

Figs. 9 and 10. A comparatively low-temperature, long-time experiment is shown in Fig. 9, which is taken from a recorder trace of an oxidation experiment conducted nominally at 1100°C (2012°F). The high degree to which this cycle approximates an isothermal exposure is clear. Figure 10 is a similar recorder trace for a high-temperature, short-time experiment. While equally fast heating and cooling rates were employed here, the very short time-at-temperature suggests that a significant fraction of the total oxidation process occurred during heating and cooling. It was considered necessary to account for these contributions in all the isothermal experiments. This process requires an accurate record of the complete time-temperature cycle.

The connection of the CODAS to the temperature measuring circuit of the MiniZWOK apparatus permitted a complete and sensitive record of the

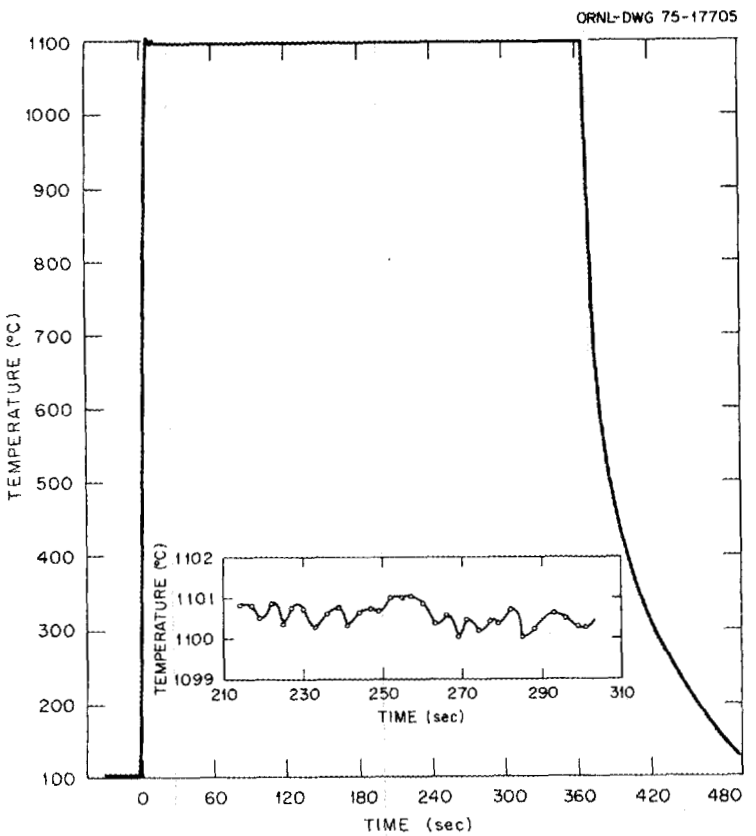

Fig. 9. Recorder Trace of Time-Temperature Record for a Typical MiniZWOK Experiment at 1100°C (2012°F). Inset shows fine scale temperature fluctuations as recorded by CODAS.

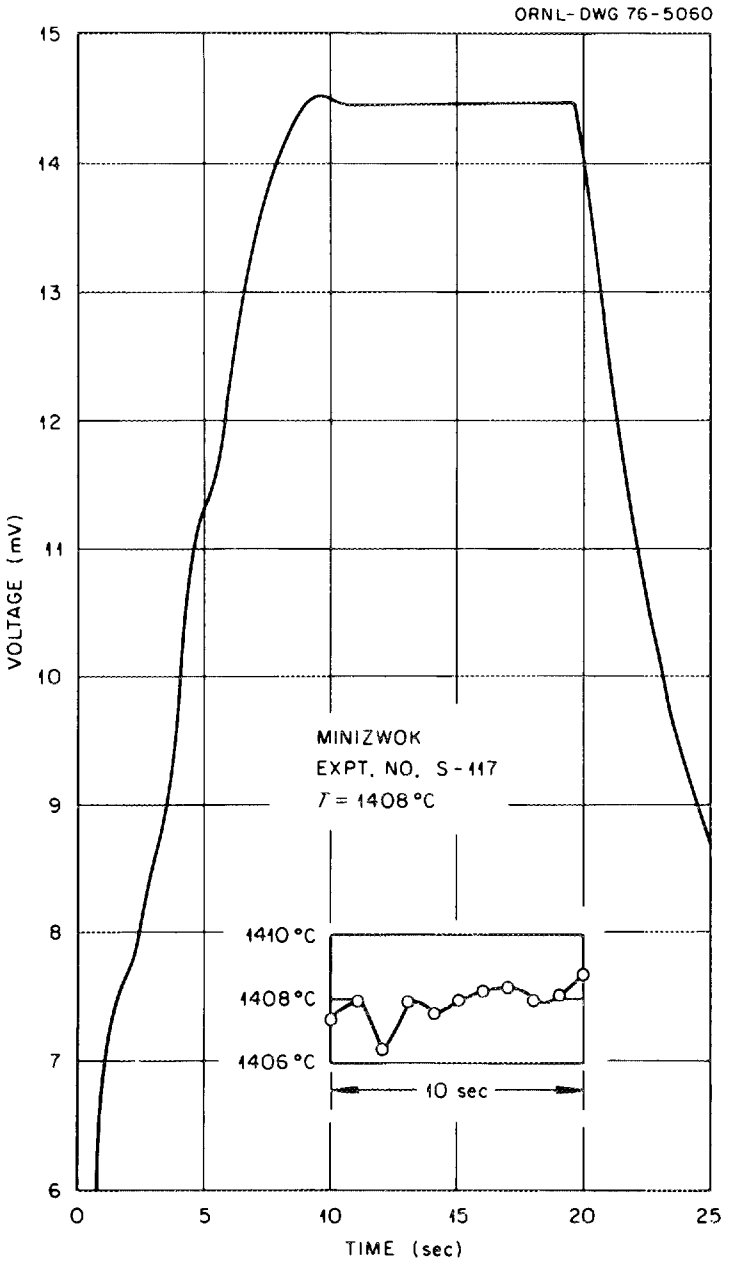

Fig. 10. Time-Temperature Excursion for Isothermal Oxidation Experiment in MiniZWOK Apparatus at Approximately 1400°C (2552°F). Main curve is drawn from recorder trace; inset curve is drawn from data taken from CODAS.

time-temperature history of each experiment to be obtained. The interface circuitry was designed so that the temperatures sensed by the two monitor thermocouples could be measured. Thermocouple emf's could be gathered by the computer in time steps as small as 50 ms over the entire duration of the experiment, stored, and recalled on demand. The CODAS computer converted thermocouple emf's to temperature according to the calibration for our Pt vs Pt—10% Rh thermocouples,[3] and frequent standardization procedures showed that the accuracy of the system was equivalent to that of the Leeds and Northrup K-3 potentiometer. Both teletype printout and paper tape records of the experiment histories were utilized. The paper tape record was subsequently used in a computer program, discussed below, for the normalization of the time-temperature data and the establishment of effective times-at-temperature for each set of isothermal experiments.

Normalization of Time-Temperature Excursions

The experimental determination of an isothermal rate constant using a multispecimen technique — where a change in a parameter is measured as a function of time — requires considerable care to insure that all variables, save time, are equivalent for each measurement. For "isothermal" experiments in either of our oxidation apparatuses, the problem is two-fold. First, the heat-up, cool-down, and stabilization times frequently constitute significant departures from isothermal conditions; secondly, it is rare that any two experiments result in precisely the same equilibrium temperature. These difficulties can be circumvented by appropriate normalization of each of the individual time-temperature excursions to an equivalent isothermal excursion at some assigned, representative temperature.

The normalization is accomplished in a manner identical to that employed by diffusion researchers to compensate for heat-up times and small differences in annealing temperatures.[26] If we assume that the rate constants for the kinetic parameters of interest in the steam oxidation of Zircaloy-4 are represented by Arrhenius relationships, we can write for any known time-temperature excursion:

$$t_{(eff)} = \frac{\int_0^t \exp[-Q/RT(t)]\, dt}{\exp[-Q/RT_{(eff)}]} \qquad (2)$$

where

$t_{(eff)}$ = equivalent time, s, at an assigned temperature, $T_{(eff)}$,
$T_{(eff)}$ = assigned temperature, °K,
$T(t)$ = actual temperature, °K, as a function of time, t,
Q = activation energy (rate constant) cal/g-mol,
R = gas constant, 1.987 cal/g-mol-°K,
t = time, s.

This expression permits the calculation of the equivalent reaction time, $t_{(eff)}$ at an arbitrary constant temperature, $T_{(eff)}$, for any given temperature-time excursion. We have written a simple computer program that accomplishes the above calculation.

For each set of isothermal experiments conducted in the oxidation apparatuses, the average temperature of the set was determined, and the equivalent time at that temperature was calculated according to Eq. (2) for each experiment. In these calculations, an activation energy of 40 Kcal/mol was assumed to apply for each rate process. However, sensitivity tests showed that the time corrections to most experiments varied only slightly for values of Q in the range of 30 to 50 Kcal/mol. Moreover, as part of a later iterative calculation check, rate constants were computed for oxide and alpha layer growth at 1253 and 1504°C (1287-2739°F) using the actual Q values for each. The average change in the range constant observed using the iterative method for computation of the times was less than 0.5%; thus, we have concluded that Eq. (2) performs accurate normalizations of the time-temperature excursions using a mean value for the activation energy. Of course, the magnitude of the correction and its sensitivity to the precise values of the activation energy will depend upon the exact shape of the time-temperature cycle in relation to the desired isothermal.

The calculations of the effective oxidation times according to Eq. (2) were performed by computer. The CODAS system provided the basic time-temperature function, T(t), which, for the very-short-time

experiments at the highest temperature, consisted of temperature readings on each thermocouple every 50 ms. For longer experiments the CODAS input to the program was appropriately modified with no appreciable loss in accuracy. It should be pointed out that where temperature differences existed between the monitor thermocouple positions during oxidation on a single specimen, the equivalent times associated with each position were generally different. The self-consistency of the calculated effective oxidation times in such cases was regarded as further evidence of the accuracy of our temperature and layer-thickness measuring procedures.

Metallographic Procedures

In order to establish the growth kinetics of the oxide and oxygen-stabilized alpha phases, it is necessary to measure accurately the phase thicknesses on each specimen. Standard metallographic techniques were relied upon to accomplish these measurements. Each oxidized specimen was carefully sectioned in the transverse direction with a slow-speed, diamond-impregnated wheel. The section was then mounted in an epoxy resin mixture containing 40% (by weight) of 1 μm alumina particles (Linde C) to aid in edge preservation during subsequent polishing. Polishing was accomplished in two stages using a Syntron vibratory polisher. The first stage consisted of a 24 hr polishing period using 0.3 μm alumina (Linde A) on a *new* Buehler Pellon polishing cloth. This was followed by a 12 to 36 hr period using 0.5 μm diamond paste on a standard nylon polishing cloth. This procedure proved particularly effective in preserving edges and the fine-structure associated with the oxide layer.

For oxidation temperatures above about 1050°C (1922°F) there was no serious problem in defining the phase boundaries during subsequent metallographic examination of specimens oxidized for relatively short times. However, in comparatively long-time oxidations, specimens exhibited irregular "incursions" of alpha that affect an observer's ability to define precisely the position of the alpha-beta interface. Similarly, at lower oxidation temperatures, notably for the series of specimens oxidized between 900 and 1000°C (1652 and 1832°F), the alpha-beta boundary was poorly defined, and a

certain degree of arbitrariness was involved in fixing its position. We found that the degree of arbitrariness could be lessened by utilizing an etch-anodization procedure to prepare the specimen for examination. This procedure led to an improved definition (by interference color) between the high-oxygen alpha phase and the low-oxygen (prior) beta phase in the specimen. Measurements made in bright-field illumination using this technique were more consistent, and variations in measurements made by different individuals were greatly reduced. The method was also suitable for examining specimens oxidized at the higher temperatures.

The etch-anodization procedure is as follows. The polished specimen is etched for 10 to 15 s with swabbing and agitation in a diluted Kroll's etchant consisting of 4 ml conc. HNO_3 and 2 ml conc. HF per liter of water. The specimen is then anodized in a 1% KOH solution to 20 v and held at this potential for 120 s by which time the current drops essentially to leakage levels. Color micrographs are useful to illustrate the advantages of this treatment; however, the improved sharpness of the alpha/beta boundary is clearly evident even in the micrographs shown in Figs. 11 and 12, which are from cross-sections of specimens oxidized at 900 and 1005°C (1652 and 1841°F).

Representative layer thickness measurements were determined for each specimen. Several different measurement schemes were investigated for obtaining these values, and both an image-shearing eyepiece and a standard filar micrometer eyepiece have been utilized. The measurements reported here were obtained using a calibrated filar micrometer eyepiece on a small Bausch and Lomb bench metallograph.

Phase Thickness Measurements

After each steam-oxidation experiment was completed, the specimen was removed from the apparatus, sectioned on a diamond-impregnated wheel, mounted in epoxy, polished, and prepared for metallographic examination by the etch-anodization treatment previously described. Care was taken to insure that the final polished section was at the elevation which included the weld positions of all three thermocouple installations. Thus, the phase thickness measurements could be made in very close proximity to the monitor thermocouple locations. In the light of the

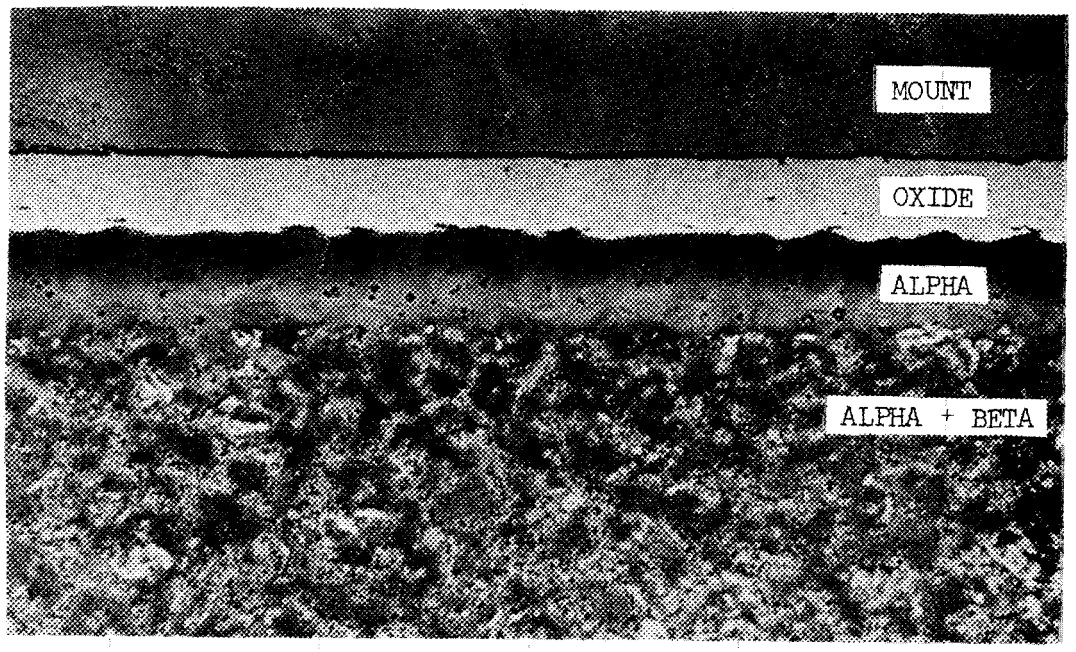

Fig. 11. Cross-Section of Zircaloy-4 PWR Tube Oxidized in the MaxiZWOK Apparatus for 858 s at 900°C (1652°F) (Expt. MAX-17). Outer surface. Etch-anodized specimen. Bright field illumination. 750×.

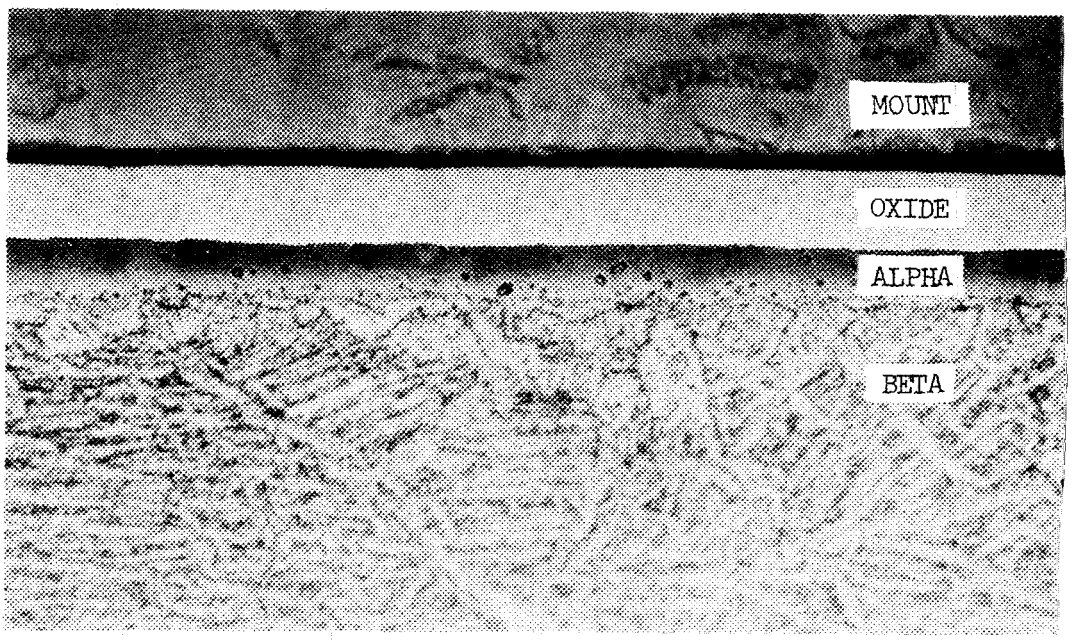

Fig. 12. Cross-Section of Zircaloy-4 PWR Tube Oxidized in the MaxiZWOK Apparatus for 99 s at 1005°C (1841°F) (Expt. MAX-23). Outer surface. Etch-anodized specimen. Bright-field illumination. 750×.

general observation that the temperature (and thus the product layer thicknesses) of the specimens oxidizing in MiniZWOK exhibited a circumferential variation, it was important to associate each phase thickness measurement position with a point on the specimen having a known time-temperature history.

The two monitor thermocouple stations on each specimen were always located in the same relative position with respect to the heating lamps within the furnace. These positions were generally the "hot" positions, and, thus, the extent of the temperature variation around a specimen could only be determined by rotating the specimen (or furnace) during oxidation or inferred by measuring the circumferential variation in product layer thicknesses after the experiment. At low temperatures, these variations were small. A plot of oxide and alpha layer thicknesses after oxidation at 1153°C (2107°F) as a function of angular position on

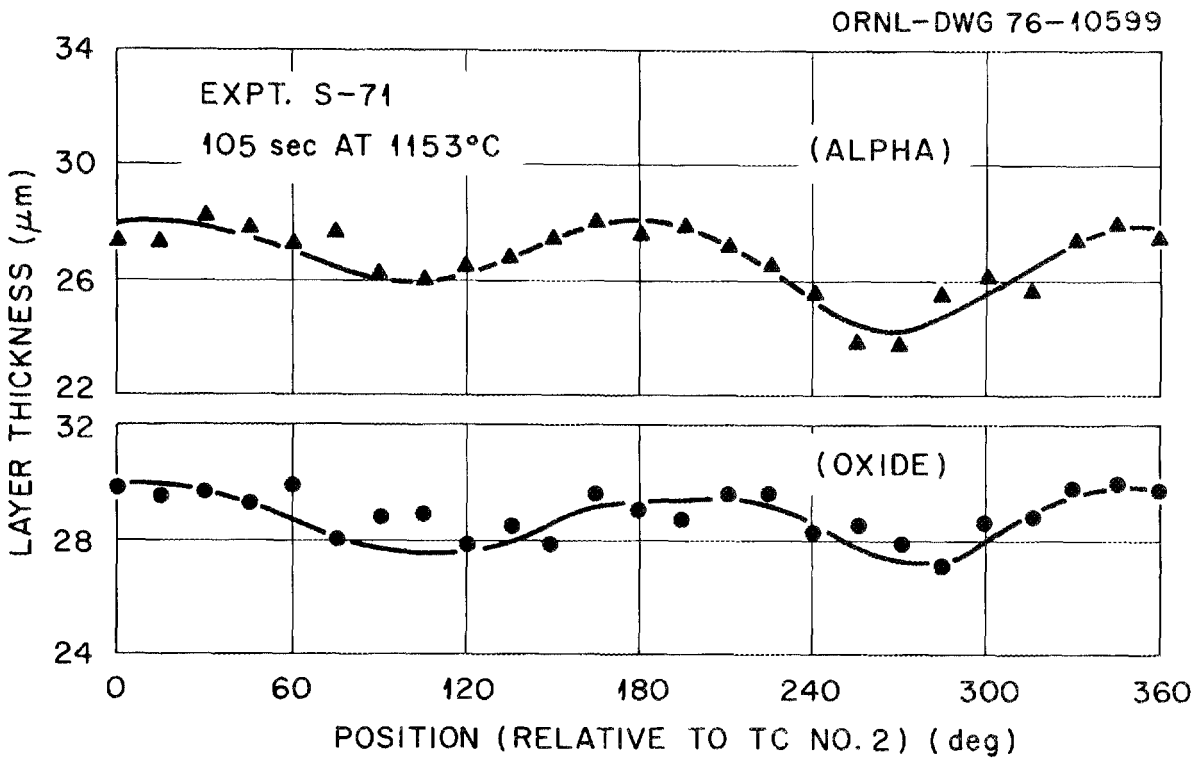

Fig. 13. Variation in Oxide and Alpha Thicknesses on Specimen S-71, Oxidized Nominally 105 s at 1153°C (2107°F). Thermocouple No. 2 located at approximately 0° and thermocouple No. 3 at approximately 180°.

the circumference of the specimens is presented in Fig. 13. While the periodicity is evident, the magnitude of the variation is seen in this case to be little more than the normal data scatter. At higher temperatures, the effect was generally more pronounced. Figure 14 illustrates the variation observed after an experiment at 1504°C (2739°F). Although in this case the temperature-time cycles recorded by the two monitor thermocouples (thermocouples Nos. 2 and 3) located at approximately 0 and 180 degrees were virtually the same, the thickness variations observed over the whole specimen imply that a maximum temperature variation of about ±15°C (27°F) existed. The periodicity of the temperature variation is consistent with the furnace geometry, and "cold" positions correspond to the location of the two furnace seams. A case where the two monitor thermocouples registered different temperatures is shown in Fig. 15. Here, the measured temperature difference accounted accurately for the

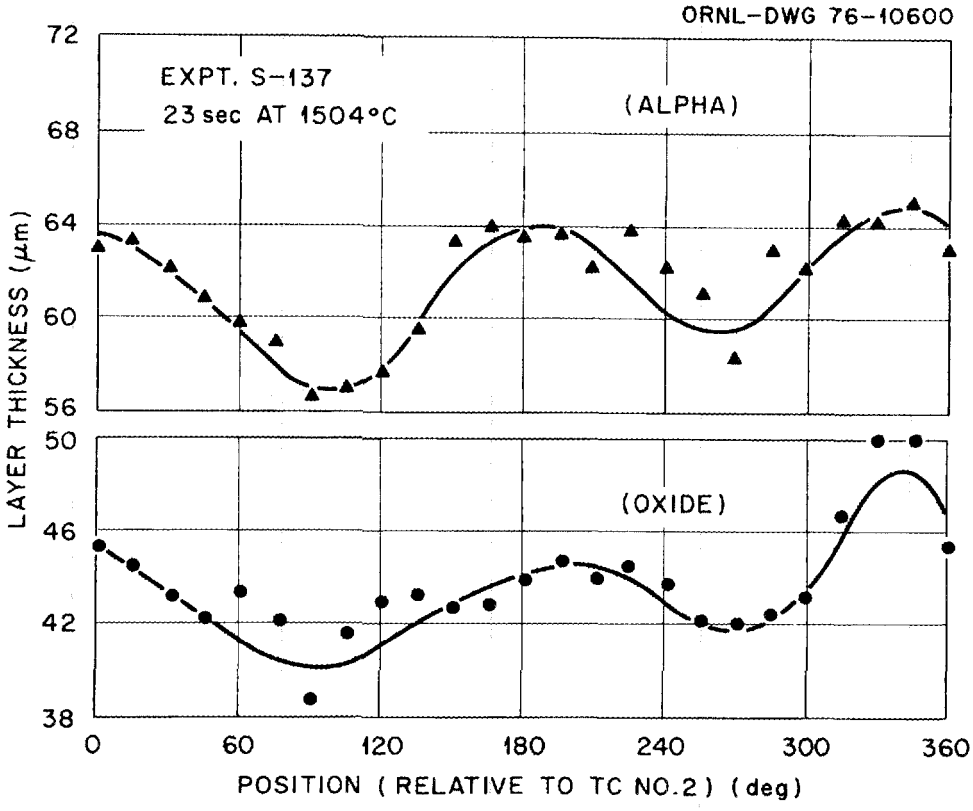

Fig. 14. Variation in Oxide and Alpha Thicknesses on Specimen S-137, Oxidized Nominally 22 s at 1504°C (2739°F). Thermocouple No. 2 located at approximately 0° and thermocouple No. 3 at approximately 180°.

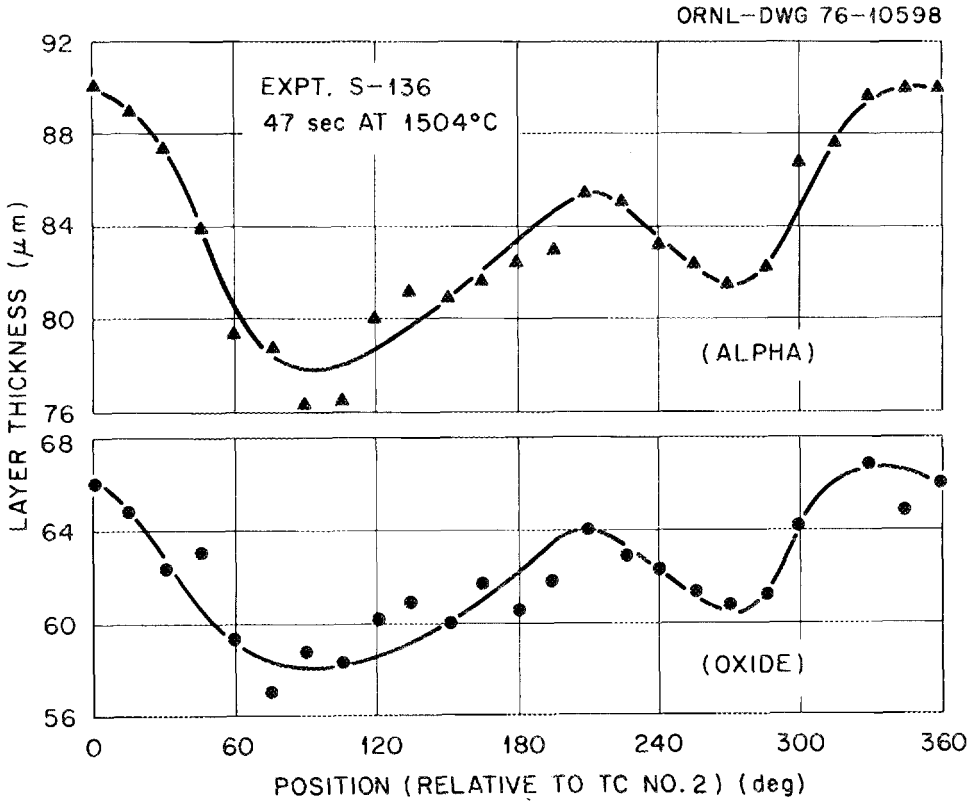

Fig. 15. Variations in Oxide and Alpha Thicknesses on Specimen S-136, Oxidized Nominally 47 s at 1504°C (2739°F). Thermocouple No. 2 located at approximately 0° and thermocouple No. 3 at approximately 180°.

measured phase thickness difference. The maximum variation in layer thicknesses over the whole specimen can be accounted for by a temperature variation of about ±20°C (36°F).

The existence of circumferential variations in temperature about a specimen made it mandatory that layer thickness measurements be made at points where the temperature is well known. Thus, layer thicknesses were measured to coincide with each of the monitor thermocouple positions. In order to reduce errors in the thickness measurements, the average of seven measurements made at 5° intervals ±15° from each thermocouple position was used.

Results

The procedures outlined above were used to obtain measurements of oxide layer thickness and alpha layer thickness as functions of time for each temperature investigated. In addition, the oxygen uptake for

each specimen was calculated from the layer thickness measurements on the basis of the model discussed earlier that assumed that all the oxide was stoichiometric, that a linear oxygen concentration gradient existed in the alpha layer, and that a simple diffusion calculation would suffice for determining the amount of oxygen in the beta phase.

The data obtained in this phase of our investigation are presented in Tables 5 to 17. We have discarded the results of experiments only when the experiment was obviously flawed. These were very few in number. The results of certain of the other experiments, also few in number, may be regarded statistically as "outliers" but have nevertheless still been included in the present data set. Additionally, for oxidation measurements at and above 1400°C (2552°F) instrumentation changes permitted complete and independent measurements of time and temperature at two positions on each specimen. For experiments below this temperature, only measurements at the No. 2 thermocouple position were considered in the analysis.

Table 5. Steam Oxidation of Sandvik Zircaloy-4 PWR Tubing at 905°C (1661°F)

Expt. No.	Time (s)	Layer Thickness		Total Oxygen Consumed (mg/cm^2)
		Oxide (μm)	Alpha (μm)	
S-15	791.9	13.5	13.2	2.37
S-16	776.6	13.8	13.5	2.42
S-17	2088.7	17.4	18.2	3.08
S-18	1148.8	15.8	16.5	2.80
S-19	420.3	11.5	9.4	1.97
S-20	2088.7	17.7	18.3	3.13
S-21	1228.2	15.1	14.1	2.63
S-22	1509.5	17.0	20.4	3.08
S-23	1623.4	17.2	21.0	3.12
S-24	370.7	11.2	10.0	1.94

Table 6. Steam Oxidation of Sandvik Zircaloy-4 PWR Tubing at 956°C (1752.8°F)

Expt. No.	Time (s)	Layer Thickness		Total Oxygen Consumed (mg/cm^2)
		Oxide (μm)	Alpha (μm)	
S-49	1344.9	26.5	24.1	4.62
S-50	977.9	23.1	18.9	3.97
S-51	1595.7	26.2	25.2	4.61
S-52	690.6	21.3	15.7	3.62
S-53	774.6	22.5	16.9	3.83
S-54	1300.2	25.1	22.3	4.37
S-55	948.7	22.0	19.9	3.83
S-56	1634.5	26.3	26.4	4.65
S-57	412.2	17.9	13.0	3.04
S-58	428.7	18.0	15.3	3.11

Table 7. Steam Oxidation of Sandvik Zircaloy-4 PWR Tubing at 1001°C (1833.8°F)

Expt. No.	Time (s)	Layer Thickness		Total Oxygen Consumed (mg/cm^2)
		Oxide (μm)	Alpha (μm)	
S-37	1130.5	40.5	23.7	7.04
S-38	725.2	32.6	23.1	5.77
S-39	301.1	22.5	15.2	3.95
S-40	925.0	37.4	24.6	6.57
S-41	300.2	20.9	14.4	3.69
S-42	483.4	26.5	18.0	4.67
S-43	678.6	29.9	20.8	5.30
S-44	1104.1	38.6	26.1	6.81
S-45	915.5	34.5	24.6	6.13
S-46	475.7	25.9	17.6	4.57
S-47	493.4	27.1	19.5	4.80
S-48	299.4	21.3	13.8	3.73

Table 8. Steam Oxidation of Sandvik Zircaloy-4 PWR Tubing at 1050°C (1922°F)

Expt. No.	Time (s)	Layer Thickness		Total Oxygen Consumed (mg/cm^2)
		Oxide (μm)	Alpha (μm)	
S-59	576.4	40.7	32.7	7.50
S-61	518.6	38.6	24.3	6.93
S-62	663.5	43.1	35.6	7.98
S-63	351.4	32.1	27.7	5.97
S-64	482.7	37.4	27.6	6.83
S-65	338.6	30.9	24.5	5.69
S-66	833.2	48.4	36.0	8.85
S-67	763.0	44.7	35.7	8.26
S-68	204.7	24.2	23.4	4.57
S-69	209.0	24.6	23.4	4.63

Table 9. Steam Oxidation of Sandvik Zircaloy-4 PWR Tubing at 1101°C (2013.8°F)

Expt. No.	Time (s)	Layer Thickness		Total Oxygen Consumed (mg/cm^2)
		Oxide (μm)	Alpha (μm)	
S-25	495.6	45.7	41.6	8.77
S-26	252.7	33.5	33.0	6.49
S-27	313.4	36.6	36.6	7.12
S-28	512.4	47.1	45.4	9.10
S-29	348.1	37.2	37.0	7.25
S-30	383.4	40.8	37.1	7.82
S-31	252.1	33.3	24.5	6.22
S-32	159.5	26.0	23.1	4.97
S-33	173.9	29.4	26.9	5.61
S-35	449.3	45.7	43.5	8.79
S-36	458.9	44.6	44.5	8.66

Table 10. Steam Oxidation of Sandvik Zircaloy-4 PWR Tubing at 1153°C (2107.4°F)

Expt. No.	Time (s)	Layer Thickness		Total Oxygen Consumed (mg/cm^2)
		Oxide (μm)	Alpha (μm)	
S-70	269.5	43.0	40.6	8.42
S-71	104.8	28.9	27.9	5.64
S-72	343.3	50.2	47.7	9.82
S-73	193.7	37.6	38.0	7.42
S-74	339.0	48.9	46.7	9.59
S-76	249.4	42.4	42.6	8.36
S-77	108.6	29.1	29.5	5.73
S-78	169.9	37.0	37.4	7.27
S-79	388.2	53.2	46.5	10.29
S-80	29.6	16.8	15.8	3.24
S-81	29.9	16.9	15.9	3.26

Table 11. Steam Oxidation of Sandvik Zircaloy-4 PWR Tubing at 1203°C (2197.4°F)

Expt. No.	Time (s)	Layer Thickness		Total Oxygen Consumed (mg/cm^2)
		Oxide (μm)	Alpha (μm)	
S-82	236.4	49.4	53.5	10.03
S-83	160.2	42.8	44.7	8.59
S-84	126.6	38.9	41.0	7.81
S-85	280.2	53.5	54.9	10.78
S-86	234.6	50.2	51.6	10.09
S-88	56.1	26.6	28.2	5.33
S-89	171.8	43.2	44.0	8.66
S-90	66.1	28.6	30.9	5.75
S-91	111.2	37.2	39.7	7.46

Table 12. Steam Oxidation of Sandvik Zircaloy-4 PWR Tubing at 1253°C (2287.4°F)

Expt. No.	Time (s)	Layer Thickness		Total Oxygen Consumed (mg/cm^2)
		Oxide (μm)	Alpha (μm)	
S-92	240.3	59.2	67.2	12.30
S-93	189.0	54.2	61.3	11.21
S-95	50.7	30.2	34.2	6.20
S-97	90.2	39.5	44.3	8.12
S-98	62.5	32.3	37.7	6.69
S-99	117.8	43.5	50.2	9.02
S-100	55.5	30.3	36.4	6.31
S-101	169.3	50.7	60.2	10.59
S-102	226.4	58.5	66.9	12.15
S-103	48.6	30.0	34.3	6.16

Table 13. Steam Oxidation of Sandvik Zircaloy-4 PWR Tubing at 1304°C (2379.2°F)

Expt. No.	Time (s)	Layer Thickness		Total Oxygen Consumed (mg/cm^2)
		Oxide (μm)	Alpha (μm)	
S-1	138.4	56.2	66.9	11.87
S-3	151.4	59.7	71.8	12.61
S-4	83.4	44.9	53.4	9.45
S-5	124.4	51.7	61.7	10.96
S-6	123.2	53.1	60.6	11.13
S-7	32.9	28.9	32.5	6.01
S-8	30.0	27.9	31.7	5.81
S-9	111.1	50.1	58.9	10.57
S-10	62.2	38.2	45.2	8.05
S-11	79.9	41.2	48.6	8.72
S-12	59.3	36.4	42.8	7.68
S-13	57.7	36.5	42.2	7.67
S-14	34.3	28.0	32.4	5.89

Table 14. Steam Oxidation of Sandvik Zircaloy-4 PWR Tubing at 1352°C (2465.6°F)

Expt. No.	Time (s)	Layer Thickness		Total Oxygen Consumed (mg/cm^2)
		Oxide (μm)	Alpha (μm)	
S-104	112.8	62.3	78.1	13.36
S-105	80.8	52.7	66.9	11.33
S-106	69.5	46.9	60.5	10.16
S-107	73.1	49.8	63.2	10.71
S-108	28.3	31.8	41.3	6.85
S-109	90.1	53.7	70.3	11.66
S-110	32.4	32.5	39.6	6.96
S-111	50.9	40.6	52.1	8.78
S-112	116.5	60.9	79.3	13.21

Table 15. Steam Oxidation of Sandvik Zircaloy-4 PWR Tubing at 1404°C (2559.2°F)

Expt. No.	Time (s)	Layer Thickness		Total Oxygen Consumed (mg/cm^2)
		Oxide (μm)	Alpha (μm)	
S-114-TC-2	72.7	58.4	78.3	12.84
S-114-TC-3	62.2	53.4	70.9	11.74
S-115-TC-2	29.7	38.7	51.0	8.45
S-115-TC-3	28.6	35.2	49.2	7.84
S-116-TC-2	45.7	45.7	62.9	10.12
S-116-TC-3	42.6	44.7	60.4	9.85
S-117-TC-2	14.3	28.0	36.8	6.08
S-117-TC-3	13.5	26.1	35.7	5.74
S-118-TC-2	11.2	24.5	31.8	5.31
S-118-TC-3	10.4	23.4	30.7	5.09
S-119-TC-2	56.4	51.6	67.5	11.29
S-119-TC-3	54.2	48.8	65.7	10.79
S-120-TC-2	44.8	47.1	62.2	10.29
S-120-TC-3	43.4	45.1	60.4	9.92
S-121-TC-2	27.5	39.1	51.1	8.47
S-121-TC-3	29.8	39.2	51.4	8.53
S-122-TC-2	74.1	59.0	77.3	12.92
S-122-TC-3	78.9	60.3	77.6	13.18
S-123-TC-2	29.3	39.0	50.4	8.46
S-123-TC-3	26.5	35.1	47.2	7.73

Table 16. Steam Oxidation of Sandvik Zircaloy-4 PWR Tubing at 1454°C (2649.2°F)

Expt. No.	Time (s)	Layer Thickness		Total Oxygen Consumed (mg/cm^2)
		Oxide (μm)	Alpha (μm)	
S-124-TC-2	57.1	61.8	81.4	13.64
S-124-TC-3	54.0	59.7	79.1	13.20
S-125-TC-2	25.1	41.5	56.5	9.20
S-125-TC-3	23.2	40.7	53.4	8.94
S-126-TC-2	27.9	45.5	59.4	9.96
S-126-TC-3	26.1	42.2	57.4	9.36
S-127-TC-3	53.3	58.7	78.0	13.01
S-128-TC-2	27.3	42.8	58.7	9.52
S-128-TC-3	26.4	42.5	57.4	9.41
S-129-TC-2	13.7	32.6	42.4	7.11
S-129-TC-3	14.9	32.6	42.0	7.14
S-130-TC-2	43.5	54.5	72.6	12.04
S-130-TC-3	43.1	54.6	72.2	12.03
S-131-TC-2	47.2	56.4	74.3	12.44
S-131-TC-3	42.0	52.6	68.9	11.61
S-132-TC-2	15.3	32.3	41.8	7.10
S-132-TC-3	14.5	31.0	40.6	6.84
S-133-TC-2	36.8	49.7	64.9	10.95
S-133-TC-3	34.5	47.5	62.9	10.51

Table 17. Steam Oxidation of Sandvik Zircaloy-4 PWR Tubing at 1504°C (2739.2°F)

Expt. No.	Time (s)	Layer Thickness		Total Oxygen Consumed (mg/cm^2)
		Oxide (μm)	Alpha (μm)	
S-134-TC-2	31.8	53.6	72.1	11.98
S-134-TC-3	28.9	50.7	68.1	11.34
S-135-TC-2	33.0	57.8	75.7	12.76
S-135-TC-3	31.2	50.3	74.2	11.53
S-136-TC-2	47.0	65.6	88.2	14.65
S-136-TC-3	42.6	61.8	83.8	13.84
S-137-TC-2	22.8	45.8	63.6	10.29
S-137-TC-3	21.9	43.8	62.8	9.93
S-138-TC-2	7.6	27.3	38.7	6.13
S-138-TC-3	8.2	28.5	38.5	6.34
S-139-TC-2	53.2	73.7	97.6	16.29
S-141-TC-2	9.2	30.0	40.7	6.68
S-141-TC-3	8.9	28.9	40.8	6.50
S-142-TC-2	49.0	62.6	93.9	14.42
S-142-TC-3	50.0	62.5	91.4	14.34
S-143-TC-2	42.4	65.9	85.6	14.51
S-143-TC-3	37.8	57.5	80.3	12.97
S-150-TC-2	13.9	37.5	48.3	8.25
S-150-TC-3	13.2	35.5	48.6	7.93

Examples of the appearance of cross-sections of oxidized specimens are given in Figs. 16–18. These are 100× micrographs taken from specimens oxidized at 1101, 1304, and 1504°C (2014, 2379, and 2739°F) and represent typical microstructures showing the oxide, alpha, and prior beta regions. The tendency for separation within the oxide layer (along the tin-rich particle line[6]) for the longer experiments at 1304 and 1504°C (2379–2739°F) was aggravated by the particular method employed in mounting the specimens. In the event of such a separation, separate measurements were made of the two parts of the oxide and the results summed to give the total oxide thickness.

Correlation of the Data

An examination of the rates of growth of the oxide and alpha layers over the temperature range of this investigation revealed that parabolic growth kinetics applied to both phases at temperatures above 1000°C (1832°F) but only to the alpha phase below this temperature. For this reason, parabolic rate constants will not be reported for oxide growth at temperatures below 1000°C (1832°F). Since the rate constants for Xi (oxide + alpha) layer growth and for total oxygen consumed involve the oxide growth parameter, they also are subject to this limitation.

The basic expression for the rate of a reaction where parabolic kinetics control is

$$\frac{dK}{dt} = \frac{1}{K}\,\frac{\delta^2_K}{2} \qquad (3)$$

where

K is a kinetic parameter [i.e., oxide layer thickness, ϕ; alpha layer thickness, α; Xi (oxide + alpha) layer thickness, ξ; or total oxygen consumed, τ], and $\frac{\delta^2_K}{2}$ is defined as the isothermal parabolic rate constant.*

*It should be emphasized, see Eq. (3), that we express the parabolic rate constants as $\delta^2/2$. These values must be multiplied by two to give the slope of a plot of K^2 vs t [c.f., Eq. (4)]. Different authors use other conventions such as designating the parabolic rate constant as being the slope of a K^2 vs t plot. The matter comes down to the question of whether the factor of 1/2 obtained during the integration of KdK (i.e., $\int_0^K KdK = K^2/2$) in Eq. (3) is or is not incorporated in the rate constant.

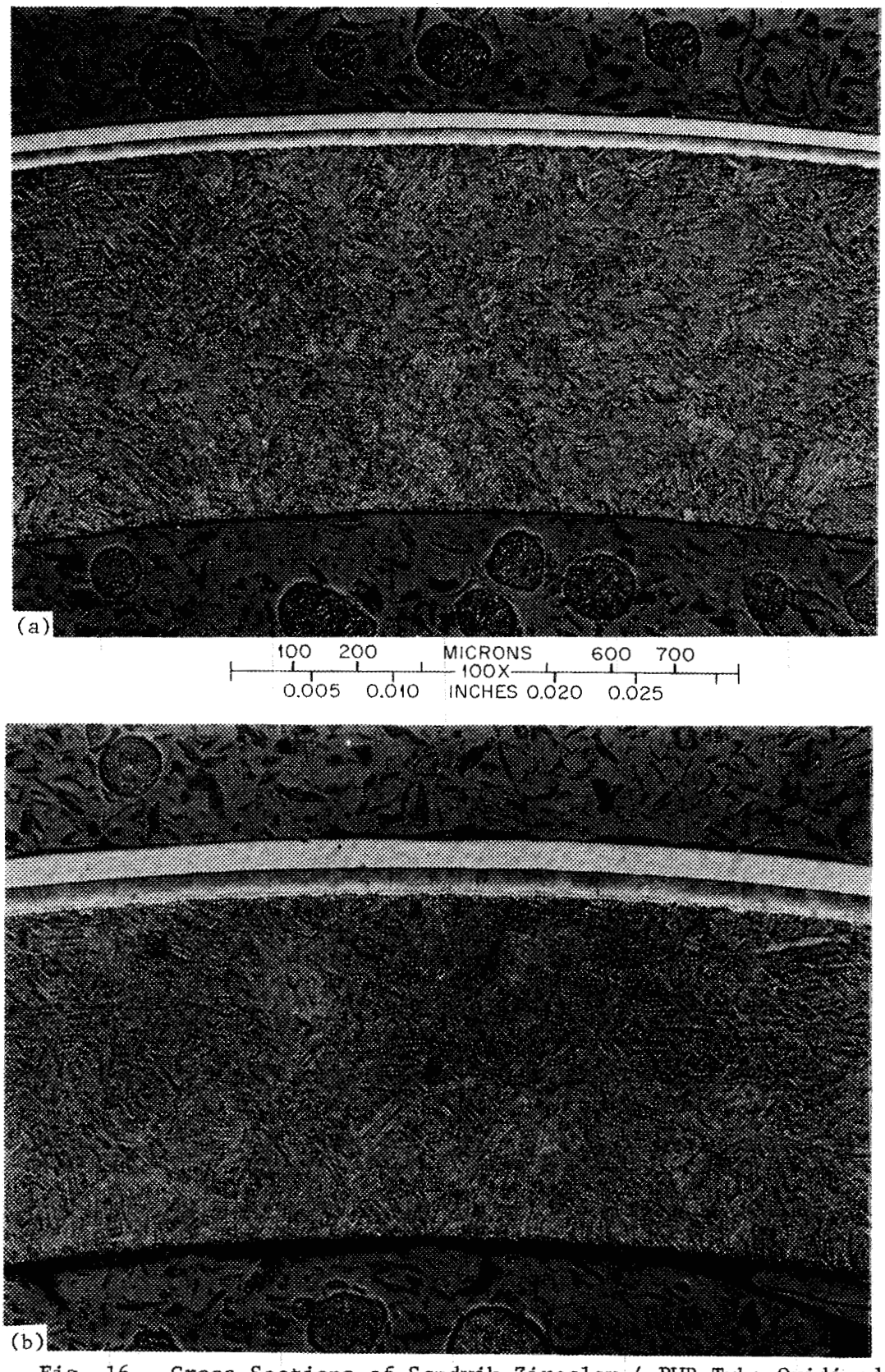

Fig. 16. Cross-Sections of Sandvik Zircaloy-4 PWR Tube Oxidized in Steam for (a) 160 s and (b) 512 s at 1101°C (1834°F). Experiments S-32 and S-28. Etch-anodized; bright-field; 100×.

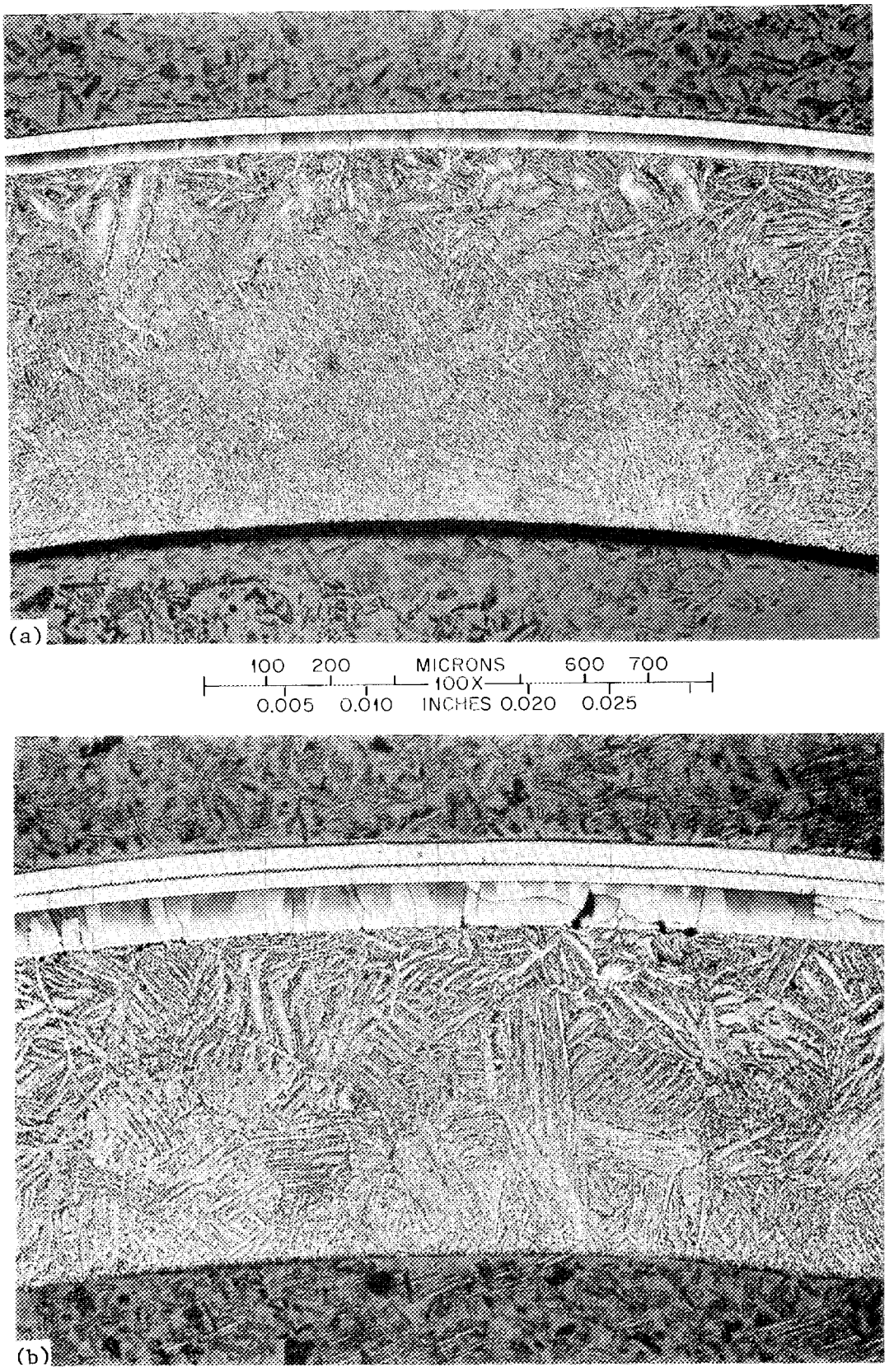

Fig. 17. Cross-Sections of Sandvik Zircaloy-4 PWR Tube Oxidized in Steam for (a) 30 s and (b) 151 s at 1304°C (2379°F). Experiments S-8 and S-3. Etch-anodized; bright-field; 100×.

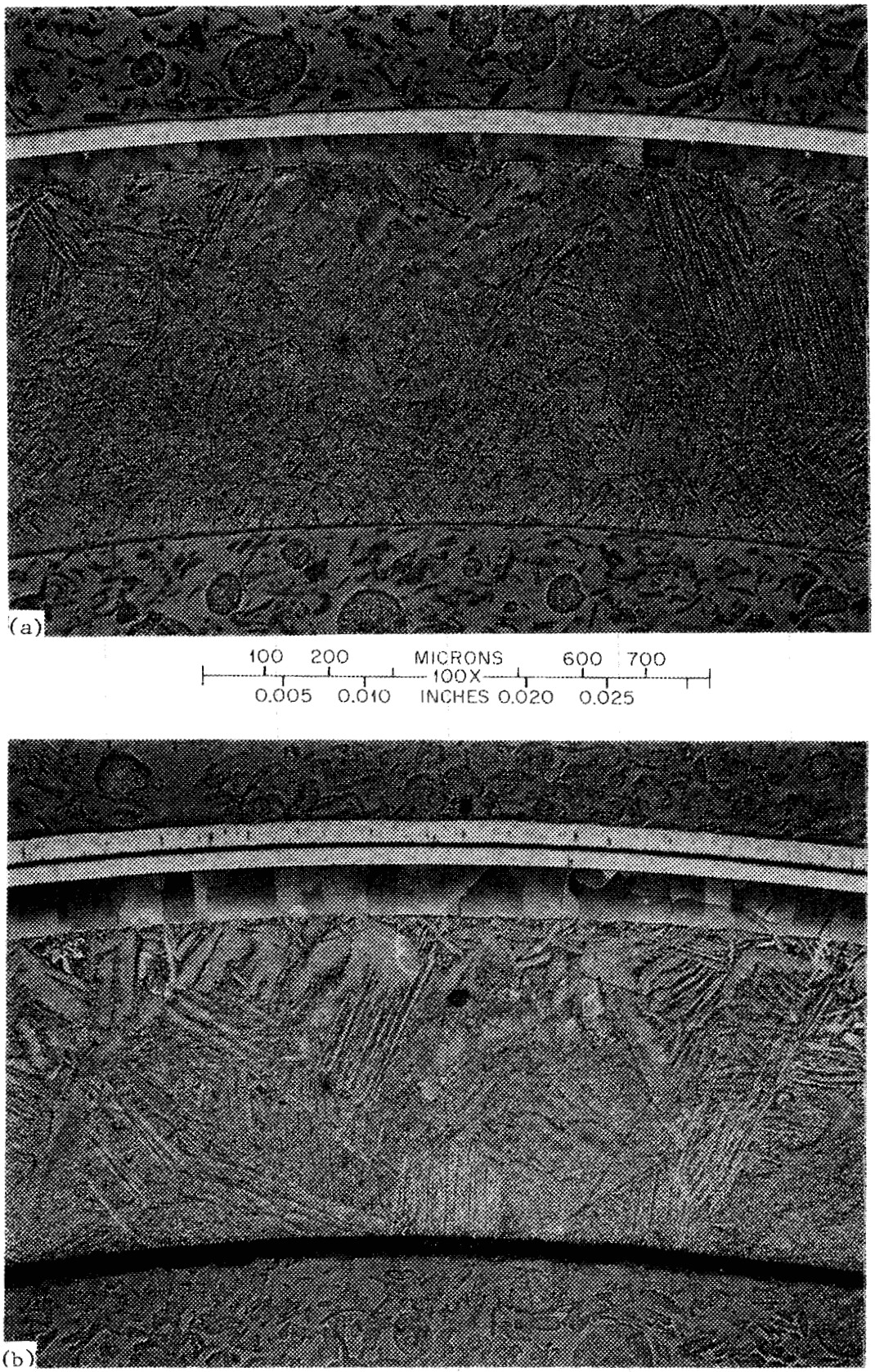

Fig. 18. Cross-Sections of Sandvik Zircaloy-4 PWR Tube Oxidized in Steam for (a) 14 s and (b) 47 s at 1504°C (2739°F). Experiments S-150 and S-136. Etch-anodized; bright-field; 100×.

The integrated form of this equation is

$$K^2 = K_o^2 + \delta_K^2 \, t \ , \tag{4}$$

and, thus, a plot of K^2 vs t should be linear with a slope of δ_K^2 and an intercept of K_o^2. Such plots of experimental data with nonzero values of K_o^2 might indicate deviations from strict parabolic behavior at short times, a pre-existing film or reaction layer on the specimen, or poor determinations of time-at-temperature for the reaction.

Parabolic rate constants for the four kinetic parameters ϕ, α, ξ, and τ were determined, where applicable, at each reaction temperature from the experimental data presented in Tables 5 through 17 by a least-squares treatment based on Eq. (4). Although we investigated both approaches, the present rate constants were calculated on the basis that $K_o = 0$, which assumes "ideal" parabolic behavior. While the observed trend in the data was for K_o to have small, positive values, virtually no loss in statistical confidence was found as a result of this arbitrary assignment. In fact, the Arrhenius correlation of the rate constants calculated in this way exhibited a lower sum of squares of error, implying that this procedure gives a more consistent final result.

Illustrations of the kinetic behavior for oxide and alpha growth for temperatures from 1001 to 1504°C (1834 to 2739°F) are given in Figs. 19 to 24. At the lower end of this temperature range [1001–1101°C (1834–2014°F)], a larger scatter exists for the alpha layer measurements. This is in large part due to the uncertainties in locating precisely the position of the alpha-beta interface at these temperatures. At temperatures below 1400°C (2552°F), each data set included measurements from only one reference point per specimen (the No. 2 thermocouple position); at higher temperatures, measurements were made at each of the two monitor thermocouple positions on each specimen, and the high degree of self-consistency of these measurements is evident. In each of these cases, as in all cases for reaction above 1000°C (1832°F), the growth rates of these phases are well represented by parabolic growth kinetics. It should be pointed out that the kinetics for Xi (oxide + alpha) layer growth, ξ, and for total oxygen consumption, τ, behave

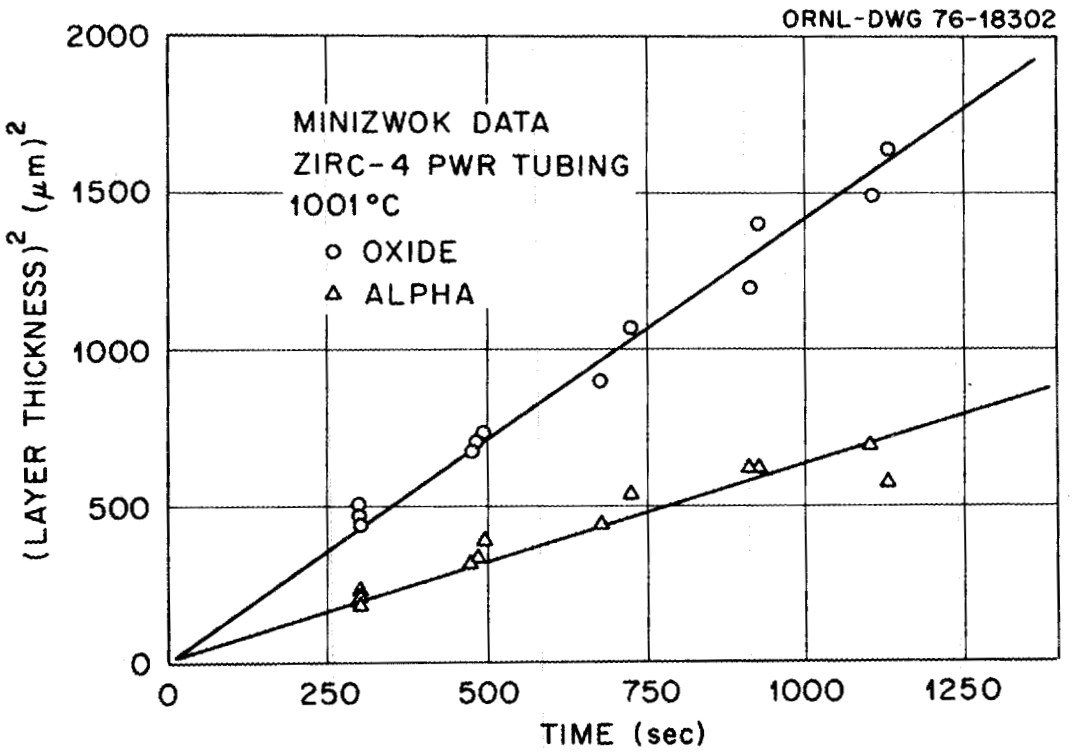

Fig. 19. Steam Oxidation of Sandvik Zircaloy-4 PWR Tubing in the MiniZWOK Apparatus at 1001°C (1834°F).

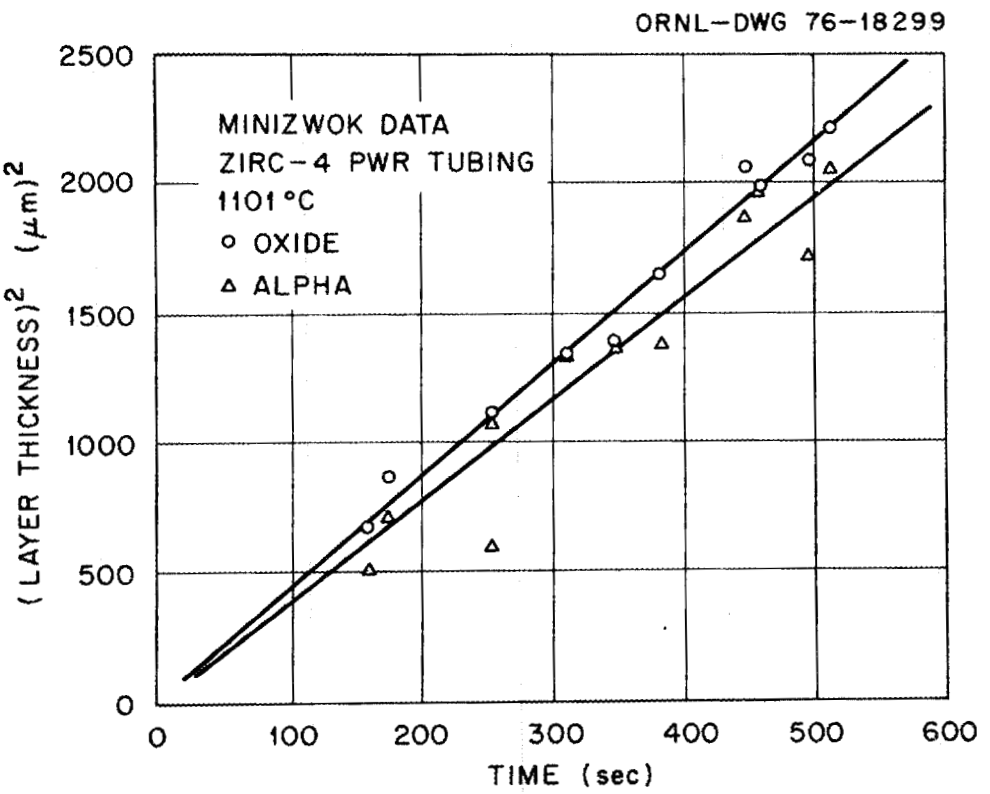

Fig. 20. Steam Oxidation of Sandvik Zircaloy-4 PWR Tubing in the MiniZWOK Apparatus at 1101°C (2014°F).

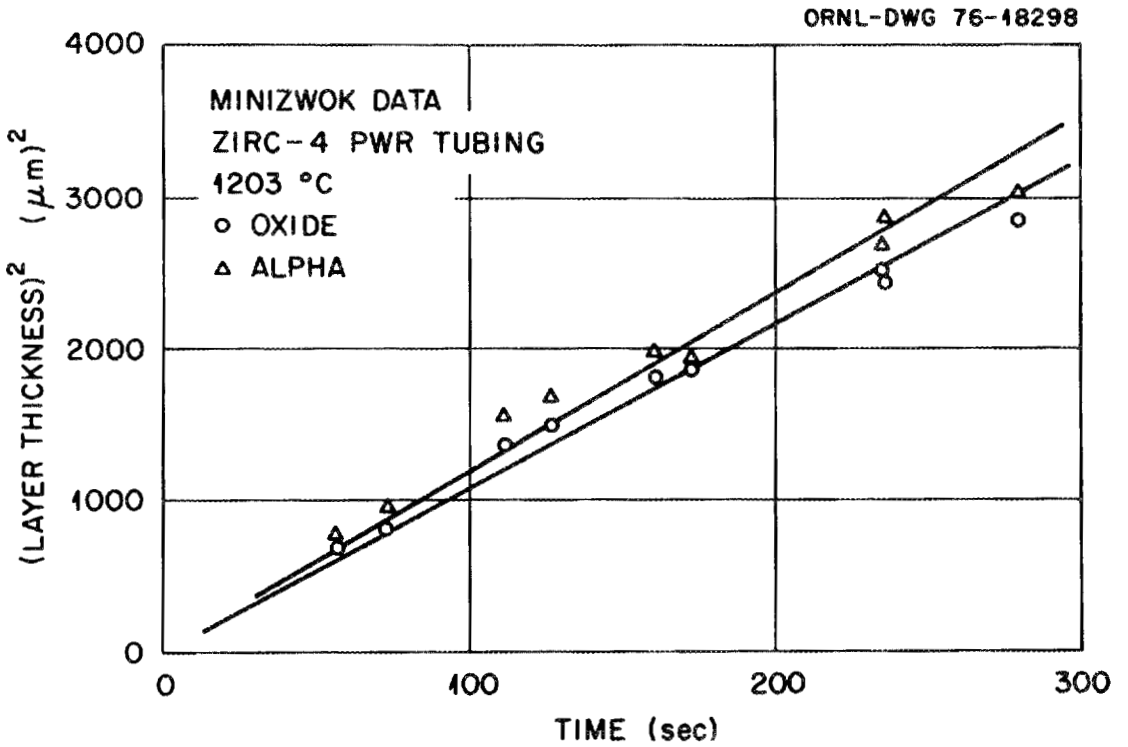

Fig. 21. Steam Oxidation of Sandvik Zircaloy-4 PWR Tubing in the MiniZWOK Apparatus at 1203°C (2197°F).

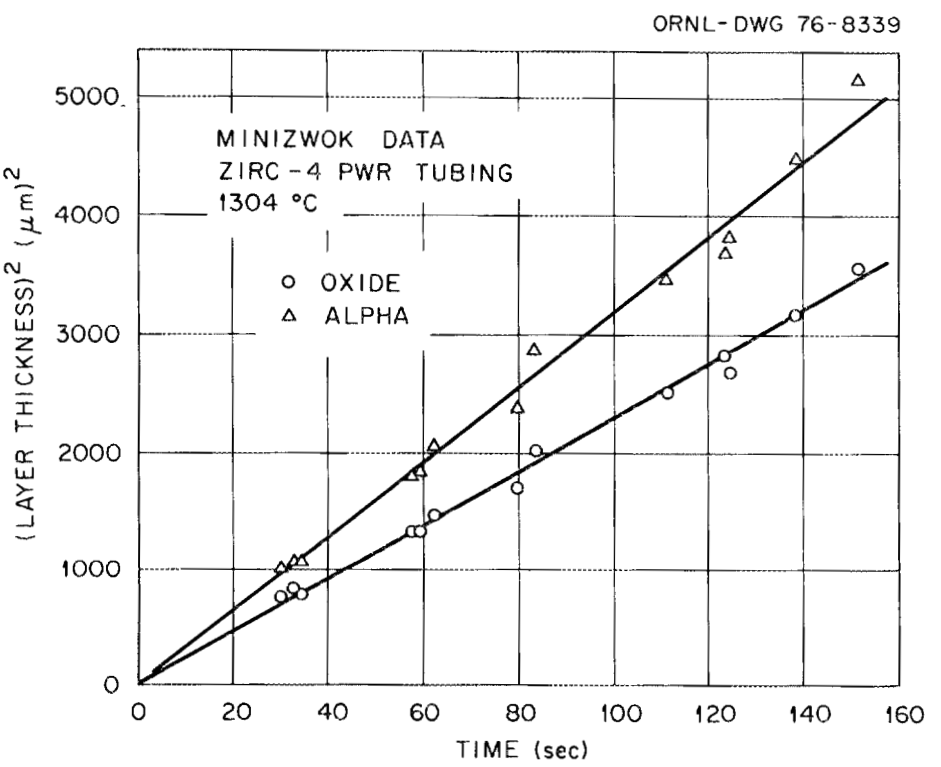

Fig. 22. Steam Oxidation of Sandvik Zircaloy-4 PWR Tubing in the MiniZWOK Apparatus at 1304°C (2379°F).

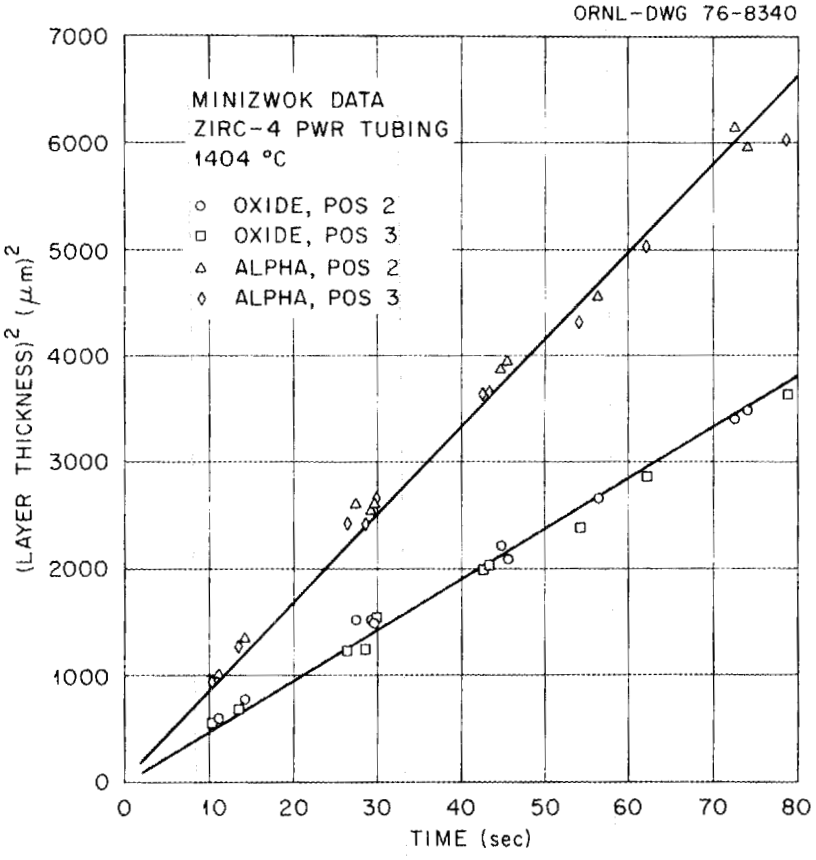

Fig. 23. Steam Oxidation of Sandvik Zircaloy-4 PWR Tubing in the MiniZWOK Apparatus at 1404°C (2559°F).

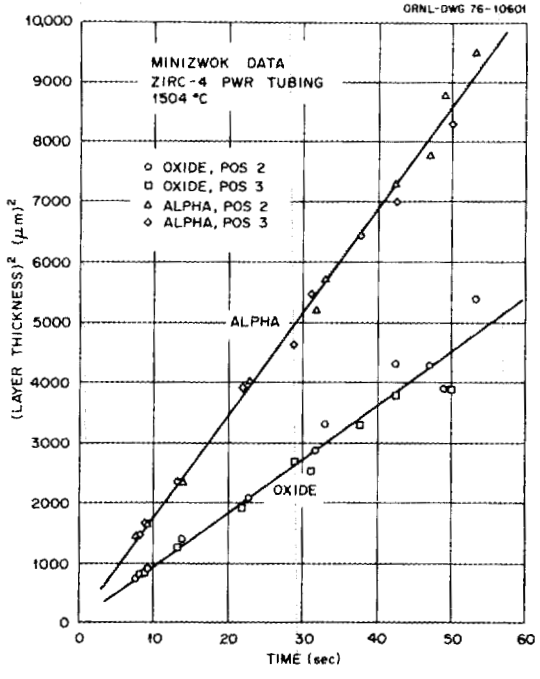

Fig. 24. Steam Oxidation of Sandvik Zircaloy-4 PWR Tubing in the MiniZWOK Apparatus at 1504°C (2739°F).

similarly. Since most of the total oxygen consumed by a specimen is located in the oxide layer, the kinetic response of this parameter is virtually identical to that for oxide layer growth.

The data for steam oxidation at 905 and 956°C (1661 and 1753°F) differ from the higher temperature results in that non-parabolic growth of the oxide layer was observed at both of these temperatures. The data set for oxidation at 956°C (1753°F) furnishes a good example of these differences. These data are presented in Fig. 25. While the growth of the alpha layer appears to be accounted for satisfactorily by parabolic kinetics, departures from this behavior clearly exist for the oxide layer growth. In fact, the growth rate of the oxide layer at this temperature is more closely represented by a cubic rate expression, as shown in Fig. 26.

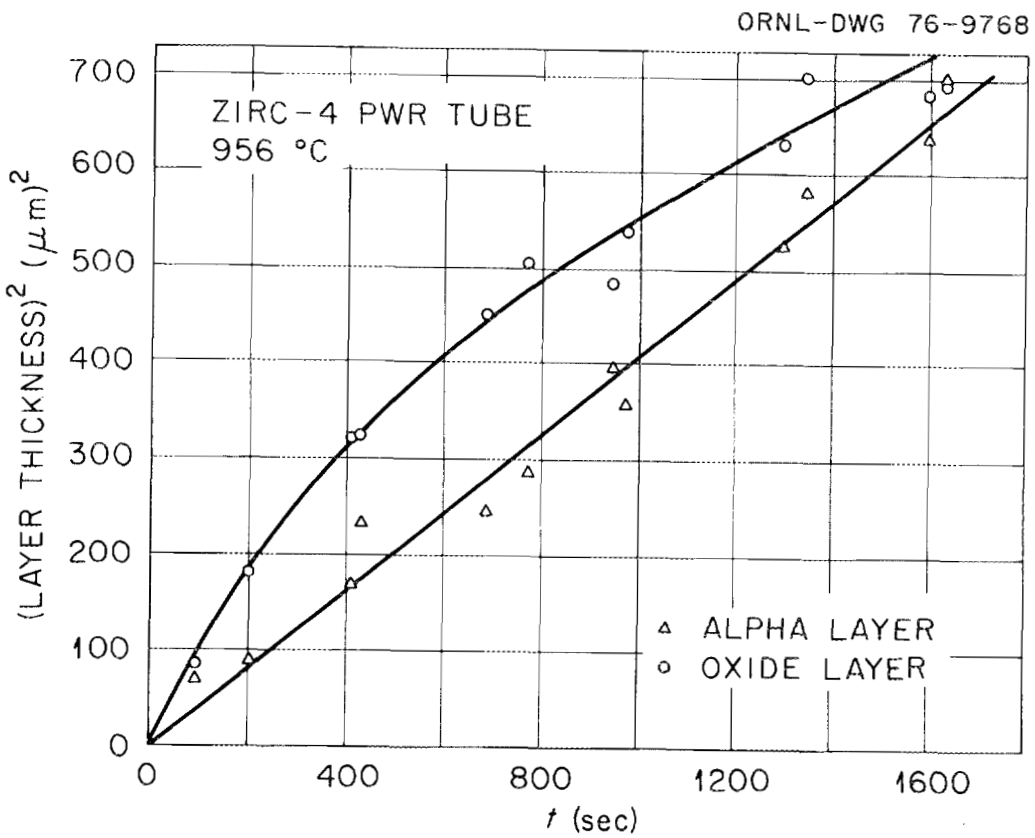

Fig. 25. Steam Oxidation of Sandvik Zircaloy-4 PWR Tubing in the MiniZWOK Apparatus at 956°C (1753°F). Example of nonparabolic growth in oxide layer.

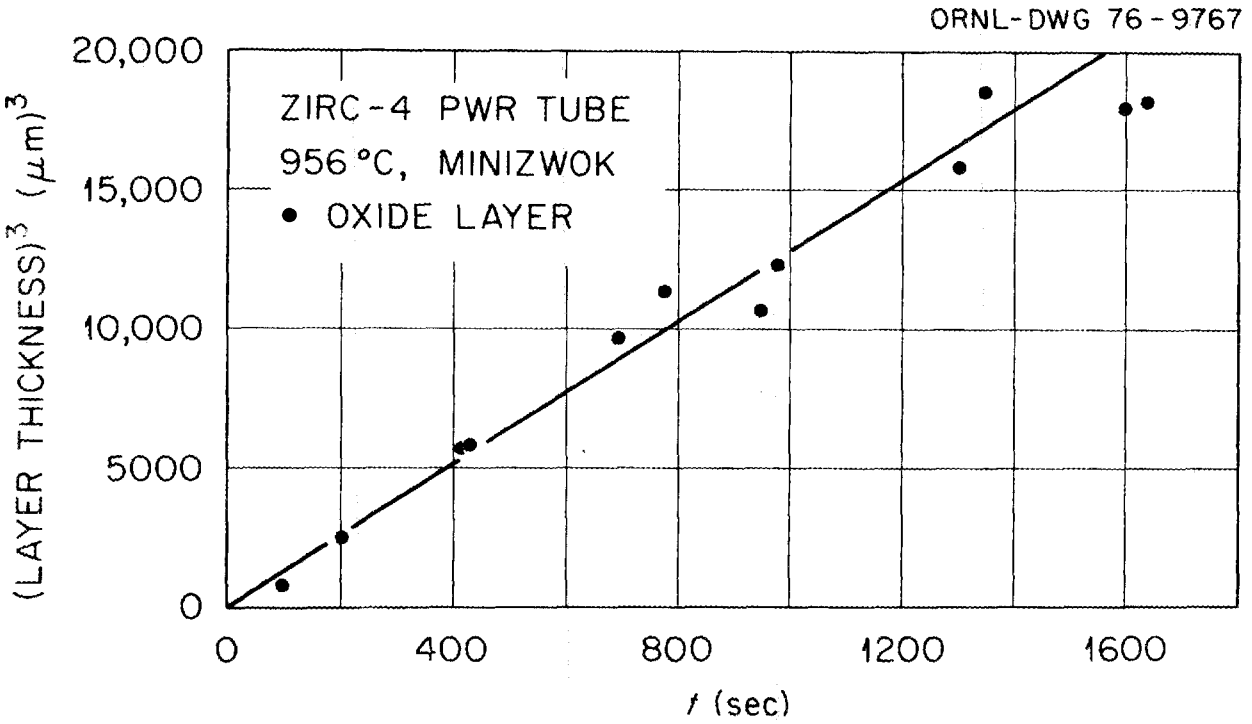

Fig. 26. Steam Oxidation of Sandvik Zircaloy-4 PWR Tubing in the MiniZWOK Apparatus at 956°C (1753°F). Cubic plot for oxide layer growth.

The parabolic rate constants from the present data sets are given in Table 18. It is interesting to observe that the scatter in the individual data, indicated by the statistical confidence in the rate constants, actually improved as the temperature increased. Part of the unexpected improvement must be associated with the fact that the measurements of interface positions are relatively more accurate at the higher temperatures because the system behaves more ideally.

Correlations of the rate constants in terms of simple Arrhenius relationships were, except for the alpha layer growth, restricted to the temperature range 1000–1500°C (1832–2732°F). In fact, because the rate constant for oxide growth at 1001°C (1834°F) appeared a little low compared to the rest of the data set, the least-squares and statistical representations were based on the data at and above 1050°C (1922°F). The four sets of parabolic rate constants are plotted in Arrhenius fashion in Figs. 27–30. The data are obviously well represented by this relationship, although a critical examination seems to indicate

Table 18. Parabolic Rate Constants for Isothermal Steam Oxidation of Sandvik Zircaloy-4 PWR Tubing

Temperature (°C)	Temperature (°F)	$\frac{\delta^2_\phi}{2}$ [Oxide] (cm^2/s)	Dev.[a] (± %)	$\frac{\delta^2_\alpha}{2}$ [Alpha] (cm^2/s)	Dev.[a] (± %)	$\frac{\delta^2_\xi}{2}$ [Xi] (cm^2/s)	Dev.[a] (± %)	$\frac{\delta^2_\tau}{2}$ [Oxygen] $(g/cm^2)^2/s$	Dev.[a] (± %)
		$\times 10^8$		$\times 10^8$		$\times 10^7$		$\times 10^7$	
905	1661			0.1012	36.9				
956	1753			0.2027	12.4				
1001	1834	0.7072	8.0	0.3139	17.2	0.1961	8.7	0.2191	7.2
1050	1922	1.399	5.8	0.8493	28.2	0.4421	13.0	0.4725	6.0
1101	2014	2.171	8.0	1.950	21.2	0.8230	12.3	0.8066	7.6
1153	2017	3.631	4.9	3.254	13.7	1.375	8.3	1.387	5.0
1203	2197	5.389	10.4	5.872	14.1	2.251	11.9	2.185	9.7
1253	2287	7.663	6.7	10.07	8.2	3.530	7.2	3.300	6.0
1304	2379	11.41	4.8	15.93	6.3	5.431	5.2	5.078	4.2
1352	2466	16.51	6.9	27.10	4.4	8.592	4.6	7.693	5.2
1404	2559	23.51	4.1	41.22	4.4	12.70	3.9	11.31	3.4
1454	2649	33.66	3.5	59.01	4.1	18.18	3.6	16.41	3.0
1504	2739	45.25	8.7	85.95	3.4	25.58	4.5	22.79	6.0

[a]Maximum uncertainty at 90% confidence level.

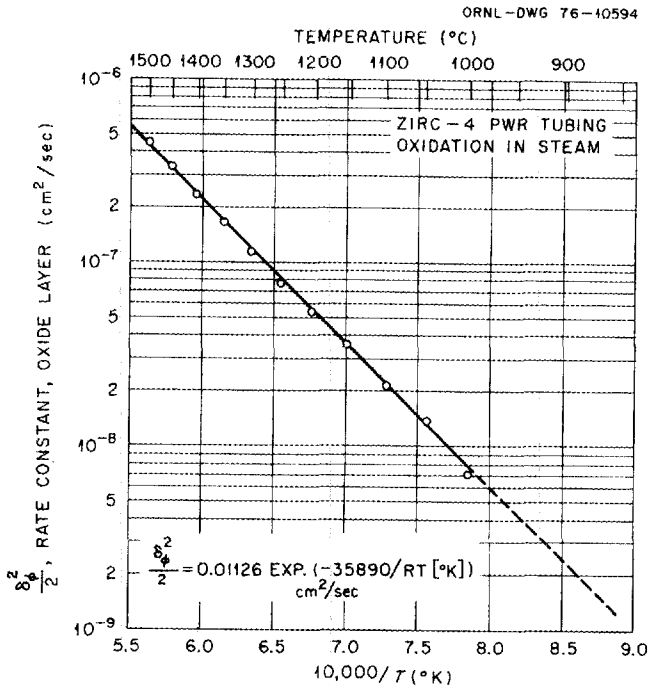

Fig. 27. Arrehnius Plot of the Parabolic Rate Constants for Oxide Layer Growth from 1000 to 1500°C (1832–2732°F). Oxidation of Sandvik Zircaloy-4 PWR tubing in steam.

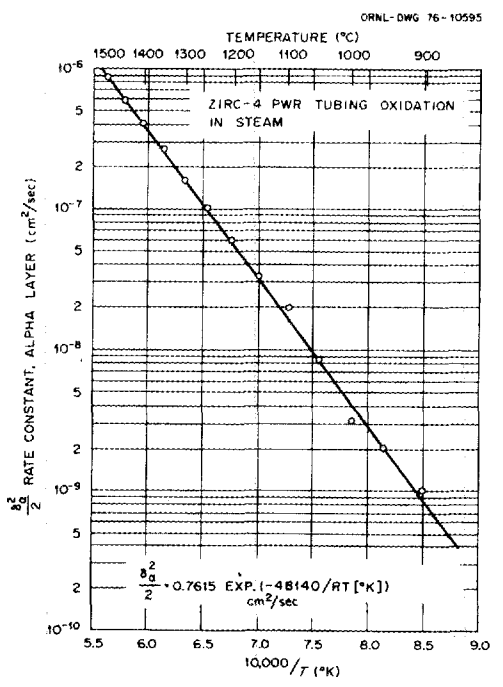

Fig. 28. Arrhenius Plot of the Parabolic Rate Constants for Alpha Layer Growth from 900 to 1500°C (1652–2732°F). Oxidation of Sandvik Zircaloy-4 PWR tubing in steam.

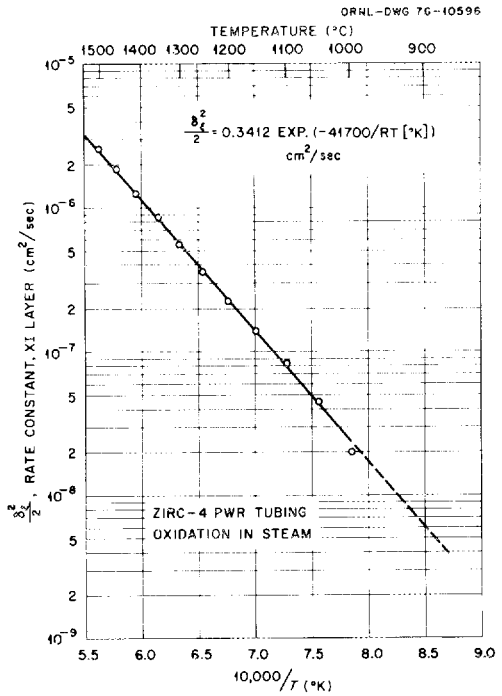

Fig. 29. Arrhenius Plot of the Parabolic Rate Constants for Xi (Oxide + Alpha) Layer Growth from 1000 to 1500°C (1832–2732°F). Oxidation of Sandvik Zircaloy-4 PWR tubing in steam.

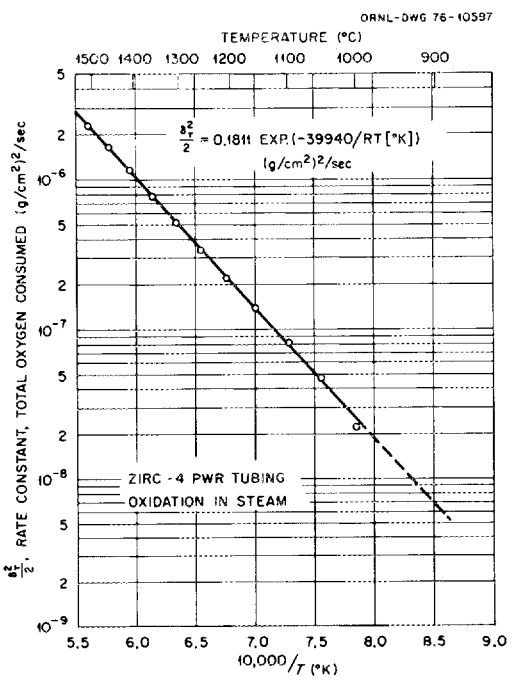

Fig. 30. Arrhenius Plot of the Parabolic Rate Constant for Total Oxygen Consumption from 1000 to 1500°C (1832–2732°F). Oxidation of Sandvik Zircaloy-4 PWR tubing in steam.

that some minor but systematic deviations exist. It should be mentioned, for example, that if the Arrhenius representation for the oxide and alpha rate constants are each linear with different slopes, then the corresponding representation for Xi *must* exhibit curvature. This effect appears negligible in the present case, and we have determined all of the expressions for the temperature dependence of the parabolic rate constant on the basis of conformity to the Arrhenius equation.

Individual confidence intervals for the pre-exponential and activation energy terms of the Arrhenius expressions for the rate constants were calculated. In addition, the joint confidence intervals for the rate constants themselves were also calculated. The computation procedures and significance of the statistical quantities have been reported previously[4] and will not be repeated here. Specifically, it was shown that

$$\frac{\delta_\phi^2}{2} = .01126 \left[{}^{+30\%}_{-23\%}\right] \exp(-35890[\pm 2.2\%]/RT) \ \mathrm{cm^2/s} \tag{5}$$

$$\frac{\delta_\alpha^2}{2} = .7615 \left[{}^{+54\%}_{-35\%}\right] \exp(-48140[\pm 2.6\%]/RT) \ \mathrm{cm^2/s} \tag{6}$$

$$\frac{\delta_\xi^2}{2} = .3412 \left[{}^{+17\%}_{-15\%}\right] \exp(-41700[\pm 1.2\%]/RT) \ \mathrm{cm^2/s} \tag{7}$$

$$\frac{\delta_\tau^2}{2} = .1811 \left[{}^{+20\%}_{-16\%}\right] \exp(-39940[\pm 1.4\%]/RT) (\mathrm{g/cm^2})^2/\mathrm{s} \quad , \tag{8}$$

where each $\frac{\delta_k^2}{2}$ is the parabolic rate constant for the kinetic parameter k calculated on the basis that $\frac{\delta_k^2}{2} = k \frac{dk}{dt}$. The quantities in the brackets refer to the *individual* 90% confidence limits on the pre-exponential and activation energy terms.

While the individual confidence intervals are useful in describing the statistics on the specific terms, the *joint* confidence intervals are more meaningful descriptions of the accuracy of the specific rate constants because the uncertainties on the pre-exponential and activation energy terms are correlated. From constructions of the joint confidence intervals, the ranges of $\frac{\delta_k^2}{2}$ at the 90% level were calculated and are given in Table 19. The confidence ranges for the rate constants shown in Table 19 are considered to be excellent. Thus, the data are consistent

Table 19. 90% Joint Confidence Intervals for the Parabolic Rate Constants for Oxide Layer Growth, Alpha Layer Growth, Xi Layer Growth and Total Oxygen Consumption

Rate Constant $\frac{\delta^2_k}{2}$	Percent Deviation from Expected Value at 1500°C (2732°F)	1250°C (2282°F)	1050°C (1922°F)
$\frac{\delta^2_\phi}{2}$	+4.3 −4.1	+2.5 −2.4	+4.9 −4.7
$\frac{\delta^2_\alpha}{2}$	+10.1 −9.2	+6.1 −5.8	+12.1 −10.8
$\frac{\delta^2_\xi}{2}$	+2.6 −2.6	+1.5 −1.5	+3.0 −2.9
$\frac{\delta^2_\tau}{2}$	+3.0 −2.9	+1.7 −1.7	+3.4 −3.3

with and represented accurately by the given Arrhenius relationships. (For a more complete exposition of the statistical treatment of the data, see Appendix A.)

Oxide-Alpha Thickness Ratios

As has been pointed out, the activation energies for oxide and alpha layer growth are 35,890 and 48,140 cal/mole, respectively. This difference is expected to produce differences in the relative rates of growth of the two phases as a function of temperature, and such a phenomenon is observed as shown in Fig. 31 where the oxide-alpha layer thickness ratio (ϕ/α) is plotted as a function of temperature. The error bars represent two standard deviations from the mean of the ratios observed.

It has been suggested that the ϕ/α ratio might be used as a measure of oxidation temperature of specimens oxidized under approximately isothermal conditions. Such an approach is certainly possible but must be used with considerable caution. As the data demonstrate, even when

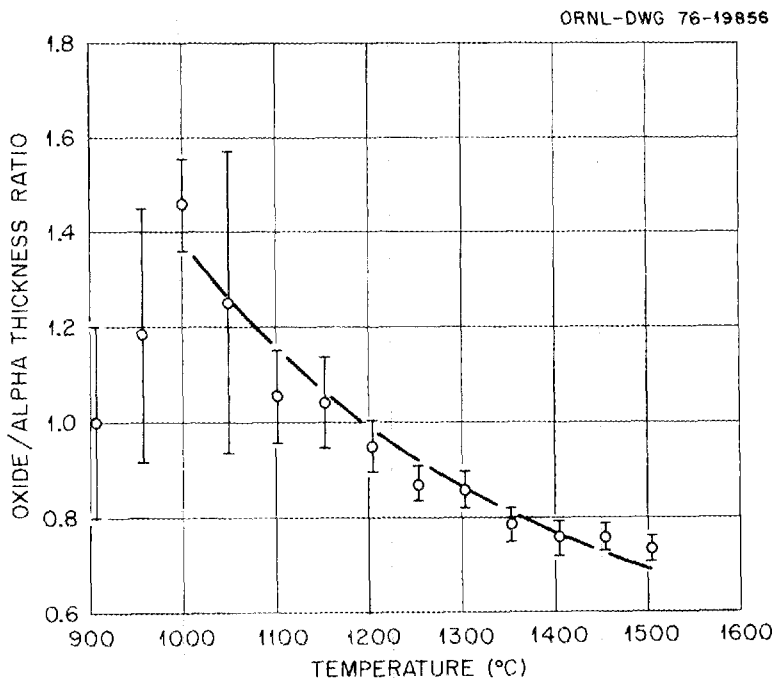

Fig. 31. Oxide/Alpha Thickness Ratios Plotted as a Function of Temperature for Zircaloy-4 Specimens Oxidized in Steam.

samples are oxidized under carefully controlled conditions, a substantial variation in the ϕ/α ratio is observed. This variation could lead to errors in temperature estimates of 100°C (180°F) or greater.

The method certainly should not be used at temperatures below 1000°C (1832°F). At 900 and 950°C (1652–1742°F) the oxide growth rate is not parabolic, and, as a consequence, the ϕ/α ratio changes as a function of oxidation time as well as temperature. This effect is illustrated in Fig. 32(b) where ϕ/α is plotted against oxidation time. At temperatures above 1000°C (1832°F), however, this ratio does not appear to vary significantly with time [see Fig. 32(a)].

Comparison of Isothermal Kinetic Data

A general comparison of the results of this investigation with previous work can be made in terms of the parabolic rate constants for total oxygen consumption, $\frac{\delta^2}{2\tau}$. The temperature dependences reported by (or derived from the data of) a number of investigators are given below. It should be remembered that we have defined these rate constants as

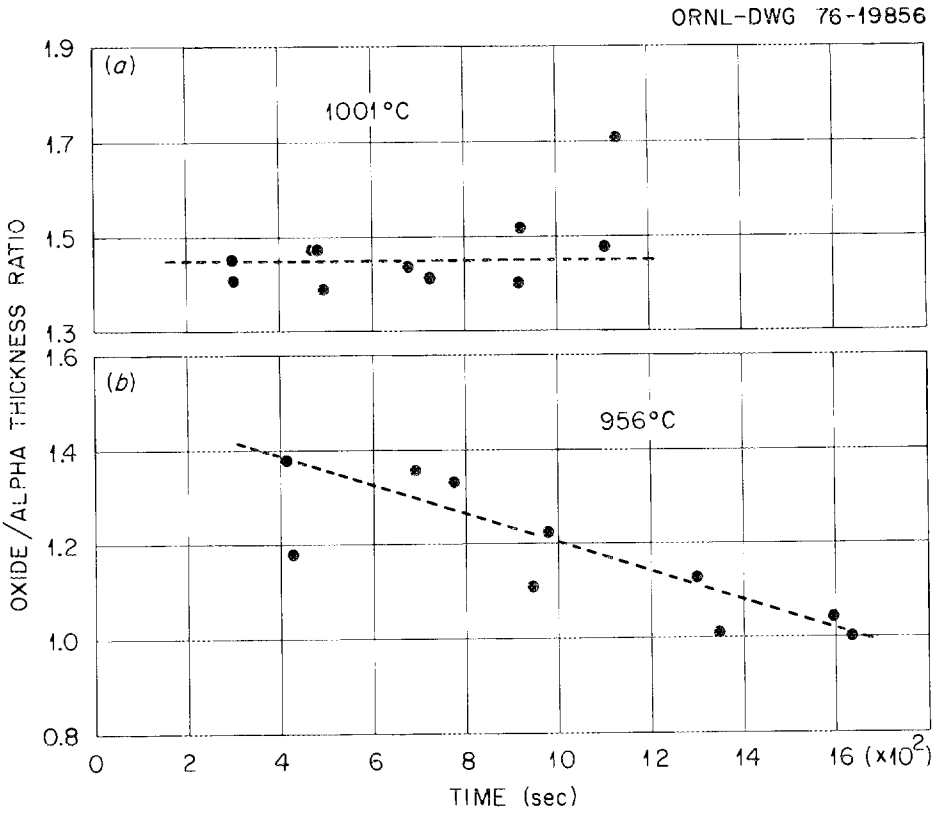

Fig. 32. Oxide/Alpha Ratios Plotted as a Function of Oxidation Time for Oxidation of Zircaloy-4 in Steam at 956 and 1001°C (1753–1834°F).

$\frac{\delta^2}{2}$ $(g/cm^2)^2/s = \tau \frac{d\tau}{dt}$, where τ is the total oxygen consumed in grams/cm^2.

Present Investigation (Based on Stoichiometric Oxide):

$$\frac{\delta^2}{2} = .1811 \exp[-39940/RT(°K)] \ (g/cm^2)^2/s$$

Present Investigation (Based on Stoichiometry Gradient in Oxide):

$$\frac{\delta^2}{2} = .1680 \exp[-39870/RT(°K)] \ (g/cm^2)^2/s$$

HOBSON[27] (Analysis of Complete Data Set):

$$\frac{\delta^2}{2} = .1553 \exp[-39290/RT(°K)] \ (g/cm^2)^2/s$$

HOBSON[27] (Point-by-Point Analyses):

$$\frac{\delta^2}{\frac{\tau}{2}} = .008311 \exp[-31110/RT(°K)] \ (g/cm^2)^2/s$$

BAKER-JUST[28]:

$$\frac{\delta^2}{\frac{\tau}{2}} = 2.0496 \exp[-45500/RT(°K)] \ (g/cm^2)^2/s$$

LEMMON[29]:

$$\frac{\delta^2}{\frac{\tau}{2}} = .028875 \exp[-34000/RT(°K)] \ (g/cm^2)^2/s$$

BIEDERMAN, et al.[17f]:

$$\frac{\delta^2}{\frac{\tau}{2}} = .01907 \exp[-33370/RT(°K)] \ (g/cm^2)^2/s$$

KLEPFER[30]:

$$\frac{\delta^2}{\frac{\tau}{2}} = .02203 \exp[-33500/RT(°K)] \ (g/cm^2)^2/s$$

KAWASAKI, et al.[31]:

$$\frac{\delta^2}{\frac{\tau}{2}} = .1994 \exp[-40500/RT(°K)] \ (g/cm^2)^2/s \quad .$$

LEISTIKOW, et al.[32] (approximated from graphical data)*

---

*The analytical expression derived for the data of Leistikow, et al. exhibits a comparatively large activation energy term, although the individual experimental rate constant values agree reasonably well with other recent data (see Appendix A). It appears that the high activation energy stems from the inclusion in this data set of the very low value of the parabolic rate constant determined at 900°C (1652°F), which produces a relatively steep slope for the Arrhenius plot. If this point is neglected, as suggested by our results that indicate the kinetics to be non-parabolic at this temperature, the activation energy decreases to less than 42000 cal/mole with a corresponding change in the pre-exponential term.

$$\frac{\delta^2}{\tau} = 2.142 \exp[-47640/RT(°K)] \ (g/cm^2)^2/s$$

$$(900°C \leq T \leq 1300°C)$$
$$(1652°F \leq T \leq 2372°F) \ .$$

While significant variations exist in both the pre-exponential and exponential terms of the various Arrhenius expressions, most of the rate constants predicted by these equations lie within a comparatively narrow band over the temperature range where they apply. Several of these data sets are compared in Fig. 33. As anticipated from an examination of the analytical expressions listed above, several of the sets are virtually identical. For example, the data of Kawasaki, et al. agrees very well with the present data; the "Klepfer correlation", as it is sometimes called, agrees well with the recent data of Biederman, et al. The Baker-Just expression is seen to produce values for the parabolic rate constant which diverge at elevated temperatures from the main body of experimental data. Further discussion of the extent of agreement among these various data sets can be found in Appendix A.

Scoping Tests

A number of tests were conducted in both of the steam oxidation apparatuses in order to assess the effect of certain experimental or system variables on the observed reaction behavior of Zircaloy. The effect of variations in the steam flow rate and steam injection temperature was determined by comparison of the data obtained in the MaxiZWOK apparatus with the standard data set. The effects of gaseous impurities in the steam and of small compositional variations in the Zircaloy were studied by additional experiments in the MiniZWOK apparatus.

Isothermal Oxidation Tests in MaxiZWOK

The MaxiZWOK apparatus was utilized to conduct oxidation tests at nominal temperatures of 900 and 1000°C (1652 and 1832°F) for comparison with the MiniZWOK data obtained for the same temperatures. The experimental conditions in MaxiZWOK, as discussed in a previous section, differ

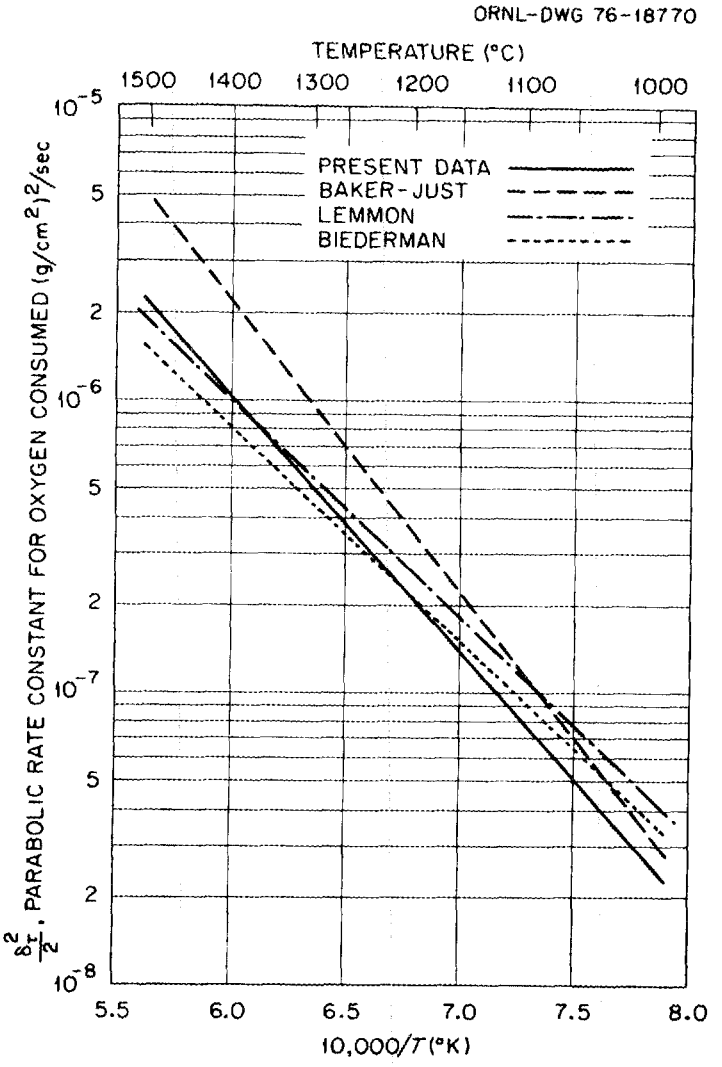

Fig. 33. A Comparison of Parabolic Rate Constants for Total Oxygen Consumption, $\frac{\delta_r^2}{2}$, from Several Investigators.

from those in MiniZWOK in two important ways: (1) the steam insertion temperature is approximately the same as the reaction temperature, and (2) the steam flow rate is maintained at about 360 g/min (0.8 lbs/min), which corresponds to a velocity of about 18 m/s (40 mph) in the reaction tube or more than order of magnitude higher than corresponding values in MiniZWOK.

Representative time-temperature excursions for experiments conducted at 900 and 1000°C (1652–1832°F) are shown in Figs. 34 and 35. Upon insertion of the specimen into the reaction tube, the specimen

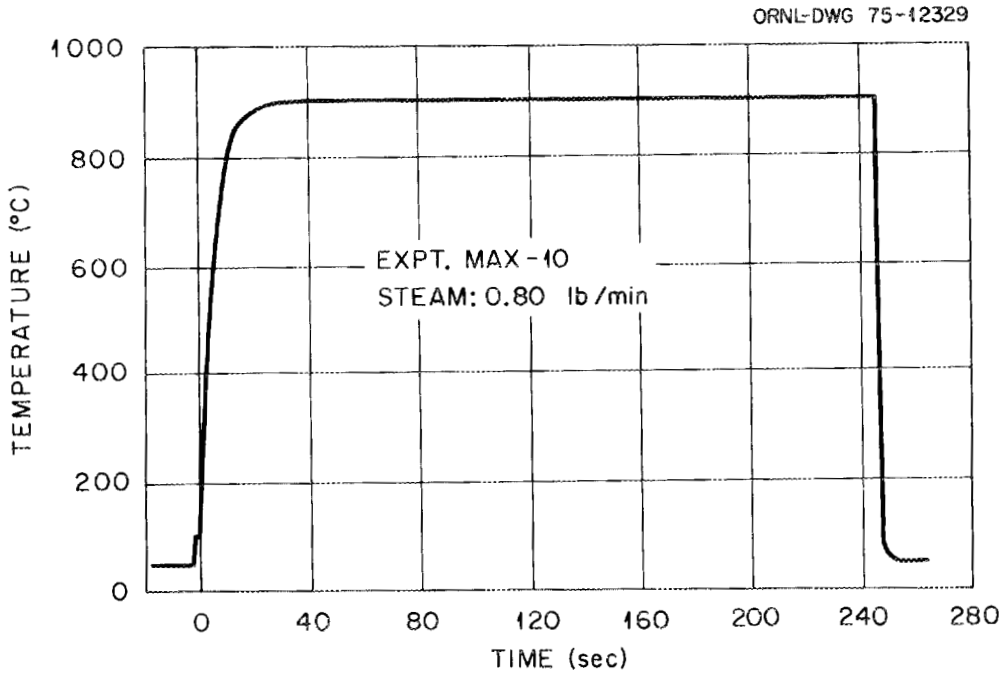

Fig. 34. Specimen Temperature as a Function of Time for MaxiZWOK Oxidation Experiment at 900°C (1652°F). Steam flow rate was 0.8 lb/min (6.0 g/s).

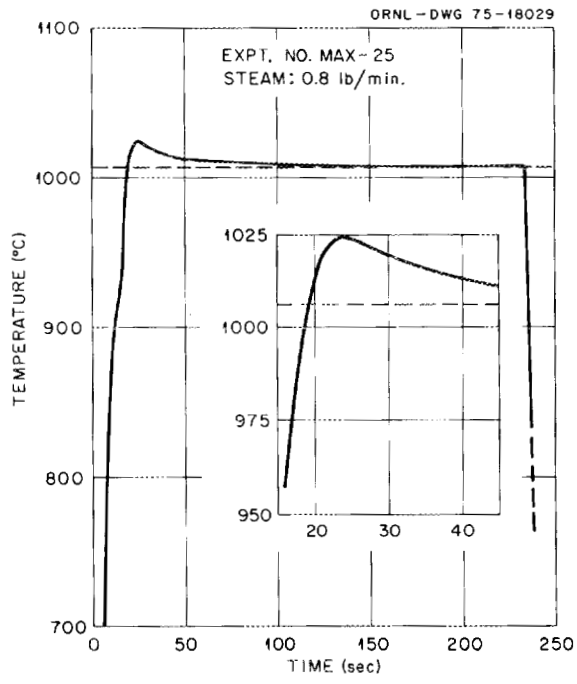

Fig. 35. Specimen Temperature as a Function of Time for MaxiZWOK Oxidation Experiment at 1000°C (1832°F). Steam flow rate was 0.8 lb/min (6 g/s).

temperature increases rapidly to the system temperature. A perturbation of the heating rate is observed due to the endothermic α-to-β transformation of the Zircaloy, which makes the rate of approach to temperature at 900°C (1652°F) somewhat sluggish. For reaction at 1000°C (1832°F), the exothermic heat of reaction is sufficient to drive the specimen temperature above that of its environment, creating the "overshoot" that was typical of MaxiZWOK experiments in this temperature range. In the particular case illustrated in Fig. 35, an overshoot of about 18°C (32°F) was observed before the specimen temperature began to return to its steady-state value, and several minutes were required for the effects of specimen self-heating to be dissipated. At the termination of each experiment, the specimen is withdrawn from the reaction chamber into the quench bath, and the temperature drops rapidly.

Data and Results — The basic experimental phase thickness measurements were obtained from the oxidized MaxiZWOK specimens using essentially the same procedures discussed in connection with the MiniZWOK apparatus. One exception in the procedure concerned the gathering of the phase thickness measurements since this apparatus produced specimens oxidized on both sides. Thus, measurements were made on each surface for comparison.

In order to check on the uniformity of the reaction, phase thickness measurements were made on several specimens as a function of angular position around their circumferences. While there were obvious local artifacts which affected the accuracy of some of the individual measurements, the circumferential variation of the phase thicknesses was considered small enough for MaxiZWOK specimens so that an "average" layer thickness was meaningful. Circumferential layer thickness measurements on the outer surfaces of two specimens oxidized at 900 and 1005°C (1652—1841°F) in the MaxiZWOK apparatus are presented in Figs. 36 and 37. Similar results were obtained for measurements on the inner surfaces. While no statistical treatment of these data has been performed, we have used such plots to justify the use of a simple data-gathering procedure involving few measurements: this procedure was to make only four measurements, approximately 90° apart, starting from a random point for both inner and outer surfaces of the specimen tube. Care

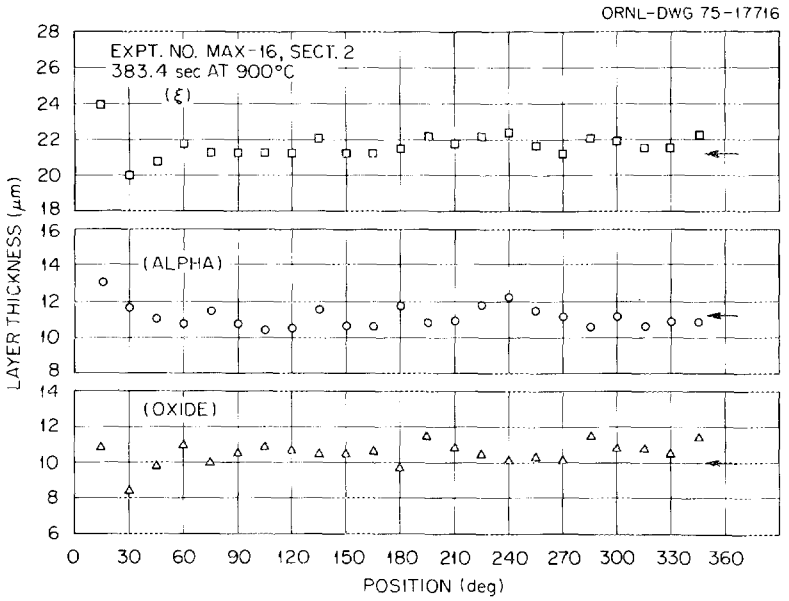

Fig. 36. Oxide, Alpha, and ξ Layer Thickness Measurements on Outer Surface of Oxidized Zircaloy-4 PWR Tube as a Function of Angular Position. Expt. MAX-16, 383.4 s at 900°C. Arrows indicate average values obtained from four measurements 90° apart starting at a random point.

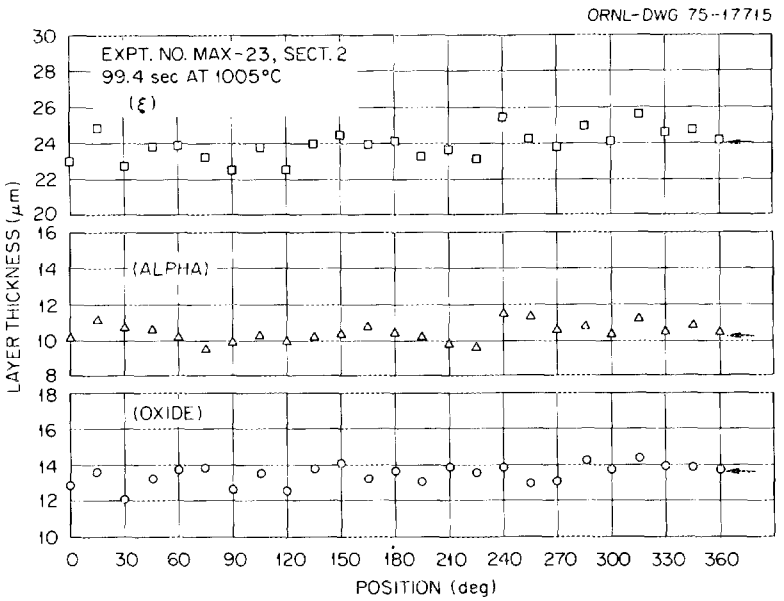

Fig. 37. Oxide, Alpha, and ξ Layer Thickness Measurements on Outer Surface of Oxidized Zircaloy-4 PWR Tube as a Function of Angular Position. Expt. MAX-23, 99.4 s at 1005°C. Arrows indicate average values obtained from four measurements 90° apart starting at a random point.

was taken to avoid obviously nonrepresentative areas. The thickness of each layer on each surface was then taken as a simple average of the four measurements. The arrows in Figs. 36 and 37 indicate the average thickness values obtained by this latter procedure for each layer. They are seen to agree well with the mean value computed from the entire data set. The MaxiZWOK data presented later in this report were obtained by this four-point method.

The equilibrium temperatures for the set of MaxiZWOK experiments nominally at 900°C (1652°F) varied from 897 to 902°C (1647–1666°F); at 1000°C (1832°F), the range was 1000 to 1009°C (1832–1848°F). Corresponding isothermal temperatures of 900 and 1005°C (1652–1841°F) were chosen to represent each of these data sets. On this basis, and the measured time-temperature excursion for each experiment, the effective time at temperature for a true isothermal oxidation was calculated as previously described.

Correlation of Data and Comparisons — Values of the oxide and alpha phase thickness measurements for the sets of oxidation experiments in MaxiZWOK at 900 and 1005°C (1652–1841°F) are presented in Tables 20 and 21. Measurements for both outer and inner surfaces of the tube are reported. It should be emphasized here that the consistency of the alpha layer thickness measurements is not as high as that obtained after oxidation at higher temperatures because of difficulties in defining the α/β or $\alpha/(\alpha+\beta)$ interface.

A parabolic plot for the growth of the outer oxide layer at 900°C (1652°F) is given in Fig. 38, which shows the extent of the departure from ideal parabolic behavior and also compares this data set with the MiniZWOK results for oxide growth at 905°C (1661°F). (Note that four additional points at short times were added to the MiniZWOK data set to aid in this comparison. These four data points were not included in Table 5.) The very good agreement between these two data sets is regarded as evidence that steam flow rate and steam insertion temperature do not affect significantly the kinetics of the steam oxidation of Zircaloy, at least in this temperature range.

Table 20. Steam Oxidation of Sandvik Zircaloy-4 PWR Tubing at 900°C (1652°F) MaxiZWOK Data

Expt. No.	Time (s)	Outer Surface			Inner Surface		
		Oxide (μm)	Alpha (μm)	Total Oxygen Consumed (mg/cm^2)	Oxide (μm)	Alpha (μm)	Total Oxygen Consumed (mg/cm^2)
Max-11	637.3	12.8	15.3	2.314	12.0	14.1	2.163
Max-12	75.8	5.6	5.0	.968	4.9	4.7	.856
Max-13	1194.0	15.7	18.6	2.833	14.4	18.0	2.624
Max-14	136.4	7.0	7.9	1.253	6.6	7.9	1.193
Max-15	46.3	5.0	3.9	.852	3.8	3.9	.670
Max-16	383.4	9.9	11.3	1.776	9.4	11.0	1.693
Max-17	857.7	13.2	17.5	2.431	12.6	17.9	2.350
Max-28	2291.1	19.6	21.7	3.500	18.3	21.4	3.296

Table 21. Steam Oxidation of Sandvik Zircaloy-4 PWR Tubing at 1005°C (1841°F) MaxiZWOK Data

Expt. No.	Time (s)	Outer Surface			Inner Surface		
		Oxide (μm)	Alpha (μm)	Total Oxygen Consumed (mg/cm^2)	Oxide (μm)	Alpha (μm)	Total Oxygen Consumed (mg/cm^2)
Max-21	367.4	25.8	17.6	4.547	24.6	17.7	4.370
Max-22	866.5	40.6	26.0	7.104	38.3	24.9	6.727
Max-23	99.4	13.7	10.2	2.436	11.8	10.1	2.147
Max-24	640.5	35.3	22.6	6.173	33.3	22.3	5.865
Max-25	234.4	20.6	14.1	3.632	20.1	13.6	3.543
Max-26	512.4	31.0	19.3	5.410	30.4	18.3	5.292

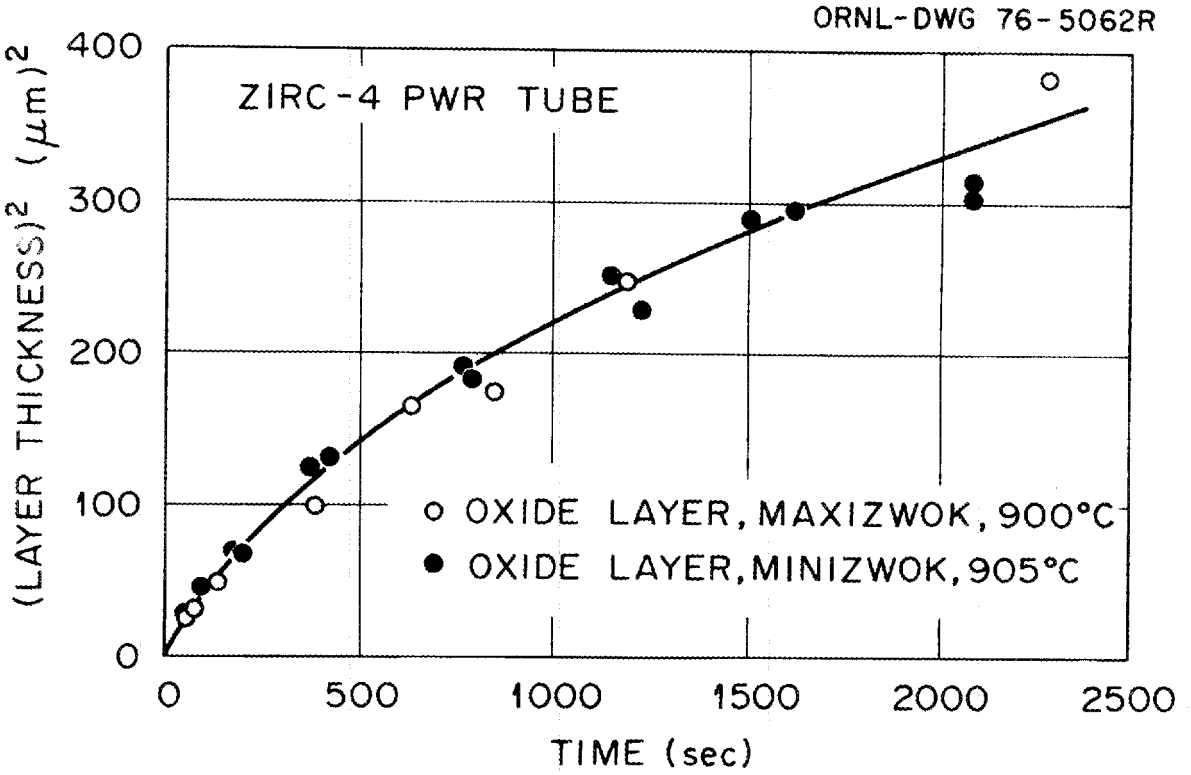

Fig. 38. Non-Parabolic Growth of Oxide Layer on Zircaloy-4 PWR Tube in the Mini- and MaxiZWOK Apparatuses at ∿ 900°C (1652°F).

The parabolic plot for the 1005°C (1841°F) MaxiZWOK data set is presented in Fig. 39, which shows the behavior for both outer and inner surfaces of the tube. The kinetic behavior at this temperature is clearly parabolic with only minor differences observed for the layer growth on the outer and inner surfaces. Small differences of this sort may be due to geometrical effects or to the different final inner-outer surface treatments used by the tube manufacturer.

A list of the parabolic rate constants for the kinetic parameters (where they apply) for oxidation in MaxiZWOK is given in Table 22. While the 900°C data compare very favorably with the values predicted from the MiniZWOK data obtained at 905°C, the comparison is not as good for the data sets at nominally 1000°C. Although the MaxiZWOK data at this temperature suggest a slightly higher value for the parabolic rate constant for oxide and alpha growth, it is interesting to observe that the actual MiniZWOK rate constant values for reaction at 1001°C are

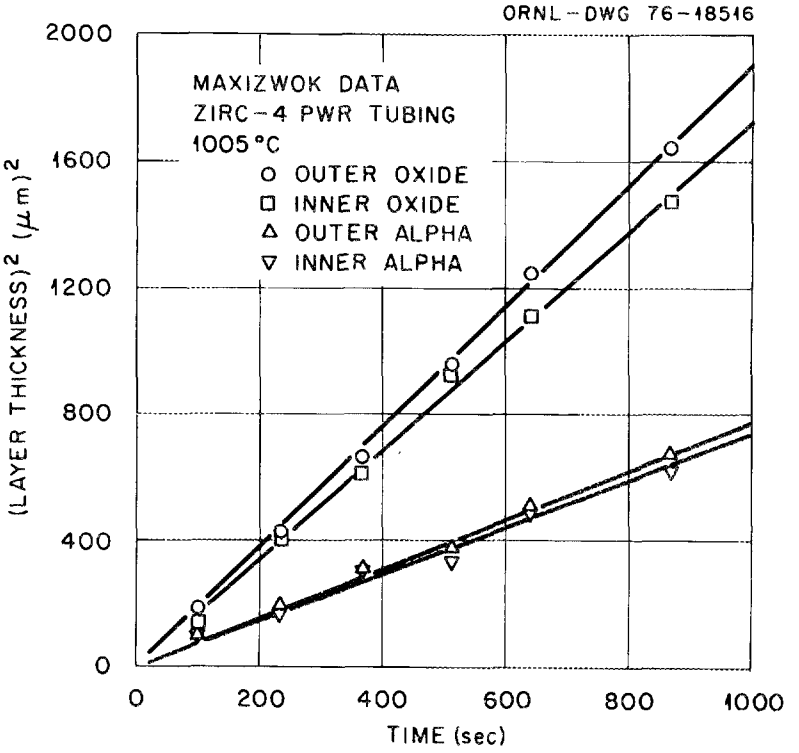

Fig. 39. Oxidation of Zircaloy-4 PWR Tube in the MaxiZWOK Apparatus at 1005°C.

Table 22. Parabolic Rate Constants for Oxidation of Sandvik Zircaloy-4 PWR Tubes in MaxiZWOK Apparatus at 900 and 1005°C (1652–1841°F)

Temperature (°C)	Temperature (°F)	Parameter	Parabolic Rate Constant $\frac{\delta^2}{2} \times 10^8$	Dev.[a] (%)
900	1652	Oxide (outer)	non-parabolic	
900	1652	Alpha (outer)	.123 cm^2/s	26.4
900	1652	Xi (outer)	non-parabolic	
900	1652	Total Ox. (outer)	non-parabolic	
900	1652	Oxide (inner)	non-parabolic	
900	1652	Alpha (inner)	.119 cm^2/s	26.2
900	1652	Xi (inner)	non-parabolic	
900	1652	Total Ox. (inner)	non-parabolic	
1005	1841	Oxide (outer)	.949 cm^2/s	4.2
1005	1841	Alpha (outer)	.393 cm^2/s	9.9
1005	1841	Xi (outer)	2.562 cm^2/s	4.2
1005	1841	Total Ox. (outer)	2.908 $(g/cm^2)^2/s$	3.6
1005	1841	Oxide (inner)	.858 cm^2/s	6.0
1005	1841	Alpha (inner)	.368 cm^2/s	16.4
1005	1841	Xi (inner)	2.349 cm^2/s	4.8
1005	1841	Total Ox. (inner)	2.649 $(g/cm^2)^2/s$	4.3

[a]Maximum uncertainty at 90% confidence level.

somewhat lower than those predicted by the Arrhenius curves considering each data set as a whole. Additionally, the fact that this temperature is within a very critical range regarding the crystal structure of the growing oxide may be responsible for these small differences in rates. This point will be discussed later with regard to transient-temperature oxidation behavior. It should also be pointed out that one additional experiment in MaxiZWOK, run under conditions where the furnace temperature was higher than the steam temperature, produced a single data point at 1050°C that agreed within experimental uncertainty with the standard data set.

Thus we argue that the variations in steam flow rate (at least for flow rates above those necessary to prevent hydrogen blanketing) and steam insertion temperature produce little effect on the isothermal rate of oxidation of Zircaloy-4. Of course, steam flow rate and temperature are recognized as important factors in determining the temperature response (i.e., the extent of temperature rise due to specimen self-heating) of a specimen in a given environment.

Mixed Gas Experiments

A number of scoping tests were performed in which specimens of the standard Zircaloy-4 PWR tubes were oxidized in steam to which small amounts of potentially reactive gases had been added. Experiments were conducted at nominally 1101 and 1304°C (2014—2379°F) with either 10 mole % N_2, 10 mole % O_2, or 5 mole % H_2 added to the flowing steam. These experiments were conducted in the MiniZWOK apparatus to which a gas injection device had been added. The gas flow rates were monitored with a calibrated flow-meter. In order to insure adequate mixing of the impurity gases with the steam, they were injected at a point just above the steam boiler.

The oxidation and data-gathering procedures used in these tests were identical to those reported previously for the basic set of isothermal data. Oxide and alpha layer thicknesses were determined at each monitor thermocouple position. The reaction time at the assigned reaction temperature was calculated by an integration scheme which

utilized the CODAS output for the entire temperature excursion. These data, plus a calculation of the total oxygen consumed by each specimen, are presented in Tables 23 through 28.

The tabulated data are presented in graphical form in Figs. 40 through 45. These are plots of the square of the oxide and alpha layer thicknesses as functions of time for the various experimental conditions. In each figure, the straight lines represent the behavior predicted for the rates of layer thickening by the analytical expressions derived from the basic data set for oxidation in pure steam.

It will be noted that in some instances the individual data points from the scoping tests differ from the baseline correlations. However, because of the comparatively small number of tests used to define the rate curves in the scoping experiments, we feel that these differences are not significant with the possible exception of the results for oxygen additions at 1101°C (2014°F).

For example, Fig. 40 compares the baseline data with those obtained after oxidation at 1101°C (2014°F) in steam containing 10 mole % N_2. It is obvious in this case that the differences in the kinetic behavior for oxide and alpha layer growth are insignificant. Indeed, the rate constants for ϕ and α calculated from the scoping test data are virtually identical to the "standard" values. On the other hand, for tests at 1101°C (2014°F) in steam containing 10 mole % O_2, Fig. 41 indicates a small, but consistent effect: the oxide layer appears to grow a little faster under these conditions, and because of the resulting enhancement of the rate of movement of the oxide-alpha boundary, the rate of growth of the alpha layer is reduced. However, while the rate constant for oxide layer growth is about 19% larger, the statistical significance of this difference is marginal. In Fig. 42, the addition of 5 mole % H_2 to the steam is shown to exhibit a negligible effect on the oxidation kinetics at 1101°C (2014°F).

The comparisons for the tests at 1304°C (2379°F), shown in Figs. 43, 44 and 45, similarly indicate no dramatic kinetic effects of impurity gas additions (at the levels studied) to the steam. Even for the case of the 10 mole % oxygen addition, the comparison with the standard data is very good. Thus, the only scoping test involving impurity gas

Table 23. Steam Oxidation of Sandvik Zircaloy-4 PWR Tubing at 1101°C (2014°F) (10 mol % Nitrogen Added to Steam)

Expt. No.	Time (s)	Layer Thickness		Total Oxygen (mg/cm^2)
		Oxide (μm)	Alpha (μm)	
S-170-TC-2	168.1	27.7	25.5	5.31
S-170-TC-3	161.7	28.4	25.9	5.42
S-171-TC-2	147.1	28.9	25.2	5.45
S-171-TC-3	162.2	27.5	23.4	5.21
S-172-TC-2	556.6	49.2	43.3	9.39
S-172-TC-3	543.1	48.6	42.8	9.28
S-173-TC-2	519.6	48.1	43.2	9.20
S-173-TC-3	523.3	47.2	40.0	8.97
S-175-TC-2	26.5	12.6	11.7	2.39
S-175-TC-3	28.5	13.5	12.1	2.55

Table 24. Steam Oxidation of Sandvik Zircaloy-4 PWR Tubing at 1101°C (2014°F) (10 mol % Oxygen Added to Steam)

Expt. No.	Time (s)	Layer Thickness		Total Oxygen (mg/cm^2)
		Oxide (μm)	Alpha (μm)	
S-188-TC-2	160.5	29.8	23.7	5.56
S-188-TC-3	157.5	29.5	24.0	5.52
S-189-TC-2	185.7	32.7	25.3	6.08
S-189-TC-3	177.5	32.2	24.7	5.97
S-191-TC-2	545.8	53.0	36.1	9.75
S-191-TC-3	510.0	51.2	34.1	9.40

Table 25. Steam Oxidation of Sandvik Zircaloy-4 PWR Tubing at 1101°C (2014°F) (5 mol % Hydrogen Added to Steam)

Expt. No.	Time (s)	Layer Thickness		Total Oxygen (mg/cm^2)
		Oxide (μm)	Alpha (μm)	
S-180-TC-2	169.8	28.2	25.5	5.39
S-180-TC-3	171.1	28.1	26.1	5.39
S-181-TC-2	182.4	29.1	27.2	5.58
S-181-TC-3	181.6	29.4	27.0	5.62
S-182-TC-2	579.9	52.0	43.2	9.82
S-182-TC-3	523.6	51.0	39.8	9.54
S-183-TC-2	585.3	51.0	42.4	9.66
S-183-TC-3	546.0	48.1	39.3	9.10

Table 26. Steam Oxidation of Sandvik Zircaloy-4 PWR Tubing at 1304°C (2379°F) (10 mol % Nitrogen Added to Steam)

Expt. No.	Time (s)	Layer Thickness		Total Oxygen (mg/cm^2)
		Oxide (μm)	Alpha (μm)	
S-174-TC-2	31.5	28.4	32.5	5.92
S-174-TC-3	27.1	26.7	31.9	5.60
S-176-TC-2	30.5	28.1	33.2	5.89
S-176-TC-3	31.5	27.7	33.8	5.85
S-177-TC-2	30.4	28.2	33.4	5.91
S-177-TC-3	25.5	25.6	30.0	5.36
S-178-TC-2	158.4	60.7	74.2	12.87
S-178-TC-3	157.0	60.1	71.2	12.68
S-179-TC-2	170.1	60.7	74.4	12.93
S-179-TC-3	167.6	61.5	73.4	13.00

Table 27. Steam Oxidation of Sandvik Zircaloy-4 PWR Tubing at 1304°C (2379°F) (10 mol % Oxygen Added to Steam)

Expt. No.	Time (s)	Layer Thickness		Total Oxygen (mg/cm^2)
		Oxide (μm)	Alpha (μm)	
S-192-TC-2	27.6	26.3	29.7	5.48
S-192-TC-3	26.5	26.6	31.2	5.55
S-193-TC-2	25.8	26.6	28.3	5.46
S-193-TC-3	24.7	27.2	28.4	5.54
S-194-TC-2	147.5	57.7	65.7	12.10
S-194-TC-3	128.0	56.2	62.0	11.67
S-195-TC-2	143.1	57.0	63.2	11.90
S-195-TC-3	147.3	58.8	66.2	12.28

Table 28. Steam Oxidation of Sandvik Zircaloy-4 PWR Tubing at 1304°C (2379°F) (5 mol % Hydrogen Added to Steam)

Expt. No.	Time (s)	Layer Thickness		Total Oxygen (mg/cm^2)
		Oxide (μm)	Alpha (μm)	
S-184-TC-2	33.8	29.5	35.1	6.19
S-184-TC-3	34.4	29.1	35.7	6.15
S-185-TC-2	32.9	28.5	34.7	6.02
S-185-TC-3	28.4	26.7	32.5	5.63
S-186-TC-2	173.8	60.2	72.1	12.80
S-186-TC-3	157.4	58.2	68.9	12.32
S-187-TC-2	152.4	57.9	68.1	12.23
S-187-TC-3	160.2	59.7	70.5	12.61

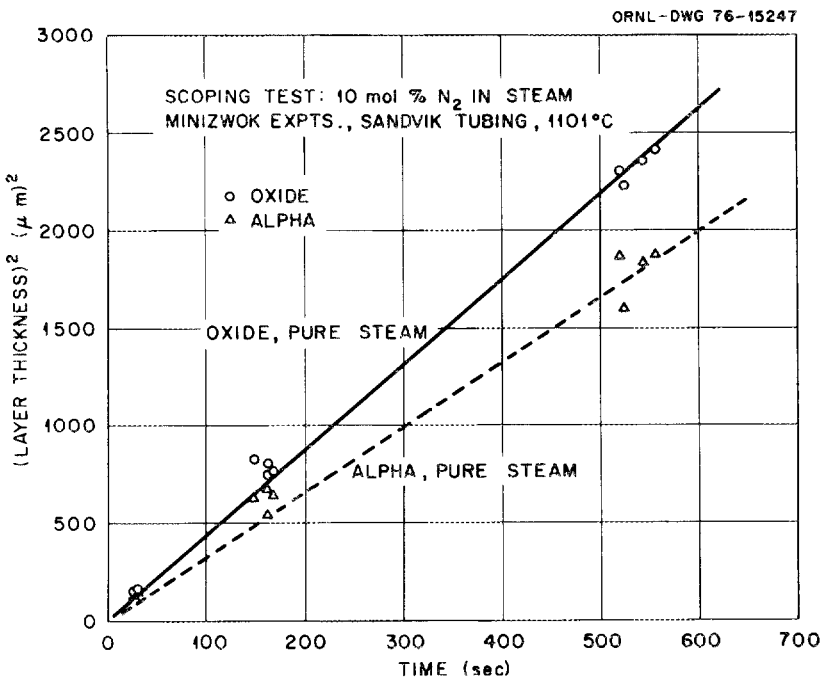

Fig. 40. Oxidation of Sandvik Zircaloy-4 PWR Tubing at 1101°C (2014°F) in Steam Containing 10 Mole % N_2. Solid and dashed lines represent parabolic oxide and alpha layer growth in pure steam.

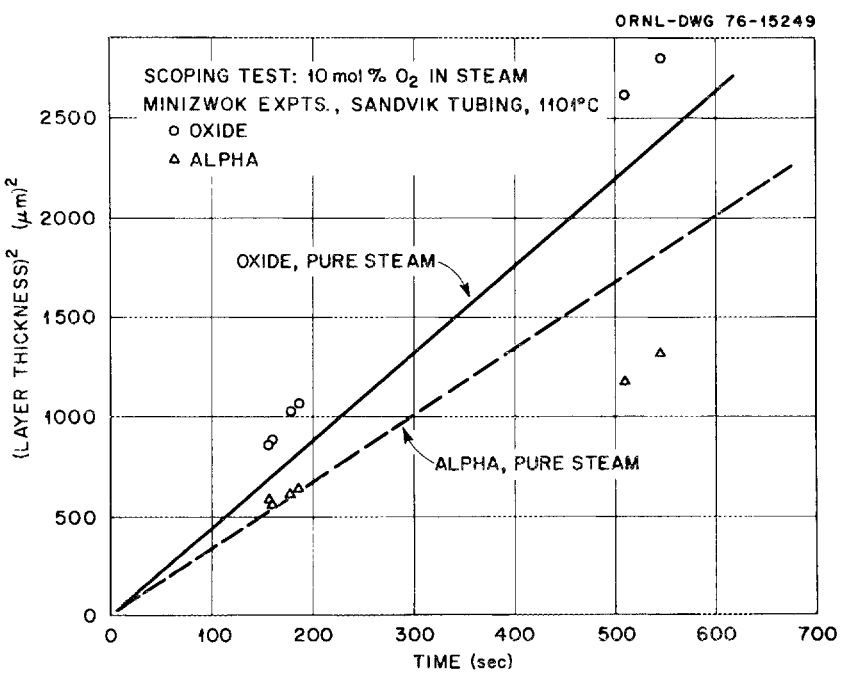

Fig. 41. Oxidation of Sandvik Zircaloy-4 PWR Tubing at 1101°C (2014°F) in Stam Containing 10 Mole % O_2. Solid and dashed lines represent parabolic oxide and alpha layer growth in pure steam.

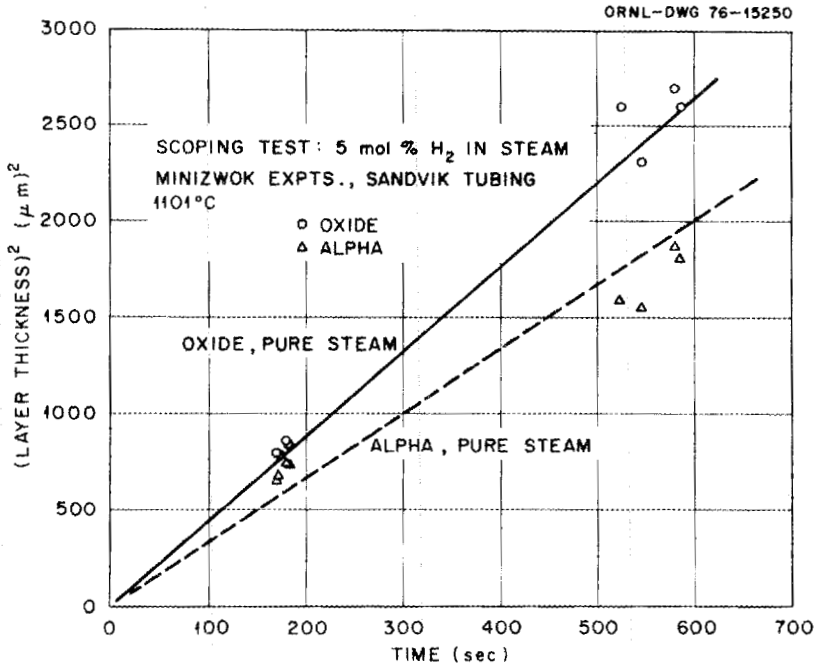

Fig. 42. Oxidation of Sandvik Zircaloy-4 PWR Tubing at 1101°C (2014°F) in Steam Containing 5 Mole % H_2. Solid and dashed lines represent parabolic oxide and alpha layer growth in pure steam.

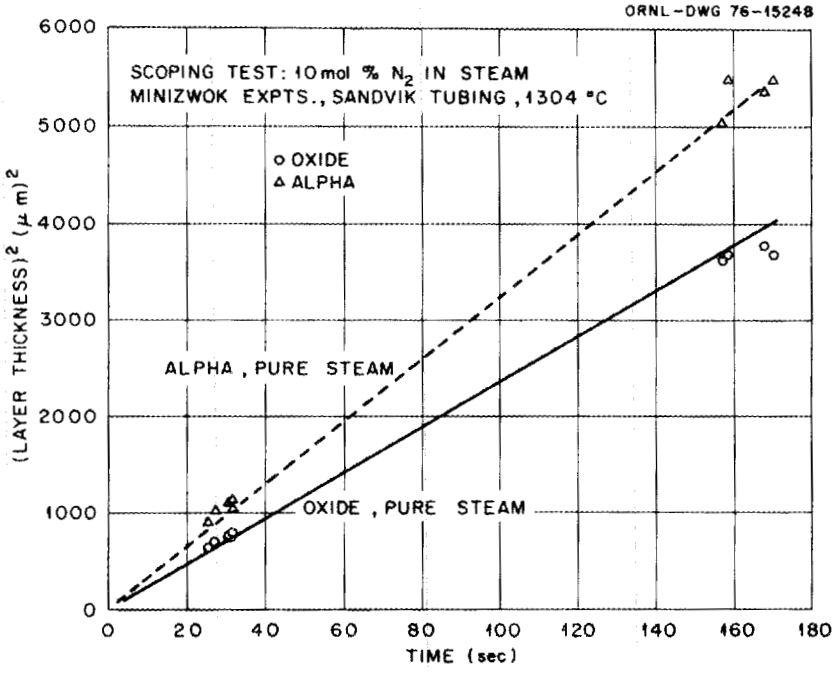

Fig. 43. Oxidation of Sandvik Zircaloy-4 PWR Tubing at 1304°C (2379°F) in Steam Containing 10 Mole % N_2. Solid and dashed lines represent parabolic oxide and alpha layer growth in pure steam.

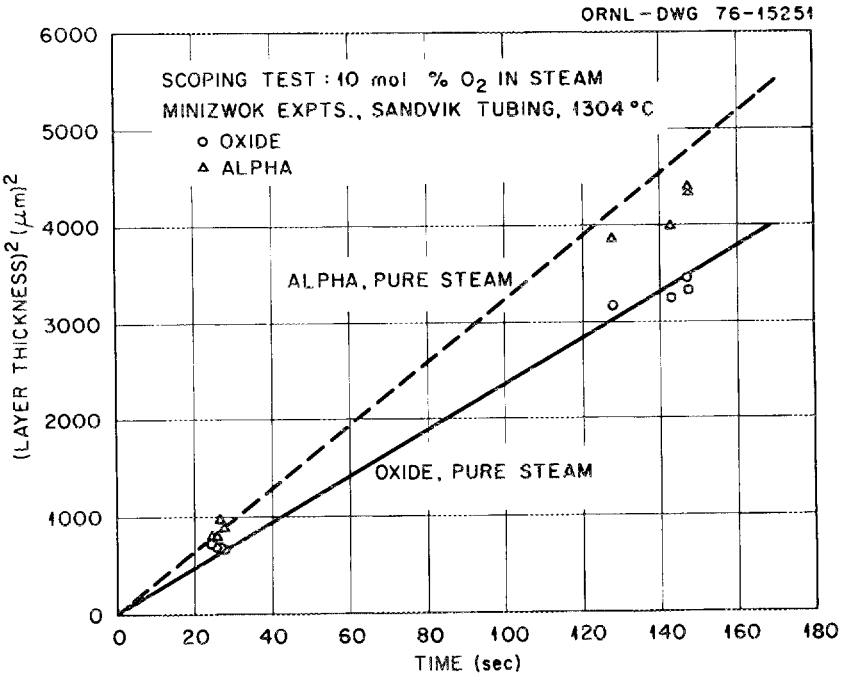

Fig. 44. Oxidation of Sandvik Zircaloy-4 PWR Tubing at 1304°C (2379°F) in Steam Containing 10 Mole % O_2. Solid and dashed lines represent parabolic oxide and alpha layer growth in pure steam.

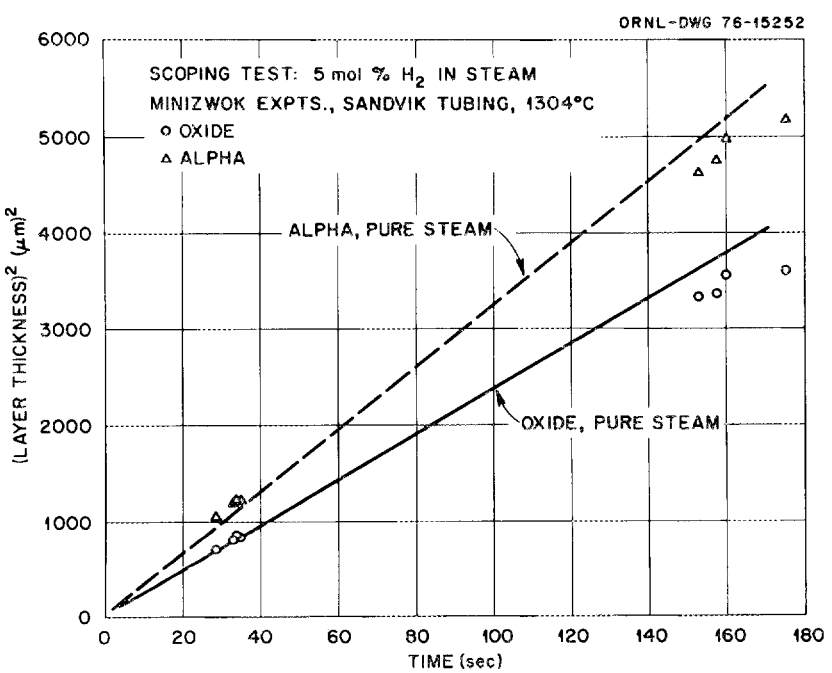

Fig. 45. Oxidation of Sandvik Zircaloy-4 PWR Tubing at 1304°C (2379°F) in Steam Containing 5 Mole % H_2. Solid and dashed lines represent parabolic oxide and alpha layer growth in pure steam.

additions to the steam in which (possibly) a kinetic effect was observed was the set for oxidation at 1101°C (2014°F) in steam containing 10 mole % O_2.

While the number of experiments in these scoping tests was relatively small, it is nevertheless possible, as mentioned above, to compute parabolic rate constants from the oxide and alpha layer thickness measurements for each set. These rate constant values are compared with those of the baseline data set in Tables 29 and 30. With the one exception, the maximum difference observed in the rate constants was less than 10%, indicating again that for the particular concentration levels studied, the influence of the gaseous impurities on the kinetics of oxidation was very small.

Alloy Composition Variation

In order to assess the possible influence of small differences in the alloy composition of reactor-grade Zircaloy-4 tubing on the oxidation kinetics, measurements were made at two temperatures on specimens obtained from an alternate tubing supply that we have designated Batch B*. Using the identical equipment and procedures documented previously, steam oxidation experiments were conducted at 1153 and 1504°C (2107–2739°F) for comparison with the standard Sandvik tubing data for these same temperatures.

The data obtained for oxidation of the Batch B tubing are given in Tables 31 and 32. Also listed in these tables are the calculated values for the total oxygen consumed by the specimens. Parabolic plots for the thickening of the oxide and alpha layer are presented in Figs. 46 and 47, which include the comparisons to the baseline Sandvik tubing data taken from the analytical representations. These comparisons show insignificant differences in the rates of alpha layer growth at these temperatures and small but apparently consistent differences in the rates of oxide layer growth. Tabulated values of the rate

*Reactor grade PWR Zircaloy-4 tubing, Batch B. Composition (wt %): 1.3 Sn, 0.22 Fe, 0.10 Cr, 0.125 O, 0.010 C, 0.0015 N, and 0.0015 H.

Table 29. Comparison of Parabolic Rate Constants for Oxidation in Steam at 1101°C (2014°F) (Impurity Gas Additions)

Data Set	Parabolic Rate Constant[a] (oxide) $\frac{\delta^2}{2}\phi$, $cm^2/s \times 10^8$	Difference[b] (%)	Parabolic Rate Constant (alpha) $\frac{\delta^2}{2}\alpha$, $cm^2/s \times 10^8$	Difference (%)
Basic (pure steam)	2.198		1.673	
10 mol % N_2 added	2.201 ± 5.4%	+.1	1.698 ± 8.4%	+1.5
10 mol % O_2 added	2.618 ± 8.1%	+19.1	1.269 ± 34.9%	−24.1
5 mol % H_2 added	2.289 ± 9.1%	+4.1	1.564 ± 16.0%	−6.5

[a]Error limits indicate uncertainty at 90% confidence level.

[b]Percent difference compared to baseline value.

Table 30. Comparison of Parabolic Rate Constants for Oxidation in Steam at 1304°C (2379°F) (Impurity Gas Additions)

Data Set	Parabolic Rate Constant[a] (oxide) $\frac{\delta_\phi^2}{2}$, $cm^2/s \times 10^7$	Difference[b] (%)	Parabolic Rate Constant (alpha) $\frac{\delta_\alpha^2}{2}$, $cm^2/s \times 10^7$	Difference[b] (%)
Basic (pure steam)	1.194		1.619	
10 mol % N_2 added	1.136 ± 4.1%	−4.9	1.652 ± 3.9%	+2.0
10 mol % O_2 added	1.170 ± 6.3%	−2.0	1.467 ± 5.2%	−9.3
5 mol % H_2 added	1.087 ± 5.5%	−9.0	1.531 ± 6.0%	−5.4

[a]Error limits indicate uncertainty at 90% confidence level.

[b]Percent difference compared to baseline value.

Table 31. Steam Oxidation of Batch B Zircaloy-4 PWR Tubing at 1153°C (2107°F)

Expt. No.	Time (s)	Layer Thickness		Total Oxygen (mg/cm^2)
		Oxide (μm)	Alpha (μm)	
AB-197-TC-2	239.4	37.4	39.5	7.51
AB-197-TC-3	231.7	37.1	39.0	7.44
AB-198-TC-2	103.5	24.2	30.7	5.01
AB-198-TC-3	103.1	24.2	30.3	5.00
AB-202-TC-2	182.4	32.8	35.1	6.59
AB-202-TC-3	174.3	32.0	34.1	6.43
AB-203-TC-2	294.4	41.0	43.9	8.26
AB-203-TC-3	284.0	40.1	42.9	8.08
AB-206-TC-2	246.6	37.6	37.2	7.48
AB-206-TC-3	241.0	38.0	37.7	7.55
AB-207-TC-2	181.6	33.4	36.7	6.73
AB-207-TC-3	165.4	31.4	35.0	6.35
AB-208-TC-2	386.0	46.4	46.0	9.25
AB-208-TC-3	374.3	45.5	44.7	9.06
AB-209-TC-2	101.8	25.7	29.3	5.19
AB-209-TC-3	92.7	24.4	28.5	4.95

Table 32. Steam Oxidation of Batch B Zircaloy-4 PWR Tubing at 1504°C (2739°F)

Expt. No.	Time (s)	Layer Thickness		Total Oxygen (mg/cm^2)
		Oxide (μm)	Alpha (μm)	
AB-210-TC-2	25.7	44.6	68.1	10.33
AB-210-TC-3	27.0	44.9	70.8	10.50
AB-211-TC-2	28.7	46.8	74.3	10.95
AB-211-TC-3	26.3	44.7	68.2	10.37
AB-212-TC-2	16.2	36.9	56.0	8.49
AB-212-TC-3	16.2	36.9	54.7	8.45
AB-213-TC-2	17.2	38.0	53.6	8.61
AB-213-TC-3	16.8	36.4	56.9	8.47
AB-214-TC-2	40.1	59.8	84.3	13.50
AB-214-TC-3	37.5	54.0	81.6	12.48
AB-215-TC-2	35.7	51.8	80.1	12.06
AB-215-TC-3	34.2	51.8	77.1	11.93
AB-216-TC-2	7.7	27.3	38.8	6.14
AB-216-TC-3	8.1	27.4	38.5	6.17
AB-217-TC-2	7.3	25.0	38.0	5.75
AB-217-TC-3	6.9	24.5	36.3	5.60
AB-218-TC-3	47.9	62.0	89.7	14.17
AB-219-TC-2	51.4	61.6	94.8	14.34
AB-219-TC-3	49.8	61.4	95.6	14.31

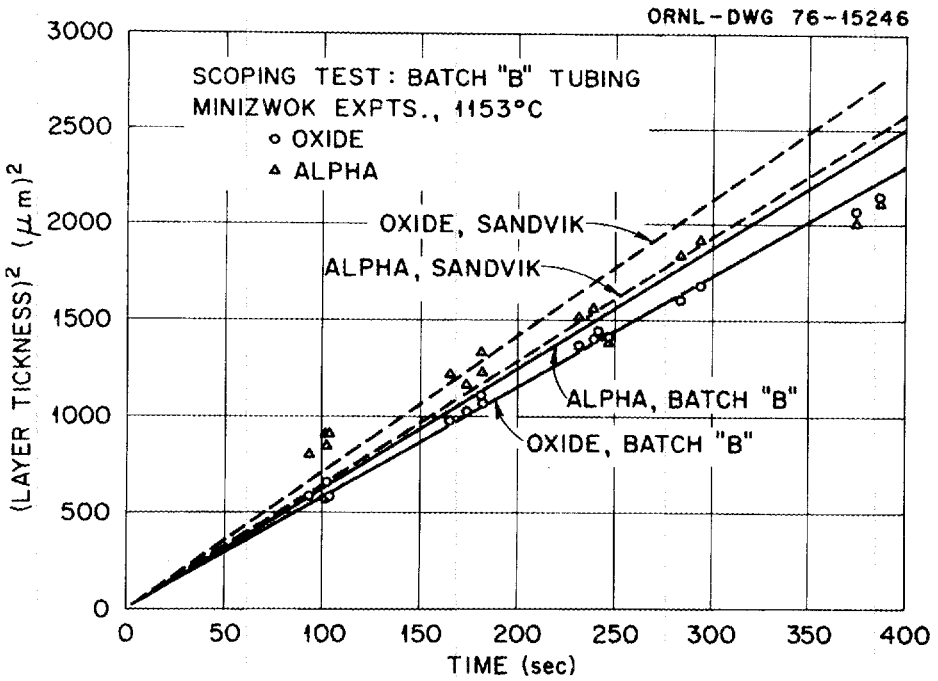

Fig. 46. Steam Oxidation of Batch B Zircaloy-4 PWR Tubing at 1153°C (2107°F). Dashed lines represent parabolic oxide and alpha layer growth on Sandvik tubing.

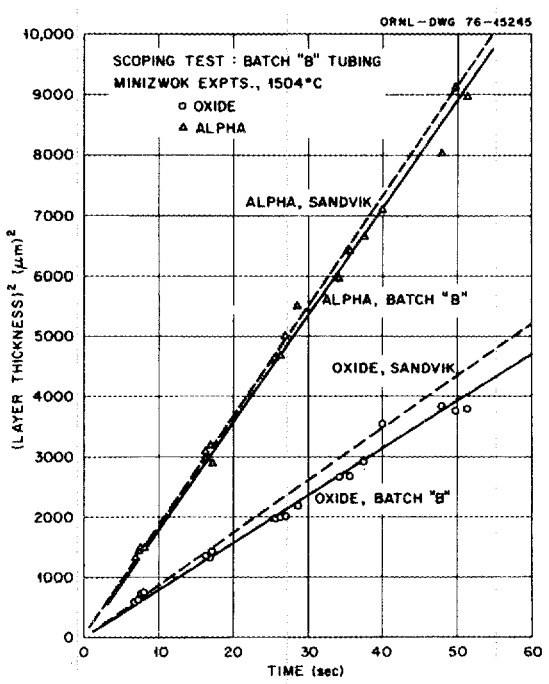

Fig. 47. Steam Oxidation of Batch B Zircaloy-4 PWR Tubing at 1504°C (2739°F). Dashed lines represent parabolic oxide and alpha layer growth on Sandvik tubing.

constants calculated from these data are given in Table 33. The percentage difference in the rate constants for oxide layer growth for the two batches of tubing is small in both cases, but is measurably less at the higher temperature.

Summary of Isothermal Scoping Test Results

(1) Variations in the steam flow rate from about 1 m/s to about 18 m/s exhibited only minor effects on the oxidation of Zircaloy-4 PWR tubing. A few preliminary tests[1c] were run with steam velocities as low as 0.2 m/s with similar results. These results are consistent with those of Biederman, et al.[17] who reported no effects even under conditios of no forced steam flow (only convective currents). Kawasaki, et al.[31] also reported no measurable effect of steam flow rate for experiments at 1000°C (1832°F) where the flow rate was varied from about 0.2 to 1.6 m/s.

(2) Variations in the steam injection temperature from approximately 150°C (202°F) to above 1000°C (1832°F) produced no significant perturbation of the oxidation kinetics. Biederman, et al.[17] reported no measurable effects for steam superheat temperatures from 66 to 316°C (150–600°F).

(3) The composition of our alternate supply of PWR tubing was slightly different from that of the standard Sandvik tubing, and this compositional variation produced only a small but consistent variation in the rate of growth of the oxide layer; alpha layer growth was unchanged. Biederman, et al.,[17] reported no significant differences in oxidation behavior for three batches of tubing, perhaps because only very small compositional variations existed.

(4) Additions of 10 mole % N_2, 10 mole % O_2 or 5 mole % H_2 to the steam were shown to have only minor, if any, effects on the oxidation rate of Zircaloy tubing.

COMPUTER CODES AND TRANSIENT-TEMPERATURE OXIDATION

Two computer codes have been developed that permit, on the basis of an ideal model, the calculation of important kinetic and oxygen

Table 33. Comparison of Parabolic Rate Constants for Sandvik and Batch 'B' Tubing at 1153 and 1504°C

Data Set	Parabolic Rate Constant[a] (oxide) $\frac{\delta_\phi^2}{2}$, $cm^2/s \times 10^8$	Difference (%)	Parabolic Rate Constant[a] (alpha) $\frac{\delta_\alpha^2}{2}$, $cm^2/s \times 10^8$	Difference[b] (%)
Sandvik, 1153°C	3.551		3.183	
Batch 'B', 1153°C	2.875 ± 4.3%	−19.0	3.112 ± 16.6%	−2.2
Sandvik, 1504°C	43.34		91.27	
Batch 'B', 1504°C	39.16 ± 5.2%	−9.6	89.17 ± 3.4%	−2.3

[a]Error limits represent uncertainty at 90% confidence level.

[b]Percent difference compared to baseline value.

distribution parameters during any given temperature excursion for Zircaloy in steam.

SIMTRAN is a Fortran IV computer program written for the IBM 360/91 system which solves SIMultaneously the TRANsport equations for both heat and mass flow for the one dimensional, multiphase, moving boundary, transient temperature transport problem in a finite geometry system defined by cylindrical coordinates. The code utilizes an ideal diffusion model based on a finite difference analysis that requires uniform layer growth of all phases and assumes the existence of thermodynamic equilibrium at all interfaces at all times.

BILD5 is a much simpler code that is a modified version of a program used in some prior analyses of the oxidation of Zircaloy.[33,34] It predicts oxide thickness, alpha thickness, and total oxygen consumption by an integration of the various rate constants for a given time-temperature cycle. A finite difference method is used to calculate the oxygen content and distribution within the beta region.

Isothermal Model Verification

The mass transport equations in our major computer code, SIMTRAN, are solved using a model based on Fick's laws of diffusion and the premise that thermodynamic equilibrium is maintained at all interfaces. The basic input to this portion of the code consists of the oxygen diffusion coefficients and equilibrium oxygen concentrations in each of the phases. With the exception of numerical values for these important input data, a detailed description of the code has been published as a topical report[2] and will not be considered here.

In order to obtain an acceptable verification of SIMTRAN for isothermal oxidation, it is then necessary to supply consistent sets of oxygen diffusivity and oxygen solubility data as functions of temperature that combine to yield good agreement with the experimental observations for layer thickness growth. Literature data for these quantities for all phases of the Zircaloy-oxygen system at elevated temperatures are scarce and are of generally unknown accuracy. Thus, care must be exercised to insure that the predictions of the code, which rely on

this input, agree with the experimental results for isothermal oxidation before comparisons are attempted for transient temperature reaction.

The equilibrium solubility values for oxygen utilized in the present version of SIMTRAN are those listed in an earlier chapter of this report, and were selected from the data of Ruh and Garrett,[21] Gebhardt, et al.,[22] Domagala and McPherson[23] for the system Zr-O, and recent results from ANL by Chung, Garde and Kassner[24] for the system Zircaloy-O. The effective oxygen diffusion coefficients were calculated from the data generated in this program. The chemical diffusion coefficient for oxygen in the beta phase of Zircaloy-4 was determined[4] by direct measurements as a function of temperature to be

$$D_{\beta} = 0.0263 \exp(-28{,}200/RT[^{\circ}K]) \ cm^2/s \quad . \tag{9}$$

The diffusion coefficients of oxygen in Zircaloy oxide and in alpha Zircaloy were determined by a treatment of the kinetic phase-growth data obtained in the present investigation. A topical report describing these calculations and results has been issued.[5] This treatment involved a consideration of the system as a classical multiphase, moving boundary, diffusion problem in which the diffusion coefficients were expressed in terms of the reaction rate constants and solubility values. The appropriate chemical diffusion coefficients for oxygen in the tetragonal oxide phase and in the oxygen-stabilized alpha phase are, respectively,

$$D_{ox} = 0.1387 \exp(-34{,}680/RT[^{\circ}K]) \ cm^2/s \tag{10}$$

$$D_{\alpha} = 3.923 \exp(-51{,}000/RT[^{\circ}K]) \ cm^2/s \quad . \tag{11}$$

Using the above values for the oxygen solubilities and diffusivities, a comparison between the SIMTRAN-predicted and the experimentally observed values for oxide layer thickness, alpha layer thickness, and oxygen consumed as a function of time was made over the temperature range 1000–1500°C (1832–2732°F). Temperatures lower than 1000°C (1832°F) were not included in this comparison because the non-parabolic kinetic behavior observed for the oxide layer at these temperatures does not conform to the SIMTRAN model, which requires diffusion controlled, parabolic kinetics.

For isothermal oxidation at 1000 to 1500°C (1832—2732°F) over the range of times reported in our experiments, SIMTRAN predictions of the important kinetic parameters compared to the parabolic representations of the experimental data were considered to be excellent (which is not surprising, since the SIMTRAN input was derived in part from the experiments themselves). For example, SIMTRAN overpredicted the oxide layer thickness by less than 3% over the whole temperature range; the agreement for alpha growth and total oxygen consumption was even better. Thus, with the noted exception for temperatures less than 1000°C (1832°F), we regard these results as a code or model verification for reaction under isothermal conditions.

An isothermal oxidation verification is redundant in the case of the BILD5 code since it makes direct use of the parabolic rate constants to compute the rates of increase of the kinetic parameters. Of course, this code in its present form also cannot be used to consider oxidation where non-parabolic behavior exists. No direct experimental verification of the accuracy of the BILD5 calculation of the oxygen distribution in the beta phase is available except to note that it compares favorably with the SIMTRAN calculation.

Mixed-Temperature Experiments

In addition to the isothermal experiments at 900 and 1005°C (1652—1841°F), we conducted several experiments in MaxiZWOK in which the steam and furnace temperatures were maintained at different values. The purpose of such experiments was two-fold. First, the furnace and steam temperatures are the principal variables governing the rate of heat transfer mechanisms. Thus, the specimen heating and temperature overshoot behavior could be examined over a range of conditions. Such information is useful for comparison with the results of SIMTRAN, which can predict such temperature excursions on the basis of an ideal model. Secondly, these data permitted an additional evaluation of the effect of inlet steam temperature, per se, on the kinetics of the steam-Zircaloy reaction.

Three mixed-temperature experiments were conducted with the steam temperatures varying from 894 to 994°C (1641—1821°F) and furnace

temperatures varying from 1040 to 1110°C (1904–2030°F). Except for the degree of overshoot, the specimen temperature response in all three runs was similar and is illustrated in Fig. 48. This drawing was made from the recorder trace for the experiment in which the steam temperature was controlled at 994°C (1821°F) while the furnace was maintained at 1110°C (2030°F). In this environment the Zircaloy-4 PWR tube specimen experienced a 43°C (77°F) temperature overshoot before its temperature decreased to an equilibrium value of 1057°C (1935°F). Thus, even at this comparatively low temperature, it is evident that appreciable specimen self-heating can occur. It would be anticipated that for similar heat transfer characteristics, the extent of self-heating would increase substantially with increasing temperature.

If the time of this pseudo-isothermal experiment is normalized to an effective value for an isothermal experiment at 1050°C, we find that

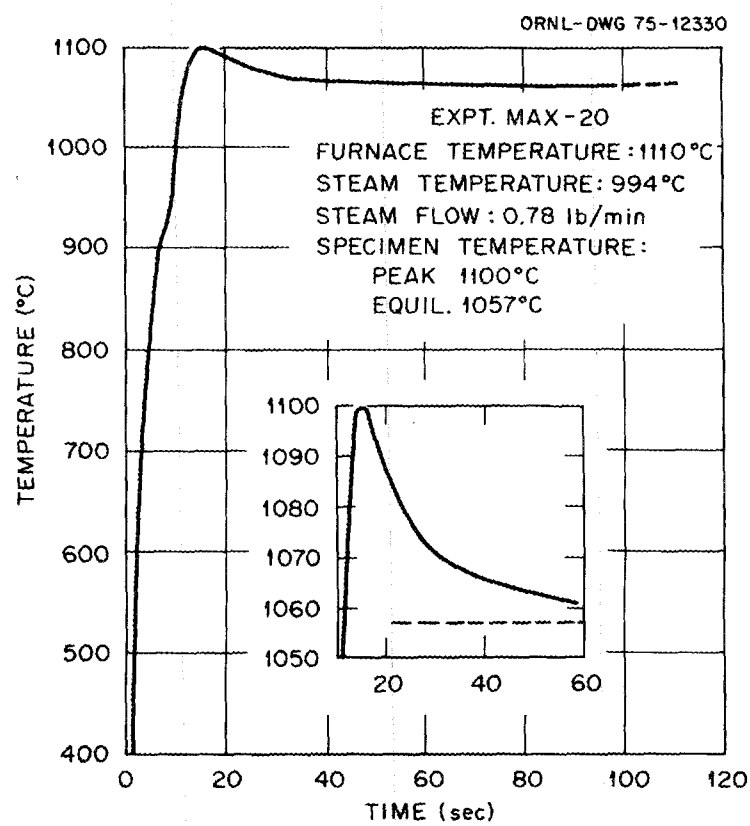

Fig. 48. Specimen Temperature as a Function of Time for Mixed Temperature MaxiZWOK Oxidation Experiment. Detail of temperature overshoot due to specimen self-heating is shown in inset.

the measured values of oxide and alpha layer thicknesses (40.3 ± 1.9 and 37.5 ± 3.1 μm, respectively) agree within the uncertainty limits with the standard experimental data set obtained in MiniZWOK for this temperature (39.0 ± 1.1 and 31.0 ± 4.4 μm, respectively). This suggests that our methods of time-temperature normalization are satisfactory and offers an additional point where a good agreement exists for data obtained in our two oxidation apparatuses.

This experiment was also used to test the temperature-time predictive capability of SIMTRAN on the basis of the physical property, heat-of-reaction and heat-transfer data input to the code. The specimen is assumed to be inserted into an environment where it receives heat by radiation from the furnace wall and by convection from the flowing steam. It was found that very good agreement between the observed and predicted temperature cycles could be obtained simply by varying the convective (steam) heat-transfer coefficient within a reasonable range. For example, a convective heat transfer coefficient of .00407 cal/s-cm^2-°C (30 Btu/hr-ft^2-°F) used as input to SIMTRAN produced the result illustrated in Fig. 49, which is a comparison with the actual experiment.

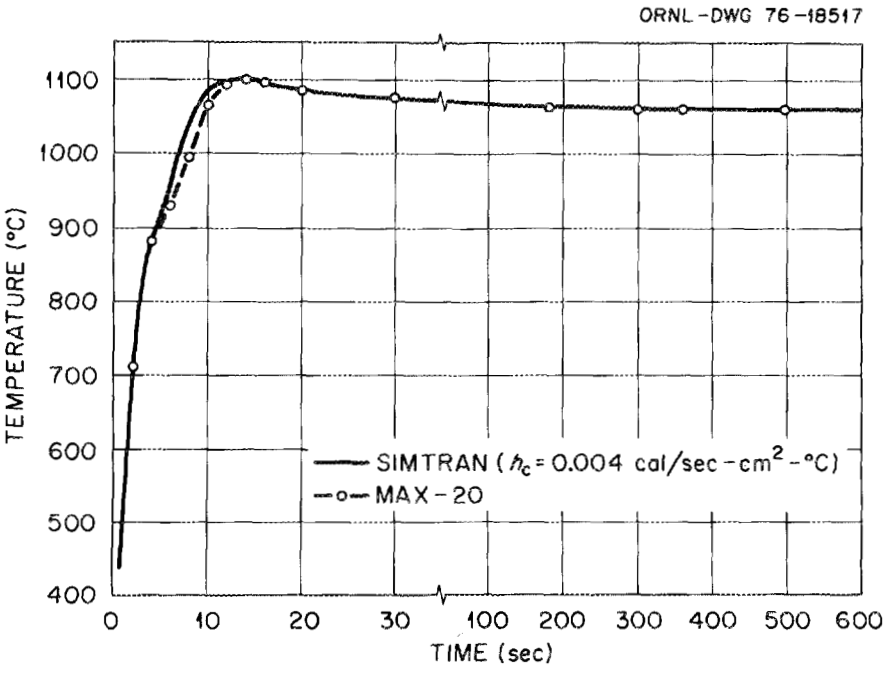

Fig. 49. A Comparison of the Observed and SIMTRAN-Predicted Time-Temperature Excursion for Expt. MAX-20.

The agreement is seen to be quite good, particularly in the light of the assumptions which go into this calculation. Such agreement lends a degree of confidence to the SIMTRAN predictions of time-temperature behavior during exposure of Zircaloy tubes at higher temperatures under known heat-transfer conditions.

Transient Temperature Oxidation Experiments

A variety of transient temperature oxidation experiments was performed in order to test the predictions of our computer codes. The temperature-time profiles used are shown in Fig. 50. The very simple transients in Fig. 50(a) were designed to investigate the effects of variations in heating and cooling rates on code predictions. The profiles in Fig. 50(b) should reveal any effects on oxidation rate related to changes in scale microstructure or other factors influenced by an increase or decrease in temperature near the beginning or the end of the transient. Curve No. 1 in Fig. 50(c) simulates a transient calculated for a particular hypothetical LOCA; curve No. 2 is similar except that the maximum temperature of the blow-down peak was increased from 900°C (1652°F) to 1400°C (2552°F).

Oxide and alpha phase thickness measurements were made for each of the transient-temperature oxidation tests. For several representative transients, as shown in Table 34, the predictions of the SIMTRAN and BILD5 codes were compared with the experimental measurements. The code predictions were made on the basis of approximate descriptions of the exact time-temperature cycles, and the code results are, therefore, thought to be slightly conservative. For the cases examined to date, except as noted below for the "two-peak" transients, both codes predict oxide thickness after transient oxidation to within about 10%. However, the tendency for the formation of "alpha incursions", as opposed to uniform alpha layer growth, during the cooling portion of a transient-temperature oxidation test represents a growth situation that is not properly modeled by the ideal growth schemes employed by the codes. In SIMTRAN, for example, the alpha-beta boundary movement is accelerated during cooling due to the changes in the equilibrium solubilities and

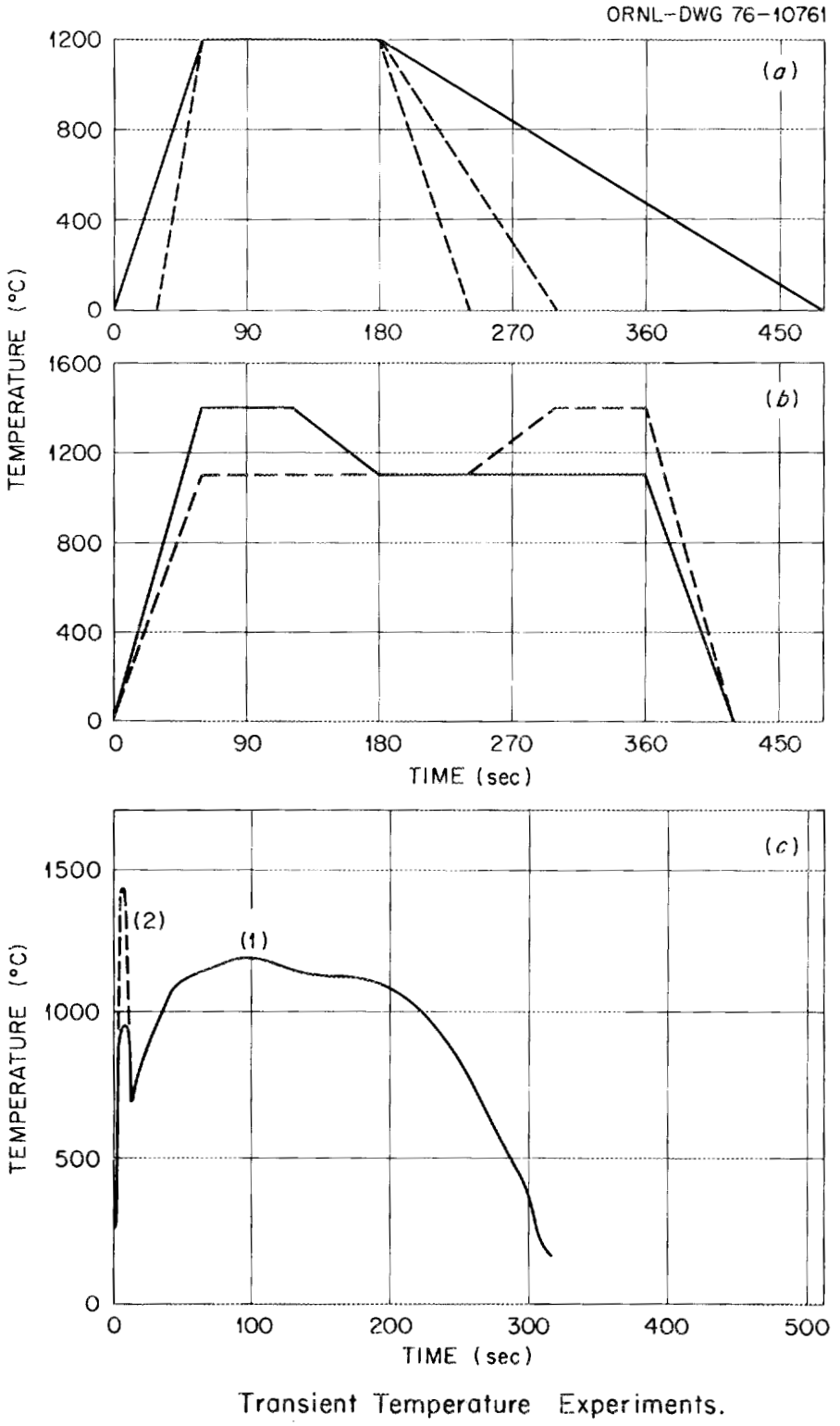

Fig. 50. Schematic Representations of the Time-Temperature Profiles of Transient Temperature Oxidation Tests.

Table 34. A Comparison of Experimental and Predicted Values for Kinetic Parameters for Transient Steam Oxidation of Zircaloy-4

Expt. No.	Transient Type (Fig. 47)	Measured		BILD5			SIMTRAN		
		Oxide (μm)	Alpha (μm)	Oxide (μm)	Alpha (μm)	Oxygen (mg/cm^2)	Oxide (μm)	Alpha (μm)	Oxygen (mg/cm^2)
S-155	a-1	39.3	46.5	40.0	39.4	7.74	41.0	64.5	7.77
S-158	a-3	35.8	40.7	36.7	36.8	7.15	37.5	55.1	7.15
S-163	b-1	65.2	82.3	71.0	85.4	14.62	74.4	132.1	14.66
S-164	b-2	65.8	86.9	73.6	88.6	15.16	73.7	141.8	14.97
S-160	c-1	45.8	49.8	48.4	45.8	9.24	49.5	77.2	9.26
S-196	c-2	40.2	52.4	49.7	47.7	9.53	51.1	78.8	9.61

the oxygen concentration gradients at this interface, but no incursions or precipitation in advance of the interface are allowed, even in the region of supersaturation. Thus, since supersaturation can be relieved in this model only by diffusion to a growth front, SIMTRAN tends to overpredict the compact alpha layer thickness. BILD5, on the other hand, appears to predict the thickness of the compact portion of the alpha layer to within about 10%. Neither program characterizes incursion formation; however, the difference in the alpha layer predictions for the two codes is related to the extent of the incursions. While no experimental values are available for comparison, the codes yield values of total oxygen consumed during transient oxidation that are in good agreement.

The metallographic structures exhibited by the transient temperature oxidized specimens are illustrated in Figs. 51–53. Figure 51 is the cross section of the specimen from Expt. S-155 (see Table 34), which was a simple "trapezoidal" transient with a peak temperature of 1200°C (2192°F) that lasted 120 s. While only a few incursions developed in this specimen, much more incursion growth and alpha precipitation were observed in the sample from Expt. S-163 (see Fig. 52) where the peak temperature was 1400°C (2552°F), and in which, consequently, a higher oxygen concentration developed near the alpha-beta interface. Most probably, a combination of excess oxygen and comparatively high

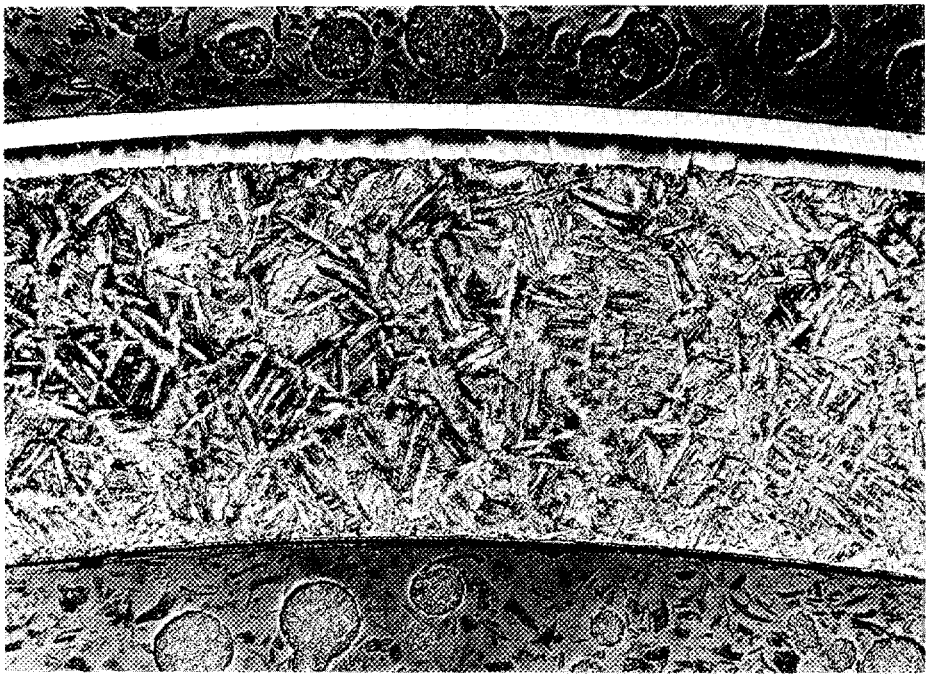

Fig. 51. Cross-Section of Sandvik Zircaloy-4 PWR Tube Oxidized in Steam According to Expt. S-155. Max. temp. = 1200°C (2192°F). Etch-anodized; bright-field; 100×.

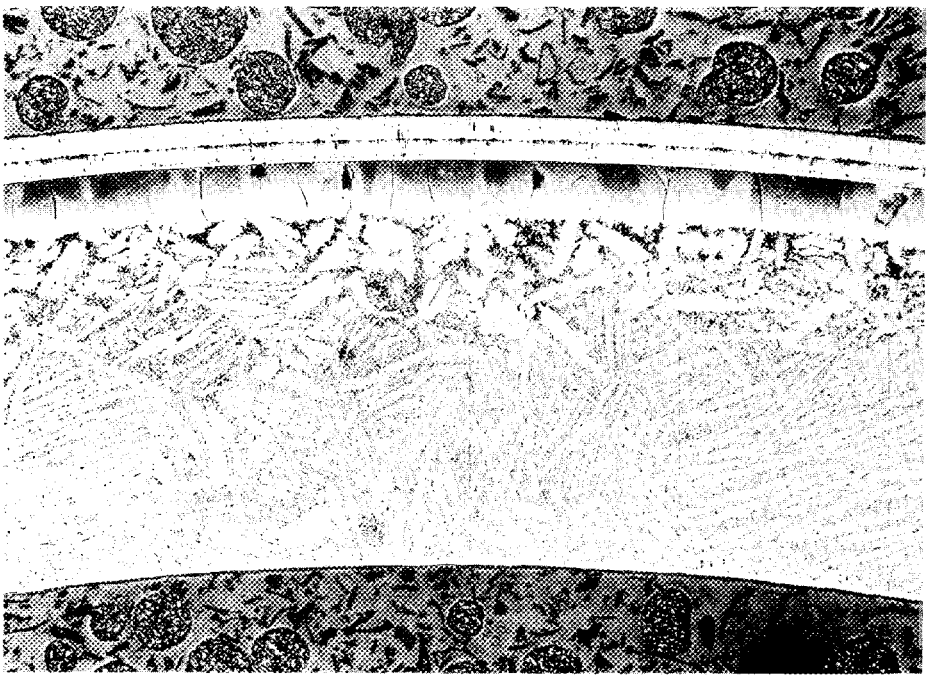

Fig. 52. Cross-Section of Sandvik Zircaloy-4 PWR Tube Oxidized in Steam According to Expt. S-163. Max. temp. = 1400°C (2552°F). Etch-anodized; bright-field; 100×.

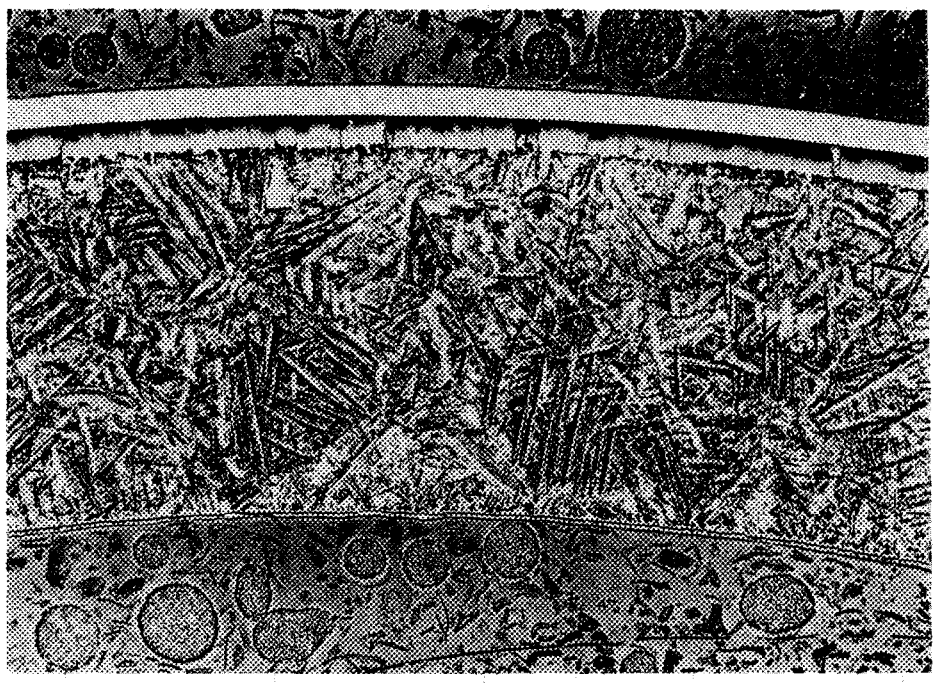

Fig. 53. Cross-Section of Sandvik Zircaloy-4 PWR Tube Oxidized in Steam According to Expt. S-160. Max. temp. = 1200°C (2192°F). Etch-anodized; bright-field; 100×.

temperatures (high oxygen mobility) favors the formation and growth of incursions on cooling. However, incursions apparently can also form in advanced stages of an isothermal reaction as the beta phase nears saturation. For example, for isothermal reaction of our Sandvik PWR tubes on one side at 1200°C (2192°F), significant numbers of incursions were observed in the microstructures after oxidation times approaching 1200 s. This general phenomenon was previously discussed by Hobson.[35]

Figure 53 is the cross section of the specimen from Expt. S-160, the LOCA-like transient shown in Fig. 50(c)-1. A few incursions are observed in the microstructure.

In terms of the total oxygen consumed by a reacting specimen, the alpha incursion modeling problem is likely to be comparatively minor. From the standpoint of the mechanical response of an oxidized specimen, however, the existence of incursions is considerably more important.[35]

Anomalous Transient Temperature Oxidation

The experimental results obtained for the two transient temperature oxidation tests illustrated in Fig. 50(c) and reported in Table 34 offer

an example of apparently "anomalous" oxidation behavior for this material. It was observed that the measured oxide layer thicknesses for the two transients were inconsistent with their known time-temperature histories: less oxide existed after transient (2) than for transient (1). This result, which appears to be identical to the "preoxidation" effect reported by Biederman, Ballinger and Dobson,[17d-f] was confirmed by subsequent experiments and, additionally, was found to exist for oxidation of pure zirconium. Also in accord with the Biederman observations was the result that the calculated values, using the BILD5 program, for the oxide layer thicknesses based on the isothermal oxidation data were consistently higher than those observed. The results of these experiments are listed in Table 35.

Since the anomalous behavior occurred only for specimens subjected to transients of the type shown in Fig. 50(c), it seemed reasonable to assume that some feature of the initial peak created the conditions necessary to produce the observed oxidation characteristics. One obvious difference from transients in which "normal" behavior is obtained is the fast cool and reheat portion of this type of transient. Thus, in order to define further the particular characteristic of the time-temperature cycle which leads to this effect, a number of steam oxidation

Table 35. Experimental and Predicted Layer Thickness Values for Transients Illustrated in Fig. 47(c)

Expt. No.	Material	Transient Type[a]	Layer Thickness			
			Measured		Calculated	
			Oxide (μm)	Alpha (μm)	Oxide (μm)	Alpha (μm)
S-160-TC-2	Zirc-4	(1)	45.8	49.8	50.5	47.9
S-162-TC-2	Zirc-4	(1)	47.5	51.0	51.6	49.7
S-196-TC-2	Zirc-4	(2)	40.2	52.4	51.2	49.6
S-199-TC-2	Pure Zr	(1)	32.6	61.4		
S-200-TC-2	Pure Zr	(2)	26.0	66.4		

[a]Type (1): First temperature maximum ≈ 900°C (1652°F); Type (2); First temperature maximum ≈ 1400°C (2552°F).

experiments were performed on Zircaloy-4 specimens in the MiniZWOK apparatus in which several key parameters of a double-peak transient were varied.

The general form of the transients used for this series of tests is illustrated in Fig. 54, which may be described as follows. The specimen is heated quickly (in approximately 10 s) to the first peak temperature T_1, and cooled, again in $\sim$ 10 s, to a specified lower temperature, T_2. The specimen is then reheated to T_3 (unless $T_2 = T_3$), held under isothermal conditions for a time, t_3, and finally cooled. The nominal test conditions for this series are listed in Table 36. Included in this table are values of the observed and calculated oxide thicknesses from which it is possible to detect the occurrence of anomalous behavior. It should be pointed out that the calculations, which utilized the BILD5 code, were made on the basis of the CODAS output for each run and not on the basis

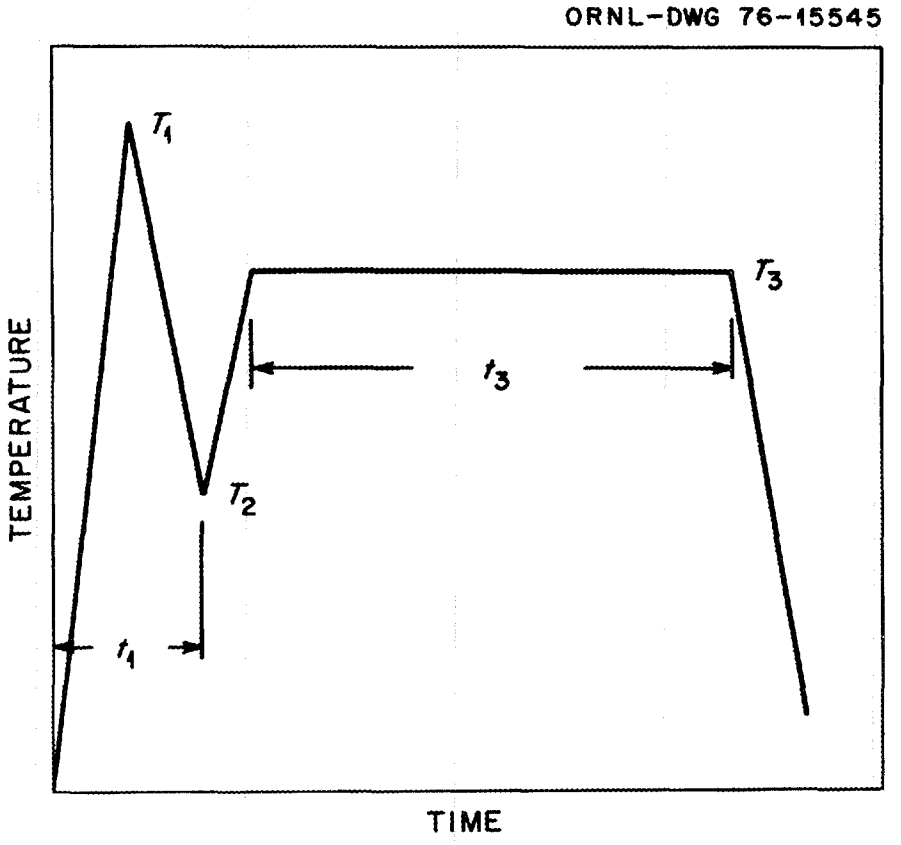

Fig. 54. Schematic Representation of Double-Peak Transients Used to Study Anomalous Transient Temperature Oxidation Effect. See Table 36 for list of nominal times and temperatures.

Table 36. Nominal Test Conditions for Anomalous Transient Temperature Oxidation Tests

Expt. No.	Maximum Temp. of First Peak T_1 (°C)	Minimum Temp. After First Peak T_2 (°C)	Plateau Temperature T_3 (°C)	Plateau Time t_3 (s)	Oxide Layer Thicknesses		Difference[a] (%)
					Calculated (μm)	Observed (μm)	
S-224	1050	650	1050	210	25.2	12.2	107
S-225	1400	650	1050	210	27.2	12.6	116
S-226	1400	650	1200	110	38.8	36.3	7
S-227	1050	650	1400	55	52.9	50.2	5
S-228	1400	650	1400	55	56.7	54.0	5
S-229	1400	1200	1200	190	51.7	49.7	4
S-230	1400	1200	1200	210	50.0	48.4	3
S-231	1400[b]	1200	1200	160	54.9	53.1	3
S-232	1400[b]	1200	1200	100	61.4	60.6	1
S-238	1400	1050	1050	200	28.4	29.4	−3
S-239	1400	650	1090	165	28.2	10.5	169

[a]Percent difference between observed and calculated layer thicknesses.

[b]Slowly cooled from T_1.

of the nominal time-temperature descriptions given for each experiment in Table 36.

Of the oxidation tests reported in Table 36, three exhibited significant differences between the observed and calculated oxide thickness values and were considered anomalous. Common to all three of these experiments were the facts that (1) each was a "two-peak" transient, (one in which the specimen was cooled significantly between heating cycles), and (2) the temperature of the second peak was less than 1200°C (2192°F). Important clues relating these facts to a viable mechanism may be obtained by comparing several of the experimental observations. For example, Expt. S-224 differs from a standard isothermal experiment at 1050°C (1922°F) only in that the specimen was cooled to 650°C (1202°F) and then reheated to 1050°C (1922°F). This difference obviously was important. Expt. S-227 involved the same initial peak as S-224, but subsequent oxidation took place at 1400°C (2552°F) rather than 1050°C (1922°F). Anomalous behavior for this experiment was not observed.

A similar sequence is found in which the initial peak temperature, T_1, was 1400°C (2552°F). Expt. S-225 differs from S-238 only in that the former specimen was cooled and reheated to the plateau temperature, 1050°C (1922°F), while the latter was simply cooled to the plateau temperature from T_1. The cooling-reheating sequence after the first temperature maximum is thus a critical parameter. Expts. S-239, S-226 and S-228 differ from S-225 only in the temperature of the second peak (or plateau), T_3. For T_3 = 1090°C (1994°F), anomalous behavior was observed; for T_3 = 1200°C (2192°F) or 1400°C (2552°F) the oxidation was considered normal.

The results of these experiments constitute a convincing set of evidence that points to the involvement of the monoclinic-tetragonal phase transformation in the oxide in the mechanism responsible for the anomalous transient temperature oxidation effect. The key characteristic appears to be the extensive temperature hysteresis associated with the transformation.[36,37]

This behavior is illustrated by the high-temperature x-ray diffraction results of Grain and Garvie,[36] shown in Fig. 55, who also demonstrated

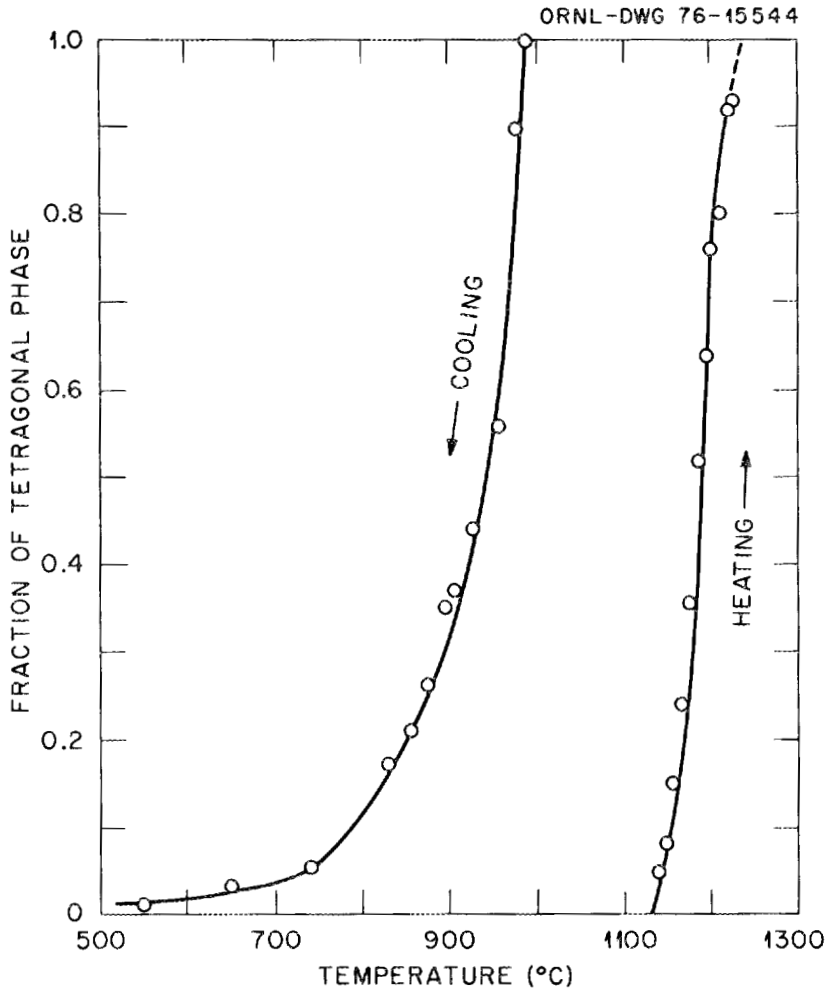

Fig. 55. Hysteresis in the Monoclinic-Tetragonal Phase Transformation in ZrO_2. After Grain and Garvie.[35,36]

that the details of the transformation depended upon the crystallite size. Upon heating, the transformation is seen to take place over a narrow temperature range near 1200°C (2204°F). On cooling, the reverse transformation is initiated near 1000°C (1832°F) but is not completed until the temperature has fallen several hundred degrees. A number of investigators have observed similar transformation behavior.[37-39] These data were obtained for ZrO_2 specimens of a specified purity and treatment which are certainly different from those of the oxide formed on Zircaloy-4 under oxidizing conditions. However, it is reasonable to assume that the general features of the transformation shown in Fig. 55 will apply to the Zircaloy oxide system.

It has been suggested by Pemsler and others[40] that tetragonal zirconia may be stabilized at lower temperatures by stress, small grain size, or high defect concentrations, and there is evidence that the growing oxide scale on Zircaloy-4 may have a tetragonal structure at temperatures lower than those indicated in Fig. 55. Thus our oxidation rate data at 1050°C (1922°F) and, to a slightly lesser extent, at 1000°C (1832°F) are completely consistent with the results at higher temperatures where the oxide is certainly tetragonal, and one is led to the idea that the oxide formed during our typical "isothermal" excursions at these temperatures is predominantly tetragonal. This conclusion is also consistent with the fact that oxidation rates observed during the first minute or two at 900 and 950°C (1652—1742°F) agree well with those predicted by extrapolations of the high temperature data.

Following Pemsler's arguments,[40] it appears likely that in the initial stages of our isothermal experiments at temperatures where the monoclinic oxide is normally stable, a thin layer of the tetragonal oxide is formed due to favorable conditions of stress, grain size, or defect structure. During further oxidation at 1000 to 1200°C (1832—2192°F), the presence of this initial tetragonal oxide layer is sufficient to stabilize the additional oxide generated in the tetragonal structure as well. The decreased oxidation rates that we observed below 1000°C (1832°F) may be rationalized in these same terms if it is assumed that the diffusion flux across a monoclinic oxide layer is smaller than that for a corresponding tetragonal scale.[40] Thus, below 1000°C (1832°F), despite the formation of an initial layer of tetragonal Zircaloy oxide, continued oxidation eventually results in the transformation of part of the oxide to the monoclinic structure, presumably due to stress relief, grain growth, etc. If this transformation resulted in the formation of layers of tetragonal and monoclinic oxide whose thickness ratio varied with time, one would expect to see the non-parabolic oxide growth kinetics that we have actually observed at 900 and 950°C (1652—1742°F).

Returning to the question of anomalous transient temperature oxidation, an explanation for the phenomenon can be put forward on the basis of a set of assumptions derived from the arguments just given and of the experimental results summarized in Tables 35 and 36.

1. The initial oxide formed during a typical isothermal experiment has a tetragonal structure.

2. If the isothermal oxidation temperature is greater than ∿ 1000°C (1832°F), the subsequently formed oxide will also be stabilized in the tetragonal structure.

3. If the initially formed tetragonal oxide is held at a sufficiently low temperature [∿ 900°C (1652°F) or lower], it transforms to the monoclinic structure, and any subsequently formed oxide will also be predominantly monoclinic unless the temperature is raised to ∿ 1200°C (2192°F).

4. The diffusion flux across a growing monoclinic Zircaloy oxide scale is smaller than that for the corresponding tetragonal oxide.

In these terms the following sequence of events may be visualized in a typical two-peak LOCA such as that hypothesized in Fig. 47(c).

1. The oxide formed during heating to the first peak temperature, T_1, (see Fig. 54) is predominately tetragonal.

2. On cooling to T_2, the oxide transforms to the monoclinic structure.

3. During the heating phase of the second peak, because of the existence of the monoclinic oxide, oxidation proceeds more slowly than would be predicted on the basis of the high temperature isothermal data, and this condition will persist until a temperature near 1200°C (2192°F) is reached, at which time the monoclinic oxide is converted to tetragonal.

Three critical features can be identified in this model for anomalous transient temperature oxidation: the minimum temperature reached after the first peak, the rate of heating from this minimum to the second peak temperature, and the second peak temperature itself. If, after the first peak temperature is attained, the temperature is maintained at a sufficiently high level to preclude transformation to the monoclinic oxide, the oxidation kinetics for the transient will be normal in the sense that the extent of oxidation will be predictable on the basis of high temperature isothermal oxidation data. Even in cases where the oxide is converted to the monoclinic structure, if the heating rate to the second peak is sufficiently fast and if the second peak temperature is sufficiently high, no perturbation of the final oxide thickness will be

observed provided the time at the second peak temperature is long enough to produce significant oxide growth. Anomalous transient temperature oxidation effects are favored by conditions where the oxide transformation occurs after the first peak, the heating rate for the second peak is low, and/or the second peak temperature is below ∿ 1200°C (2192°F).

The existence of the anomalous transient temperature effect obviously raises questions concerning the techniques currently being used to predict transient temperature oxidation behavior. Computer codes based on typical isothermal oxidation results will tend to overpredict oxide layer thicknesses and, hence, total oxygen consumption (although not necessarily the quantity of oxygen dissolved in the beta region) for a hypothetical two peak LOCA such as those shown in Fig. 50(c). The critical factors in such a case are the minimum temperature reached after the first peak, the maximum temperature of the second peak, and the rate at which this second temperature is reached. The prospects for more precise predictions of oxidation behavior during single peak LOCA's are better, although the rate at which the maximum temperature is attained could also be important. Clearly, however, the problem of transient temperature oxidation predictions deserves further study.

CONCLUSIONS AND RECOMMENDATIONS

A variety of conclusions may be drawn and recommendations made on the basis of results obtained in the ZMWOK Program.

1. The Program has yielded a set of isothermal reaction rate data for the oxidation of Zircaloy-4 in steam between 900 and 1500°C (1652–2732°F). The conditions under which these data were obtained have been carefully characterized, and the experimental procedures used in the study were fully documented. In addition the data were subjected to an extensive statistical analysis in order to establish appropriate confidence limits for the results, and an analysis of the maximum absolute errors inherent in the procedures was performed. Within the limits thus established and for the comparatively ideal set of oxidation conditions used, we consider this data set to be highly reliable.

2. The ZMWOK data set provides a basis for quantifying the degree of conservatism of the Baker-Just correlation for the oxidation rate of Zircaloy. Under the conditions used for our experiments, the Baker-Just relationship predicts oxidation rate constants 32, 78, and 147% higher than ours at temperatures of 1000, 1200, and 1500°C (1832, 2192, and 2732°F), respectively.

3. A study of the influence of deformation during oxidation on the oxidation rate of Zircaloy is beyond the scope of the ZMWOK program. The effects of deformation could, however, alter the oxidation behavior of Zircaloy. Under hypothetical loss-of-accident conditions in a PWR, ballooning and possibly some bending of the fuel rods is anticipated. Any oxide on the surface of the rod at such a time would tend to undergo cracking with a resulting increase in oxidation rate. Whether the total oxygen consumption per cm^2 during the LOCA is significantly increased would depend to a large extent on the temperature and time into the LOCA at which deformation occurred. If tube rupture and, hence, ballooning, are complete at temperatures near 900°C (1652°F), then the influence of deformation on the high temperature oxidation process might be restricted to increases in the rate at which the beta regions of the tube fill up with oxygen, an increase related to the thinning of the tube wall during ballooning. We recommend, however, that the effect of deformation on oxidation be taken into consideration in best estimate computer codes such as FRAP-T. Data from other RSR-sponsored projects, e.g., the Multirod Burst Test Program, should provide useful information in this regard.

4. Oxide layer growth at 900 and 950°C (1652–1742°F) is not describable in terms of parabolic kinetics. Extrapolation below ∿ 1000°C (1832°F) of high temperature rate constant data for oxide or Xi layer growth or total oxygen consumption will yield overpredictions of these quantities. However, the error resulting from such an extrapolation is likely to be negligible if the time of oxidation at the lower temperatures does not exceed ∿ 100 s (but see Par. 7 below).

5. Neither steam flow rate (above levels leading to steam starvation); steam temperature; the presence in the steam of reasonable concentrations of oxygen, nitrogen, or hydrogen; nor small variations

in alloy composition significantly influence the isothermal rate of oxidation of Zircaloy-4. Obviously, however, both steam temperature and flow rate are important parameters in heat transfer calculations, and any failure to remove the heat of the Zircaloy-steam reaction from the fuel cladding can result in an increase in the temperature of the cladding. We have shown that the extent of this temperature increase can be calculated with the SIMTRAN computer code given an input of appropriate heat transfer coefficients.

6. Except as described in Par. 7 below, the SIMTRAN and BILD5 computer codes can be used together to provide adequate predictions of the thickness of oxide and oxygen-stabilized alpha layers and probably of total oxygen consumption during transient temperature oxidation. Neither code, however, models the formation of alpha incursions or precipitates in the beta regions of a sample during the cooling phase of most transients. It is likely that the presence of such precipitates will influence the mechanical properties of the prior-beta regions, and we recommend that a further correlation be developed between alpha incursion formation during transient temperature oxidation and the mechanical properties of the Zircaloy fuel tubes.

7. The two computer codes also overpredict oxide thickness and, therefore, total oxygen consumption in certain hypothetical two-peak LOCAs. This phenomenon is described in the body of the text (see p. 109) as "anomalous transient temperature oxidation". Its occurrence is probably related to the manner in which the monoclinic-to-tetragonal phase transformation occurs in the oxide and to the extent that the tetragonal oxide is stabilized at low temperatures by stress, departures from stoichiometry, and other factors. Accurate predictions of overall oxidation rates under these conditions clearly require that additional research be done. It should be emphasized, however, that while overall oxygen consumption during anomalous transient temperature oxidation is less than expected, there is every reason to believe that the rate of oxygen solution in the beta phase continues to be that predicted on the basis of calculations using the high temperature data, that is, a reduction in the rate of oxide formation does not reduce the rate of embrittlement of the beta phase due to oxygen solution.

ACKNOWLEDGMENTS

The authors gratefully acknowledge the help received from many sources during the course of this research. The excellent metallographic work of E. T. Rose and N. M. Atchley was essential to the program. R. L. Anderson, T. G. Kollie, and J. L. Horton of the Metrology Research and Development Laboratory, Instruments and Controls Division, ORNL, were responsible for the calibration of the thermocouples used and contributed many helpful suggestions regarding thermometry problems. D. L. McElroy and R. K. Williams also worked on thermometry problems and supplied advice concerning several phases of the program. R. S. Graves and F. J. Weaver helped with instrumentation, and T. G. Godfrey made possible the use of the CODAS to collect experimental data. C. K. Bayne of the Computer Sciences Division, ORNL performed the statistical analysis included in the Appendix. D. O. Hobson and R. A. Perkins reviewed the manuscript and made numerous helpful comments during the course of the research. We also received invaluable assistance from many members of the Instruments and Controls, Plant and Equipment, and Analytical Chemistry Divisons at ORNL; it is impossible to list all these people but certainly special thanks are due to R. F. Stone, C. D. Wicker, R. W. Tucker, Wayne King, and Paul Stafford. We are appreciative of the patience and skill of Mrs. Sharon Buhl in preparing this report. Finally, we wish to acknowledge the support and advice given by several members of the Fuel Behavior Branch, Division of Reactor Safety Research, NRC and of M. L. Picklesimer in particular.

REFERENCES

1. *Quarterly Progress Report on the Zirconium Metal-Water Oxidation Kinetics Program Sponsored by the NRC Division of Reactor Safety Research for*

   (a) *April–June 1974*, ORNL/TM-4655
   (b) *July–September 1974*, ORNL/TM-4729
   (c) *October–December 1974*, ORNL/TM-4805
   (d) *January–March 1975*, ORNL/TM-4914
   (e) *April–June 1975*, ORNL/TM-5021
   (f) *July–September 1975*, ORNL/TM-5148
   (g) *October–December 1975*, ORNL/TM-5248
   (h) *January–March 1976*, ORNL/NUREG/TM-17
   (i) *April–June 1976*, ORNL/NUREG/TM-41
   (j) *July–September 1976*, ORNL/NUREG/TM-62.
   (k) *October–December 1976*, ORNL/NUREG/TM-87
   (l) *January–March 1977*, ORNL/NUREG/TM-110.

2. S. Malang, *SIMTRAN I — A Computer Code for the Simultaneous Calculation of Oxygen Distributions and Temperature Profiles in Zircaloy During Exposure to High-Temperature Oxidizing Environments*, ORNL-5083 (November 1975).

3. J. V. Cathcart, et al., *Zirconium Metal-Water Oxidation Kinetics I. Thermometry*, ORNL-5102 (February 1976).

4. R. A. Perkins, *Zirconium Metal-Water Oxidation Kinetics II. Oxygen-18 Diffusion in β-Zircaloy*, ORNL/NUREG/TM-19 (July 1976).

5. R. E. Pawel, *Zirconium Metal-Water Oxidation Kinetics III. Oxygen Diffusion in Oxide and Alpha Zircaloy Phases*, ORNL/NUREG-5 (October 1976).

6. G. J. Yurek, J. V. Cathcart, and R. E. Pawel, "Microstructures of the Scales Formed on Zircaloy-4 in Steam at Elevated Temperatures," *Oxidation of Metals* 10:255 (1976).

7. R. E. Pawel, R. A. Perkins, R. A. McKee, J. V. Cathcart, G. J. Yurek, and R. E. Druschel, *The Diffusion of Oxygen in Beta-Zircaloy and the High Temperature Zircaloy-Steam Reaction*, to be published in ASTM Symposium Book on "Zirconium in the Nuclear Industry," Quebec City, Canada, Aug. 19–12 (1976).

8. "The International Practical Temperature Scales of 1968," (adopted by the Comite International des POids et Mesures) *Metrologia* 5(2): 35–44 (1969).

9. W. T. Gray and D. I. Finch, "Accuracy of Temperature Measurements" *Temperature, Its Measurement and Control in Science and Industry*, 4(2): 1381–1392, ed. by Harmon H. Plumb, Society of America, 1972.

10. D. T. Hawkins and R. Hultgren, "Constitution of Binary Alloys," in *Metals Handbook*, Vol. 8, American Society for Metals, Metals Park, Ohio, 1973, p. 33.

11. M. Hansen, *Constitution of Binary Alloys*, McGraw Hill, New York, 1958, p. 1226.

12. T. G. Kollie, D. L. McElroy, R. K. Adams, and J. M. Jansen, "Measurement Accuracy of a Computer-Operated-Data-Acquisition System," in *Temperature, Its Measurement and Control in Science and Industry*, Vol. 4, Part 2, H. H. Plumb, ed., Instrument Society of American, Pittsburg, PA, 1972, pp. 1457–1466.

13. Summaries of pertinent phenomena, approaches, and remedies are given in (a) A. J. Otter, *Thermocouples and Surface Temperature Measurement*, AECL-3062 (March 1968) or (b) *Manual on the Use of Thermocouples in Temperature Measurement*, American Society for Testing and Materials, Spec. Tech. Publ. 470A, Philadelphia, 1974, particularly Chapter 9.

14. M. Jakob, *Heat Transfer*, Vol. II, Wiley, NY, 1957, p. 147.

15. L.M.K. Boelter et al., *An Investigation of Aircraft Heaters, XXVIII – Equations for Steady-State Temperature Distribution Caused by Thermal Sources in Flat Plates Applied to Calculation of Thermocouple Errors, Heat-Meter Corrections, and Heat Transfer by Pin-Fin Plates*, NACA-TN-1452 (1948).

16. L.M.K. Boelter and R. W. Lockhart, *Thermocouple Conduction Error Observed in Measuring Surface Temperatures*, NACA-TN-2427 (1951).

17. R. R. Biederman, R. G. Ballinger and W. G. Dobson, *A Study of Zircaloy-Steam Oxidation Reaction Kinetics*, Research Project No. 249-1, Electric Power Research Institute, Palo Alto, California.

    (a) First Interim Progress Report, January–March 1975
    (b) Second Interim Progress Report, April–June 1975
    (c) Third Interim Progress Report, July–September 1975
    (d) Fourth Interim Progress Report, October–December 1975
    (e) Fifth Interim Progress Report, January–March 1976
    (f) Final Report, September 1976.

18. R. K. Williams, "A Study of the Resistivity of Zone-Refined Tungsten at High Temperatures," *J. Appl. Phys.* 46: 475–490 (1975).

19. D. L. McElroy and J. P. Moore, "Radial Heat Flow Methods for the Measurement of the Thermal Conductivity of Solids" in *Thermal Conductivity*, Vol I, R. P. Tye, ed., Academic Press, New York, 1969, p. 190.

20. On the assumption that the oxide at the oxide/gas interface will be approximately stoichiometric ZrO_2 with a density of 5.82 g/cm^3.

21. Calculated from phase diagram for Zr-O presented by R. Ruh and H. J. Garrett, "Nonstoichiometry of ZrO_2 and Its Relation to Tetragonal-Cubic Inversion in ZrO_2," *J. Am. Ceram. Soc.* 50: 257 (1967). It should be noted that it is possible that impurities (such as those found in the Zircaloy series of alloys) would influence the defect concentrations.

22. E. Gebhardt, H. D. Seghezzi and W. Dürrschnabel, "Untersuchungen in System Zirconium-Sauerstoff," *J. Nucl. Mater.* 4: 255 (1961).

23. R. F. Domagala and D. J. McPherson, "System Zirconium-Oxygen," *J. Met.* 6:, *Trans. AIME* 200: 238 (1954).

24. Analytical representation of data of H. M. Chung, A. M. Garde, and T. F. Kassner, Argonne National Laboratory, by S. Malang, Gesellschaft für Kernforschung, Karlsruhe, W. Germany. Private communication and ANL-75-58 (September 1975).

25. R. H. Chapman, *Characterization of Zircaloy-4 Tubing Procured for Fuel Cladding Research Programs,* ORNL/NUREG/TM-29 (July 1976).

26. For example, S. H. Makin, A. H. Rowe, and A. D. LeClaire, "Self Diffusion in Gold," *Proc. Phys. Soc.* 70: 545–52 (1957).

27. Unpublished results, D. O. Hobson and R. E. Pawel, ORNL (1973). Original data from D. O. Hobson and P. L. Rittenhouse, *Embrittlement of Zircaloy-Clad Fuel Rods by Steam during LOCA Transients*, ORNL-4758 (January 1972).

28. L. Baker and L. C. Just, *Studies of Metal-Water Reactions at High Temperatures; III. Experimental and Theoretical Studies of the Zirconium-Water Reaction,* ANL-6548 (May 1962).

29. A. W. Lemmon, Jr., *Studies Relating to the Reaction Between Zirconium and Water at High Temperatures,* BMI-1154 (January 1957).

30. H. H. Klepfer, reported in G. J. Scatina, *Fuel Cladding Embrittlement during a Loss-of-Coolant Accident,* NEDO-10674 (October 1972).

31. S. Kawasaki, T. Furuta, and M. Hashimoto, *Reaction of Zircaloy Cladding with Steam under Simulated Loss-of-Coolant Accident Conditions,* JAERI-M-6181 (July 1975).

32. S. Leistikow, H. v. Berg, and D. Jennert, "Comparative Studies of Zircaloy-4/High Temperature Steam Oxidation under Isothermal and Temperature Transient Conditions," in *Proceedings, CSNT Specialist Meeting on the Behavior of Water Reactor Fuel Elements under Accident Conditions,* Spatind, Nord-Torpa, Norway, September 13–16, 1976, in press.

33. R. E. Pawel, "Diffusion in a Finite System with a Moving Boundary," *J. Nucl. Mater.* 49: 281 (1974).

34. R. E. Pawel, "Oxygen Diffusion in Beta Zircaloy during Steam Oxidation," *J. Nucl. Mater.* 50: 247 (1974).

35. D. O. Hobson, "Ductile-Brittle Behavior of Zircaloy Fuel Cladding" in *Topical Meeting on Water Reactor Safety,* March 26–28, 1973, G. A. Freund, compiler, pp. 274–288. USAEC-TIC CONF 730304.

36. C. F. Grain and R. C. Garvie, *Mechanism of the Monoclinic to Tetragonal Transformation of Zirconium Dioxide,* U.S. Bureau of Mines Report 6619 (1965).

37. P. Kofstad and D. J. Ruzicka, "On the Defect Structure of ZrO_2 and HfO_2," *J. Electrochem. Soc.* 110: 181 (1963).

38. For example, F. A. Mupton and R. Roy, "Low Temperature Equilibria Among ZrO_2, ThO_2 and UO_2," *J. Am. Ceram. Soc.* 43: 234 (1960).

39. W. L. Baun, "Phase Transformation at High Temperatures in Hafnia and Zirconia," *Science* 140: 1330 (1963).

40. J. P. Pemsler, "The Kinetics and Mechanism of Oxide Film Growth on Zirconium," *Electrochem. Tech.* 4: 128 (1966).

APPENDIX A

ERROR ANALYSIS

INTRODUCTION

The experimental method used in this study requires the determination of three parameters, viz., temperature, time, and phase thicknesses, in order that a rate of oxidation may be estimated. In this section we analyze the uncertainties associated with these measurements in an effort to establish rational error limits for the data presented.

Two basic approaches are used. In the first the data are subjected to a statistical analysis to establish the degree of self-consistency of the results. Such a treatment reflects the reproducibility of the data and sets confidence limits on the overall results; however, it provides no information concerning any possible systematic errors inherent in the techniques used.

In the second approach an attempt is made to establish limits for these systematic errors through an analysis of the determinant errors associated with the measuring techniques used and through an estimate of the indeterminant errors involved insofar as they are reflected in the raw data. An overall estimate of the absolute error limits is then obtained by summing the determinant and indeterminant errors. It should be emphasized that the results of this procedure represents the *maximum possible* error for the data; the difference between the measured and true values of a given parameter is expected in a very large majority of instances to be significantly less than this maximum error.

STATISTICAL TREATMENT OF ISOTHERMAL OXIDATION RATE DATA

A statistical analysis of the isothermal oxidation rate data generated in this program was performed. The analysis provided estimates of the parameters of the Arrhenius prediction equation and, in addition, provided 90% joint and individual confidence intervals for the rate

constants and the parameters. The details of these calculations were outlined in a previous report[1] covering the diffusion results and will not be repeated here.

Data

The isothermal steam oxidation rate data were assumed to be represented by the parabolic rate of reaction kinetic model in time (t):

$$\frac{dK}{dt} = \frac{1}{K}\frac{\delta_K^2}{2} \tag{A1}$$

where K is a kinetic parameter (i.e., oxide layer thickness, ϕ; alpha layer thickness, α; Xi (oxide + alpha) layer thickness, ξ; and total oxygen consumed, τ) and $\delta_K^2/2$ is defined as the isothermal parabolic rate constant. The isothermal parabolic rate constant can be estimated from the integrated form of Eq. (A1): $K^2 = K_0 + \delta_K^2 t$ by the method of least squares. The estimated values of $\delta_K^2/2$ were calculated on the basis that $K_0 = 0$, which assumes "ideal" parabolic behavior, and these estimated values are tabulated in Table A1. The parabolic rate constants in Table A1 were rounded to three significant figures for the statistical treatments outlined below. Thus, the prediction equations from this analysis are not precisely those presented earlier where rounding was not done. The differences in the statistical parameters, however, are negligible.

The treatments for the rate constants for the oxide layer and subsequently for the ξ layer and τ were restricted to the temperature range 1050–1504°C (1922–2739°F) for reasons discussed in the body of this report. The alpha layer rate constants were examined for the temperature range of 905–1504°C (1661–2739°F).

Prediction Equations for Rate Constants

The theoretical prediction equation for a rate constant, $\delta_K^2/2$ is:

$$\delta_K^2/2 = A\exp(-Q/RT) \quad , \tag{A2}$$

Table A1. Parabolic Rate Constant Data, $\delta_K^2/2$

Temperature (°C)	Oxide Layer ($cm^2/s \times 10^8$)	Alpha Layer ($cm^2/s \times 10^8$)	Oxide + Alpha Layer ($cm^2/s \times 10^7$)	Total Oxygen $[(g/cm^2)^2/s] \times 10^7$
905		.101		
956		.203		
1001		.314		
1050	1.40	.849	.442	.472
1101	2.17	1.95	.823	.807
1153	3.63	3.25	1.38	1.39
1203	5.39	5.87	2.25	2.18
1253	7.66	10.1	3.53	3.30
1304	11.4	15.9	5.43	5.08
1352	16.5	27.1	8.59	7.69
1404	23.5	41.2	12.7	11.3
1454	33.7	59.0	18.2	16.4
1504	45.2	85.9	25.6	22.8

where A and Q are constants to be determined from experimental data, R[1.987 cal/(mole • kelvin)] is the gas constant and T is temperature (kelvin). Equation (A2) is linearized by taking logarithms, $\ln \delta_K^2/2 = \ln A - (Q/R)\ 1/T$, and, assuming this linear model is the correct representation of the data, the following computations can be made:

1. Calculate by the method of least squares a prediction equation:

$$\widehat{\ln \delta_K^2/2} = \widehat{\ln A} - (\widehat{Q/R})\ 1/T \quad .$$

2. Calculate the individual and joint 90% confidence intervals on the expected values of the estimates $\widehat{\ln A}$ and $(\widehat{Q/R})$.
3. Calculate the 90% confidence interval for the expected predicted values of $\widehat{\ln \delta_K^2/2}$.
4. Calculate the 90% confidence interval for the expected values of $\hat{A}$ and $\hat{Q}$.

The symbol "^" over a letter means "the estimate of". For example, $\ell n\hat{}A$ is "the estimate of" the constant ℓn A.

Let $\hat{Y}_i = \hat{\ell n}(\delta_K^2/2)_i$ be the predicted value of the logarithm of a rate constant at temperature T_i where i = 1, 2, ..., n (number of data points) and let Y_i be the observed experimental value of the logarithm of a rate constant at temperature T_i. The correct model for the observed values is assumed to be $Y_i = E\{\hat{Y}_i\} + \varepsilon_i$, where the error random variables, ε_i's, are independent and identically distributed with zero mean and constant variance (σ^2), and $E\{\hat{Y}_i\}$ represents the expected value of the predicted value. In addition, the errors are assumed to be normally distributed for the purposes of calculating confidence intervals.

The estimates of the constants in the prediction equation are found by minimizing the sum of the squares for error:

$$SSE = \sum_{i=1}^{n} \varepsilon_i^2 = \sum_{i=1}^{n} (Y_i - \hat{Y}_i)^2 \quad .$$

The solutions to this minimization for each rate constant are tabulated in Table A2.

Table A2. Prediction Equations for the Logarithm of the Rate Constants

Model	Prediction Equation	Applicable Range (°C)
Oxide	$\hat{\ell n}\ \delta_\phi^2/2 = -4.48868 - 18060(1/T)$	1050–1504
Alpha	$\hat{\ell n}\ \delta_\alpha^2/2 = -0.27230 - 24230(1/T)$	905–1504
Oxide + Alpha	$\hat{\ell n}\ \delta_\xi^2/2 = -1.07462 - 20990(1/T)$	1050–1504
Total Oxygen	$\hat{\ell n}\ \delta_\tau^2/2 = -1.70986 - 20100(1/T)$	1050–1504

The observed and predicted values of the rate constants and the 90% confidence intervals for the predicted values are tabulated in Table A3. Columns 5 and 7 of the table express the confidence interval as a percentage of the predicted values at the extremes and approximate mean of the observed reciprocal temperatures. These same data are displayed graphically in Figs. A1–A4. The confidence interval lines (dashed lines)

Table A3. Observed and Predicted Values and 90% Confidence Intervals for the Predicted Values of $\ln \frac{\delta^2}{2}$

Temperature (°C)	Observed Value	Predicted Value	Lower 90% CI For Mean	Uncertainty (%)	Upper 90% CI (%)	Uncertainty (%)
			Oxide			
1050	−18.0842	−18.1381	−18.1862	−4.0	−18.0899	+5.0
1101	−17.6459	−17.6315	−17.6705		−17.5925	
1153	−17.1314	−17.1523	−17.1837		−17.1208	
1203	−16.7361	−16.7234	−16.7498		−16.6969	
1253	−16.3846	−16.3225	−16.3468	−2.4	−16.2982	+2.5
1304	−15.9870	−15.9398	−15.9649		−15.9148	
1352	−15.6173	−15.6016	−15.6296		−15.5737	
1404	−15.2636	−15.2571	−15.2894		−15.2247	
1454	−14.9031	−14.9453	−14.9825		−14.9081	
1504	−14.6095	−14.6511	−14.6934	−4.1	−14.6088	+4.3
			Alpha			
905	−20.7133	−20.8375	−20.9520	−10.8	−20.7229	+12.1
956	−20.0152	−19.9842	−20.0801		−19.8883	
1001	−19.5790	−19.2880	−19.3699		−19.2061	
1050	−18.5843	−18.5838	−18.6535		−18.5141	
1101	−17.7528	−17.9042	−17.9649		−17.8434	
1153	−17.2420	−17.2613	−17.3174		−17.2051	
1203	−16.6508	−16.6858	−16.7419	−5.4	−16.6298	+5.8
1253	−16.1081	−16.1481	−16.2075		−16.0887	
1304	−15.6543	−15.6347	−15.6999		−15.5895	
1352	−15.1211	−15.1810	−15.2530		−15.1089	
1404	−14.7022	−14.7187	−14.7989		−14.6386	
1454	−14.3431	−14.3005	−14.3888		−14.2122	
1504	−13.9674	−13.9058	−14.0022	−9.3	−13.8094	+10.1
			Oxide + Alpha			
1050	−16.9345	−16.9371	−16.9666	−2.9	−16.9076	+3.0
1101	−16.3128	−16.3484	−16.3722		−16.3245	
1153	−15.7960	−15.7915	−15.8107		−15.7722	
1203	−15.3071	−15.2930	−15.3092		−15.2768	
1253	−14.8567	−14.8271	−14.8420	−1.5	−14.8123	+1.5
1304	−14.4261	−14.3824	−14.3978		−14.3671	
1352	−13.9674	−13.9894	−14.0065		−13.9723	
1404	−13.5764	−13.5890	−13.6088		−13.5691	
1454	−13.2166	−13.2267	−13.2495		−13.2039	
1504	−12.8755	−12.8848	−12.9107	−2.6	−12.8589	+2.6
			Total Oxygen			
1050	−16.8688	−16.8993	−16.9322	−3.2	−16.8664	+3.3
1101	−16.3325	−16.3356	−16.3622		−16.3089	
1153	−15.7887	−15.8023	−15.8238		−15.7808	
1203	−15.3387	−15.3249	−15.3430		−15.3068	
1253	−14.9241	−14.8789	−14.8955	−1.6	−14.8623	+1.7
1304	−14.4927	−14.4530	−14.4702		−14.4359	
1352	−14.0781	−14.0766	−14.0957		−14.0576	
1404	−13.6932	−13.6932	−13.7153		−13.6711	
1454	−13.3208	−13.3463	−13.3717		−13.3209	
1504	−12.9913	−13.0189	−13.0478	−2.9	−12.9900	+2.9

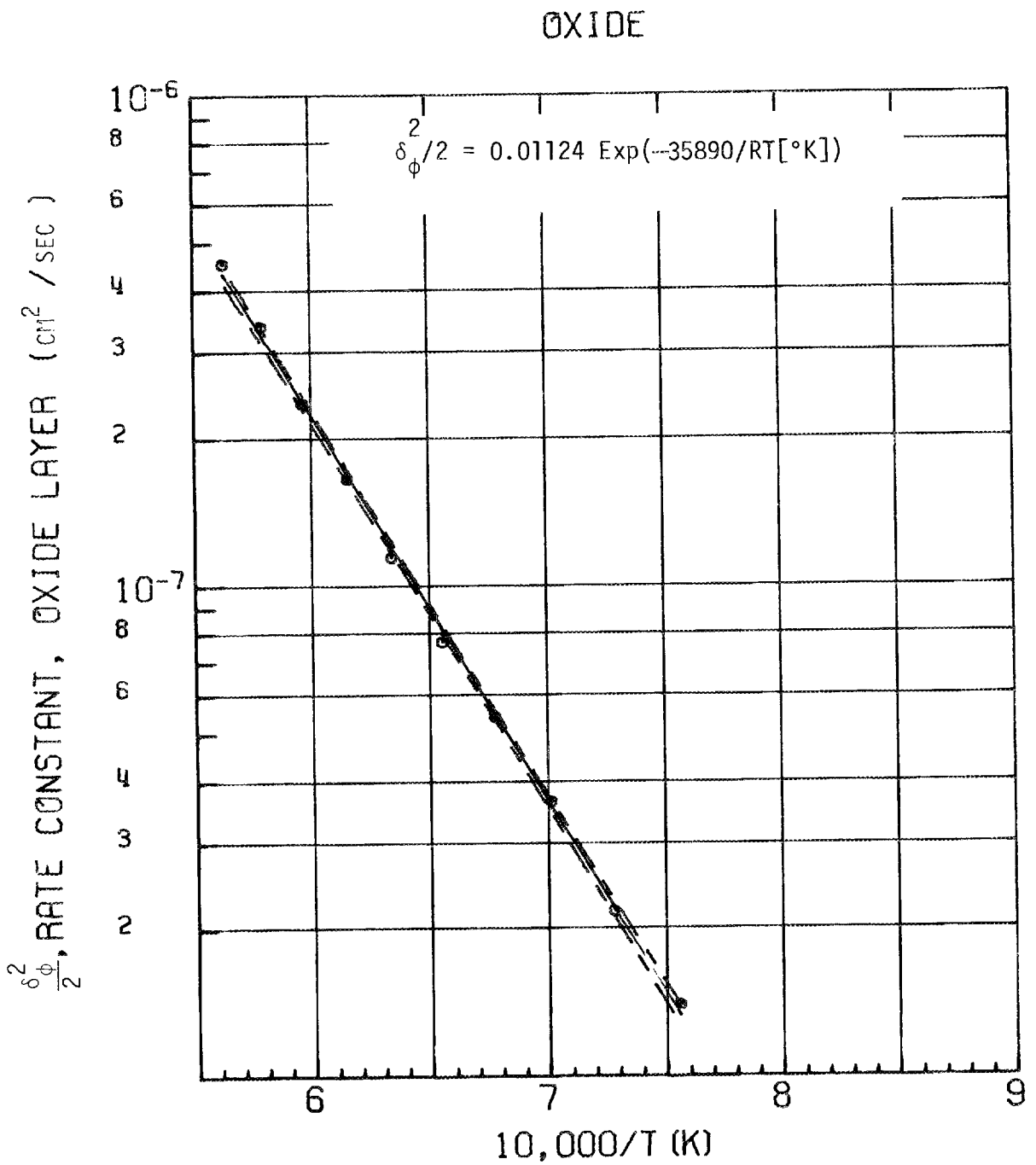

Fig. A1. Prediction Equation and 90% Confidence Intervals (Dashed Lines) for the Parabolic Rate Constants for Oxide Layer Growth from 1050 to 1504°C (1922–2739°F). Oxidation of Sandvik Zircaloy-4 PWR tubing in steam.

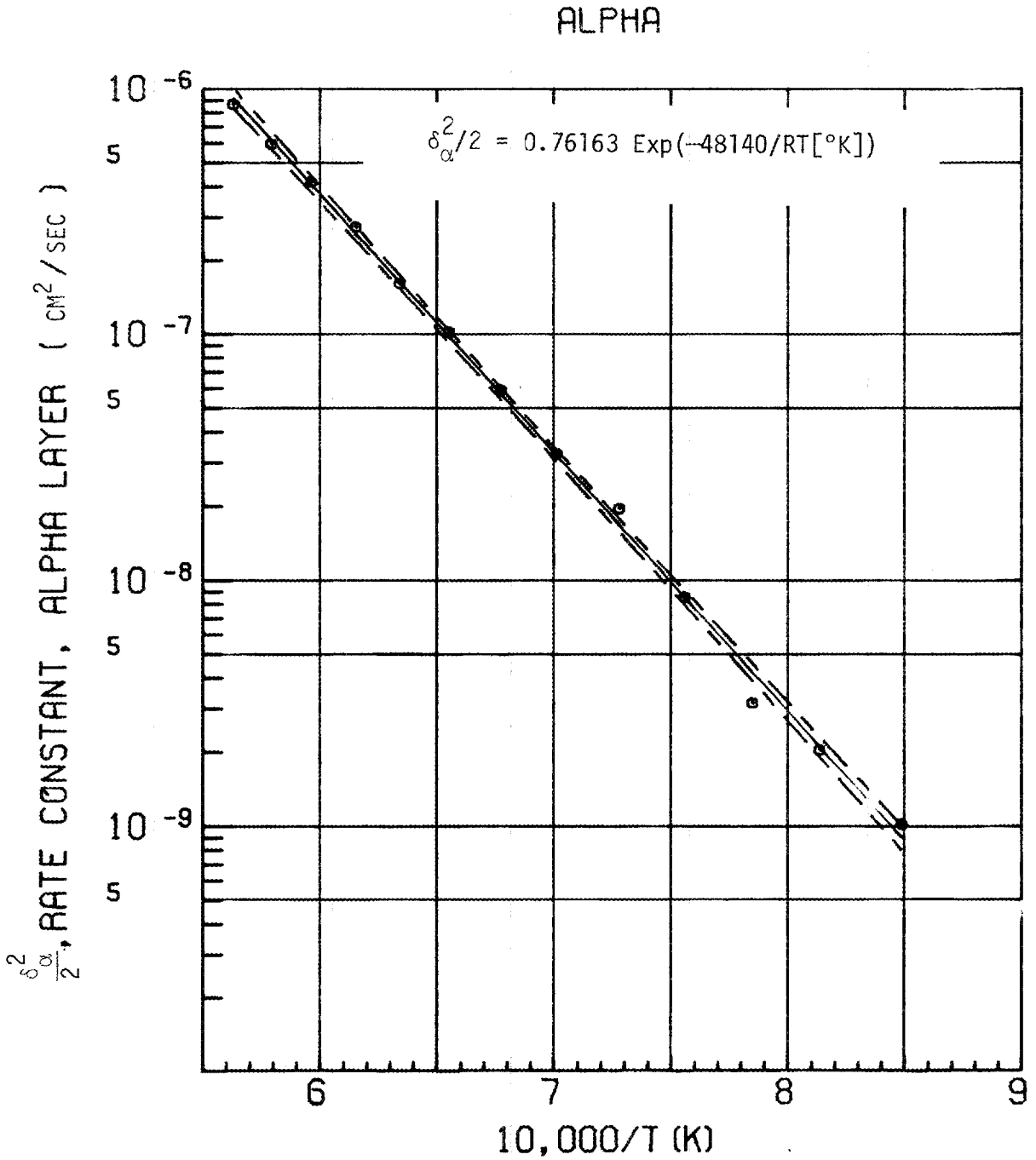

Fig. A2. Prediction Equation and 90% Confidence Intervals (Dashed Lines) for the Parabolic Rate Constants for Alpha Layer Growth from 905 to 1504°C (1661–2739°F). Oxidation of Sandvik Zircaloy-4 PWR tubing into steam.

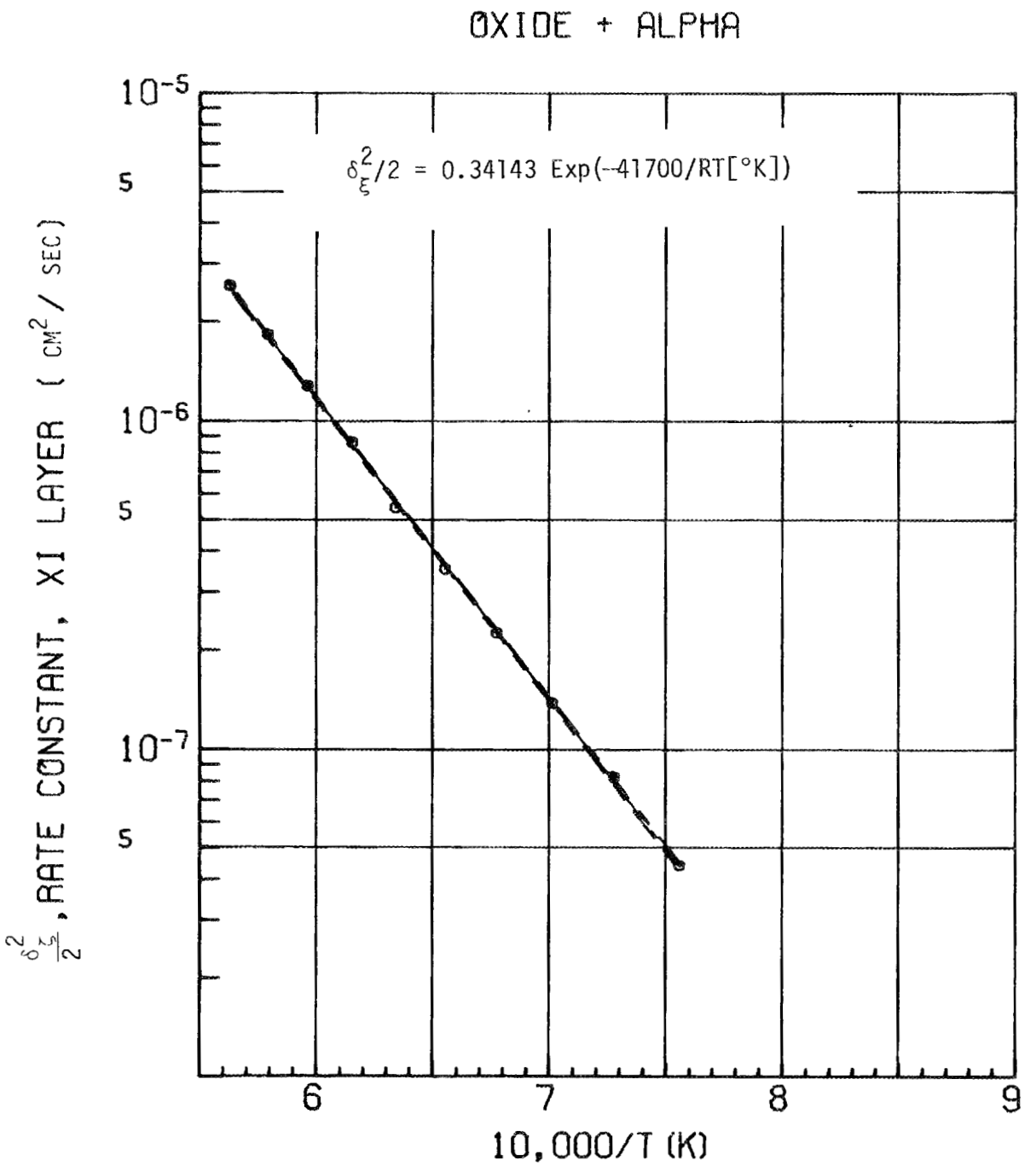

Fig. A3. Prediction Equation and 90% Confidence Intervals (Dashed Lines) for the Parabolic Rate Constants for the Xi (Oxide + Alpha) Layer Growth from 1050 to 1504°C (1922–2739°F). Oxidation of Sandvik Zircaloy-4 PWR Tubing in Steam.

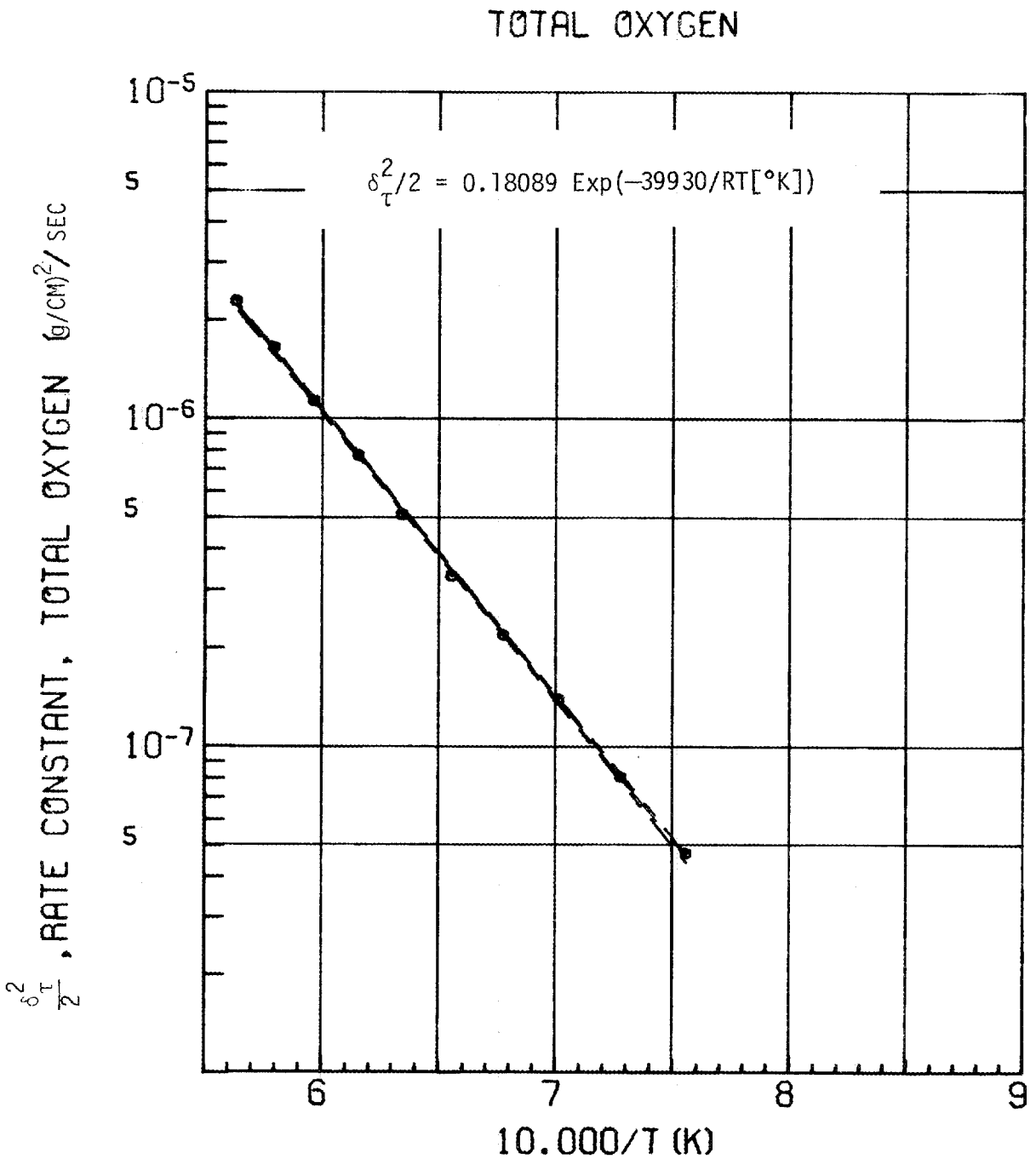

Fig. A4. Prediction Equation and 90% Confidence Intervals (Dashed Lines) for the Parabolic Rate Constant for Total Oxygen Consumption from 1050 to 1504°C (1922–2739°F). Oxidation of Sandvik Zircaloy-4 PWR tubing in steam.

in the figures are so narrow for the ξ and τ measurements that it is difficult to distinguish them from the prediction lines.

The estimated values, $\widehat{\ln} A$ and $(\hat{Q}/R)$ are unbiased estimates of the true values of $\ln A$ and (Q/R). The 90% confidence intervals for the individual expected values of the estimators are listed in Table A4.

Table A4. Individual 90% Confidence Intervals for the Expected Values of $\widehat{\ln} A$ and (Q/R)

Estimator	Lower 90% Confidence Interval	Estimated Value	Upper 90% Confidence Interval
Oxide			
$\widehat{\ln} A$	−4.74691	−4.48868	−4.23045
$(\hat{Q}/R)$	17670	18060	18460
Alpha			
$\widehat{\ln} A$	−0.70658	−0.27230	0.16198
$(\hat{Q}/R)$	23600	24230	24850
Alpha + Oxide			
$\widehat{\ln} A$	−1.23275	−1.07462	−0.91649
$(\hat{Q}/R)$	20750	20990	21230
Total Oxygen			
$\widehat{\ln} A$	−1.88638	−1.70986	−1.53334
$(\hat{Q}/R)$	19830	20100	20370

The individual confidence intervals on $\ln A$ and (Q/R) are appropriate for specifying ranges for an individual estimator irrespective of the value of the other estimator. To interpret the possible values of the estimators of $\ln A$ and (Q/R) simultaneously, which takes into account the covariance and the relative sizes of the variances of the two estimators, joint 90% confidence regions are given in Figs. A5–A8. Each pair of points ($\ln A$, (Q/R)) inside the confidence region (the ellipse) determines a prediction line contained inside the confidence interval about the corresponding prediction line in Fig. A1–A4. Those points on the confidence region boundary in Figs. A5–A8 determine prediction lines which are tangent to the confidence interval boundaries on the corresponding prediction lines.

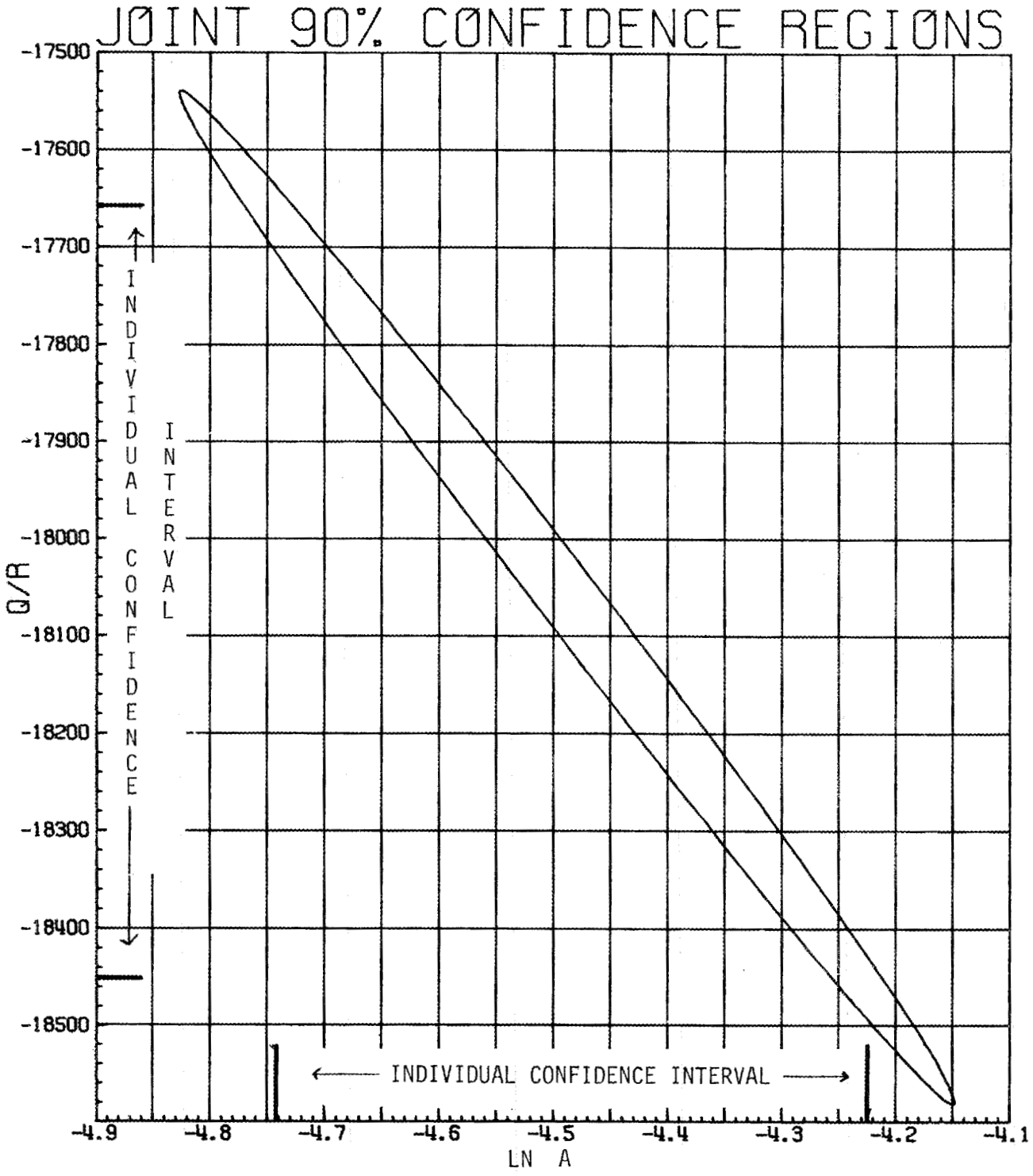

Fig. A5. Joint Confidence Region for the Coefficients of the Oxide Model: $\ell n\ \hat{\delta}^2_\phi/2 = -4.48868 - 18060\ (1/T)$.

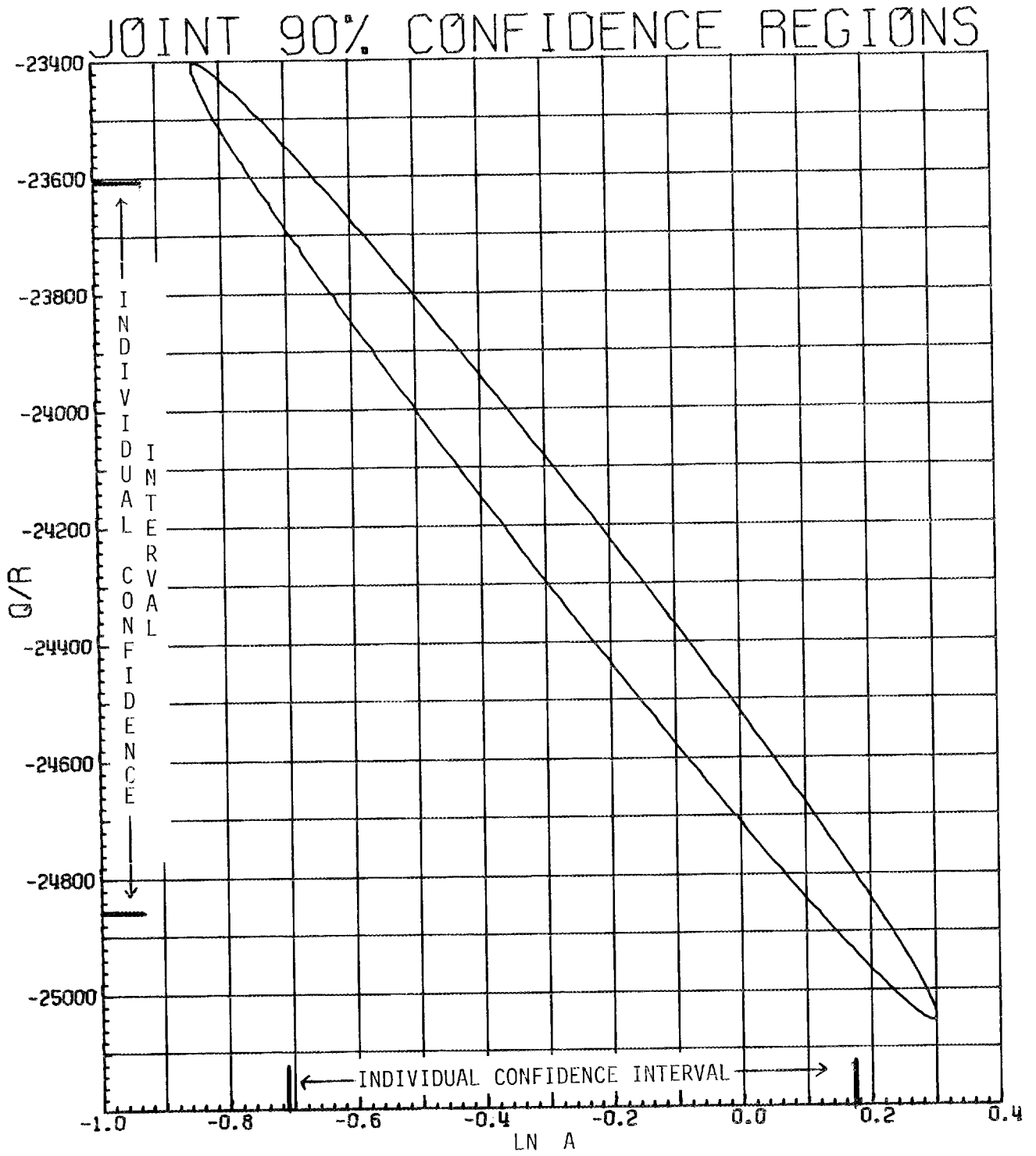

Fig. A6. Joint Confidence Region for the Coefficients of the Alpha Model: $\ln \hat{\delta}_{\alpha}^{2}/2 = -0.27230 - 24230\ (1/T)$.

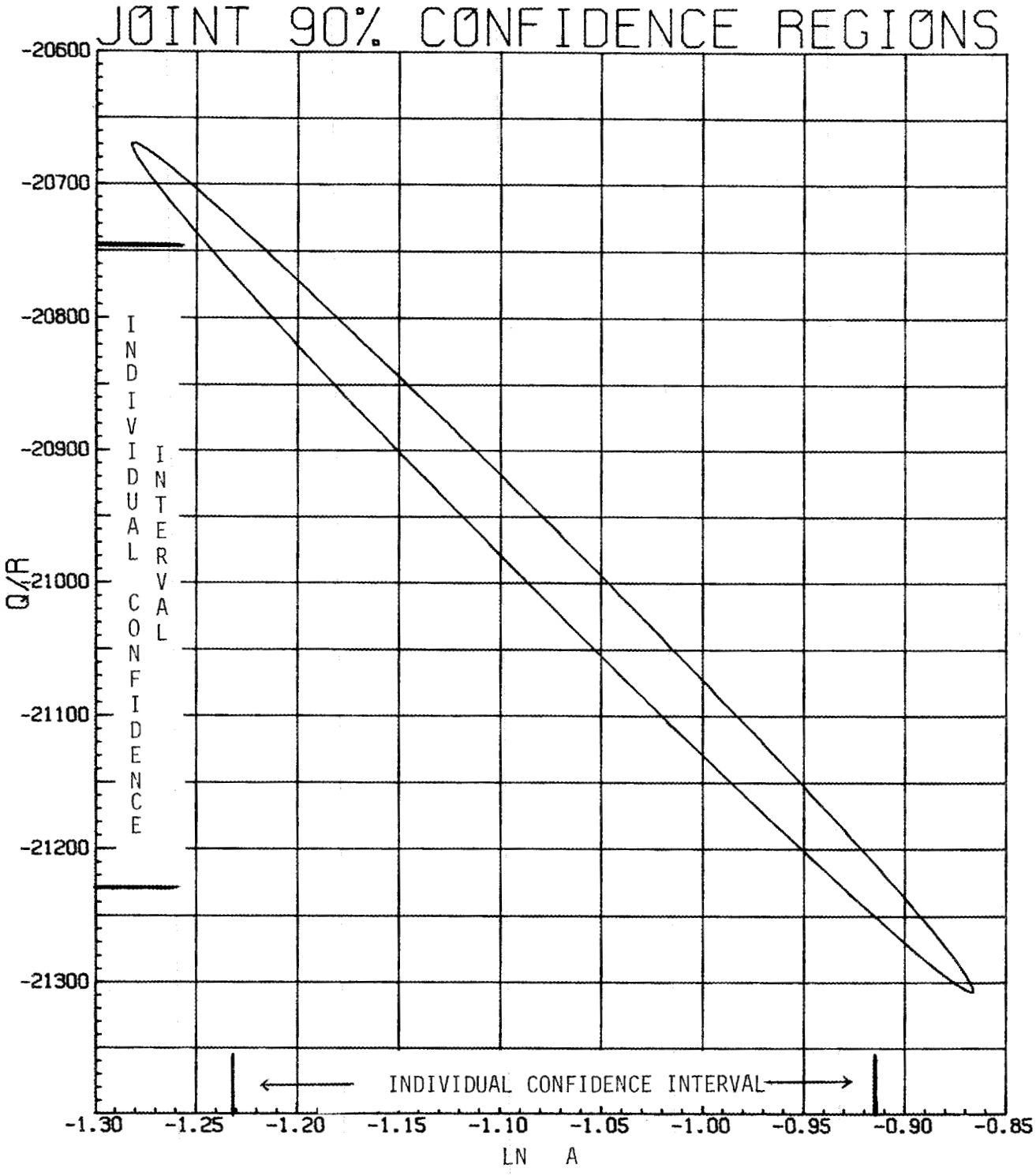

Fig. A7. Joint Confidence Region for the Coefficients of the (Alpha + Oxide) Model: $\ln \hat{\delta}_{\xi}^{2}/2 = -1.07462 - 20990\ (1/T)$.

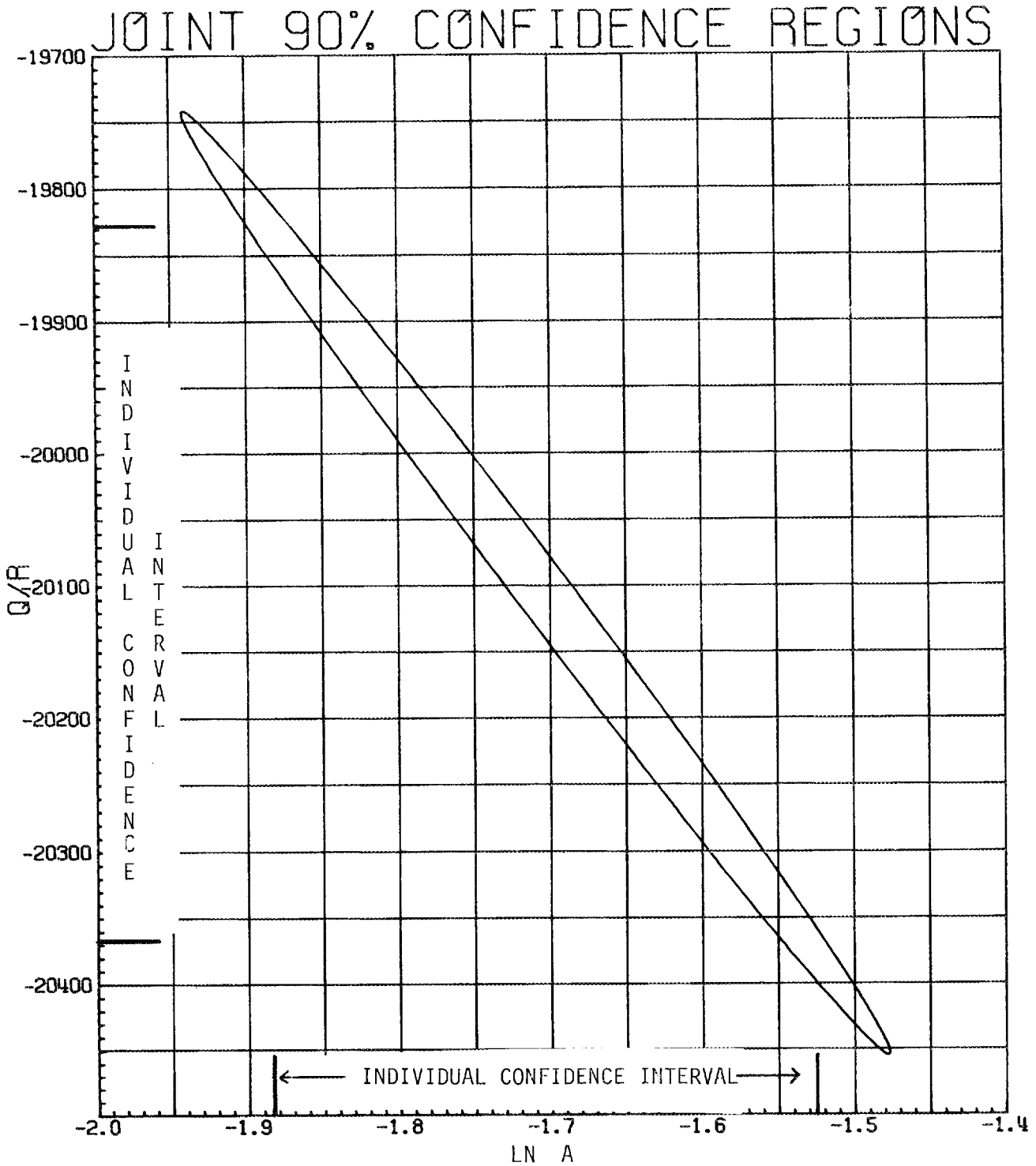

Fig. A8. Joint Confidence Region for the Coefficients of the Total Oxygen Model: $\ell\hat{n}\ \delta_{\tau}^{2}/2 = -1.70986 - 20100\ (1/T)$.

Because the evaluation of confidence intervals and confidence regions depend on the assumption that the errors are normally distributed, the residuals (observed values — predicted values), were examined to see if there was any indication that this assumption might be false.

The residuals were standardized by dividing by the estimated standard deviation (S) of the error random variables and then plotted versus the predicted value. None of the residuals is three standard deviations from zero, and, except for one residual point for the alpha layer data, all remaining points are within two standard deviations from zero. Therefore, there are no apparent outliers. To test for normality, Bowman and Shenton's test[2] on the skewness and kurtosis statistics was used at the 10% significance level with no significant results for any of the data sets. There did appear to be some trends in the residual plots but because of the small number of points, only gross deviations from the assumption could have been detected. The examination of the residuals did not indicate that any assumptions were false.

To estimate the constants A and Q in Eq. (A2), the estimators $\ell\hat{n}\ A$ and $(\hat{Q}/R)$ from the linear prediction equations are used. The estimators of the two constants are:

$$\hat{A} = \exp\{\ell\hat{n}\ A\}, \text{ and} \tag{A3}$$

$$\hat{Q} = R(Q/R) \quad . \tag{A4}$$

The estimator $\hat{Q}$ is an unbiased estimate of Q but $\hat{A}$ is a slightly biased estimator of A with the expected value of $\hat{A}$ being $\exp[(\sigma_o^2/2)A]$, where σ_o^2 is the variance of $\ell\hat{n}\ A$. If the estimate of σ_o^2 is used, the bias can be shown to be less than 1% of the true value for all four data sets. Since the bias is so small, the correction for bias will not be used. Table A5 lists the values of $\hat{A}$ and $\hat{Q}$ and their corresponding confidence intervals.

Table A5. Estimated Values and 90% Confidence Intervals for A and Q

Estimator	Lower 90% Confidence Interval	Estimated Value	Upper 90% Confidence Interval
Oxide			
$\hat{A}$	0.00868	0.01124	0.01455
$\hat{Q}$	35100	35890	36670
Alpha			
$\hat{A}$	0.49333	0.76163	1.17584
$\hat{Q}$	46900	48140	49390
Alpha + Oxide			
$\hat{A}$	0.29149	0.34143	0.39992
$\hat{Q}$	41220	41700	42190
Total Oxygen			
$\hat{A}$	0.15162	0.18089	0.21581
$\hat{Q}$	39400	39930	40470

Confidence Intervals at the 95% Level

Throughout this report we have chosen to discuss statistical uncertainties on the data in terms of 90% confidence levels. As pointed out in the introduction to this appendix, the basic purpose of a statistical analysis of a data set is to provide an objective measure of the self-consistency and reproducibility of the data. From this point of view, the particular confidence level selected for use is to a large degree a matter of individual judgment, the 90% confidence level being one frequently chosen by many experimenters. On the other hand, the 95% level is also popular, and in this section we summarize our statistical results based on calculations at that confidence level.

Individual Confidence Limits

Values for the upper and lower individual 90% confidence limits on $\hat{A}$ and $\hat{Q}$ are listed in Table A5 for oxide, alpha, oxide + alpha, and total oxygen. To change the upper and lower 90% levels to the 95% levels, we can multiply the uncertainty, in each upper value by the ratio (upper 95%/upper 90%) and each lower value by the ratio (lower 95%/lower 90%). Since the arguments given below for deriving these two ratios are

symmetrical and the numerical values of the ratios are identical, only the ratio (upper 95%/lower 90%) is derived. Note also that the ratios given below may be used only when the uncertainties at the 90% confidence level are expressed as a percentage uncertainty in the estimator; they are not directly applicable in converting the absolute numerical values of the 90% confidence limits to corresponding values at the 95% level.

(Upper 95%/Upper 90%) for Estimator $\hat{A}$ — For a $(1-\alpha)\%$ confidence interval, an upper $(1-\alpha)\%$ value for the estimator $\hat{A}$, expressed as a fraction of $\hat{A}$, is defined by

$$\text{upper } (1-\alpha)\% = \frac{\exp[\ell n\ \hat{A} + t_{\alpha/2}\ (\nu)\ S_1] - \exp(\ell n\ \hat{A})}{\exp(\ell n\ \hat{A})} \tag{A5}$$

where

$1-\alpha$, expressed as percent, represents the desired confidence level,

$\ell n\ \hat{A}$ is the estimator of $\ell n\ A$ (see Tables A4 and A6). (Note that the value of $\ell n\ \hat{A}$ is independent of the value of α chosen.),

S_1 is the standard deviation of $\ell n\ \hat{A}$ for the given data set (see Table A6), and

$t_{\alpha/2}(\nu)$ is the $\alpha/2$ percentage point of the t-distribution with (ν) degrees of freedom.

Therefore,

$$\frac{\text{upper } 95\%}{\text{upper } 90\%} = \frac{\exp(t_{0.025}(\nu)\ S_1) - 1}{\exp(t_{0.05}(\nu)\ S_1) - 1} \quad . \tag{A6}$$

Evaluation of the ratio in Eq. (A6) requires knowledge of the appropriate values of the $t_{\alpha/2}(\nu)$'s and of the standard deviations for the estimators. These quantities are listed in Table A6; note that $t_{\alpha/2}(\nu)$ is dependent on the degrees of freedom and, hence, the number of observations for a given data set. Substituting these quantities in Eq. (A6), one obtains the desired ratios, which are tabulated in Table A7. As may be seen, the change from a 90% to a 95% confidence interval increases the uncertainties on $\hat{A}$ by amounts varying from about 26 to 31%; e.g., if the uncertainty on the $\hat{A}$ value in the expression for the oxide parabolic rate were ±10% at the 90% confidence level, it is ±12.8% at the 95% level.

Numerical values for the upper and lower limits for the 95% individual confidence intervals for $\hat{A}$ are given in Table A8.

Table A6. Values of and the Standard Deviations for the Estimators $\ell N\ \hat{A}$ and $(\hat{Q}/R)$ and the Degrees of Freedom and Appropriate $t_{\alpha/2}(\nu)$ Values for the Various Data Sources

Source	Estimator	Estimated Value	Estimator Standard Deviation	Degrees of Freedom	$t_{.05}(\nu)$	$t_{.025}(\nu)$
Oxide				8	1.860	2.306
	$\ell n\ \hat{A}$	-4.48868	0.13883			
	$(\hat{Q}/R)$	18060	212			
Alpha				11	1.796	2.201
	$\ell n\ \hat{A}$	-0.27230	.24180			
	$(\hat{Q}/R)$	24230	348			
Xi (oxide + alpha)				8	1.860	2.306
	$\ell n\ \hat{A}$	-1.07462	0.08501			
	$(\hat{Q}/R)$	20990	130			
Total Oxygen				8	1.860	2.306
	$\ell n\ \hat{A}$	-1.70986	0.09490			
	$(\hat{Q}/R)$	20100	145			

Table A7. Ratios to be Used in Converting Uncertainties at the 90% Confidence Level to Uncertainties at the 95% Confidence Level. Conversion Applicable to Individual Confidence Limits Only

Source	Ratio (Upper 95%/Upper 90%)
Oxide	1.281
Alpha	1.314
Xi	1.264
Total Oxygen	1.267

Table A8. Estimated Values and 95% Individual Confidence Intervals for the Estimators $\hat{A}$ and $\hat{Q}$

Estimator	Lower 95% Confidence Interval	Estimated Value	Upper 95% Confidence Interval
Oxide			
$\hat{A}$	0.00816	0.01124	0.01547
$\hat{Q}$	34910	35890	36860
Alpha			
$\hat{A}$	0.4473	0.7616	1.297
$\hat{Q}$	46620	48140	49670
Alpha + Oxide			
$\hat{A}$	0.2807	0.3414	0.4154
$\hat{Q}$	41110	41700	42300
Total Oxygen			
$\hat{A}$	0.1453	0.1810	0.2252
$\hat{Q}$	39270	39930	40600

<u>(Upper 95%/Upper 90%) for $\hat{Q}$</u> — For a $(1-\alpha)\%$ confidence interval, an upper $(1-\alpha)\%$ limit for the estimator $\hat{Q}$, expressed as a fraction of $\hat{Q}$, is defined by

$$\text{Upper}(1-\alpha)\% = \frac{R(\hat{Q}/R) + Rt_{\alpha/2}(\nu)S_2 - R\ (\hat{Q}/R)}{R(\hat{Q}/R)}$$

or

$$\text{Upper}(1-\alpha)\% = t_{\alpha/2}(\nu)S_2/(\hat{Q}/R) \tag{A7}$$

where

$\hat{Q}/R$ is the estimator of Q/R,

R is the gas constant, and

S_2 is the standard deviation of $\hat{Q}/R$.

Therefore

$$\frac{\text{Upper 95\%}}{\text{Upper 90\%}} = \frac{t_{0.025}(\nu)}{t_{0.05}(\nu)} = \begin{cases} 1.240 \text{ for } \nu = 8 \\ 1.226 \text{ for } \nu = 11 \end{cases} \tag{A8}$$

The numerical values at the right of Eq. (A8) were obtained by inserting appropriate values of $t_{\alpha/2}(\nu)$ from Table A6. See Table A8 for numerical values of the 95% confidence limits on $\hat{Q}$.

Joint Confidence Intervals

The joint confidence interval on $\hat{\delta}/2$, in contrast to the individual confidence limits for $\hat{A}$ and $\hat{Q}$, varies over the width of an Arrhenius plot, being minimum at the mean of the reciprocal temperature observations. For this reason no single conversion factor can be used to convert uncertainties at the 90% level to corresponding values at the 95% level. We have, therefore, recalculated these confidence intervals using the F-distribution statistics appropriate for the 95% level. The results are given in Table A9, which may be compared to Table A3 where the corresponding 90% level values are summarized. Graphical representations of these data in the form of joint confidence ellipses are presented in Figs. A9–A12. The joint confidence regions at the 90% level are also displayed.

MAXIMUM ABSOLUTE ERROR LIMITS FOR EXPERIMENTAL PROCEDURES

Temperature Measurement Errors

Temperature measurement errors in this program were extensively analyzed in a previous report.[3] Potential error sources considered included thermal shunting, electrical shunting, parasitic emf's, data acquisition system errors, thermocouple calibration errors, temperature gradients in the sample, decalibration of thermocouples, and tab attachment effects. It was concluded that the maximum probable temperature measurement error in the MiniZWOK apparatus ranged from ±4°C (7.2°F) at 900°C (1652°F) to ±6°C (10.8°F) at 1500°C (2732°F). The validity of these limits was confirmed by the subsequent *in situ* determination of the alpha-to-beta phase transformation temperature for pure zirconium (see p. 30); the additional *in situ* melting point determination (p. 31) did not bear directly on the question of the extent of thermal shunting errors, but this result did show that the contributions of the other potential error sources to the uncertainties of temperature measurements lie well within the limits given above.

Table A9. Predicted Values for the Estimators $\ln \hat{\delta}^2/2$ and 95% Confidence Intervals for the Expected Predicted Values. Percentage Uncertainties on $\hat{\delta}^2/2$ are Also Shown

Temperature (°C)	$\ln \hat{\delta}^2/2$ Observed Value	$\ln \hat{\delta}^2/2$ Predicted Value	Lower 95% CL For $\ln \hat{\delta}^2/2$	Uncertainty on $\hat{\delta}^2/2$ (%)	Upper 95% CL For $\ln \hat{\delta}^2/2$	Uncertainty on $\hat{\delta}^2/2$ (%)
			Oxide			
1050	−18.0842	−18.1381	−18.1978	−5.8	−18.0784	+6.1
1101	−17.6459	−17.6315	−17.6798		−17.5832	
1153	−17.1314	−17.1523	−17.1913		−17.1133	
1203	−16.7361	−16.7234	−16.7562		−16.6905	
1253	−16.3846	−16.3225	−16.3527	−3.0	−16.2924	+3.1
1304	−15.9871	−15.9398	−15.9710		−15.9087	
1352	−15.6173	−15.6016	−15.6363		−15.5670	
1404	−15.2636	−15.2571	−15.2972		−15.2169	
1454	−14.9031	−14.9453	−14.9915		−14.8992	
1504	−14.6095	−14.6511	−14.7036	−5.1	−14.5987	+5.4
			Alpha			
905	−20.7133	−20.8375	−20.9779	−13.1	−20.6970	+15.1
956	−20.0152	−19.9842	−20.1017		−19.8666	
1001	−19.5790	−19.2880	−19.3884		−19.1876	
1050	−18.5843	−18.5838	−18.6692		−18.4984	
1101	−17.7528	−17.9042	−17.9786		−17.8297	
1153	−17.2420	−17.2613	−17.3301		−17.1925	
1203	−16.6508	−16.6858	−16.7545	−6.6	−16.6172	+7.1
1253	−16.1081	−16.1481	−16.2209		−16.0753	
1304	−15.6543	−15.6347	−15.7147		−15.5548	
1352	−15.1211	−15.1810	−15.2693		−15.0927	
1404	−14.7022	−14.7187	−14.8170		−14.6205	
1454	−14.3431	−14.3005	−14.4087		−14.1923	
1504	−13.9674	−13.9058	−14.0240	−11.1	−13.7877	+12.5
			Oxide + Alpha			
1050	−16.9345	−16.9371	−16.9737	−3.6	−16.9005	+3.7
1101	−16.3128	−16.3484	−16.3780		−16.3188	
1153	−15.7960	−15.7915	−15.8153		−15.7676	
1203	−15.3071	−15.2930	−15.3131		−15.2729	
1253	−14.8567	−14.8271	−14.8456	−1.8	−14.8087	+1.9
1304	−14.4261	−14.3824	−14.4015		−14.3634	
1352	−13.9674	−13.9894	−14.0106		−13.9682	
1404	−13.5764	−13.5890	−13.6135		−13.5644	
1454	−13.2166	−13.2267	−13.2549		−13.1984	
1504	−12.8755	−12.8848	−12.9169	−3.2	−12.8526	+3.3
			Total Oxygen			
1050	−16.8688	−16.8993	−16.9401	−4.0	−16.8585	−4.2
1101	−16.3325	−16.3356	−16.3686		−16.3025	
1153	−15.7887	−15.8023	−15.8289		−15.7756	
1203	−15.3387	−15.3249	−15.3474		−15.3025	
1253	−14.9241	−14.8789	−14.8995	−2.0	−14.8583	+2.1
1304	−14.4927	−14.4530	−14.4743		−14.4318	
1352	−14.0781	−14.0766	−14.1003		−14.0530	
1404	−13.6932	−13.6932	−13.7206		−13.6658	
1454	−13.3208	−13.3463	−13.3779		−13.3148	
1504	−12.9913	−13.0189	−13.0548	−3.5	−12.9830	+3.7

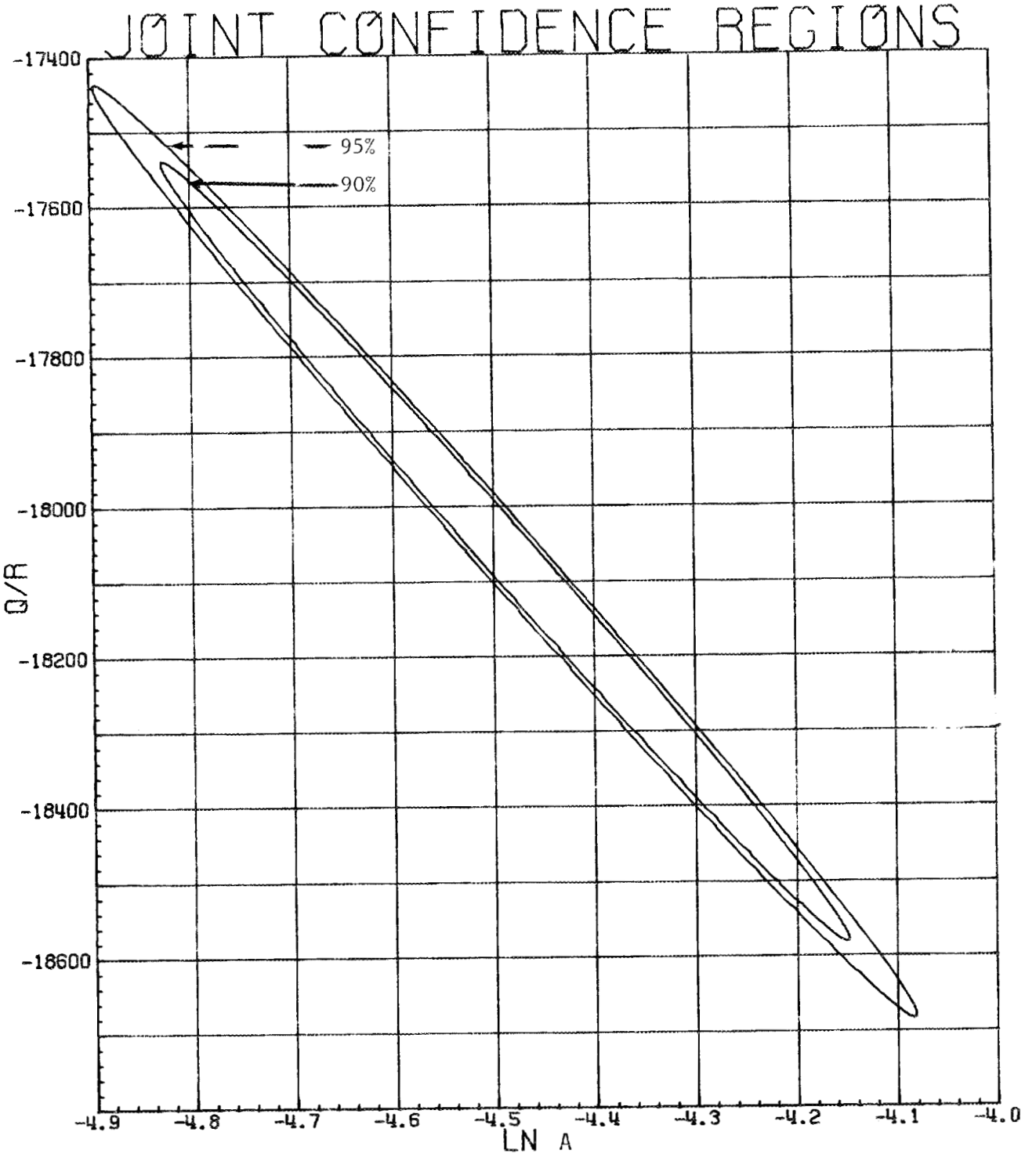

Fig. A9. Joint Confidence Region for the Coefficients of the Oxide Model: $\hat{\ell n}\ \delta_{\phi}^{2}/2 = -4.48868 - 18060.28\ (1/T)$.

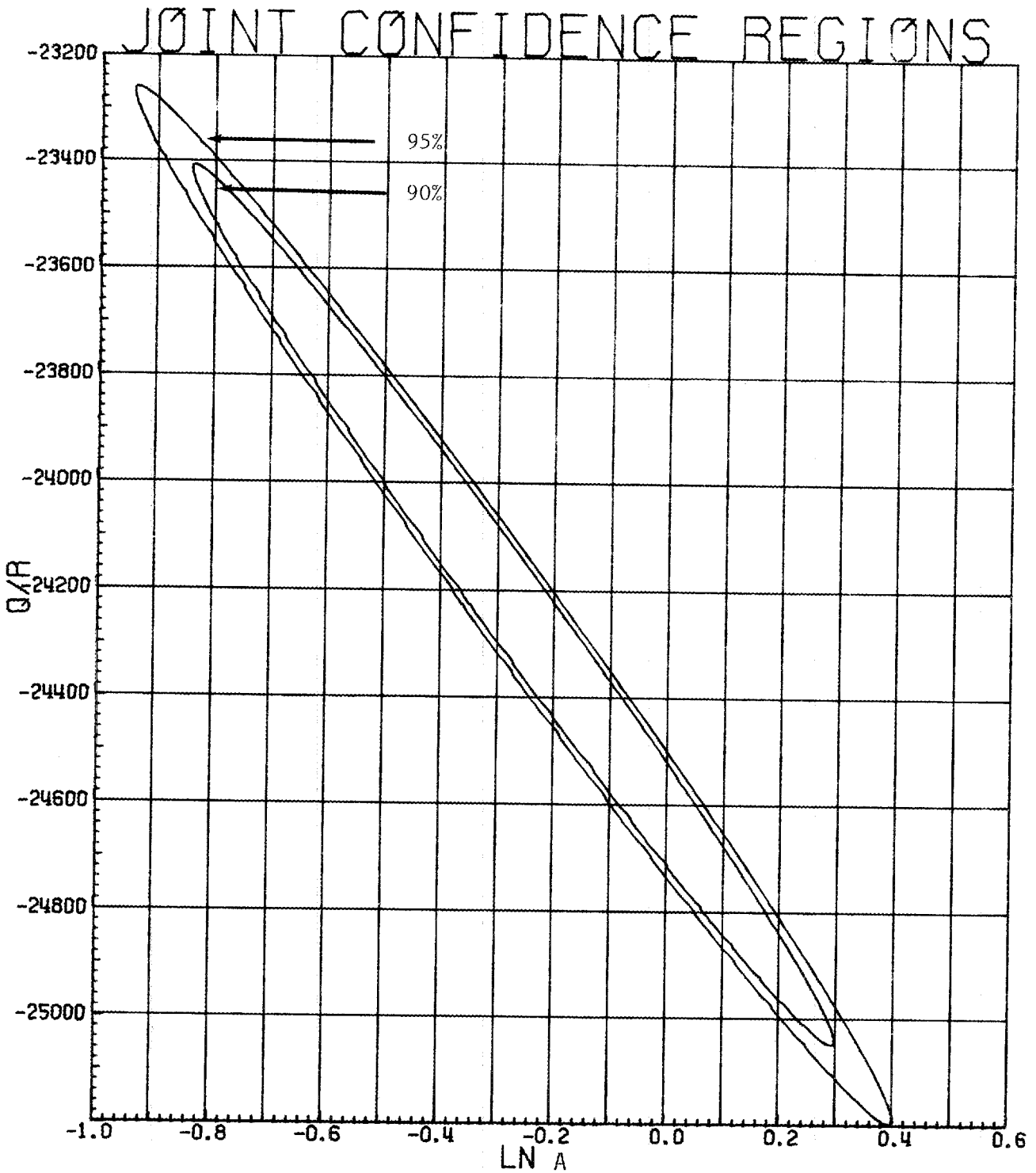

Fig. A10. Joint Confidence Region for the Coefficients of the Alpha Model: $\ell\hat{n}\ \delta_\alpha^2/2 = -0.27230 - 24228.91\ (1/T)$.

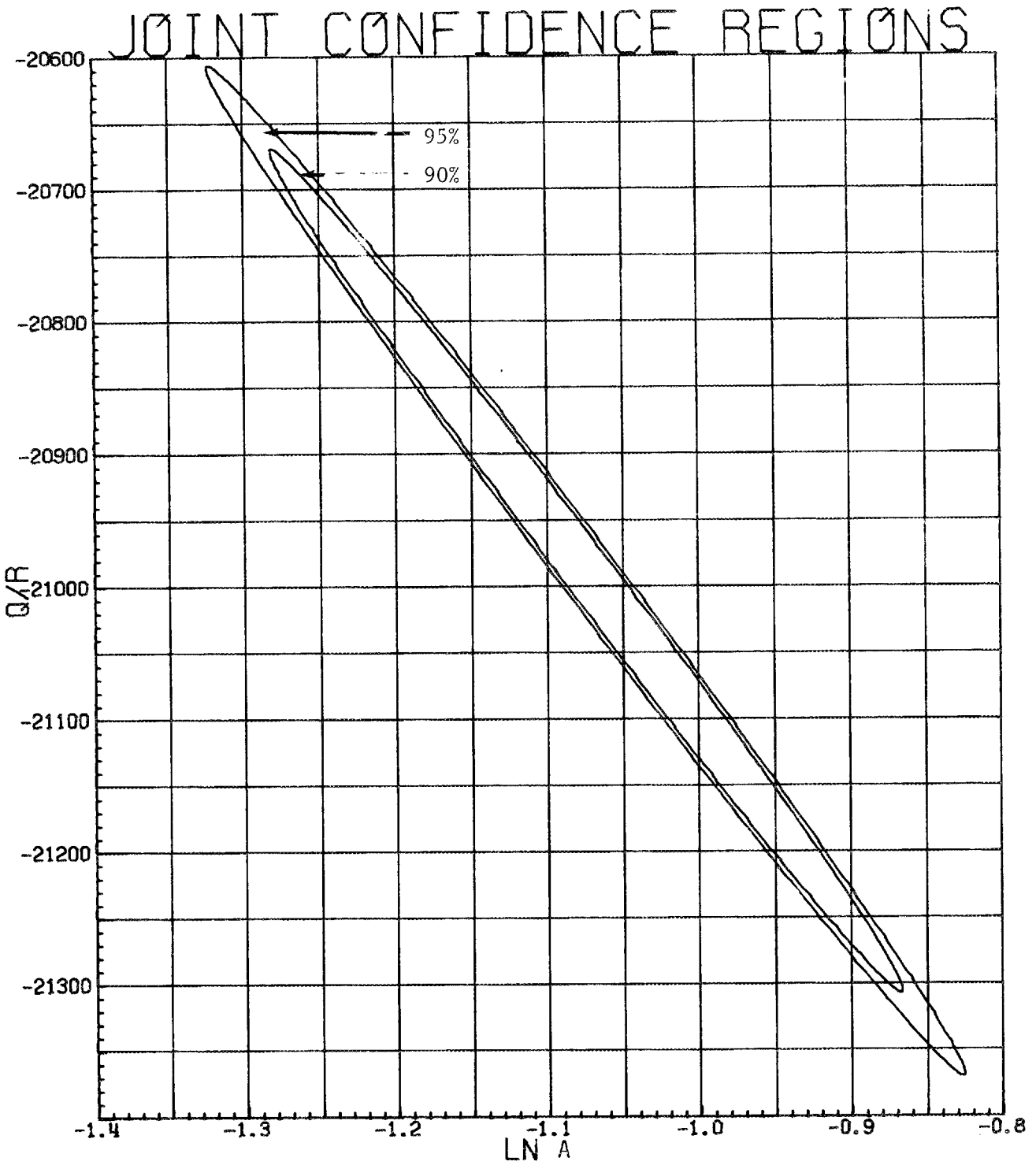

Fig. A11. Joint Confidence Region for the Coefficients of the (Alpha + Oxide) Model: $\hat{\ell n}\ \delta^2_{Xi}/2 = -1.07462 - 20988.50\ (1/T)$.

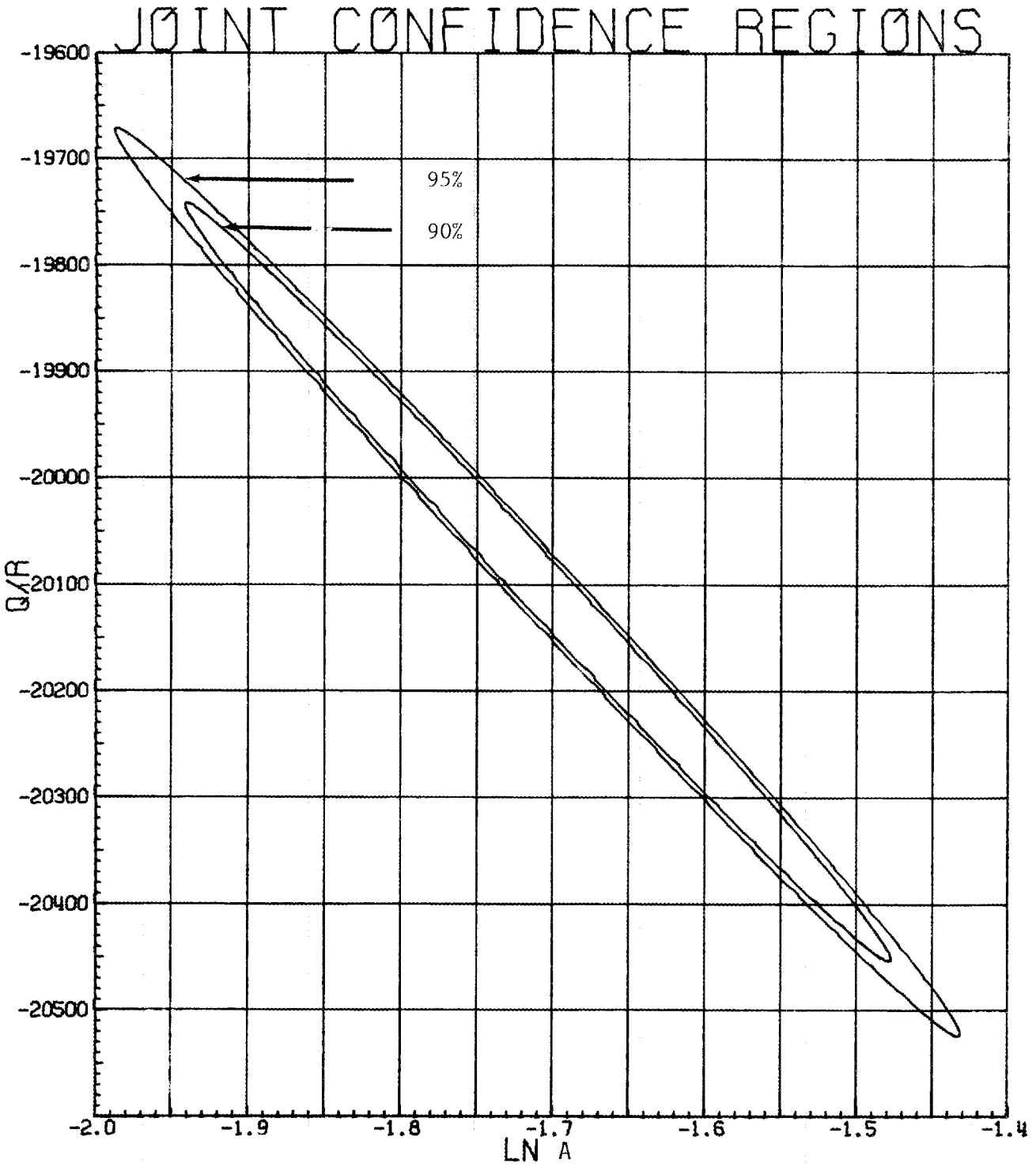

Fig. A12. Joint Confidence Region for the Coefficients of the Total Oxygen Model: $\ell\hat{n}\ \delta_{\tau}^{2}/2 = -1.70986 - 20097.96\ (1/T)$.

Time Measurement Errors

Absolute measurements of time in virtually all experiments were made using the Computer Operated Data Acquisition System (CODAS). CODAS utilizes a quartz crystal clock whose accuracy is warranted to ±13 μs. There is, however, an uncertainty as large as 2 ms in the time of triggering of the CODAS clock at the beginning of an experiment, and 2 ms may thus be regarded as the maximum error in our absolute time measurements. The effect of this error on the oxidation results is obviously negligible.

A second source of error in the oxidation times reported stems from the necessity for normalizing the time-temperature record for each experiment to an equivalent time of isothermal oxidation at some average temperature. The technique used, which is described in detail in the body of the report (p. 43), utilizes the expression

$$t_{(eff)} = \frac{\int_0^t \exp[-Q/RT(t)]dt}{\exp[-Q/RT_{(eff)}]} , \qquad (A9)$$

where $t_{(eff)}$ is the equivalent oxidation time for strictly isothermal conditions, $T_{(eff)}$ is the temperature (°K) to which the data are to be normalized, T(t) is the actual temperature of the experiment expressed as a function of time, Q is the activation energy for the process, and R is the gas constant. Application of Eq. (A9) thus allows one to correct for oxidation during heat-up and cool-down and for small variations in set-point position of the temperature controller in experiments performed at some nominal temperature.

Implicit in Eq. (A9) is the assumption that the reaction being considered, e.g., the growth of the oxide layer, can be described in terms of a single process (i.e., single activation energy) over the entire temperature range of interest. Inspection of the Arrhenius plots for the oxide and alpha layer kinetic data (Figs. 27 and 28) shows that this assumption is surely valid from ∿1000 to 1500°C (1832–2732°F). Below this temperature range a change in oxidation mechanism does occur at relatively long oxidation times; however, the

amount of oxidation taking place at temperatures below 1000°C (1832°F) at heating rates of ∿100°C/s (180°F/s) will be small. Furthermore, as shown below, changes in t_{eff} produced by relatively large changes in the value of Q used in Eq. (A9) occasioned only minor changes in the $\delta^2/2$ values calculated from K^2 vs $t_{(eff)}$ plots; thus, unless the true activation energy below 1000°C (1832°F) is radically different from that at higher temperatures, the time correction given by Eq. (A9) should be approximately valid.

As experimental data were gathered during the course of this study, it was, of course, necessary to use Eq. (A9) to construct oxidation rate curves and, ultimately, the Arrhenius plots from which values of the activation energy could be obtained. Since accurate values of Q were not available at that time, we chose 40,000 cal/mole as a reasonable approximation. Strictly speaking, once experimental values of Q were determined, these new values of Q could have been used in Eq. (A9) and an iterative procedure applied to the entire data set to obtain the best possible evaluation of Q. However, when the experimental activation energies (35,890 and 48,140 cal/mole for oxide and alpha layers, respectively) were used, tests on several representative data sets revealed that the resulting small changes in oxidation time never produced changes greater than ∿1% in the slopes of the oxidation rate curves. Thus the time corrections made are rather insensitive to the precise value of Q used in Eq. (A9), and we concluded that time corrections are responsible for no more than a 1% error in the parabolic rate constants.

Thickness Measurement Errors

Errors in the measurements of oxide and alpha layer thickness can arise from several sources. For well-defined, uniform scales the reproducibility of readings with the filar eyepiece used in these determinations was ∿±0.25 μm, producing thickness uncertainties ranging from ±2.0 to ±0.25% in thickness determinations for the thinnest and thickest scales measured. In some instances the interface between

different phases, particularly the alpha/prior-beta boundary at low temperatures was ill defined, and measurement uncertainties under these conditions were somewhat greater.

Accurate phase thickness measurements require that specimens be mounted so that they can be sectioned perpendicular to the tube wall. The maximum mounting error was $\sim 5°$, resulting in a thickness uncertainty of +0.4%.

As described in the body of the report, oxide and alpha layer thicknesses represent the average of seven measurements made at 5° intervals over a 30° arc centered on the bead of a measuring thermocouple. This procedure was adopted because of the circumferential temperature gradient in the specimens and because of the existence of small variations in layer thicknesses over short distances caused by other factors. We consider that this procedure minimizes uncertainties in layer thickness.

An estimate of these uncertainties was made by computing the mean $\pm 2\sigma$, where σ is a standard deviation, for the seven layer thicknesses measured in each experiment. The 2σ's were then expressed as a percentage of the mean thickness. A typical data set at 1203°C (2197°F) is shown in Table A10.

From 10 to 20 individual mean thickness determinations were used to define the rate curve at each temperature, and the values of $\pm 2\sigma_K/\bar{K}$, where $\bar{K}$ represents the mean thickness of either the oxide or the alpha layer, were summed and averaged and a value for two standard deviations, $2\sigma'$, for the mean computed. The resulting quantity, $\overline{\pm 2\sigma_K/\bar{K}} \pm 2\sigma'$, for each temperature is to be interpreted as the *maximum* uncertainty (expressed as a percentage of $\bar{K}$) in thickness measurements at the confidence level (approximately 95%) represented by two standard deviations. Tables A11 and A12 list values for this *maximum* uncertainty at several temperatures under the heading "Thickness Variability". It should be noted that $\overline{2\sigma_K/\bar{K}} \pm 2\sigma'$ contains the uncertainties related to the reproducibility of individual measurements but does not take into account the possibility that the measured section was not cut precisely perpendicular to the specimen wall.

Table A10. Estimates of Mean Oxide and Alpha Layer Thicknesses and Their Standard Deviations for Experiments at 1203°C (2197°F)

Expt. No.	$\bar{\phi}$[a] (μm)	$2\sigma_\phi$[b] (μm)	$2\sigma_\phi/\bar{\phi}$ (%)	$\bar{\alpha}$[c] (μm)	$2\sigma_\alpha$[b] (μm)	$2\sigma_\alpha/\bar{\alpha}$ (%)
S-82	49.46	±1.64	±3.3	53.54	±1.04	±2.0
S-83	43.13	2.32	5.4	44.74	1.06	2.4
S-84	38.86	1.63	4.2	40.97	0.96	2.3
S-85	53.52	1.33	2.5	54.62	1.35	2.5
S-86	50.22	1.96	3.9	51.66	1.04	2.0
S-87	58.10	1.35	2.3	64.79	0.91	1.4
S-88	26.64	1.41	5.3	28.23	0.55	2.0
S-89	43.21	1.37	3.2	44.01	1.06	2.4
S-90	28.79	1.23	4.3	30.87	0.81	2.6
S-91	37.23	1.03	2.8	39.74	2.61	6.6

$\overline{\pm 2\sigma_\phi/\bar{\phi}} \pm 2\sigma'_\phi = \pm 3.72 \pm 2.18\%$[d]

$\overline{\pm 2\sigma_\alpha/\bar{\alpha}} \pm 2\sigma'_\alpha = \pm 2.62 \pm 2.88\%$

[a] $\bar{\phi}$ = mean oxide layer thickness.

[b] σ_K = standard deviation of layer thickness measurements in a single experiment; K = ϕ or α.

[c] $\bar{\alpha}$ = mean alpha layer thickness.

[d] σ'_x = standard deviation of the mean $\overline{2\sigma'_K/\bar{K}}$; K = ϕ or α.

Table A11. Probable Maximum Determinant Errors in Oxide Growth Rate Measurements

Error Source	Error at						
	905°C (1661°F)	1001°C (1884°F)	1101°C (2014°F)	1203°C (2197°F)	1304°C (2397°F)	1404°C (2559°F)	1504°C (2739°F)
Temperature measurement uncertainty (°C)	±4.0	±4.3	±4.7	±5.0	±5.3	±5.7	±6.0
Uncertainty in $\delta_\phi^2/2$ due to time correction (%)		±1.0	±1.0	±1.0	±1.0	±1.0	±1.0
Thickness measurement uncertainties							
Mounting error (%)	+0.4	+0.4	+0.4	+0.4	+0.4	+0.4	+0.4
Thickness variability (%)	±16.1	±11.3	±6.5	±5.9	±6.7	±6.9	±11.7
Total (%)	+16.5 −15.7	+11.7 −10.9	+6.9 −6.1	+6.3 −5.5	+7.1 −6.3	+7.3 −6.5	+12.1 −11.3
Calculated uncertainty in $\delta_\phi^2/2$ (%)		+29.2 −27.6	+19.3 −17.7	+17.7 −16.1	+19.0 −17.4	+19.3 −17.7	+28.6 −27.0

Table A12. Probable Maximum Determinant Errors in Alpha Layer Growth Measurements.

Error Source	Error at						
	905°C (1661°F)	1001°C (1884°F)	1101°C (2014°F)	1203°C (2197°F)	1304°C (2397°F)	1404°C (2559°F)	1504°C (2739°F)
Temperature measurement uncertainty (°C)	±4.0	±4.3	±4.7	±5.0	±5.3	±5.7	±6.0
Uncertainty in $\delta_\alpha^2/2$ due to time correction (%)	±1.0	±1.0	±1.0	±1.0	±1.0	±1.0	±1.0
Thickness measurement uncertainties							
Mounting error (%)	+0.4	+0.4	+0.4	+0.4	+0.4	+0.4	+0.4
Thickness variability (%)	±22.6	±15.6	±13.2	±5.5	±6.4	±4.9	±3.9
Total (%)	+23.0 −22.2	+16.0 −15.2	+13.6 −12.8	+5.9 −5.1	+6.8 −6.0	+5.3 −4.5	+4.3 −3.5
Calculated uncertainty in $\delta_\alpha^2/2$ (%)	+54.0 −52.4	+39.4 −37.8	+34.2 −32.6	+18.4 −16.8	+19.8 −18.2	+16.5 −14.9	+14.2 −12.6

This method of assessing the uncertainty in thickness measurements in relative terms, i.e., as a fraction of the observed mean thickness, implies that the uncertainty increases with increasing thickness. Although a careful examination of the raw data does reveal such a trend, it is a weak one, and the error band defined on K^2 vs t plots using the uncertainties in thickness, K, given in Tables A11 and A12 easily encompasses all of the experimental data points. Thus the thickness uncertainties listed are quite conservative and tend to overestimate the thickness errors.

Under these circumstances it might be argued that a more realistic estimate of the uncertainty in thickness variability would be given by the variance (σ^2) or the actual values of the 2σ's for the mean of the thickness determinations. As may be seen in Table A10, 2σ for the oxide thickness determinations is, with one exception, less than ±2 mμ for oxidation at 1203°C (2197°F). The present method was, nonetheless, chosen (1) because it does provide somewhat conservative estimates of thickness uncertainties, and (2) because it expresses the thickness error in relative terms that are especially convenient in evaluating relative errors in the rate constants.

Uncertainty in Parabolic Rate Constants

The fractional error in the parabolic rate constant may be estimated from the sum of the uncertainties in layer thickness and time measurements. The rate constant, $\delta^2/2$, is related to layer thickness, K, and time, t, through the parabolic rate equation:

$$K^2 = \delta^2 t \quad . \tag{A10}$$

Solving for δ^2 and taking the total derivative, one obtains

$$\frac{d(\delta^2)}{\delta^2} = \frac{2dK}{K} + \frac{dt}{t} \quad . \tag{A11}$$

In Eq. (A11) $\frac{d(\delta^2)}{\delta^2}$ is the fractional uncertainty in $\delta^2/2$ occasioned by the fractional uncertainties, dK/K and dt/t, in K and t, respectively.

All signs on the right hand side of Eq. (A11) are taken as positive on the assumption that in the worst possible case all errors are additive.

While Eq. (A11) provides an estimate of the errors in $\delta^2/2$ due to uncertainties in K and t, it should be noted that implicit in Eqs. (A10) and (A11) is the assumption that the temperature, T, is known exactly. Such, of course, is never the case, and an additional uncertainty in $\delta^2/2$ arises from uncertainties in T. Consider, for example, a situation in which K and t can be measured exactly but where T is measurable only to $T \pm \varepsilon$, where $\pm\varepsilon$ is the uncertainty in the temperature measurement. If a series of experiments is performed in which specimens are oxidized for various times at the nominal temperature T but in which the true temperature varies randomly about T in the range $\pm\varepsilon$, then a plot of K^2 versus t, whose slope is proportional to the rate constant, will show a scatter of data points about the best estimate line. Thus even though K and t are known exactly, an uncertainty in $\delta^2/2$ will exist because of the uncertainty, $\pm\varepsilon$, in the measurements of T.

The contribution of these temperature uncertainties may be estimated by making use of the Arrhenius equation:

$$\delta^2/2 = A \exp(-Q/RT) \quad . \tag{A12}$$

Again taking the total derivative of $\delta^2/2$, one obtains

$$\frac{d(\delta^2)}{\delta^2} = \frac{-Q}{RT}\frac{dT}{T} \quad , \tag{A13}$$

where the last term on the right gives the contribution of the fractional uncertainty in temperature, dT/T, to the uncertainty in $\delta^2/2$.

We, therefore, take as the *maximum possible determinant error* in $\delta^2/2$ the sum

$$d(\delta^2)/\delta^2 = 2d\xi/\xi + dT/t + (Q/RT)(dT/T) \quad . \tag{A14}$$

The resulting calculated uncertainties in $\delta^2/2$ are summarized in Tables A11 and A12.

Uncertainties in A and Q

Treating the quantities A and Q in Eq. (A12) as variables and differentiating as before, it can be shown that

$$\frac{dQ}{Q} + \frac{RT}{Q}\frac{dA}{A} = \frac{RT}{Q}\frac{d(\delta^2)}{\delta^2} - \frac{dT}{T} \quad . \tag{A15}$$

The terms on the left side contain the uncertainties dQ/Q and dA/A in the activation energy, Q, and the pre-exponential term, A, respectively, and the equation expresses these quantities in terms of errors in $\delta^2/2$ and T. The right hand side may be evaluated using information from Tables A11 and A12. For example, for oxide layer growth at 1203°C (2197°F), $(RT/Q)(d(\delta^2)/\delta^2)$ is .015 and dT/T = 0.003. Assuming all errors to be additive, dQ/Q + RT/Q dA/A = 0.018 or 1.8%. However, Eq. (A15) contains two unknowns, dQ/Q and dA/A, and it is impossible to specify either uniquely. For estimates of dQ/Q and dA/A, therefore, we rely on the statistical analysis given in the first part of the Appendix.

Indeterminant Errors

Any experimental program is subject to indeterminant errors, i.e., errors that by definition are not known to exist but may be present and may be either systematic or random. In general, the only way their presence can be detected is through the comparison of a given data set with a comparable set determined by an independent method.

The only internal evidence for the lack of indeterminant errors in the present program is the relatively good agreement between results obtained in the MiniZWOK and MaxiZWOK apparatuses.

Table A13 gives a comparison of the parabolic rate constants for total oxygen consumption found in the present results with correlations obtained by other investigators. There is excellent agreement between our results and those of Kawasaki.[4] The agreement with the Hobson data[5] set is also reasonable. Less good agreement exists with the results of Biederman,[6] Klepfer,[7] and Lemmon.[8] The activation energies determined by the latter three workers are all somewhat smaller than that reported

Table A13. Percent Difference[a] Between Parabolic Rate Constants for Total Oxygen Determined in this Study[b] and Those Calculated From Other Correlations

Temperature (°C)	(°F)	Kawasaki	Hobson[c]	Biederman	Klepfer	Lemmon	Baker-Just
1000	1832	7.5%	16.3%	−48.3%	−62.7%	−75%	−31.7%
1200	2192	4.6	12.7	−4.6	−15.6	−27.7	−78.3
1500	2732	0.7	9.0	28.1	20.0	9.1	−147.0

[a]The differences are calculated relative to the results of the present study.

[b]The correlation based on the assumption of a stoichiometric gradient in the oxide is used (see p. 85).

[c]Correlation based on analysis of complete data set (see p. 85).

by us, and on an Arrhenius plot their best estimate lines cross ours at temperatures somewhat above 1200°C (2192°F).

There is in addition a recently completed set of measurements by Leistikow, Berg, and Jennert.[9] They report an activation energy of 47 kcal/mole for the rate constant for total oxygen consumption. Their analytical expression for $\delta_\tau^2/2$ is biased, however, by the fact that they included a rate determination at 900°C (1652°F) in their calculation. A point by point comparison of their results at 1000, 1100, 1200, and 1300°C (1832, 2012, 2192, and 2372°F) showed that their experimental values for $\delta_\tau^2/2$ at these temperatures differed from ours by 22, 11, 5, and 2%, respectively. Thus in the range 1000 to 1300°C (1832–2372°F) the measurements of Leistikow, et al. appear to be in reasonable agreement with ours.

It is difficult to use these comparisons as a basis for any quantitative estimates of the indeterminant errors in our experimental procedures. The various data sets appear to fall into two clusters, our results and those of Kawasaki, Hobson, and Leistikow, et al. in one and those of Biederman, Klepfer, and, to a lesser extent, Lemmon in the other. Furthermore, unless total oxygen consumption is determined directly

(i.e., gravimetrically or by hydrogen release), quantitative comparisons of data sets are somewhat uncertain unless specific information is available on the computational technique and oxygen solubility data used in the calculation of total oxygen. For these reasons we have chosen not to include any estimate of the magnitude of indeterminant errors in our total absolute error calculations. We feel, in any case, that such errors are small.

SIGNIFICANCE OF ABSOLUTE ERROR ESTIMATES

The theory of propagation of errors[10] requires that for a calculated quantity, x,

$$x = f(a,b,c,\ldots) \quad ,$$

where a, b, c,... are experimentally measured variables, the error in x be taken as the sum of the errors related to each measured variable. Thus this procedure describes the worst possible case: all measurement errors are assumed to be maximum and systematic and to have the same sign. *The purpose of the exercise is not to give a realistic estimate of the magnitude of the actual error in x but rather to set a maximum upper bound for that error.*

This absolute error analysis is included in this report in order to provide such an upper bound. It must be borne in mind, however, that it is highly unlikely that the various experimental errors discussed did, in fact, occur systematically and were of the same sign. To the extent that the various experimental measurement errors are random, the uncertainty on $\delta^2/2$ would be best described by the confidence limits derived from a statistical treatment of the data. In other words, errors in thickness, time, or temperature measurements for any given single oxidation specimen would tend to be averaged out in the 10 to 20 such sets of measurements used to define the oxidation rate curve and, hence, $\delta^2/2$, at any temperature. Furthermore, a similar averaging occurs during the construction of an Arrhenius plot, thus minimizing further the effects of random errors.

As already noted in the section on indeterminant errors, it is impossible to prove absolutely that unknown, systematic errors do not exist in our data. For the reasons already given, however, we believe that such errors, if they exist at all, are small, and we feel that the best available description of the uncertainties in the data is that derived from the statistical treatment of the results. Thus, although the absolute error analysis yields uncertainties in the parabolic rate constant for oxide growth of $\sim\pm16\%$ at 1050°C (1922°F), $\sim\pm19\%$ at 1250°C (2282°F) and $\sim\pm28\%$ at 1500°C (2732°F), a better approximation to the real uncertainty is given by the statistical results: $\sim\pm5\%$ at 1050°C (1922°F), $\sim\pm2.5\%$ at 1250°C (2282°F), and $\sim\pm4\%$ at 1500°C (2732°F).

REFERENCES

1. R. A. Perkins, *Zirconium Metal-Water Oxidation Kinetics II. Oxygen-18 Diffusion in β-Zircaloy*, ORNL/NUREG/TM-19 (July 1976).

2. K. O. Bowman and L. R. Shenton, "Omnibus Test Contours for Departure from Normality Based on $\sqrt{b_1}$ and b_2," *Biometrika* 62: 243–250 (1975).

3. J. V. Cathcart, D. L. McElroy, R. E. Pawel, R. A. Perkins, R. K. Williams, and G. J. Yurek, *Zirconium Metal-Water Oxidation Kinetics, I. Thermometry*, ORNL-5102 (February 1976).

4. S. Kawasaki, T. Furuta, and M. Hashimoto, *Reaction of Zircaloy Cladding with Steam under Simulated Loss-of-Coolant Accident Conditions*, JAERI-M-6181 (July 1975).

5. D. O. Hobson and R. E. Pawel, unpublished results, ORNL (1973). Original data from D. O. Hobson and P. L. Rittenhouse, *Embrittlement of Zircaloy-Clad Fuel Rods by Steam during LOCA Transients*, ORNL-4758 (January 1972).

6. R. R. Biederman, R. G. Ballinger, and W. G. Dobson, *A Study of Zircaloy-Steam Oxidation Reaction Kinetics*, Research Project No. 249-1, Electric Power Research Institute, Palo Alto, Calif., Final Report, September 1976.

7. H. H. Klepfer, reported in G. J. Scatina, *Fuel Cladding Embrittlement during a Loss-of-Coolant Accident*, NEDO-10674 (October 1972).

8. A. W. Lemmon, Jr., *Studies Relating to the Reaction Between Zirconium and Water at High Temperatures*, BMI-1154 (January 1957).

9. S. Leistikow, H. v. Berg, and D. Jennert, "Comparative Studies of Zircaloy-4/High Temperature Steam Oxidation under Isothermal and Temperature Transient Conditions," in *Proceedings, CSNI Specialist Meeting on the Behavior of Water Reactor Fuel Elements under Accident Conditions*, Spatind, Nord-Torpa, Norway, September 13–16, 1976, in press.

10. See, for example, S. L. Meyer, *Data Analysis for Scientists and Engineers*, John Wiley and Sons, New York, N.Y., 1975, p. 39.

APPENDIX B

HYDROGEN ANALYSES FOR OXIDIZED SPECIMENS

INTRODUCTION

Hydrogen, like oxygen, can dissolve in large quantities in zirconium or Zircaloy and in certain circumstances is capable of embrittling Zircaloy seriously. Because hydrogen is one of the products of the steam-Zircaloy reaction, one is always concerned about the possibility of hydrogen pick-up during steam oxidation. Fortunately, the presence of an oxide film greatly retards the rate at which hydrogen is absorbed by Zircaloy; nonetheless, we considered it important to obtain a series of hydrogen analyses for specimens used in the present investigation.

These analyses showed that many of the MiniZWOK specimens had absorbed considerable quantities of hydrogen during oxidation. In this Appendix the analytical results are summarized, the manner in which the hydrogen entered the specimens is discussed, and experimental evidence is cited to show that the presence of hydrogen did not significantly influence the observed rates of oxidation of the samples.

ANALYTICAL RESULTS

A variety of samples were submitted for hydrogen analysis. Included were sections of as-received tubes as well as samples oxidized on both sides (two-sided oxidation) in several different apparatuses. This latter set contained standard MaxiZWOK samples, specimens from the high pressure steam apparatus (SuperZWOK), and several tubes oxidized in a preliminary version of MiniZWOK where specimens were oxidized on both the inside and outside surfaces. In addition analyses were obtained for a large number of samples oxidized under both isothermal and transient temperature conditions in the standard MiniZWOK apparatus where oxidation occurred primarily on the outer surfaces of the specimens (one-sided oxidation). Also included in the category of one-sided oxidation experiments were three specimens oxidized in a specially modified version of

MiniZWOK; these samples, designated as "MiniZWOK, full length", were cut to such a length that their ends extended beyond the top and bottom of the apparatus. These tubes were held in place with O-rings, and the interior of the tubes was filled with slowly flowing, high purity helium. This design made it possible to exclude steam rigorously from the interior of the tubes.

Samples to be submitted for hydrogen analyses were obtained from oxidized specimens in the following manner. A ring section, approximately 0.5 cm (3/16 in.) wide and containing the tabs to which the thermocouples are attached, was cut from the approximate center of the specimen and was used for metallographic evaluation of oxide and alpha layer thicknesses. A second ring section of about the same dimensions was then removed from that end of the remaining portions of the specimen that was adjacent to the section removed for metallographic purposes, and this ring, after being cut in half, was submitted for analysis. In general, the analytical laboratories cut smaller aliquots from the sample submitted before performing the actual analysis. It should also be noted that in some instances where multiple analyses were obtained on the same specimen, a second ring section, further removed from the central specimen, was used.

Prior to submission for analysis, all specimens were washed in a detergent solution, rinsed thoroughly with alcohol and water, and dried to make certain that no organic surface contaminants were left on the samples. Specimens were analyzed in both the as-oxidized condition and after both the outside and inside surfaces had been machined down to bare metal. No significant differences in reported hydrogen concentrations were noted for specimens prepared in these two different ways.

Because the initial hydrogen analyses obtained for the standard MiniZWOK specimens showed considerable scatter, samples were submitted for analysis at three different laboratories: the Analytical Chemistry Division, ORNL; the Analytical Laboratory of the Wah Chang, Albany Corp.; and the Plant Analytical Laboratory at the Y-12 facility in Oak Ridge. Techniques used in the analyses included vacuum fusion, inert-gas fusion, and hot, vacuum extraction. The results of these analyses are summarized in Table B1.

Table B1. Hydrogen Analyses of Zircaloy-4 Specimens

Description of Specimen	Expt. No.	Experimental Conditions t(s)	Experimental Conditions T(°C)	Tubing Source	Hydrogen Content (ppm by wt) ORNL	Hydrogen Content (ppm by wt) Wah Chang	Hydrogen Content (ppm by wt) Y-12[a]	Hydrogen Content (ppm by wt) Y-12[b]
As-received tubes				Sandvik	20,23,26,	15,17	23	
				Sandvik	19,20,25,			
				Sandvik	26,22,17,			
				Sandvik	24,			
As-received tubes				Batch "B"	14,14,11			
Two-Sided Oxidation								
MiniZWOK[c]	10-16-1142	188	1200	Batch "B"	14,16	14		
MiniZWOK[c]	10-16-1408	142	1200	Batch "B"	16,32			
MiniZWOK[c]	10-18-1051	546	1180	Batch "B"	15	18		
MiniZWOK[c]	10-18-1404	171	1200	Batch "B"	16,17			
MiniZWOK[c]	10-18-1438	62	1200	Batch "B"	17			
MiniZWOK[c]	10-11-1042	56	1210	Batch "B"	10			
MiniZWOK[c]	10-11-1318	50	1190	Batch "B"	23			
MiniZWOK[c]	10-11-1533	65	1204	Batch "B"	26			
MaxiZWOK	Max-26	383	900	Sandvik	27,28,24	19		
MaxiZWOK	Max-24	640	1005	Sandvik	35,26,25	17	21	
SuperZWOK	Z-13	380	905	Sandvik	36,27	40		18
One-Sided Oxidation								
MiniZWOK, full-length[d]	SL-244	170	1038	Sandvik	25		11	
MiniZWOK, full-length[d]	SL-246	180	1068	Sandvik	27		25	
MiniZWOK, full-length[d]	SL-247	65	1153	Sandvik	22		21	

Table B1. (Continued)

Description of Specimen	Expt. No.	Experimental Conditions t(s)	Experimental Conditions T(°C)	Tubing Source	Hydrogen Content (ppm by wt) ORNL	Hydrogen Content (ppm by wt) Wah Chang	Hydrogen Content (ppm by wt) Y-12[a]	Hydrogen Content (ppm by wt) Y-12[b]
One-Sided Oxidation (Continued)								
MiniZWOK, standard	S-80	30	1153	Sandvik		9		93
MiniZWOK, standard	S-71	105	1153	Sandvik		81		368
MiniZWOK, standard	S-73	194	1153	Sandvik		380		150
MiniZWOK, standard	S-76	249	1153	Sandvik		320		425
MiniZWOK, standard	S-79	388	1153	Sandvik		740		1096
MiniZWOK, standard	S-118	11	1404	Sandvik	35	50		20
MiniZWOK, standard	S-115	30	1404	Sandvik	46	130		73
MiniZWOK, standard	S-116	46	1404	Sandvik	146	36		30
MiniZWOK, standard	S-119	56	1404	Sandvik	92	61		213
MiniZWOK, standard	S-122	74	1404	Sandvik	187	75		77
MiniZWOK, standard	S-19	420	905	Sandvik	109,67	500		
MiniZWOK, standard	S-23	1623	905	Sandvik	119,103	230		
MiniZWOK, standard	S-90	66	1203	Sandvik	42,45	43		
MiniZWOK, standard	S-82	236	1203	Sandvik	294,449,427			
MiniZWOK, standard	S-138	8	1504	Sandvik	37,37	30		
MiniZWOK, standard	S-136	47	1504	Sandvik	30,188	190		
MiniZWOK, 5% H_2 added	S-180	170	1101	Sandvik	255,130	320		
MiniZWOK, 5% H_2 added	S-185	33	1304	Sandvik	48,160,83	32		

Table B1. (Continued)

Description of Specimen	Expt. No.	Experimental Conditions t(s)	Experimental Conditions T(°C)	Tubing Source	Hydrogen Content (ppm by wt) ORNL	Hydrogen Content (ppm by wt) Wah Chang	Hydrogen Content (ppm by wt) Y-12[a]	Hydrogen Content (ppm by wt) Y-12[b]
Transient Temperature Oxidation (One-Sided)								
MiniZWOK, 2-peak LOCA	S-160			Sandvik	940	1140		
MiniZWOK, 2-peak LOCA	S-196			Sandvik	978	1160		
MiniZWOK, trapezoidal transient	S-155			Sandvik	487			
MiniZWOK, trapezoidal transient	S-156			Sandvik	509			
MiniZWOK, 1400/1100°C transient	S-163			Sandvik	497			
MiniZWOK, 1100/1400°C transient	S-164			Sandvik	>827			

[a]Y-12 high vacuum, hot extraction analysis.

[b]Y-12 inert gas fusion analysis.

[c]Preliminary MiniZWOK experiments, Batch B tubing.

[d]Modified MiniZWOK apparatus; see text.

EVALUATION OF ANALYTICAL DATA

Inspection of Table B1 will reveal a considerable scatter in the data obtained from the three laboratories for standard MiniZWOK specimens. Two causes for this variability suggest themselves: (1) inaccuracies in the analytical procedures and (2) an inhomogeneous distribution of hydrogen in the samples.

All laboratories cited uncertainties of $\sim\pm10$ to 20% of reported values for the results of vacuum- or inert-gas fusion techniques, with the higher uncertainties being applicable in the 20 ppm H_2 range. The hot extraction methods are thought to be somewhat more accurate, especially the High Vacuum Hot Extraction technique employed by the Y-12 Plant Laboratory where uncertainties less than 1 ppm are claimed in the 1 to 20 ppm range. These error estimates appear to be more or less consistent with the relatively small variations in hydrogen content reported for the as-received Zircaloy tubes and for specimens subjected to oxidation on both sides. They are not sufficiently large to allow the variations in the reported hydrogen contents of the MiniZWOK samples to be reconciled, however.

Given the manner in which hydrogen gets into the specimens (see below), it is possible that hydrogen is not distributed homogeneously throughout a sample despite the very high diffusion rates expected for hydrogen in Zircaloy at high temperatures. Lack of homogeneity would certainly lead to varying results for the hydrogen concentrations measured. Furthermore, there is no *a priori* reason to assume that the hydrogen content of one oxidized sample will be completely consistent with that for another, and this type of variability could contribute to the *apparent* inconsistency of some of the results as well. This question is considered further in connection with the mechanism of hydrogen solution in the samples.

While it has not been possible to exorcise all doubts concerning the accuracy of the hydrogen analyses, particularly at high hydrogen concentrations, we have concluded that rather high hydrogen concentrations existed in many of the MiniZWOK samples and that a substantial

part of the variability in the results is attributable to an inhomogeneous distribution of hydrogen in the samples.

DISCUSSION OF THE ANALYTICAL RESULTS

As-Received Tubing

As already pointed out, analyses of the as-received tubes were quite self-consistent (see Table B1). Sandvik tubing exhibited hydrogen concentrations ranging from 15 to 26 ppm, twelve determinations yielding a mean value of 21.3 ppm with a standard deviation of ±3.6 ppm. The hydrogen content of the "Batch B" tubing was somewhat smaller: 11 to 14 ppm.

Two-Sided Oxidation

Specimens oxidized on both sides, whether made of the "Batch B" or the standard Sandvik tubing and whether oxidized in the MaxiZWOK, SuperZWOK, or preliminary MiniZWOK apparatuses, yielded hydrogen concentrations in this same general range. This result is in agreement with the previously reported data of Biederman, et al.[1] and Kawasaki, et al.[2] for Zircaloy-4. This result is also consistent with the observations of Gulbransen and Andrew[3] who found that hydrogen absorption by zirconium was greatly impeded by the presence of a surface oxide film. For a further discussion of this question, see a recent review by Cox.[4] Thus it seems clear that as long as the oxygen potential over a Zircaloy sample is high enough to produce significant oxide formation, the rate of hydrogen pickup will be very small, at least for short time oxidation at high temperatures.

One-Sided Oxidation

The situation with regard to specimens oxidized on the outside only is quite different. Virtually all of the standard MiniZWOK specimens exhibited a tendency to pick up hydrogen, and many exhibited hydrogen concentrations in the range 100 to 300 ppm.

An exception to this general statement is to be found in the analytical results for the three specimens designated "MiniZWOK, full length" (see Expts. SL-224, 246, and 247, Table B1). The hydrogen concentrations in these specimens are very close to those for the as-received Sandvik tubes, and the agreement between the analyses obtained at ORNL and those from the Y-12 laboratory is quite satisfactory. It will be recalled that the "MiniZWOK, full length" experiments were designed so that steam was rigorously excluded from the interior of the sample tubes, and these analytical results demonstrate that when no source of hydrogen is present in the interior of a specimen, no more hydrogen is absorbed by the Zircaloy sample during one-sided oxidation than would be the case for two-sided oxidation. These same results also strongly suggest that the hydrogen present in the standard MiniZWOK specimens must have been absorbed through the surface of the inner wall of the specimen tube.

Further clues as to the manner in which hydrogen enters the samples may be obtained from Figs. B1 and B2. In Fig. B1 hydrogen concentration is plotted as a function of total oxygen consumed, τ, by the isothermally-oxidized, standard MiniZWOK samples. The very considerable scatter of the data is evident, but within this scatter there is no discernible correlation between hydrogen concentration and τ when data at all temperatures are considered together. Such a result is not surprising in light of the fact that we have already concluded that hydrogen does not enter the specimen in significant quantities through the heavily oxidized outer surface of the tube.

Figure B2 shows hydrogen concentration as a function of oxidation time for the same set of samples. Here, despite the scatter in the data, a trend may be detected; the longer the oxidation time, the greater is the chance that high hydrogen concentrations will be observed.

Mechanism of Hydrogen Absorption

The standard specimen used in the MiniZWOK apparatus is a 3 cm (1.2 in.) long PWR Zircaloy tube held between two specially ground quartz tubes in the center of a steam-filled reaction chamber. A slight positive pressure of helium is maintained inside the specimen to prevent

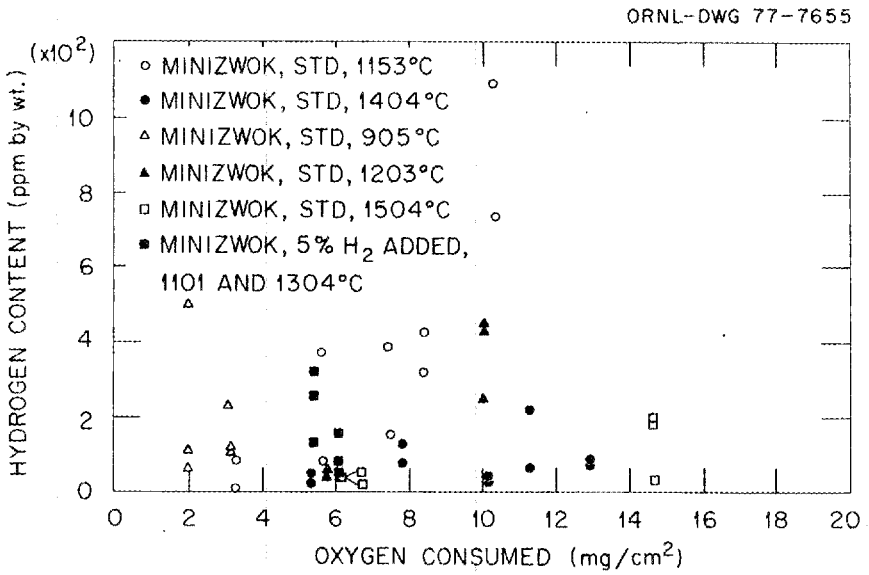

Fig. B1. Hydrogen Content of Zircaloy-4 PWR Tube Specimens Isothermally Oxidized in the MiniZWOK Apparatus Plotted as a Function of the Oxygen Consumed.

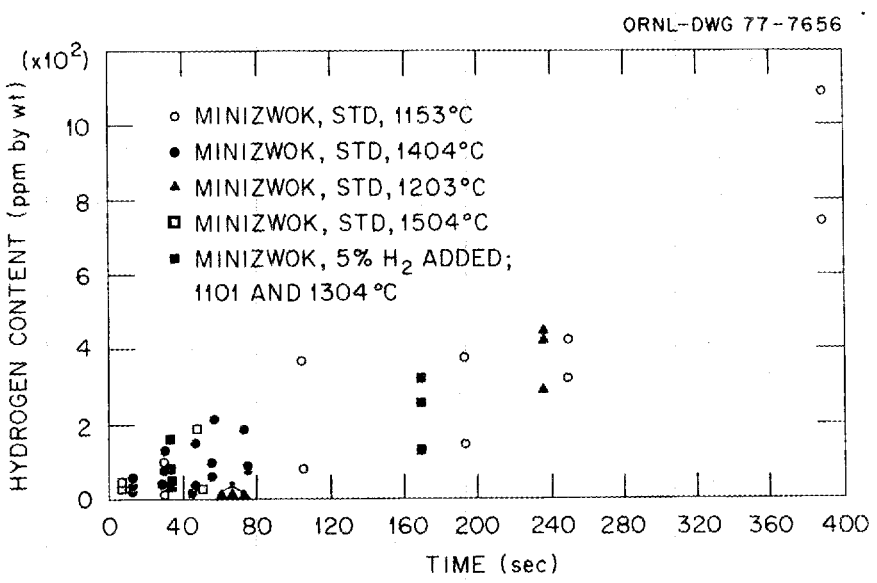

Fig. B2. Hydrogen Content of Zircaloy-4 PWR Tube Specimens Isothermally Oxidized in the MiniZWOK Apparatus Plotted as a Function of Time of Oxidation.

ingress of steam to the inner surface of the tube. Thin tantalum washers, which oxidize when the temperature is increased to the desired oxidation range, also help in sealing off the ends of the specimen.

However, despite these precautions small amounts of steam have been known to leak into the center of the specimens in some experiments. Observations on longitudinal sections through oxidized specimens have, in fact, revealed the presence of a thin layer of oxide on the inner surface of the tube; this oxide layer is thickest at the end of the tube and tapers down to nothing as the center of the tube is approached. Thus it appears that in many MiniZWOK experiments small amounts of steam have leaked around the ends of the specimens and reacted at the inner surface of the tube, creating oxide and releasing hydrogen. The Zircaloy acts as an efficient getter for the steam so that the center of the specimen is under virtual steam starvation conditions. The Zircaloy surface there is either free of oxide or covered by only a thin oxide layer. Under these conditions hydrogen is easily absorbed as has been shown by Kawasaki, et al.[2]

This scenario explains a number of observations relative to hydrogen absorption. The amount of hydrogen absorbed will depend in two ways on the leak rate of steam into the center of the specimen. To begin with, to obtain significant hydrogen absorption the leak rate must be less than a certain maximum value; above this level the entire inner surface of the specimen will be oxidized, steam starvation conditions will not prevail, and little hydrogen pickup will be observed. The comparatively low hydrogen concentrations observed for the specimen oxidized for 1623 min at 905°C (1661°F) (see Expt. S-23, Table B1) may, perhaps, be accounted for on this basis.

For leak rates below this maximum, the extent of hydrogen absorption should depend primarily on absolute magnitude of the leak rate and on the time of oxidation. This conclusion can account for the correlation with time noted in Fig. B2 and for the scatter in the analytical results. Variations in leak rate could produce variations in the extent of coverage by oxide of the inner specimen surface, thus also accounting for the apparently inhomogeneous distribution of hydrogen in the specimens.

Transient Temperature Oxidation

As may be noted in Table B1, specimens subjected to transient temperature oxidation exhibited particularly high hydrogen levels. The most likely explanation of this phenomenon rests on the fact that the coefficient of expansion of a Zircaloy specimen is much larger than that of the quartz tubes that hold it in place in the oxidation apparatus. Thus when the specimen expands or contracts in the various stages of a transient, the upper quartz tube, which is lightly spring loaded, must move up and down if the seal between it and the specimen is to be maintained. It seems plausible that such motion could produce a slight unseating of the tantalum gaskets at the ends of the specimen, thus increasing the steam leak rate slightly and enhancing hydrogen absorption.

Another mechanism that cannot be discounted involves our explanation of anomalous transient temperature oxidation (see p. 109 of the main body of this report). We suggested the possibility of the transformation of an initially tetragonal oxide scale to a monoclinic structure during portions of certain types of temperature transients, e.g., the two-peak LOCA's tested in Experiments S-160 and S-196 (see Table B1). Evidence exists[5] that during oxidation at relatively low temperatures where the monoclinic oxide is stable, hydroxyl ions may diffuse through the oxide, releasing hydrogen at the oxide-metal interface. We can cite no evidence in support of this mechanism as a means for introducing hydrogen into our specimens, but it remains a possibility.

POSSIBLE EFFECTS OF DISSOLVED HYDROGEN ON OXIDATION RATES

Having established that the rather high hydrogen concentrations observed in many MiniZWOK specimens in all probability were the result of a characteristic of the apparatus, we considered it important to address the question of whether hydrogen dissolved in the metal phases of the specimens might have influenced the measured rates of oxidation. There is a considerable body of indirect evidence that suggests that no such perturbation of the oxidation rates occurred, but as an additional check we also carried out a special series of oxidation experiments in

which the MiniZWOK specimens were oxidized in pure oxygen rather than steam. In this section we describe these various observations and results and conclude finally that the presence of hydrogen in the metal did not, within the sensitivity of our measurements, influence oxidation rates.

Indirect Evidence

Self-Consistency of Rate Data

Inspection of Table B1 and Figs. B1 and B2 shows that the hydrogen content of the MiniZWOK specimens tended to increase with the total time of oxidation essentially independent of temperature or total oxygen consumption. Thus when a series of specimens was oxidized for varying lengths of time at a fixed temperature in order to generate an oxidation rate curve, the specimens oxidized for shorter times contained, in general, less hydrogen than those oxidized for longer periods [cf., MiniZWOK specimens oxidized at 1153°C (2107°F), Table B1]. Yet no significant deviation from parabolic behavior was observed in the corresponding rate curves as might have been expected had hydrogen dissolved in the metal had a major effect on the kinetics.

A similar argument may be made regarding oxidation at different temperatures. Specimens oxidized at 1404°C (2559°F), for example, contained less hydrogen than those oxidized at 1153°C (2107°F) (see Table B1) because oxidation times at the higher temperatures were shorter. However, inspection of the Arrhenius plots of the rate data shows that the high temperature results are entirely consistent with those obtained at lower temperatures, again suggesting that the hydrogen dissolved in the metallic phases of the Zircaloy had no effect on oxidation rates.

We conclude, therefore, that the self-consistency of the oxidation rate data is itself evidence against spurious oxidation results relating to the absorption of hydrogen by the MiniZWOK specimens.

Comparison with Other Data

Oxidation rate data obtained with the MiniZWOK apparatus (relatively high hydrogen contents) agrees well with data obtained in the MaxiZWOK apparatus (low hydrogen) at 900 and 1000°C (1652–1832°F) and in the high

pressure apparatus (SuperZWOK) where the hydrogen content of the specimens was also low (cf., Table B1). Similar good agreement can be cited between our data and those of Kawasaki, et al.[6] and Leistikow, et al.,[7] both the latter investigations involving specimens with low hydrogen contents. Thus a comparison of our MiniZWOK results with other data sets also supports the conclusion that hydrogen dissolved in Zircaloy has no appreciable effect on its oxidation rate.

Experiments in Pure Oxygen

Although the indirect evidence just cited suggests strongly that the hydrogen found in the MiniZWOK specimens did not influence their oxidation rate, we felt that the possibility of "hydrogen effects" actually occurring should not be dismissed out of hand. For example, the formation of O-H complexes, which could alter the diffusion rates of oxygen, has been observed near room temperature and below in niobium containing hydrogen and oxygen.[8,9] These complexes tend to dissociate at temperatures slightly above room temperature, making remote the likelihood of their existence in Zircaloy at temperatures of interest in this study. Nevertheless, we have performed experiments in pure oxygen in order to provide a reference state against which possible hydrogen effects in Zircaloy can be judged.

Analysis of Possible Effects

At high temperatures ZrO_2 is generally assumed to be an n-type conductor with diffusion proceeding via an anion vacancy mechanism. Thus if hydrogen dissolved in the metal phases of a specimen has no effect on the oxidation rate and if no changes in stoichiometry, defect concentration, or ionic mobilities occur in the oxide, oxidation in pure oxygen should be identical with that observed for steam oxidation in the MiniZWOK apparatus. On the other hand, changes in mobility or equilibrium oxygen solubilities in oxide, alpha, or beta phases should cause oxidation behavior in pure oxygen to be different from that in steam, and it is possible to predict trends in the growth rates of oxide and oxygen-stabilized alpha layers on the basis of any such differences.

The velocity of any phase boundary in an oxidizing Zircaloy specimen is proportional to the difference between the oxygen fluxes into and out of the boundary. For example, the velocity, $\nu_{i,j}$ of the i,j boundary is given by

$$\nu_{i,j} = (J_{i,j} - J_{j,i})/\Delta c_{i,j} \tag{B1}$$

and

$$J_{i,j} = -D_i \nabla c_{i,j} \tag{B2}$$

where $J_{i,j}$ is the oxygen flux to the i,j boundary, the first subscript indicating the phase in which the flux is measured; $\nabla c_{i,j}$ is the oxygen concentration gradient in the i'th phase at the i,j boundary; D_i is the diffusion coefficient in the i'th phase; and $\Delta c_{i,j} = c_i - c_j$; with c_i and c_j being the equilibrium oxygen concentrations in the i'th and j'th phases, respectively, at the i,j boundary. Thus any change in $\nu_{i,j}$ must involve changes in diffusion coefficients or equilibrium oxygen concentrations or both. (Strictly speaking, the denominator of Eq. (B1) should be written as $V_{i,j}\ C_{i,j} - C_{j,i}$, where $V_{i,j}$ is the ratio of equivalent volumes of the i'th to the j'th phase. At the oxide-alpha boundary V has a value of 1.5 and is essentially unity at the α/β interface. In the discussion to follow the actual value of $V_{i,j}$ does not enter into consideration, and for the sake of notational simplicity we shall use Eq. (B1) in the form shown with the understanding that $\Delta C_{i,j} \equiv V_{i,j}\ C_{i,j} - C_{j,i}$.)

Effects in the Alpha and Beta Phases — It would appear that the only possible effect of hydrogen on D_α or D_β would be that of decreasing the diffusivities. As mentioned previously, changes in the diffusion coefficient for oxygen in Nb containing dissolved hydrogen could be brought about by the formation of the O-H complexes observed at low temperatures. It is most unlikely, however, that such complexes could retain any degree of stability in Zircaloy at the high temperatures used in this study; but if they do, the presence of the complexes should, if anything, reduce oxygen mobility. Both oxygen and hydrogen diffuse

interstitially in Zircaloy, and the jump frequency, γ_{O-H}, for an O-H pair is related to the jump frequencies, Ω_O and Ω_H, of isolated oxygen and hydrogen atoms, respectively, by

$$\gamma_{O-H} = \Omega_O\Omega_H/(\Omega_O + \Omega_H) = \Omega_O/(1 + \Omega_O/\Omega_H) \quad , \tag{B3}$$

and $\Omega_H > \Omega_O$. Therefore,

$$\gamma_{O-H} \leq \Omega_O \quad . \tag{B4}$$

Thus the formation of O-H pairs should either reduce the diffusivity of oxygen or leave it unchanged. D_α or D_β might also be decreased if, as a result of the presence of hydrogen, the correlation factor for oxygen were reduced below the value of unity expected for interstitial diffusion. An increase in the diffusivity, on the other hand, would require that the strain field associated with dissolved hydrogen produce an increase in the jump frequency, Ω_O, for oxygen. In light of the smallness of the hydrogen atoms and their high rate of diffusion, however, such a possibility is dismissed, and we conclude that only decreases in D_α and D_β can occur as a result of the presence of hydrogen.

C. Roy[10] reports that when a crystal-bar zirconium sample, previously charged with 44 ppm tritium, was oxidized in oxygen at 500°C (932°F) long enough to produce an oxide film 2.5 μm thick, subsequent autoradiographs revealed no tritium in the oxide or in the underlying metal zone highly enriched in oxygen. When the oxidized specimens were annealed at 800°C (1472°F) to dissolve the oxide scale and then either slow cooled or quenched, "very little hydrogen was found in the thick layer of metal enriched in oxygen". Clearly, the introduction of oxygen into a Zircaloy specimen will reduce the solubility of hydrogen in the metal, and this result suggests the existence of a solubility product relationship

$$[a_O][a_H] = k \quad , \tag{B5}$$

where a_O and a_H are the activities of oxygen and hydrogen, respectively, and k is the solubility product. Roy's experimental results indicate that the magnitude of any hydrogen effect in the alpha will surely be

small, and the solubility product relationship suggests that hydrogen in the beta phase could only reduce the equilibrium oxygen solubility. Since a reduction of the solubility of oxygen in the beta would also lead to a reduction in $Vc_{\beta,\alpha}$, we can conclude that solubility changes due to hydrogen in the beta will produce only decreases in the oxygen flux, $J_{\beta,\alpha}$, into the beta [cf., Eq. (B2)].

Effects in the Oxide — Kofstad's[11] summary of the properties of ZrO_2 makes it clear that transport mechanisms in ZrO_2 are not fully understood. The predominant characteristics of ZrO_2 are those of an oxygen-deficit, n-type semiconductor with material transport occurring via anion vacancy diffusion. Given the great stability of zirconia, the assumption of most investigators that ZrO_2 is stoichiometric in either steam or oxygen at one atmosphere might appear justified. With regard to the possible effects of the hydrogen liberated by the steam-Zircaloy reaction, we have already cited evidence for the limited solubility of hydrogen in ZrO_2,[10] and any effect of such small quantities of hydrogen on the vacancy diffusion rate in the oxide should be insignificant. On the basis of such arguments one would predict that oxygen mobilities and interfacial concentrations in the oxide would be the same during oxidation in oxygen or in steam.

On the other hand, electrical conductivity measurements at 1550°C (2822°F) and below provide somewhat controversial evidence for a component of p-character in the conductivity of ZrO_2. In such a case, the rate of oxidation might be some function of oxygen pressure. Furthermore, McClaine and Coppel[12] reported differences in the conductivity of ZrO_2 measured in H_2-H_2O atmospheres as compared to data obtained in CO-CO_2 mixtures having the same oxygen partial pressure. They attributed their results to hydrogen entering the ZrO_2 as an interstitial positive ion with an associated electron. These observations raise the possibility that during oxidation of Zircaloy in steam, small quantities of hydrogen dissolve in the oxide and change its defect concentration. For example, either an interstitial proton or a proton trapped on a vacant cation site would produce an increase in the oxygen vacancy concentration in the oxide. The influence of such hydrogen impurity atoms would be most

important at the gas-oxide interface where the intrinsic vacancy concentration is virtually zero; at the oxide-alpha interface, however, the intrinsic vacancy concentration is so high (∿8%) as to make extrinsic contributions negligible. The net effect, then, of hydrogen dissolved in the oxide would be that of reducing slightly the defect concentration gradient across the scale by reducing the oxygen concentration in the oxide at the oxide-gas interface. For additional information see also Refs. 4 and 5.

The above comments relate to the properties of relatively pure ZrO_2. The oxide formed on Zircaloy contains small amounts of various alloying additions such as Sn, Fe, and Cr. Depending on their oxidation state, these impurity elements could contribute to the extrinsic defect concentration in Zircaloy oxide. However, in principle, at least, the various arguments given above should apply to both pure ZrO_2 and the oxide formed on the alloy.

We conclude from this discussion that it is difficult to suggest a mechanism by which oxygen mobility in the oxide can be affected by the oxidizing medium. However, the possibility of a variation in equilibrium solubilities cannot be dismissed. If such a change does occur, one should recognize that it is a natural consequence of oxidizing Zircaloy in two widely differing media, and the change should not be described as a "hydrogen effect" in the sense of possible effects on oxidation rates produced by hydrogen dissolved in the alpha or beta regions.

Experimental Results for Oxidation in Oxygen

With these various possibilities in mind, oxidation rate curves were determined for Zircaloy-4 in 5–9's oxygen at 1253 and 1404°C (2287–2559°F). Ten specimens were used to define each curve, and the specimens and procedures used were identical to those employed in the standard MiniZWOK experiments except that pure oxygen at one atmosphere pressure was substituted for steam.

The results obtained are summarized in Table B2 in terms of parabolic rate constants for oxide and α-layer growth. The uncertainties listed are for the 90% confidence level. For ease of comparison the corresponding rate constants obtained for oxidation in steam are also listed. Values

Table B2. Parabolic Rate Constants for the Oxidation of Zircaloy-4 in Oxygen and Steam at 1253 and 1404°C (2287–2995°F)

Temperature [°C (°F)]	$\delta_\phi^2/2$ ($cm^2/s \times 10^7$)	Dev.[a] (%)	$\delta_\alpha^2/2$ ($cm^2/s \times 10^7$)	Dev.[a] (%)	$\delta_\xi^2/2$ ($cm^2/s \times 10^7$)	Dev.[a] (%)	$\delta_\tau^2/2$ [$(g/cm^2)^2/s \times 10^7$]	Dev.[a] (%)
				Oxidation in Oxygen				
1253 (2287)	0.9275	±3.1	0.9875	±4.9	3.827	±2.0	3.5847	±1.9
1404 (2559	2.681	±2.6	3.830	±5.2	12.92	±3.1	11.55	±2.1
				Oxidation in Steam[b]				
1253 (2287)	0.7663	±6.7	1.007	±8.2	3.530	±7.2	3.300	±6.0
1404 (2559)	2.351	±4.1	4.122	±4.4	12.70	±3.9	11.31	±3.4

[a]Uncertainty (%) at the 90% confidence level.

[b]Kinetic parameters in steam calculated from actual data at each temperature.

of oxidation times, observed oxide and alpha layer thicknesses, and total oxygen consumed (calculated) are tabulated in Tables B3 and B4.

Discussion of Results

Inspection of Table B2 shows that the rate of oxide growth is smaller in steam than in oxygen, while the rate of alpha growth is slightly greater in steam than in oxygen. At both temperatures investigated the differences in the two data sets are small, but for $\delta_\phi^2/2$ and $\delta_\tau^2/2$ these differences lie outside the statistical uncertainty limits at the 90% confidence levels. The uncertainty intervals of $\delta_\alpha^2/2$ and $\delta_\xi^2/2$ do overlap at the 90% level. For both these parameters, however, the trends in the experimental data are clear; the growth rate of the alpha layer is slightly greater in steam than in oxygen, while the reverse is true for Xi layer growth. We conclude, therefore, that the oxidation behavior of Zircaloy-4 in oxygen is not equivalent to oxidation in steam, and that

$$\phi|_{H_2O,\underline{H}} < \phi|_{O_2} \tag{B6}$$

$$\alpha|_{H_2O,\underline{H}} > \alpha|_{O_2} \quad , \tag{B7}$$

where ϕ and α are the oxide and alpha layer thicknesses, respectively. One may also infer from Eq. (B6) that

$$\nu_{\phi,\alpha}|_{H_2O,\underline{H}} < \nu_{\phi,\alpha}|_{O_2} \quad . \tag{B8}$$

Hydrogen Effects in the Beta Phase Only — The most immediate explanation that suggests itself for these differences is the possibility of a hydrogen effect in the beta phase. As already pointed out, most of the hydrogen in the MiniZWOK specimens must have been concentrated in the beta phase, and reasonable arguments can be made that other effects in the oxide and alpha layers should be minor. Consider, therefore, the following postulate, which we will prove false.

Postulate I. A hydrogen effect occurs in the beta phase only. It follows from the postulate that mobilities and equilibrium oxygen concentrations are undisturbed in the oxide and alpha layers.

Table B3. Oxidation of Sandvik Zircaloy-4 PWR Tubing in Pure Oxygen at 1253°C (2287°F)

Expt. No.	Time (s)	Oxide Layer (μm)	Alpha Layer (μm)	Total Oxygen (mg/cm^2)
S-255-TC-2	31.5	25.1	23.8	4.854
S-255-TC-3	34.1	25.6	24.7	4.972
S-256-TC-2	259.5	68.9	75.1	13.676
S-256-TC-3	254.5	67.1	73.4	13.351
S-257-TC-2	273.1	69.4	74.2	13.76
S-257-TC-3	266	70.1	71.3	13.755
S-258-TC-2	168.6	57.5	54.6	11.131
S-258-TC-3	158.7	55.7	53.5	10.802
S-259-TC-2	162.6	55.4	55.7	10.839
S-259-TC-3	152.9	54.3	54.4	10.606
S-260-TC-2	100.6	45	44.7	8.758
S-260-TC-3	103	45.4	44.1	8.809
S-261-TC-2	8.6	15.5	14.4	2.94
S-261-TC-3	9.5	15.8	14	2.985
S-262-TC-2	110.3	46.1	45.7	8.99
S-262-TC-3	102.8	44.9	44.7	8.753
S-263-TC-2	99.4	43.5	41.8	8.448
S-263-TC-3	100.2	43.2	40.4	8.366
S-264-TC-2	23.5	23.2	20.2	4.401
S-264-TC-3	23	23.1	21.6	4.424

Table B4. Oxidation of Sandvik Zircaloy-4 PWR Tubing in Pure Oxygen at 1404°C (2559°F)

Expt. No.	Time (s)	Oxide Layer (μm)	Alpha Layer (μm)	Total Oxygen (mg/cm^2)
S-265-TC-2	53	53.8	62	11.085
S-265-TC-3	52.2	53.3	61.3	10.979
S-266-TC-2	59.6	56.3	69.5	11.763
S-266-TC-3	60.5	57	66.4	11.777
S-267-TC-2	52.5	52.4	62.3	10.885
S-267-TC-3	53	53.3	62.6	11.03
S-268-TC-2	57.6	54.9	65.6	11.415
S-268-TC-3	57.9	55.4	68.8	11.59
S-269-TC-2	41.6	47	58.4	9.832
S-269-TC-3	41.5	46.8	57.7	9.78
S-270-TC-2	11.7	26.8	31.8	5.511
S-270-TC-3	12	27	30.5	5.495
S-271-TC-2	11.9	27.6	31.5	5.623
S-271-TC-3	12.7	28.1	33.6	5.783
S-272-TC-2	23.6	35.4	43	7.375
S-272-TC-3	23.8	36.4	43.4	7.535
S-273-TC-2	27.3	38.5	48.8	8.073
S-273-TC-3	27.6	38.4	45.8	7.97
S-274-TC-2	41.7	47.9	56.4	9.901
S-274-TC-3	38.9	45.6	53.8	9.446

We shall now examine the experimental results for oxidation in steam and oxygen. The pertinent data are represented schematically in Fig. B3 where the positions of the various phase boundaries are referenced to the original metal surface. We consider the relative velocities of the oxide-alpha (ϕ-α) interfaces in steam and oxygen.

$$\nu_{\phi,\alpha} = (J_{\phi,\alpha} - J_{\alpha,\phi})/\Delta C_{\phi,\alpha} \quad . \tag{B9}$$

Therefore,

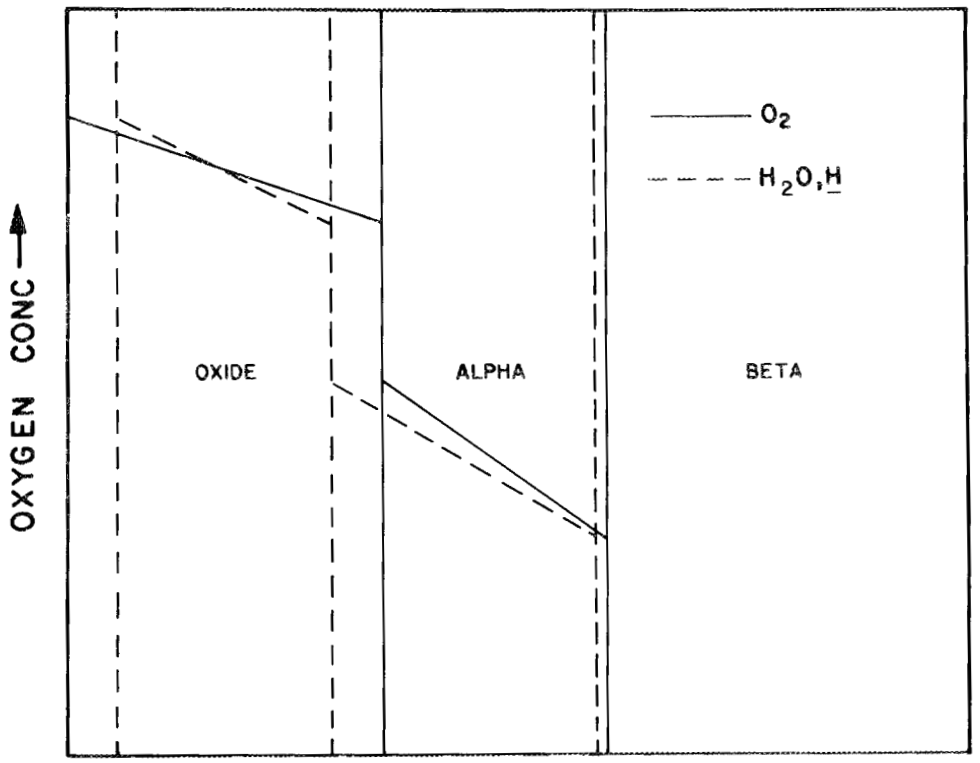

Fig. B3. Schematic Representation of Oxygen Concentration Gradients in Oxide and Oxygen-Stabilized Alpha Layers. The linear gradient shown in the oxide is a very good approximation of reality; the gradient in the alpha layer is certainly curved but is shown as linear in order to emphasize the differences in slope in steam as compared to oxygen. The arguments presented in the text turn on the relative values of ∇C at the various interfaces, and the relative differences in the values are the same whether the actual gradient across the phase is linear or a function of position.

$$\nu_{\phi,\alpha}\big|_{H_2O,\underline{H}} - \nu_{\phi,\alpha}\big|_{O_2} = \frac{1}{\Delta c_{\phi,\alpha}} \Big[\underbrace{(J_{\phi,\alpha}\big|_{H_2O,\underline{H}} - J_{\phi,\alpha}\big|_{O_2})}_{\text{Term 1}} - \underbrace{(J_{\alpha,\phi}\big|_{H_2O,\underline{H}} - J_{\alpha,\phi}\big|_{O_2})}_{\text{Term 2}} \Big] \tag{B10}$$

It can be seen in Fig. B3 that $\nabla c_{\phi,\alpha}\big|_{H_2O,\underline{H}} > \nabla c_{\phi,\alpha}\big|_{O_2}$ and $\nabla c_{\alpha,\phi}\big|_{H_2O,\underline{H}} < \nabla c_{\alpha,\phi}\big|_{O_2}$, and recalling that $J_{i,j} = D_i \nabla c_{i,j}$,

$$J_{\phi,\alpha}\big|_{H_2O,\underline{H}} > J_{\phi,\alpha}\big|_{O_2} \tag{B11}$$

and

$$J_{\alpha,\phi}\big|_{H_2O,\underline{H}} < J_{\alpha,\phi}\big|_{O_2} \ . \tag{B12}$$

Referring Eqs. (B11) and (B12) to Eq. (B10), it is evident that Postulate I requires the right side of Eq. (B10) to be a positive quantity, while the experimental observation [cf. Eq. (B8)] shows that the left side of the equation is negative. Therefore, Postulate I is false; the differences between oxidation in steam and in oxygen cannot be explained in terms of a hydrogen effect in the beta alone.

Effects in the Oxide Only — We consider now a second postulate concerning the possibility that the decrease in oxide growth rate and the increase in the alpha growth rate in steam relative to oxygen is due to a decreased oxygen flux into the oxide for oxidation in steam. We shall show that this idea is consistent with the experimental results.

Postulate II. The oxygen flux into the oxide is smaller in steam than in oxygen, and oxygen mobilities in the α and β phase remain unchanged as do the equilibrium oxygen concentrations at the ϕ,α and α,β boundaries.

This postulate is consistent with the experimental observations as may be seen from the following arguments. By Postulate II

$$J_{\phi,\alpha}\big|_{H_2O,\underline{H}} < J_{\phi,\alpha}\big|_{O_2} \quad ; \tag{B13}$$

therefore, the first term on the right side of Eq. (B10) is negative. Referring again to the oxygen concentration gradients in the alpha phase (Fig. B3), it is evident that Eq. (B12) holds in this case also; therefore, the second term on the right of Eq. (B10) is negative and makes a net positive contribution in light of the negative sign in front of it. The left side of the equation is negative, requiring only that

$$|\text{Term 1}| > |\text{Term 2}|$$

in order to satisfy the experimental observations.

This type of analysis can also be extended to take into account the relative velocities of the α/β interface.

$$\nu_{\alpha,\beta}\big|_{H_2O,\underline{H}} - \nu_{\alpha,\beta}\big|_{O_2} = \frac{1}{\Delta c_{\alpha,\beta}} \Big[\underbrace{(J_{\alpha,\beta}\big|_{H_2O,\underline{H}} - J_{\alpha,\beta}\big|_{O_2})}_{\text{Term 1}}$$

$$- \underbrace{(J_{\beta,\alpha}\big|_{H_2O,\underline{H}} - J_{\beta,\alpha}\big|_{O_2})}_{\text{Term 2}} \Big] \quad . \tag{B14}$$

The experimental observation is that

$$\xi\big|_{H_2O,\underline{H}} < \xi\big|_{O_2} \quad , \tag{B15}$$

where ξ is the combined oxide and alpha layer thickness, and when the position of the α/β interface was referenced to the original metal surface, we found

$$\nu_{\alpha,\beta}\big|_{H_2O,\underline{H}} \leq \nu_{\alpha,\beta}\big|_{O_2} \quad . \tag{B16}$$

Therefore, the left side of Eq. (B14) is equal to or slightly less than zero. As previously, Term 1 on the right side of Eq. (B14) is negative. Since the position of the α,β boundary is almost the same in the two oxidizing media, it is likely that Term 2 in Eq. (B14) is close to zero, but in any event, we only require that $|\text{Term 1}| \geq |\text{Term 2}|$. Thus we conclude that Postulate II is consistent with the experimental results.

It is, in fact, possible to offer supplementary evidence that changes in oxide stoichiometry are responsible for the observed differences for oxidation in steam and in oxygen. This additional evidence involves the observation that a line of metallic particles, rich in tin, is found in cross sections through the oxide formed on Zircaloy tubes oxidized in either steam or oxygen. This phenomenon has been reported in detail previously,[13] and the key fact is that the oxide is divided into inner and outer regions by the particle line with the ratio of the inner oxide layer thickness, ϕ_i, to that of the outer layer, ϕ_o, being essentially constant with oxidation time. Since the oxygen concentration gradient across the oxide is virtually linear, the constancy of ϕ_o/ϕ_i indicates that the metallic particles must form and move along a plane of constant oxygen potential in the oxide.

Values of ϕ_o and ϕ_i were obtained for specimens oxidized in steam and in oxygen at 1253 and 1404°C (2287—2559°F), and the results are summarized in Table B5. In both oxidizing media the ratio of inner to outer oxide thickness, ϕ_i/ϕ_o, is constant with both time and total oxide thickness; however, the inner oxide is relatively thicker in steam than oxygen.

These results underscore some interesting aspects of the differences in the oxidation behavior of Zircaloy in steam and oxygen. Assuming only that the constant oxygen potential at which the metallic particles form is the same in both media, the fact that ϕ_i/ϕ_o is different in the two cases means that the equilibrium oxygen content of the oxide at one or both interfaces is different in steam than in oxygen. Furthermore, as will be demonstrated graphically below, the fact that $\phi_i/\phi_o|_{H_2O,\underline{H}} > \phi_i/\phi_o|_{O_2}$ indicates that the difference between the oxygen concentration

Table B5. Comparison of Growth Rates and Thickness Ratios of Inner and Outer Oxide Layers Formed in Steam and Oxygen

	Temperature [°C (°F)]	
	1253 (2287)	1404 (2559)
$\delta_\phi^2/2\|_{O_2} \times 10^8$ (outer oxide)	3.44 ± 10.6%	8.47 ± 11.8%
$\delta_\phi^2/2\|_{O_2} \times 10^8$ (inner oxide)	1.45 ± 5.9%	5.12 ± 4.9%
$\delta_\phi^2/2\|_{H_2O,\underline{H}} \times 10^8$ (outer oxide)	2.33 ± 9.7%	7.40 ± 6.9%
$\delta_\phi^2/2\|_{H_2O,\underline{H}} \times 10^8$ (inner oxide)	1.55 ± 7%	5.25 ± 3.2%
$\phi_i/\phi_o\|_{O_2}$	.649	.777
$\phi_i/\phi_T\|_{O_2}$	.394	.437
$\phi_i/\phi_o\|_{H_2O,\underline{H}}$	.815	.842
$\phi_i/\phi_o\|_{H_2O,\underline{H}}$	.449	.457

at the oxide-gas interface, $c_{\phi,g}$, and that, $c_{\phi,a}$, at the oxide-alpha interface in steam is less than the corresponding difference, $c_{\phi,g}-c_{\phi,\alpha}$, in oxygen. This condition is precisely one of the phenomena in the oxide previously suggested as a cause of the differences in the oxidation behavior of Zircaloy in oxygen and steam.

These experimental results can be used as a quantitative basis for assessing the extent and nature of the "hydrogen effect" in the oxide. Figure B4 is a schematic representation of the oxygen concentration gradient across a Zircaloy oxide scale. Note that the triangle $C_{\phi,g}$,A,$C_{\phi,\alpha}$ is similar to the triangle C,B,$C_{\phi,\alpha}$; therefore,

$$\frac{C - C_{\phi,\alpha}}{\phi_i} = \frac{C_{\phi,g} - C_{\phi,\alpha}}{\phi_T} \tag{B17}$$

or

$$\frac{\phi_i}{\phi_T} = \frac{C - C_{\phi,\alpha}}{C_{\phi,g} - C_{\phi,\alpha}} \quad , \tag{B18}$$

where $\phi_T = \phi_o + \phi_i$ is the total oxide thickness. Equation (B18) is valid for oxidation in either steam or oxygen. Note also that Eq. (B18) demonstrates that the ratio ϕ_i/ϕ_T is independent of any effect attributable to the presence of dissolved hydrogen in the oxygen-stabilized α or the β phases.

One may now form the ratio

$$\frac{(\phi_i/\phi_T)|_{H_2O,\underline{H}}}{(\phi_i/\phi_T)|_{O_2}} = \frac{\dfrac{C - C_{\phi,\alpha}}{C_{\phi,g}|_{H_2O,\underline{H}} - C_{\phi,\alpha}}}{\dfrac{C - C_{\phi,\alpha}}{C_{\phi,g}|_{O_2} - C_{\phi,\alpha}}} \tag{B19}$$

or

$$\frac{(\phi_i/\phi_T)|_{H_2O,\underline{H}}}{(\phi_i/\phi_T)|_{O_2}} = \frac{C_{\phi,g}|_{O_2} - C_{\phi,\alpha}}{C_{\phi,g}|_{H_2O,\underline{H}} - C_{\phi,\alpha}} \quad . \tag{B20}$$

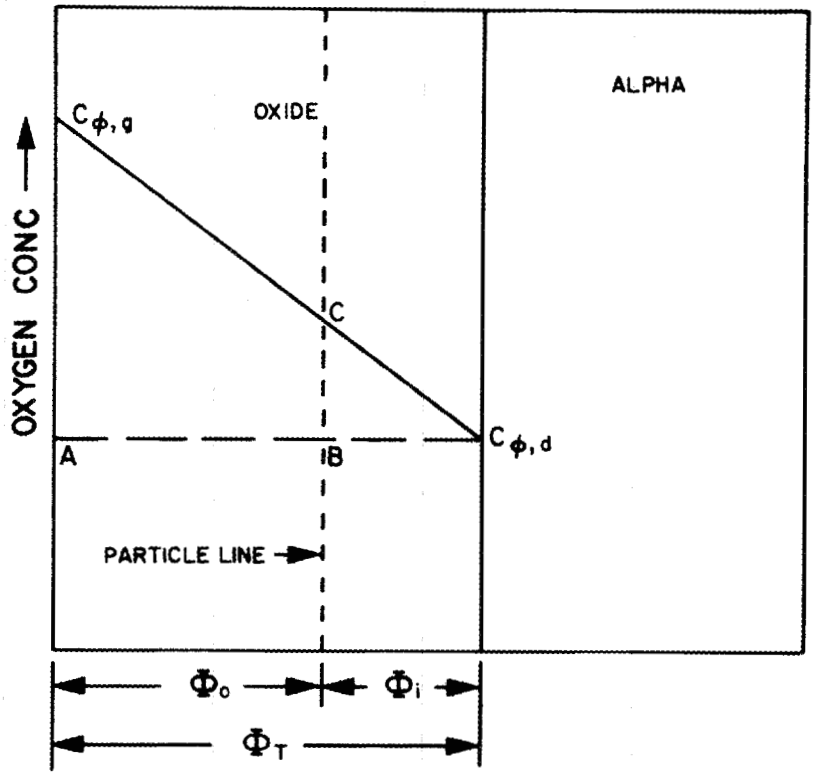

Fig. B4. Schematic Representation of Oxygen Concentration Gradient in the Oxide Layer Showing Position of the Tin-Rich Particle Line.

On the basis of phase diagram information the equilibrium oxygen concentrations at the oxide-alpha boundary, $C_{\phi,\alpha}$, are 1.403 and 1.391 gm/cc at 1253 and 1404°C (2287–2559°F), respectively.[14] Taking the oxide at the oxide-gas interface to be stoichiometric in pure oxygen ($C_{\phi,g}|_{O_2}$ = 1.511 gm/cc), the appropriate experimental values of ϕ_i/ϕ_T (Table B5) may be used to calculate $C_{\phi,g}|_{H_2O,\underline{H}}$. The result at both temperatures is $C_{\phi,g}|_{H_2O,\underline{H}}$ = 1.50 gm/cc, which is equivalent to $ZrO_{1.99}$.

The "particle line" observations thus indicate that oxidation in steam produces a reduction in $\nabla C_{\phi,\alpha}$ as compared to oxidation in oxidation in oxygen. However, the flux across the oxide-gas interface is the product of $\nabla C_{\phi,\alpha}$ and the chemical diffusion coefficient, D_ϕ, for the oxide.

$$J_{\phi,g} = -D_\phi \nabla C_{\phi,\alpha} \quad . \tag{B21}$$

We now demonstrate that the variation of $\nabla C_{\phi\ \alpha}$ deduced from the particle line observations can alone account for the differences in oxidation in oxygen as compared to steam, in other words, that $D_\phi|_{O_2} = D_\phi|_{H_2O,\underline{H}}$.

An analytical expression for D_ϕ may be obtained from Eq. (B21) by noting that the gradient in the oxide is essentially linear. Thus[14]

$$J_{\phi,g} = D_\phi \nabla C_{\phi,\alpha} = -D_\phi (C_{\phi,g} - C_{\phi,\alpha})/\phi = d\tau/dt \quad , \tag{B22}$$

where τ is the total oxygen consumed by the sample. From the fundamental equations describing parabolic oxidation kinetics, we have

$$d\tau/dt = (\delta_\tau^2/2)/\tau \quad , \tag{B23}$$

$$\tau = \delta_\tau \sqrt{t} \quad , \tag{B24}$$

and

$$\phi = \delta_\phi \sqrt{t} \quad . \tag{B25}$$

Using Eqs. (B23) and (B24),

$$d\tau/dt = \delta_\tau/2\sqrt{t} \quad , \tag{B26}$$

and substituting Eq. (B26) into Eq. (B22), using Eq. (B25), and solving for D_ϕ, we obtain

$$D_\phi = \delta_\tau \delta_\phi / 2(C_{\phi,g} - C_{\phi,\alpha}) \quad . \tag{B27}$$

Equation (B27) is valid for both oxidizing media; therefore, we may form the ratio

$$\frac{D_\phi|_{H_2O,\underline{H}}}{D_\phi|_{O_2}} = \frac{(\delta_\tau \delta_\phi)_{H_2O,\underline{H}}}{(\delta_\tau \delta_\phi)_{O_2}} \left[\frac{C_{\phi,g}|_{O_2} - C_{\phi,\alpha}}{C_{\phi,g}|_{H_2O,\underline{H}} - C_{\phi,\alpha}}\right] \quad . \tag{B28}$$

If the diffusion coefficient in the oxide is the same for oxidation in steam as in oxygen, obviously, the ratio $D_\phi|_{H_2O,\underline{H}}/D_\phi|_{O_2}$ must be unity.

We evaluate Eq. (B28) using the value of $C_{\phi,g}|_{H_2O,\underline{H}} = 1.50$ gm/cc obtained from the "particle line" observations; values for $C_{\phi,\alpha}$ are based on the phase diagram data already cited; $C_{\phi,g}|_{O_2} = 1.511$ gm/cc; and δ_τ and δ_ϕ values are derived from the oxidation data for oxidation in oxygen (see Table B2) and from the values for $\delta_\tau^2/2$ and $\delta_\phi^2/2$ obtained from the standard MiniZWOK data set at 1253 and 1404°C (2287–2559°F) (see pp. 51–57 of this report). The results obtained were

$$D_\phi|_{H_2O,\underline{H}}/D_\phi|_{O_2} = 0.971 \text{ at } 1253°C \ (2287°F) \tag{B29}$$

and

$$D_\phi|_{H_2O,\underline{H}}/D_\phi|_{O_2} = 1.02 \text{ at } 1404°C \ (2559°F) \quad . \tag{B30}$$

These results show that the ratio of oxide diffusion coefficients is certainly unity within experimental uncertainty, and it is interesting to dwell on the implications of this conclusion. Unlike Eq. (B20), where all quantities on the left side of the equation are direct observations and independent of hydrogen effects in either the α or β regions, the right side of Eq. (B28) involves the product of δ_τ and δ_ϕ, both of which could be influenced by hydrogen effects in the α and β. Furthermore, while δ_ϕ is an experimental quantity based on observations of oxide thickness as a function of time, δ_τ is a calculated value in our study. Its

evaluation requires not only direct measurements of oxide and alpha layer thicknesses, but also information concerning oxygen diffusivity in the beta and oxygen interfacial equilibrium concentrations in the various phases. All the latter values were determined (by us or others) in the absence of hydrogen. Thus the numerical evaluation of the right side of Eq. (B28) as we have performed it is "biased" in the sense that a significant hydrogen effect in the α or β phases, if it existed, would cause the real value of δ_τ to be different from that which we calculated with the result that the ratio of diffusivities would depart from unity. However, no such bias is evident in the results shown in Eqs. (B29) and (B30), and we are led to the following conclusions.

1. The value of $\nabla C_{\phi,g}$ for oxidation in oxygen is greater than that in steam because of a reduction in $C_{\phi,g}$ during oxidation in steam.

2. The differences in oxidation behavior in the two media may be rationalized solely in terms of a variation in $\nabla C_{\phi,g}$; D_ϕ remains unchanged.

3. Implicit in these results is the conclusion that hydrogen dissolved in the alpha and beta phases does not change the oxygen interfacial concentrations in either the α or β, nor does it influence oxygen diffusivity in the beta.

This last conclusion may be tested more directly through a calculation of the diffusivity, D_α, for oxygen in the alpha. Pawel[14] has shown that D_α may be expressed as

$$D_\alpha = \frac{1}{F}\left\{\left[\left(\frac{\delta_\alpha^2}{2} + \frac{\frac{1}{V}\,\delta_\phi\delta_\alpha}{2}\right)\left(\frac{C_{\alpha,\beta} - C_{\beta,\alpha}}{C_{\alpha,\phi} - C_{\alpha,\beta}}\right)\right] + \left[\frac{\delta_\alpha\sqrt{D}_\beta\,(C_{\beta,\alpha} - C_\beta)}{\sqrt{\pi}\,(C_{\alpha,\phi} - C_{\alpha,\beta})}\right]\frac{\left[\exp - \left(\frac{\delta_\alpha + \frac{1}{V}\,\delta_\phi}{2\sqrt{D_\beta}}\right)^2\right]}{\left[1 - \mathrm{erf}\left(\frac{\delta_\alpha + \frac{1}{V}\,\delta_\phi}{2\sqrt{D_\beta}}\right)\right]}\right\} \tag{B31}$$

where

C_β is the initial oxygen concentration in the beta phase, and

$$F = \frac{\dfrac{\delta_\alpha}{\sqrt{\pi D_\alpha}} \exp - \left(\dfrac{\delta_\alpha + \frac{1}{V}\delta_\phi}{2\sqrt{D_\alpha}}\right)^2}{\operatorname{erf}\left(\dfrac{\delta_\alpha + \frac{1}{V}\delta_\phi}{2\sqrt{D_\alpha}}\right) - \operatorname{erf}\left(\dfrac{\frac{1}{V}\delta_\phi}{2\sqrt{D_\alpha}}\right)} .$$

Inspection of Eq. (B31) shows that all the parameters on the right side, except V, could, in principle, be changed by the existence of a hydrogen effect in the alpha or beta phases. Note also that the δ_i's are quantities derived directly from our experimental data, while values for D_β and the equilibrium oxygen concentrations have been obtained only in the absence of significant amounts of dissolved hydrogen in the α and β phases. Thus the use of Eq. (B31) to evaluate $D_\alpha|_{O_2}$ and $D_\alpha|_{H_2O,\underline{H}}$ is "biased" in the sense that the existence of any hydrogen effect that changes D_β or the oxygen concentration terms would produce a change in the calculated D_α. Consequently, if one finds, on the basis of Eq. (B31), that $D_\alpha|_{O_2} \neq D_\alpha|_{H_2O,\underline{H}}$, a hydrogen effect in the alpha or beta is strongly suggested. On the contrary, the finding that $D_\alpha|_{O_2}$ equals $D_\alpha|_{H_2O,\underline{H}}$ provides compelling evidence that no significant hydrogen effect exists.

Substitution of appropriate values for the parameters in Eq. (31) yields the results shown in Table B6. Clearly, within experimental accuracy $D_\alpha|_{O_2} = D_\alpha|_{H_2O,\underline{H}}$, and we conclude as before that the presence of dissolved hydrogen in the α and β phases had no significant effect on the observed rates of oxidation of our standard MiniZWOK specimens.

Table B6. Comparison of D_α Calculated from Oxidation Rate Data Obtained in Steam and Oxygen

Temperature °C	Temperature (°F)	$D_\alpha\|_O$ ($cm^2/s \times 10^7$)	$D_\alpha\|_{H_2O}$ [a] ($cm^2/s \times 10^7$)	Diff. [b] (%)
1253	(2287)	1.99	1.95	2.1
1404	(2559)	8.67	8.86	−2.1

[a] Values calculated from analytical expressions for diffusion coefficients derived from standard MiniZWOK data (see Ref. 14).

[b] Difference relative to oxidation in steam.

The arguments presented thus far demonstrate that the differences observed in oxidation behavior of Zircaloy in oxygen and in steam are consistent with differences in the oxygen flux into the oxide in the two media and are inconsistent with the existence of an appreciable hydrogen effect in the α or β phases. One final test of the experimental results can be cited in support of this conclusion. We again suggest an oxidation model (that will be shown to be incorrect) that is not inconsistent with the interface velocity equations [Eqs. (B10) and (B14)], and we require the following assumptions:

$$J_{\phi,\alpha}\big|_{H_2O,\underline{H}} < J_{\phi,\alpha}\big|_{O_2} \tag{B32}$$

$$J_{\alpha,\beta}\big|_{H_2O,\underline{H}} < J_{\alpha,\beta}\big|_{O_2} \tag{B33}$$

and

$$J_{\beta,\alpha}\big|_{H_2O,\underline{H}} < J_{\beta,\alpha}\big|_{O_2} \quad . \tag{B34}$$

This model cannot be correct, however, because, as we shall now demonstrate, the conditions contained in Eqs. (B32)—(B34) require a departure from parabolic growth kinetics for both oxide and alpha layer growth.

Consider the implications of Eq. (B32)—(B34). Not only is the flux into the oxide different in steam compared to oxygen [Eq. (B32)], but the hydrogen dissolved in the alpha and beta regions is also assumed to reduce the oxygen flux into these phases. We suppose now that the Zircaloy is oxidized in steam under conditions where no hydrogen dissolves in the metallic phases of the specimen, and we contrast the resulting oxidation behavior to that exhibited when "hydrogen effects" are present in both the α and β. Since steam is the oxidizing medium in both cases, we expect no differences in interfacial equilibrium oxygen concentrations or mobilities in the oxide. By contrast, the postulate that hydrogen dissolved in the specimen reduces the flux of oxygen in the α and β phases means that the "hydrogen effect", by reducing $J_{\alpha,\phi}$, actually increases the velocity of the oxide-alpha interface relative to its velocity in steam in the absence of dissolved hydrogen; that is

$$\nu_{\phi,\alpha}\big|_{H_2O,\underline{H}} > \nu_{\phi,\alpha}\big|_{H_2O} \quad , \tag{B35}$$

where the notation "$|_{H_2O}$" refers to steam oxidation in the absence of dissolved hydrogen. In other words, if Eqs. (B32)—(B34) are valid, the rate of oxide growth in steam in the absence of dissolved hydrogen is less than that in the case where hydrogen is present. The resulting oxidation rate curves are shown schematically in Fig. B5.

As already noted, hydrogen analyses of oxidized MiniZWOK specimens exhibited considerable variability, but there was a general tend for hydrogen content to increase with oxidation time. The analytical data are not good enough to establish a functional relationship between hydrogen content and time, but in no case is there any evidence that the specimens become saturated with hydrogen (cf., Table B1). Therefore, it follows from the model that the rate of oxide growth for a specimen oxidized for a short time should be less influenced by hydrogen than would be the case for a relatively long oxidation time. The resulting rate curve would then be expected to have the form defined by the points A, B, and C in Fig. B5; short-time specimens should yield oxide thicknesses close to those predicted by Curve 1 (e.g., point A). On the other hand

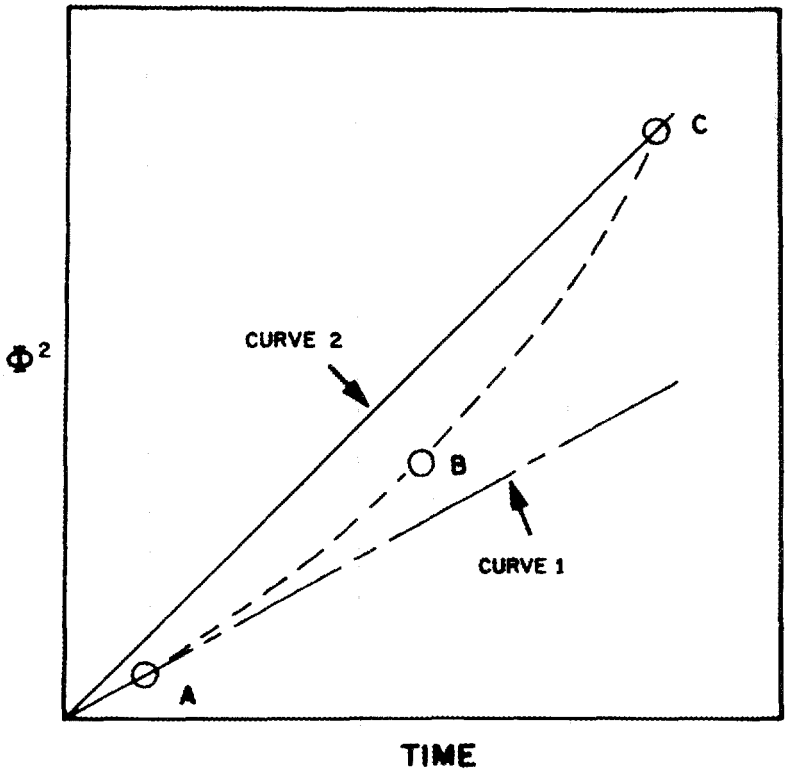

Fig. B5. Schematic Representation of Hypothetical Oxide Growth Rates for Zircaloy Without Dissolved Hydrogen (Curve 1) and with Dissolved Hydrogen (Curve 2). The dashed line shows the expected rate curve assuming a "hydrogen effect" and given the condition that the hydrogen content increases with time.

a long-time specimen should produce a datum such as point C near Curve 2. The net result would be an oxidation rate curve that is concave upward. Inspection of the oxidation rate curves (see Figs. 19–24, pp. 63–65 in the main body of the report) show no such trend. We estimate that a "hydrogen effect" that led to a maximum increase in oxide thickness of 10% for long time samples would produce a very obvious upward curvature in the rate curve and that a 5% effect should be detectable. Clearly, the postulated "hydrogen effects" either do not exist or are, at worst, small.

Another way of stating the above argument is to note that a "hydrogen effect" that increases with time would perturb the kinetics of oxidation, causing a departure from the Parabolic Rate Law. Thus the discussion above relative to the growth rate of the oxide is also applicable to the growth of the alpha layer. As in the case of oxide, inspection of the alpha-layer rate curves shows that they are well represented by a parabolic oxidation model and exhibit no indication of a hydrogen effect.

CONCLUSIONS

The dissolved hydrogen detected in MiniZWOK specimens was shown to be an artifact of the experimental procedure used. A variety of tests were performed to determine whether this dissolved hydrogen influenced the measured rates of oxidation. These tests included

1. The internal consistency of the data;
2. Comparisons with other data sets (our own and those of other investigators);
3. Oxidation rate measurements in pure oxygen.

In no case was any evidence of a "hydrogen effect" found, and we conclude that within the limits of experimental uncertainty our measured values of oxide and alpha layer growth rates were unaffected by the presence of hydrogen in the metallic phases of the specimens.

REFERENCES

1. R. R. Biederman, R. G. Ballinger, and W. G. Dobson, *A Study of Zircaloy-Steam Oxidation Kinetics*, Research Project No. 249-1, Electric Power Research Institute, Palo Alto, California, Final Report, September 1976.

2. S. Kawasaki, T. Furuta, and K. Homma, *Progress of the LWR Reactor Safety Research in JAERI*, Reactor Safety Research Center, Japan Atomic Energy Research Institute, September 1976.

3. E. A. Gulbransen and K. F. Andrew, *J. Electrochem. Soc.* 101: 348 (1954).

4. B. Cox, "Oxidation of Zirconium and Its Alloys," *Advances in Corrosion Science and Technology*, Vol. 5, M. G. Fontana and R. M. Staehle, Eds., Plenum Press, 1976, pp. 173–391.

5. K. Hauffe and V. Martinez, "Oxidation and Corrosion of Tin-Coated Zircaloy-4," *J. Electrochem. Soc.* 123: 595–602 (1976).

6. S. Kawasaki, T. Furuta, and H. Hashimoto, *Reaction of Zircaloy Cladding with Steam Under Simulated Loss-of-Coolant-Accident Conditions*, JAERI-M-6181 (July 1975).

7. S. Leistikow, H. v. Berg, and D. Jennert, "Comparative Studies of Zircaloy-4/High Temperature Steam Oxidation Under Isothermal and Temperature Transient Conditions," in *Proceedings, CSNT Specialist Meeting on the Behavior of Water Reactor Fuel Elements under Accident Conditions*, Spatind, Nord-Torpa, Norway, September 13–16, 1976, in press.

8. R. F. Mattas and H. K. Brinbaum, "Isotopic Effects on the Motion of O-H Clusters in Nb," *Acta Met.* 23: 973–77 (1975).

9. C. Baker and H. K. Birnbaum, "Anelastic Studies of Hydrogen Diffusion in Niobium," *Acta Met.* 21: 865–72 (1973).

10. C. Roy, "An Experiment to Clarify the Effect of Dissolved Oxygen on the Terminal Solubility of Hydrogen in Zirconium," *J. Nucl. Mater.* 13: 275–7 (1964).

11. P. Kofstad, *Nonstoichiometry, Diffusion and Electrical Conductivity in Binary Metal Oxides*, Wiley-Interscience, New York, N.Y., 1972, pp. 152–165.

12. L. A. McClaine and C. P. Coppel, "Electrical Conductivity Studies of Tetragonal Zirconia," *J. Electrochem. Soc.* 113: 80–85 (1966).

13. G. J. Yurek, J. V. Cathcart, and R. E. Pawel, "Microstructures of the Scales Formed on Zircaloy-4 in Steam at Elevated Temperatures," *Oxidation of Metals* 10: 255–76 (1976).

14. R. E. Pawel, *Zirconium Metal-Water Oxidation Kinetics III. Oxygen Diffusion in Oxide and Alpha Zircaloy Phases*, ORNL/NUREG-5 (October 1976).

ORNL/NUREG-17
Dist. Category NRC-3

INTERNAL DISTRIBUTION

1. C. K. Bayne
2. M. Bender
3. J. R. Buchanan
4. J. J. Campbell
5. K. R. Carr
6–31. J. V. Cathcart
32. R. H. Chapman
33. W. B. Cottrell
34. F. L. Culler
35. D. G. Davis
36. R. E. Druschel
37. G. G. Fee
38. D. E. Ferguson
39. J. H. Freels
40. J. A. Hawk
41. R. A. Hedrick
42–44. M. R. Hill
45. D. O. Hobson
46. G. Hoffman
47. S. H. Jury
48. T. G. Kollie
49. B. C. Leslie
50. T. S. Lundy
51. F. C. Maienschein
52. D. L. McElroy
53. C. J. McHargue
54. R. A. McKee
55. C. S. Meadors
56. F. H. Neill
57. R. E. Pawel
58. R. A. Perkins
59. H. Postma
60. E. T. Rose
61. R. L. Shipp
62. D. B. Trauger
63. J. R. Weir
64. R. K. Williams
65. Patent Office
66–67. Central Research Library
68. Document Reference Section
69–73. Laboratory Records Department
74. Laboratory Records, RC

EXTERNAL DISTRIBUTION

75–79. Director, Division of Reactor Safety Research, Nuclear Regulatory Commission, Washington, DC 20545
80. Director, Reactor Division, ERDA, ORO
81. Director, Research and Technical Support Division, ERDA, ORO
82–84. R. F. Fraley, ACRS
85. M. Levenson, Electric Power Research Institute, 3412 Hillview Avenue, P.O. Box 10412, Palo Alto, CA 94305
86–87. W. Loewenstein, Electric Power Research Institute, 3412 Hillview Avenue, P.O. Box 10412, Palo Alto, CA 94305
88. H. Seipel, Der Bundesminister fur Forschung and Technologie, 53 Bonn 12, Postfach 120370, Federal Republic of Germany
89–408. Given distribution as shown in NRC category 3 (25 copies — NTIS)

☆ U.S. GOVERNMENT PRINTING OFFICE: 1977-748-189/174